NOTICE

The quality of this microform is heavily dependent upon the quality of the original thesis submitted for microfilming. Every effort has been made to ensure the highest quality of reproduction possible.

If pages are missing, contact the university which granted the degree.

Some pages may have indistinct print especially if the original pages were typed with a poor typewriter ribbon or if the university sent us an inferior photocopy.

Reproduction in full or in part of this microform is governed by the Canadian Copyright Act, R.S.C. 1970, c. C-30, and subsequent amendments.

AVIS

La qualité de cette microforme dépend grandement de la qualité de la thèse soumise au microfilmage. Nous avons tout fait pour assurer une qualité supérieure de reproduction.

S'il manque des pages, veuillez communiquer avec l'université qui a conféré le grade.

La qualité d'impression de certaines pages peut laisser à désirer, surtout si les pages originales ont été dactylographiées à l'aide d'un ruban usé ou si l'université nous a fait parvenir une photocopie de qualité inférieure.

La reproduction, même partielle, de cette microforme est soumise à la Loi canadienne sur le droit d'auteur, SRC 1970, c. C-30, et ses amendements subséquents.

FAST AND EFFICIENT TECHNIQUES FOR THE DESIGN OF 2-D ELLIPTICALLY AND CIRCULARLY SYMMETRIC FIR AND IIR DIGITAL FILTERS USING MCCLELLAN TRANSFORMATION

Natarajan Nagamuthu

A Thesis

in

The Department

of

Electrical and Computer Engineering

Presented in Partial Fulfillment of the Requirements
for the Degree of Doctor of Philosophy at
Concordia University
Montréal, Québec, Canada

August, 1989

ISBN 0-315-51328-4

ABSTRACT

FAST AND EFFICIENT TECHNIQUES FOR THE DESIGN OF 2-D ELLIPTICALLY AND CIRCULARLY SYMMETRIC FIR AND IIR DIGITAL FILTERS USING MCCLELLAN TRANSFORMATION

Natarajan Nagamuthu, Ph. D.,
Concordia University, 1989.

This thesis is concerned with the problem of developing analytical techniques to design two-dimensional (2-D) elliptically and circularly symmetric FIR and IIR digital filters using McClellan transformation.

The scaling problem of 2-D digital filters with elliptical and circular cutoff contours is analyzed. Several new simple formulas for finding the extreme values of the transformation function are presented. Using these extreme values, simple formulas for scaling factors and scaled transformations are derived. Scaling-free transformations and the condition for their existence are also derived. It is shown that the number of independent coefficients in such transformations varies from 0 to 2, compared to 3 in the original McClellan transformation. A new scaling formula is developed, and some of its properties and advantages are discussed.

Several fast and efficient analytical techniques are developed for finding the coefficients of the first-order McClellan transformation for the design of 2-D zero-phase FIR and IIR digital filters with circularly symmetric contours and elliptically symmetric contours of arbitrary orientations. Original and scaling-free transformations are employed for the filters with circular and normal elliptical contours. Generalized and scaling-free generalized transformations are utilized in the case of filters with rotated elliptical contours. A number of new formulas is derived for finding the coefficients of all these transformations by using an approximation approach in which the coefficients

of the lower-order significant terms in the power series expansion of a linear error function are forced to zero. All the results presented are both for the cosine- and sine- form transformations and are general in their formats. The formulas derived are extremely simple, and because of their analytical nature, the developed filter design techniques employing these formulas are faster than the existing ones.

The scaled coefficients for the circular contours are shown to be constants and independent of frequency specifications. These coefficients are also shown to yield a better approximation of circular contours than the McClellan's coefficients. In order to demonstrate the validity of the derived formulas and the efficiency of the proposed design schemes, a number of examples is presented. Through these examples, it is shown that the design techniques provide results with a reasonably good accuracy even for large frequency values It is shown that the design results agree well with those achieved by using optimization and other analytical techniques, and the CPU time for the design is only a fraction of those of the conventional methods.

ACKNOWLEDGMENTS

I would like to record my sincere gratitude to my supervisor Dean M.N.S. Swamy for his guidance, encouragement, and support during the course of this research. I also would like to record my sincere thanks to Professor M.O. Ahmad for spending several hours with me and correcting the initial draft of this thesis which resulted in improvement of the presentation. The comments of the committee members are gratefully acknowledged.

I wish to express my heartfelt appreciation to Professor G.A. Jullien, Department of Electrical Engineering, University of Windsor, for first introducing the area of digital signal processing (DSP) to me, and suggesting some of the challenging problems in the area of multidimensional DSP. I am very thankful to other faculty members in the Signals and Systems Group for further stimulating my research interest in the latter area.

This research work was supported in part by the Natural Sciences and Engineering Research Council of Canada under Grant A7739, and in part by the Fonds pour la Formation de Chercheurs et l'Aide la Recherche, awarded to Dean M.N.S. Swamy. These financial assistances are very much acknowledged.

I consider myself very lucky to have made many new wonderful friends in Montreal. They would always be in my memory along with the joyous moments that we shared together. I thank all of them for keeping my spirits alive during these years of research.

Last but not least, I extend with pride my sincerest thanks to our family members, without their love and help, though far away, this work would not have been accomplished.

To My Parents

T.M. Natarajan and M. Kunjammal

TABLE OF CONTENTS

LIST OF FIGURES

LIST OF TABLES

LIST OF ABBREVIATIONS AND SYMBOLS

2-D	two-dimensional
3-D	three-dimensional
BP	band-pass
BS	band-stop
FIR	finite impulse response
HP	high-pass
IIR	infinite impulse response
LANDSAT	land satellite
LMS	least mean square
LP	low-pass
MFM	maximally flat magnitude
MSE	mean square error
N-D	N-dimensional
RADARSAT	radar satellite
ROM	read only memory
SOPOT	sum-of-powers-of-two
VLSI	very large scale integration

C_1 , C_2	scaling factors
E_1 (E_2)	nonlinear (linear) error function
$E_{i\ \max}$	maximum absolute error of nonlinear ($i = 1$) (linear ($i = 2$)) error function

$E_{i\ MSE}$	mean square error of nonlinear ($i = 1$) (linear ($i = 2$)) error function
$E_{i\ RMS}$	root mean square error of nonlinear ($i = 1$) (linear ($i = 2$)) error function
$F(\omega_1,\omega_2)$	cosine-form 2-D original McClellan transformation function
$F'(\omega_1,\omega_2)$	scaled cosine-form 2-D original McClellan transformation function
$F_{g\,1}(\omega_1,\omega_2)$	two-dimensional generalized McClellan transformation function with one first-order sine term
$F_{g\,2}(\omega_1,\omega_2)$	two-dimensional generalized McClellan transformation function with two second-order sine terms
$F_{\max}$	maximum value of $F(\omega_1,\omega_2)$
$F_{\min}$	minimum value of $F(\omega_1,\omega_2)$
$G(\omega_1,\omega_2)$	sine-form 2-D original McClellan transformation function
$G'(\omega_1,\omega_2)$	scaled sine-form 2-D original McClellan transformation function
$G_{g\,1}(\omega_1,\omega_2)$	sine-form 2-D generalized McClellan transformation function with one first-order sine term
$G_{g\,2}(\omega_1,\omega_2)$	sine-form 2-D generalized McClellan transformation function with two second-order sine terms
$g(s_1,s_2)$	right side of 1-D to 2-D analog transformation
$g(z_1,z_2)$	right side of 1-D to 2-D digital transformation
J_1 (J_2)	nonlinear (linear) objective function
l_2	error norm for LMS approximation
l_∞	error norm for minimax or Chebyshev approximation
M×M	order of a 2-D filter

n_1	ω_1 frequency index
N_f	total number of equally spaced frequency points in the set R_p
p_{ij}	coefficients of sine-form 2-D original McClellan transformation
P_{ij}	scaled coefficients corresponding to p_{ij}'s
q_{ij}	part of the coefficients of sine-form 2-D generalized McClellan transformation (p_{ij} : remaining coefficients)
r_{a1} (r_{a2})	transition-ratio of a 2-D type-A filter for the ω_1- (ω_2-) axis
r_{b1} (r_{b2})	transition-ratio of a 2-D type-B filter for the ω_1- (ω_2-) axis
r_ω (w_ω)	transition- ratio (width) of a 1-D filter
R_p	discrete set of frequency points on the ω_1-axis in a limited range
s	one-dimensional analog frequency variable
s_1 , s_2	two-dimensional analog frequency variables
s_{ij}	coefficients of sine terms of 2-D generalized McClellan transformation
S_{ij}	scaled coefficients corresponding to s_{ij}'s
t	vector of transformation coefficients to be optimized
t_{ij}	coefficients of cosine-form 2-D original McClellan transformation
T_{ij}	scaled coefficients corresponding to t_{ij}'s
U_{ij}	coefficients of scaled and scaling-free 2-D original transformations
w_{a1} (w_{a2})	transition-width of a 2-D type-A filter for the ω_1- (ω_2-) axis
w_{b1} (w_{b2})	transition-width of a 2-D type-B filter for the ω_1- (ω_2-) axis
z	one-dimensional digital frequency variable
z_1 , z_2	two-dimensional digital frequency variables

$\rightarrow$	mapping operator
α	a constant
β	angle of rotation for rotated filters
ω	one-dimensional frequency variable
ω'	new 1-D frequency
ω_0	one-dimensional pass-band cutoff frequency
ω_0'	new 1-D pass-band cutoff frequency
ω_1 , ω_2	two-dimensional frequency variables
ω_a	two-dimensional minor-axis pass-band cutoff frequency
ω_b	two-dimensional major-axis pass-band cutoff frequency
ω_c	two-dimensional minor-axis stop-band cutoff frequency
ω_d	two-dimensional major-axis stop-band cutoff frequency
ω_e	two-dimensional pass-band cutoff radius
ω_f	two-dimensional stop-band cutoff radius
ω_p	another 1-D pass-band cutoff frequency ($\omega_p < \omega_0$)
ω_s	one-dimensional stop-band cutoff frequency
θ	angle of rotation in anticlockwise direction

CHAPTER 1

INTRODUCTION

1.1 GENERAL

Signals are integral parts of almost all physical systems and, therefore, have become a subject of extensive study in a number of important disciplines such as acoustics, telemetry, biomedicine, communications, control and robotic systems, power systems, and computer engineering. Most signals in the real world are multidimensional or more precisely N-dimensional (N-D, $N \geq 2$). For example, image signals and geophysical signals are two-dimensional (2-D) in nature, and moving image signals are in three-dimensional (3-D) in form. Signals received by distributed sensors in seismic, sonar, and radio astronomical systems can be of even higher dimensions.

A major objective of signal processing is to get the required information or to remove the unwanted noise from the signal. Processing the signals digitally rather than in their analog form offers the traditional advantages associated with digital systems [1], [2]. One of the important and powerful means for processing of multidimensional digital signals is to employ multidimensional digital filters. Two major types of digital filters are: (i) finite impulse response (FIR) or nonrecursive filter and (ii) infinite impulse response (IIR) or recursive filter. Relative advantages and disadvantages of these filters, and techniques for their design in the case of 1-D are well known [1-3]. In two and higher dimensions, the design of digital filters satisfying prescribed magnitude and/or group-delay specifications while guaranteeing stability remains a challenging and interesting problem.

An important domain in the area of 2-D filter design [4]-[81] is the technique of spectral transformation [18], [19], [23], since it has a number of advantages, *e.g.*, it allows the use of an already available vast resource of 1-D filter designs. Therefore, in

the following two sections, some of the existing spectral transformation techniques for the design of 2-D FIR and IIR filters are briefly reviewed.

1.2 Review of 2-D FIR Filter Design Techniques

Many design techniques reported for 2-D linear-phase FIR filters are generalizations of the familiar 1-D design techniques. The techniques available for the design of 2-D FIR filters are [5], [11], [15], [16]: 1) window technique, 2) frequency sampling technique, 3) optimization technique, and 4) separable filter technique, and 5) transformation technique.

Of these, the window technique is the easiest to apply and it is the most general, for it can be used to find filters of any order with arbitrary magnitude and phase responses. Though this technique results in a short design time, it is not optimal in any sense. Using the frequency sampling technique, though filters as large as 25×25 can be designed, the design time is excessive. The optimization technique yields optimum filters which are more selective than those designed by the first two techniques. But, it is computationally very expensive. Linear programming is slow and has been limited to the design of 9×9 filters [17] because of the complexity of the problem. For example, the design of an optimum 31×31 FIR filter involves optimization of over $16 \times 16 = 256$ parameters. In terms of cost, the optimization technique is only worthwhile for filters with relatively small impulse responses [5]. The separable filter technique requires relatively less computer time, but it is generally not optimal. The transformation technique is a powerful design method for 2-D zero-phase FIR filters. Its efficiency far exceeds the efficiency of the optimization technique. In the following paragraphs, the definition and classification of spectral transformations, and design approaches which are also applicable for 2-D IIR filters are presented. Some of the transformation techniques [18], [19], [23] for the design of 2-D FIR filters are also briefly reviewed.

Complex transformations, with domains and co-domains consisting of rational

transfer functions which map one transfer function into another transfer function with a different frequency response maintaining some desirable characteristics (*e.g.* ripple in pass-band and stop-band of magnitude response and stability) are defined as "spectral transformations".

One- and two- dimensional spectral transformations can be classified into any one of the three categories: 1) analog transformations, 2) digital transformations, and 3) conversion transformations. An analog transformation transforms an analog filter into another analog filter. Similarly, a digital transformation transforms a digital filter into another digital filter. But, a conversion transformation transforms an analog filter into a digital filter or a digital filter into an analog filter. The first two categories exist for 1-D to 2-D spectral transformations. The 1-D spectral transformations are well known [1-3]. However, a short review for the 2-D and 1-D to 2-D spectral transformations is in order.

Starting from a 1-D analog filter to design a 2-D digital filter, there are two distinct approaches. In approach A, a 1-D to 2-D analog transformation is followed by a 2-D conversion transformation. In approach B, a 1-D conversion transformation is followed by a 1-D to 2-D digital transformation. Unlike 1-D where both the approaches are almost equally advantageous, in 2-D the advantages and disadvantages of the two approaches differ significantly.

In approach A, it is difficult to control the cutoff contour of a 2-D filter. Also, the 1-D to 2-D analog transformation [23] should be such that the denominator of the resulting 2-D transfer function is a very strict Hurwitz polynomial; otherwise, nonessential singularities of the second kind may occur which in turn may lead to an unstable filter when double bilinear transformation is applied [20]. This approach is very useful for the design of 2-D IIR filters, but, not so useful for the design of FIR filters.

Approach B is useful for the design of a restricted class FIR and IIR filters. In this approach, the warping effect can be eliminated by directly starting from a 1-D digital filter. Moreover, it is relatively easy to control the cutoff contour of the 2-D filter,

especially when the desired 2-D response is constant in certain regions of the (ω_1,ω_2)-plane. This approach is very convenient for the design of 2-D filters.

Both in approaches A and B, the starting 1-D filter can be designed by using various types of 1-D spectral transformations. These approaches yield filters with only first quadrant impulse response. However, by proper combination of two or more quarter-plane filters or by properly processing the input data, one can achieve zero-phase response or other useful symmetries [4].

Several spectral transformations have been reported in the literature [18], [19]. The 1-D to 2-D analog transformation [21-23], $s = g(s_1,s_2)$ followed by the double bilinear transformation is less successful mainly because it is difficult to prewarp the 2-D cutoff contours. The 1-D to 2-D digital transformation [24-26], $z = g(z_1,z_2)$ requires interpolations or it is applicable only for circularly symmetric or fan filters.

The McClellan transformation [17] is by far the most popular method due to its simplicity and flexibility. Several design techniques which use this transformation are reported in the literature [4], [5], [16-18], [27-48]. Most of these techniques are for the design of 2-D zero-phase FIR filers, and they are obtained by applying McClellan transformation on 1-D zero-phase FIR filters. Some efforts have also been made for the design of 3-D spherically- and N-D hyper-spherically- symmetric FIR filters [29]-[31]

The idea of converting a 1-D zero-phase FIR filter into a 2-D one through a substitution of variables was first proposed by McClellan [17]. This is an attractive technique for a number of reasons. It utilizes a vast resource of the already very well developed 1-D filter design techniques [1], [2]. It is simpler and faster, and requires less memory compared to the direct design methods [5], [15]. Even higher order filters (*e.g.* 61×61) can be designed using the McClellan transformation in a modest amount of computer time [27]. If the 1-D filter is optimal in the Chebyshev sense, then, the 2-D filter obtained by using this transformation with the coefficients suggested in [17] is also optimal in the Chebyshev sense. If the 1-D filter has maximally flat magnitude (MFM)

characteristic, then the 2-D filter obtained by using the McClellan transformation also has MFM characteristic [49]. Since the transformation has only cosine terms, it is limited to the design of 2-D filters with quadrantal symmetry [50]. This type of symmetry however, is present in many practical 2-D filters such as elliptically and circularly symmetric filters, and fan filters.

Mersereau *et al.* [27] have extended the first-order original McClellan transformation to higher orders and presented some optimal algorithms for finding its coefficients. They showed that 2-D filters with different shapes such as square, diamond, and ring could be designed by using higher order transformations. Mersereau [32] further extended the technique to the design of arbitrary 2-D zero-phase FIR filters by adding a sine term with the original transformation. The idea of increasing the capability of the original transformation to generate 2-D functions possessing real frequency response without quadrantal symmetry was first suggested by Rajan and Swamy [50].

McClellan transformation can be applied on 1-D zero-phase filters having different types of structures such as direct, cascade, and parallel. Also, efficient implementations [5], [16] which are faster than the direct convolution and fast Fourier transform (FFT) approaches, exist for the 2-D zero-phase FIR filters of moderate filter size (up to 51×51) designed by using this transformation.

In all the above mentioned methods, the transformation coefficients are found such that the transformation maps the 1-D cutoff frequency onto the desired 2-D cutoff contour. The constrained optimization methods are computationally more expensive than the unconstrained methods [4]. Also, among the unconstrained linear [27], [29-32] and nonlinear [18], [28], [45-47] optimization methods, the former methods take more computational time [4]. The nonlinear optimization methods are generally sensitive to the initial guess and suffer from the problem of local minima. The computations of the optimization methods often exceed the arithmetic and/or speed capability of low cost, standalone, 2-D signal processors and therefore, are not suitable for real-time applications.

To overcome these problems, some analytical methods have been developed for the design of 2-D filters with elliptical [34-37], circular [38-41], and rotated elliptical [42], [43] cutoff contours. The methods of Reddy and Hazra [34], [40], [42] are more complex, and hence, involve a considerable amount of computations compared to the methods [35]-[37], [41], and [43]. Fettweis [38], and Kurogochi and Makino [39] have used higher order transformations to achieve better circular symmetry for the 2-D filters. The use of higher order transformation is not preferred, since it results in 2-D filters with higher order. Also, these methods do not give circular contours over a band of frequencies. Some of the transformations given in [38] do not map certain real frequency points in the (ω_1,ω_2)-plane onto the ω-axis which is real. The method given in [35] for a rotated elliptical contour produces unnecessary extra pass-bands.

Most of the methods mentioned above, reformulate the contour approximation problem which is nonlinear in nature, into a linear approximation problem by assuming the that 1-D to 2-D mapping is exact. Therefore, this approach is a suboptimum. This is not a serious problem, since for a first-order McClellan transformation, the minimization of the linear error function effectively minimizes the nonlinear error function [27].

A common problem in all the design methods using McClellan transformation is that even if the 1-D prototype filter and the transformation coefficients are optimum, the resulting 2-D filter may not be optimum. The reason for this is that the transformation may not preserve the response of the 1-D filter exactly on the ω_1 and ω_2 axes of the 2-D plane. Generally, the 2-D filter obtained by using the McClellan transformation is suboptimum. The transformation coefficients given by McClellan [17], however, provide optimum 2-D approximately circularly symmetric filter if the 1-D filter is optimum. The optimization techniques [5], [15] used for designing optimum 2-D filters take considerable amount of computer time and require large amount of memory [4].

1.3 REVIEW OF 2-D IIR FILTER DESIGN TECHNIQUES

Most of the design techniques reported for 2-D IIR filters are extensions of the familiar 1-D IIR filter design techniques with incorporation of stability conditions or stability testing and group-delay specifications in the design procedure. Unlike the design of 2-D FIR filter, the design of 2-D IIR filter is not an easy task, since these modifications are difficult to incorporate. The techniques available for the design of 2-D IIR filters are [4], [5], [11], [15]: 1) spatial-domain technique, 2) magnitude squared technique, 3) optimization technique, 4) separable technique, and 5) transformation technique.

Spatial-domain techniques are useful in applications which call for a filter whose response to a particular input approximates a well-defined signal. In other situations, where the desired characteristics of the filter are specified in the frequency-domain, other techniques, may be more useful. Frequency-domain techniques are popular for several reasons [5], [11]. First, the approximating function is easily written in a closed form as a function of the filter coefficients. Second, they offer more flexibility in filter design (*e.g.* specifications with or without group-delay response) and implementation (*e.g.* various VLSI schemes). Magnitude squared techniques are used in applications where the magnitude squared response of the filter should approximate some real, desired response.

Optimization techniques are general and they are suitable for designing optimum filters with arbitrary frequency specifications. The optimization techniques can be used to match the requirements of VLSI implementations Also, they can be used to further refine the responses of the filters designed by other techniques. Both linear and nonlinear optimization algorithms are employed to design 2-D IIR filters. A main disadvantage of the optimization technique is their high computational complexity and memory requirement. In these techniques, the computational time is proportional to the square of the number of iterations. For example, the test results of a direct design reported in [4] indicate a computer time of more than three hours on IBM 3031 for 100 iterations using the well known Fletcher and Powell's algorithm. The memory requirement reported for the

technique is 170 K-bytes. Least mean square (LMS) error criterion was used and the initial guess for the parameter vector, the number of optimization parameters, and the number of grid points were 1, 20, and 231 respectively.

In the separable techniques, the time consuming 2-D stability testing problem is avoided because it reduces to that of a 1-D problem which is considerably simpler. Moreover, separable IIR filters are economical to implement [53], although they generally do not satisfy the specifications as closely as the nonseparable filters. Three kinds of separable filters exist: (i) product separable filters, (ii) two term denominator separable filters, and (iii) three term denominator separable filters. Transformation techniques are the simplest and fastest of all the techniques, though the filters designed by them are not optimum. In the following paragraphs, some of the transformation techniques [18], [19] used for the design of 2-D IIR filters are briefly reviewed.

Shanks *et al.* [21] first presented a technique by following approach A. They considered a 1-D analog filter as a 2-D analog filter which varies in 1-D only. They suggested two 1-D to 2-D analog transformations to rotate the (s_1,s_2)-plane by an angle β, onto the (s_1' ,s_2')-plane. Finally, by applying double bilinear transformation, the required 2-D filter was obtained. By cascading several prototype 1-D filters, rotated by various angles, 2-D filters having different characteristics can be designed. This technique, in spite of its simplicity suffers from a lack of control of the 2-D cutoff contour and also from a lack of stability guarantee of the 2-D filter.

Costa and Venetsanopoulos [22] made the above procedure more exact, showing how to obtain a desired cutoff frequency in a given direction with a specified maximum error. In addition, they proved that the rotated filters are marginally stable, if the angle β lies in between $(3/2)\pi$ and 2π. Using this technique, a 2-D IIR filter with good circular symmetry is achieved by cascading two elliptically shaped filters each of which is a cascade of second-order Butterworth filters. Since, several rotated filters are used, it is difficult to control the cutoff contour and attenuation at different contours.

The same authors proposed an algorithm by which the frequency response is approximated in as many directions as the number of rotated filters being cascaded [11]. The cutoff frequency of each rotated filter is adjusted separately and iteratively, according to the frequency response of the overall filter. This approach gives better circularly symmetric frequency response and is suitable for designing noncircularly symmetric filters. In the algorithm, however, there is a compromise between accuracy in the cutoff frequency and the number of directions in which it is specified. The rotated filter designed by this technique suffers from hardware complexity problem in its implementation.

Dubois and Blostein [54] designed 2-D IIR filters by applying double bilinear transformation on the transfer function of a two-variable passive network. Filter stability is assured as long as the parameters of the network are positive. Thus, the need for stability test is eliminated.

Ahmadi *et al.* [55] applied a two-variable reactance function on a 1-D analog transfer function, and then applied double bilinear transformation to obtain a first-quadrant 2-D IIR filter. Similarly, second-, third-, and fourth- quadrant filters can be obtained by using proper recursion for 2-D variables. A 2-D zero-phase IIR filter is obtained by cascading all the four filters. The 1-D analog transformation is a positive real function and so is the 1-D to 2-D reactance function. Since the application of a positive real function on another positive real function leads to a positive real function, the stability of the filter designed is guaranteed. As pointed out in [20], the reactance function used does not produce any nonessential singularity of the second kind. It is a locally type-preserving function [23].

King and Kayran [56] used a second-order two-variable reactance function and a guard filter [57] to design a 2-D zero-phase circularly symmetric IIR filter. This technique has a superior performance with less hardware complexity than the methods of [22] and [55].

Fahmy and Sobhy [58] used a 1-D to 2-D analog transformation and designed 2-D analog filters. Since this transformation may produce nonessential singularity of the second kind [20], the authors have imposed some conditions in the design procedure to meet the stability requirements. It is globally type-preserving [23] and permits a better control on the filter responses [57] than the reactance transformation in [55]. The filters designed using this technique have near circular symmetry when all the variables are used to optimize the magnitude response. In the case of simultaneous magnitude and group-delay optimization, the symmetry deteriorates. Finally, 2-D digital filters can be obtained from the analog counterpart, through the double bilinear transformation.

Mendonca *et al.* [59] described a procedure for the design of 2-D rotated digital filters satisfying prescribed specifications. Their scheme is a modification of the techniques in [22] and [60]. The rotations are carried through a somewhat more general transformation obtained by combining the transformations in [21] and [55]. Various types of 2-D filters can be designed using this scheme. Even though the scheme eliminates some of the problems associated with the techniques of [21] and [55], it suffers from others.

Two-dimensional IIR filters can be designed using 1-D to 2-D digital transformations and following approach B. Existing stable 2-D IIR filters can be transformed to different 2-D IIR filters that are stable by using 2-D digital transformations. Pendergrass *et al.* [61] studied such transformations and proposed single and two variable transformations. It is desirable that the transformations preserve some characteristics of the magnitude response, such as peak ripple, while altering other characteristics such as cutoff frequencies. They have found and catalogued ten stable all-pass functions that met these requirements.

Chang and Aggarwal [24] rotated the frequency response of product separable 2-D digital filters by using a 1-D to 2-D digital transformation which has rational powers of z_1 and z_2. Their technique, however, is also applicable for nonseparable 2-D digital

filters [19]. When the filters designed are realized using interpolation functions, there are two inherent problems: (i) high frequency attenuation in the vicinity of the Nyquist frequencies, and (ii) contraction of the Nyquist region.

Iijima *et al.* [25] used a simpler form of the transformation in [24] for designing 2-D circularly symmetric filters. Even though this avoids the interpolation process, it is used to design filters with a cutoff radius less than $\pi/\sqrt{2}$ only.

Kayran and King [26] developed a technique for designing 2-D FIR and IIR fan filters by the application of a complex transformation to a 1-D low-pass FIR or IIR filter. The resulting fan filters are inherently stable and no optimization is needed. The technique, however, is limited to the design of 2-D fan filters and their implementation involves causal recursions.

Gerheim [62] has given a synthesis procedure for 90° fan filters following approach B. In this synthesis, a 2-D digital filter is obtained by using the method of Hirano and Aggarwal [63]. Then, it is rotated by 45° using the index transformation in [24]. It can be implemented as a series-parallel combination of four 1-D all-pass filters. This technique is restricted very much and applicable only to 90° fan filters.

Harn and Shenoi [64] presented a theory for the design of 2-D IIR filters with circular, elliptic, and fan-like contours using a 1-D to 2-D product separable digital transformation. The transformation in the product is the well known 1-D low-pass to low-pass digital transformation [1], [2]. Though the 1-D to 2-D transformation is analogous to the McClellan transformation, it produces two unnecessary pass-bands in the (ω_1,ω_2)-plane. To avoid these extra pass-bands, the authors used a rectangular or square-shaped 2-D low-pass guard filter. In their technique a 2-D filter is a cascade of two rotated filters with each containing two 1-D filters. In the case of circular contours, the technique gives less than 10% error only for a cutoff radius $\geq 0.55\pi$. For lower cutoff radius, the filter realization requires interpolation. Also, the 1-D search procedure used by the authors is not the best.

Goodman [60] designed 2-D circularly symmetric low-pass filters by following approach B. This technique is based on a new 1-D to 2-D digital transformation. This approach retains most of the advantages of the original analog technique [22], permits design entirely in the discrete domain, yields filters with better stability characteristics, and facilitates frequency response optimization via nonlinear programming.

Ali [65] used the 1-D to 2-D digital transformation in [60] and designed an inherently stable 2-D IIR filter imitating the behavior of a 1-D analog filter. Using this technique good circular symmetry is achieved at low frequencies by cascading only two single-quadrant filters as opposed to many other filters [22].

Thyagarajan [66] designed 2-D IIR filters with circular symmetry by transforming 1-D IIR filters. The transformation proposed is such that the resulting 2-D filter has elliptical symmetry. In order to obtain circular symmetry, two such filters rotated with respect to each other by 90° are cascaded. Since each filter section in the cascade is of first-order, stability can be tested very easily.

Ramachandran and Ahmadi [67] proposed some methods of generating very strict Hurwitz polynomials and applied them to design 2-D IIR filters with specified magnitude and group-delay characteristics. Nonlinear optimization algorithm and double bilinear transformation are employed in their techniques.

Reddy and Hazra [68] proposed a modification of the technique [64], for the case of circularly symmetric filters. In the modified scheme, better results were obtained by minimizing the parameters of optimization in subsets and in sequence during each iteration.

Swamy and Thyagarajan [69] gave a method for deriving the 1-D digital transformations. They showed that the reactance transformation of an analog filter corresponds to an all-pass function transformation in the case of a digital filter. Erfani *et al* [70] gave a similar approach to derive 2-D digital transformations from 2-D analog reactance functions, and this is an extension of the procedure in [69].

An explicit formula for establishing the relationship between the original coefficients of a single-variable polynomial and the coefficients of the transformed polynomial upon application of the general biquadratic transformation has been derived in [71]. This formula is useful in the transformation technique of filter design.

McClellan transformation [17] was originally developed to transform 1-D zero-phase FIR filters into 2-D zero-phase FIR filters. But, it can also be utilized in the design of 2-D IIR filters [4], [18], [44]-[47]. Since the 2-D zero-phase IIR filter obtained by applying the McClellan transformation on a 1-D zero-phase IIR filter is unstable, it is necessary to spectrally factorize this filter to get stable 2-D IIR filters.

Bernabo *et al.* [44] designed a 2-D circularly symmetric low-pass filter using McClellan transformation. This filter is a cascade of four all-pole filters and a FIR filter. Obviously, this filter is inefficient from the hardware point of view.

A modification of this scheme was reported in [45]. It is used to achieve prescribed magnitude and constant group-delay specifications through a single factorized filter. A stability error criteria which is formed on the basis of complex cepstrum and has been included in the design to guarantee the stability of the filters. A nonlinear optimization algorithm is employed to find the McClellan transformation coefficients, and to perform the magnitude and group-delay approximations. The technique is simple and fast, and requires less memory compared to many direct designs. It can also be used to stabilize unstable 2-D filters.

This technique was improved and generalized in [18]. The improved design starts from a 1-D digital filter. It retains the advantages of the original technique while permitting the design entirely in the digital domain, yielding a simple relation for the 2-D cutoff contour, and facilitating the frequency response optimization. In 2-D IIR filters, a general class of filters, *viz*, half-plane filters [4] have more capability in approximating arbitrary frequency responses than the sub-class of quarter-plane filters. Therefore, this technique was further improved by generalizing the scheme to the design of optimum

half-plane filters [46]. In this technique, by using various types of transformations, various types of 2-D filters (*e.g.* circularly symmetric filters, fan filters) can be designed. A 2-D zero-phase IIR filter can be implemented by proper combination of two or more of factorized filters (quarter-plane or half-plane filters). A review of half-plane filter designs is also given in [46]. Extension of these techniques to the design of N-D filters was reported in [47]. Two-factor and four-factor factorization results in half-plane and quarter-plane filters, respectively. The technique is based on the existence and computation of (i) 1-D to N-D spectral transformation, (ii) N-D spectral factorization, and (iii) N-D stability error and stability test based on complex cepstrum.

Nguyen and Swamy [48] proposed a separable denominator 2-D IIR filter design technique. Using this technique a class of filters can be designed via the McClellan transform. They can be implemented by using multiprocessors [53] or by causal recursion [26].

Two- and higher- dimensional symmetry conditions [72]-[76] can be utilized to simplify the analysis and design of multidimensional FIR and IIR digital filters. Considering the various types of symmetries in the magnitude responses of transfer functions, conditions were reported in [72] and [73]. In [74] and [75], the various symmetries were expressed in a general frame work. Also, the interrelationships in the inverse Fourier transform samples as a result of various symmetries in the frequency response of 2-D filters were derived. In [76], the type of symmetry induced in one function (Fourier or inverse Fourier transform) as a result of a particular symmetry in the other function were reported in a unified manner. These results are applicable to both continuous- and discrete- domain cases. Several papers have been published based on the utilization of symmetry conditions (*e.g.* [15], [28]-[30], [33]-[43], [50]-[52], [77]-[80]). The class of McClellan transformations that are used to generate 2-D filters possessing 4-fold rotational symmetry in their frequency response are reported in [81].

1.4 MOTIVATION

Every year, a vast amount of data are received from radars and satellites. For example, LANDSAT-D, with its high resolution images sends $\approx 3.7 \times 10^{15}$ bits/year [16]. Therefore, there is a growing need for real-time adaptive 2-D digital filter design and filtering due to the complex nature of signals and large volume of data. The future satellites such as RADARSAT which is mainly planned for remote sensing will have on-board signal processors to preprocess the huge amount of data that will be collected during every rotation around the earth. The 2-D signal processor for such aerospace applications must have some characteristics such as high throughput rate, low power consumption, reasonable accuracy, small size, and low cost. The research work in this thesis, takes into account these challenging demands, and provides a handy solution to some of the existing problems.

The 2-D digital filters which are used to process the images in applications like video signal transmission and computer vision should generally have linear phase (constant group-delay) or zero-phase characteristic. FIR filters having this characteristic can be easily designed, but not the IIR filters. Since the latter filters offer greater speed of filtering (because of lower filter order), some researchers (refer previous Sec.) addressed this problem. Most of the IIR design techniques do not address this problem because, it will increase the complexity of the design which is already complex due to the stability problem. Since the McClellan transformation is a 1-D to 2-D digital transformation, it is applicable for the design of 2-D zero-phase FIR and IIR filters. Also, it has several advantages over analog and other digital transformations (refer Sec.s 1.2 & 1.3). Therefore, it is chosen as the basic transformation for the research and it brings all its advantages to the proposed design techniques.

The 2-D signals that are encountered in real world have a wide variety of characteristics. Therefore, it more beneficial to process them depending upon their characteristics and our requirements from them. The signal to be processed may have equal or

unequal spatial variations and these may or may not coincide with the spatial coordinates. Also, while sampling the signal, the sampling rates along them may be the same or different. To adopt to this type of situations or to process this kind of signals, 2-D filters having different frequency response characteristics such as circular, elliptical, and rotated elliptical contours are needed. Therefore, it is the aim of this research to come up with design techniques for these filters.

1.5 Scope and Organization of the Thesis

The thesis presents several fast and efficient analytical techniques for the design of 2-D elliptically† and circularly symmetric FIR and IIR digital filters using McClellan transformation. The method of obtaining 2-D zero-phase filters from 1-D zero-phase filters using this transformation is known. Therefore, given the 1-D and 2-D cutoff frequencies, the nature of 2-D cutoff contour, and the types of 1-D and 2-D filters, the problem of designing 2-D filters reduces to the problem of finding suitable transformation coefficients to meet the specifications. In short, the filter design problem becomes a contour approximation problem. In the thesis, the results are presented for both cosine- and sine- form McClellan transformations. They are valid for the design of 2-D low-pass (LP), high-pass (HP), band-pass (BP), and band-stop (BS) filters from 1-D LP, HP, BP, and BS filters, respectively. In other words, the transformations employed are type preserving transformations [19]. Specifically, the transformations employed for the design of 2-D filters with common and rotated elliptical contours are locally type preserving and those employed for the 2-D filters with circular contours are globally type preserving [19]. The main contents of each chapter are given next.

In Chapter 2, analytical formulas are presented for finding the extreme values of the transformation function for filters with elliptical and circular contours. Using these

† A 2-D elliptically symmetric filter is defined as a 2-D filter for which the contours of the magnitude response are in the form of ellipses and all of them have the same ratio of major axis to minor axis.

values, scaling factors, and scaled and scaling-free transformations are derived for the various cases of each type of contour. It is shown that in the scaling-free transformations, depending on the case, the number of independent coefficients vary from 0 to 2 compared to 3 in the original McClellan transformation [17]. A new scaling formula is proposed and some of its applications are discussed.

Some analytical techniques are developed in Chapter 3 for finding the coefficients of first-order original and scaling-free transformations for the design of 2-D elliptically symmetric filters. Following an approximation approach, ordinary, simplified, and scaling-free formulas are derived for the various cases of both vertical and horizontal elliptical contours. The analytical method of [34] which is for vertical elliptical contours is extended to horizontal contours as well. For both these methods, approximation techniques are developed and they offer certain advantages in hardware implementation. The results of various techniques are compared and some filter design examples are provided to demonstrate the accuracy and application of the formulas and transformations.

Similar to Chapter 3, in Chapter 4, some techniques are developed for the design of 2-D circularly symmetric filters. For the various cases of a circular contour, several extremely simple analytical formulas are derived by following the approximation approach. It is shown that the McClellan's coefficients [17] for approximately circular contours can be obtained as a special case from one of the scaling-free formulas. The scaled coefficients are shown to be constants and independent of the frequency specifications. These coefficients provide a better approximation of circular contours than that achieved by the McClellan's coefficients. Some numerical and filter design examples are presented.

In Chapter 5, some analytical techniques are developed for finding the coefficients of generalized and scaling-free generalized transformations for the design of 2-D elliptically symmetric filters with arbitrary orientations. Generalized transformations with two sine terms and with one sine term are employed for the approximation problem, and

several formulas are derived for the various cases of both vertical and horizontal elliptical contours. The effects of rotation angle on the coefficient values and the relative advantages of the techniques are discussed. The results of various techniques for different specifications are summarized and compared.

The last chapter, Chapter 6, presents the conclusions drawn from the research work of this thesis and points out the possible extensions of the results to more specific problems and new open problems.

CHAPTER 2

SCALED AND SCALING-FREE MCCLELLAN TRANSFORMATIONS FOR THE DESIGN OF 2-D DIGITAL FILTERS

2.1 INTRODUCTION

In this chapter, first, the conventional method of scaling 2-D McClellan transformation coefficients is described. Then, analytical formulas for finding the maximum and minimum values of the transformation function for elliptical and circular cutoff contours are derived. Using these extreme values, scaling factors and scaled transformations for these two classes of contours are derived. Scaling-free transformations for the same classes of contours are found. Finally, a new scaling formula for scaling the coefficients is presented and its properties, applications, and its effects on filter design are discussed.

2.2 CONVENTIONAL METHOD OF SCALING

2.2.1 Cosine-Form McClellan Transformation

The design of 2-D zero-phase filters using original McClellan transformation [17] involves a 1-D to 2-D mapping given by

$$\begin{aligned}\cos(\omega) &= t_{00} + t_{01}\cos(\omega_2) + t_{10}\cos(\omega_1) + t_{11}\cos(\omega_1)\cos(\omega_2) \\ &= F(\omega_1,\omega_2).\end{aligned} \tag{2.1}$$

For $0 \leq \omega \leq \pi$, the left side of (2.1) *i.e.* $\cos(\omega)$ varies between -1 and 1. Therefore, the right side of (2.1) must satisfy the constraint

$$|F(\omega_1,\omega_2)| \leq 1, \quad 0 \leq \omega_1 \leq \pi, \quad 0 \leq \omega_2 \leq \pi. \tag{2.2}$$

The McClellan transformation coefficients (t_{ij}'s, $(i,j) \in (0,1)$) in (2.1) are generally found using an optimization technique [27] so that the 1-D pass-band cutoff frequency ω_0 is mapped onto the desired 2-D pass-band cutoff contour.

If both 1-D and 2-D filters are low-pass, one of the desirable requirement is that the 1-D origin be mapped onto the 2-D origin *i.e.* 0→(0,0). This imposes the constraint

$$t_{00} + t_{01} + t_{10} + t_{11} = 1. \tag{2.3}$$

Using (2.3), any one coefficient can be expressed as a function of the other three. Thus, the total number of independent coefficients to be optimized reduces from 4 to 3.

The coefficients obtained by an optimization technique are usually such that some area in the 2-D plane corresponds to complex values of the 1-D frequency ω. This means that the constraint (2.2) is not satisfied. As a practical matter, the transformation (2.1) will be useful only if the coefficients satisfy the constraint (2.2). Mersereau *et al.* [27], therefore, proposed a linear scaling scheme so that the optimized coefficients are modified satisfying (2.2). The scaled transformation function is given by

$$F'(\omega_1,\omega_2) = C_1 F(\omega_1,\omega_2) - C_2 \tag{2.4}$$

where C_1 and C_2 are the scaling factors defined as

$$C_1 = 2 / (F_{max} - F_{min}) \quad \text{and} \quad C_2 = C_1 F_{max} - 1 \tag{2.5}$$

in which F_{max} and F_{min}, respectively are the maximum and minimum values of $F(\omega_1,\omega_2)$. These extreme values are usually found numerically. Obviously, this scaling does not change the shape of the contours $F(\omega_1,\omega_2) =$ constant; all that changes is the 1-D frequency associated with each contour. The scaled McClellan transformation is

$$\begin{aligned} \cos(\omega') &= T_{00} + T_{01}\cos(\omega_2) + T_{10}\cos(\omega_1) + T_{11}\cos(\omega_1)\cos(\omega_2) \\ &= F'(\omega_1,\omega_2) \end{aligned} \tag{2.6}$$

where T_{ij}'s are the scaled McClellan transformation coefficients corresponding to the t_{ij}'s. The new 1-D frequency ω' corresponding to $F'(\omega_1,\omega_2)$ is

$$\omega' = \cos^{-1}\{C_1\cos(\omega) - C_2\}. \tag{2.7}$$

The entire area in the (ω_1,ω_2)-plane, now corresponds to real values of ω' $(0 \le \omega' \le \pi)$.

Eq. (2.7) implies that the 1-D prototype filter must be designed after the transformation has been found. If F_{max} and F_{min} used in (2.5) are not evaluated accurately, spurious responses occur in the stop-band of the 2-D filter, usually along the ω_1 and ω_2 axes where $\cos(\omega_1)$ and $\cos(\omega_2)$ attain their extreme values. This is a very common design problem. The order of the 2-D filter increases with increase in the order of the transformation. For this reason, only the first-order transformation is considered in this thesis. Since, (2.1) has cosine terms, it is only suitable for designing 2-D quadrantally symmetric filters [50]. This type of symmetry however, is inherent in many practical filters such as those possessing elliptical, circular, and fan-like contours in their frequency response.

2.2.2 Sine-Form McClellan Transformation

The original McClellan transformation *i.e.* (2.1) can be expressed using sine terms as

$$\begin{aligned}\sin^2(\omega/2) &= p_{00} + p_{01}\sin^2(\omega_2/2) + p_{10}\sin^2(\omega_1/2) + p_{11}\sin^2(\omega_1/2)\sin^2(\omega_2/2) \\ &= G(\omega_1,\omega_2).\end{aligned} \tag{2.8}$$

The advantage of this form, as pointed out by Rajan and Swamy in [28], is that it is easy to visualize this mapping, since $\sin(\theta)$ is a monotonically increasing function of θ in the range 0 to $\pi/2$, and for low values of θ, $\sin(\theta) \approx \theta$. In this case, the scaled McClellan transformation for (2.8) is

$$\begin{aligned}\sin^2(\omega'/2) &= P_{00} + P_{01}\sin^2(\omega_2/2) + P_{10}\sin^2(\omega_1/2) + P_{11}\sin^2(\omega_1/2)\sin^2(\omega_2/2) \\ &= G'(\omega_1,\omega_2)\end{aligned} \tag{2.9}$$

where P_{ij}'s are the scaled McClellan transformation coefficients corresponding to the p_{ij}'s and

$$\omega' = 2\sin^{-1}\{C_1'\sin^2(\omega/2) - C_2'\}^{1/2}. \tag{2.10}$$

Both cosine- and sine- form transformations have been widely used in the literature. The results developed in this thesis are presented in both the forms so that they may easily be compared with the existing results. Conversion formulas for cosine-form to sine-

form, and sine-form to cosine-form are given in Appendix A. Using these formulas, t_{ij}'s/p_{ij}'s (T_{ij}'s/P_{ij}'s) can be found for any given p_{ij}'s/t_{ij}'s (P_{ij}'s/T_{ij}'s).

2.3 Simple Formulas for Maximum and Minimum Values

Nguyen and Swamy [51] have presented two simple formulas for calculating the maximum and minimum values of the function and hence the scaling factors for filters with vertical elliptic-contour (called type-A contour) frequency responses. In [52], they have extended this work by encompassing the analysis of all cases of vertical elliptic response. In this section, the study of [51] and [52] is further generalized, and also the horizontal elliptic and circular responses are considered. New simple formulas for calculating the maximum and minimum values, F_{max} and F_{min} are presented. In this context, the similarities and differences between different types of responses are brought out.

2.3.1 Location of Maximum and Minimum Values

The derivation for locating the maximum and minimum values of the transformation function (2.1) is given in Appendix B. It is found that in the first quadrant, maximum and minimum values of the function $F(\omega_1,\omega_2)$ lie only at the corner frequency points, *viz*, (0,0), (0,π), (π,0), and (π,π). The functional values at these points and therefore, the locations of the global maxima and minima depend on the values of the coefficients.

2.3.2 Type-B Contours

When the frequency response of a filter is horizontally elliptic, its contours are classified as type-B contours. It should be noted that for type-A contours the smaller cutoff frequency occurs on the ω_1-axis, while it occurs on the ω_2-axis for type-B contours For type-A contours, the conditions for the four possible cases and the formulas for F_{max} and F_{min} have been reported in [52].

An example of a type-B contour is shown in Fig. 2.1. Let

$$p_1 = t_{10} + t_{11} \tag{2.11a}$$

and

$$p_2 = t_{01} + t_{11}. \tag{2.11b}$$

Substituting $\omega_2 = 0$ or $\omega_1 = 0$ in (2.1), and using (2.11a) and (2.11b), respectively, yields the following equations.

$$F(\omega_1,0) = 1 - p_1\{1 - \cos(\omega_1)\} \tag{2.12a}$$

$$F(0,\omega_2) = 1 - p_2\{1 - \cos(\omega_2)\} \tag{2.12b}$$

The values of the function at the corner frequencies can be obtained readily from (2.12) as

$$\begin{aligned} F(0,0) &= 1 & F(0,\pi) &= 1 - 2p_2 \\ F(\pi,0) &= 1 - 2p_1 & F(\pi,\pi) &= 1 - 2(t_{01} + t_{10}). \end{aligned} \tag{2.13}$$

Type-B contours must satisfy the condition

$$p_2 > p_1 > 0. \tag{2.14}$$

Using the inequalities of (2.14) in (2.13), gives

$$F(0,0) > F(\pi,0) > F(0,\pi). \tag{2.15}$$

Complication arises from the value of $(t_{01} + t_{10})$ in (2.13). Depending on the values of t_{01} and t_{10}, its value may lie in one of the four possible intervals defined by the inequality (2.14). Accordingly, $F(\pi,\pi)$ assumes a value that lies in an appropriate sub-interval of (2.15). The conditions and formulas for the four cases are given below.

Case (i): $(t_{01} + t_{10}) < 0$:

The condition $p_2 > p_1 > 0 > (t_{01} + t_{10})$ reduces to $(t_{01} + t_{10}) < 0$ because of the previous condition (2.14). The condition $(t_{01} + t_{10}) < 0$ along with (2.14) implies $F(\pi,\pi) > F(0,0) > F(\pi,0) > F(0,\pi)$. Therefore, $F_{max} = 1 - 2(t_{01} + t_{10})$ and

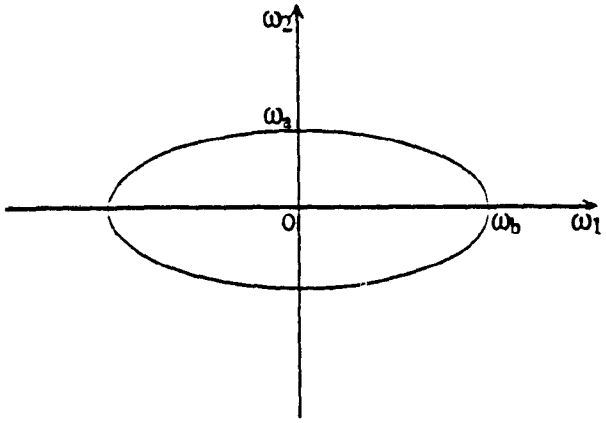

Fig. 2.1 Example of a Type-B (Horizontal) Elliptical Cutoff Contour ($\omega_b > \omega_a$).

$F_{min} = 1 - 2p_2$.

This case occurs for contours having strong components [52] on the diagonal $\omega_2 = \omega_1$. For example, this will happen for an ellipse with rotation angle close to $\pi/4$ *i.e.* $\pi/6 \leq \theta < \pi/4$ (Fig. 2.2a)†. Consequently, t_{11} as obtained from (2.3), has a high value.

Case (ii): $t_{11} > t_{01}$:

The condition $t_{11} > t_{01}$ along with (2.14) implies $F(0,0) > F(\pi,\pi) > F(\pi,0) > F(0,\pi)$. Therefore, $F_{max} = 1$ and $F_{min} = 1 - 2p_2$.

This case occurs for contours having strong components on the ω_1-axis (*e.g.* ellipses with low rotation angle *i.e.* $\pi/9 \leq \theta < \pi/6$ (Fig. 2.2b)).

Case (iii): $t_{01} > t_{11} > t_{10}$:

The condition $t_{01} > t_{11} > t_{10}$ along with (2.14) implies $F(0,0) > F(\pi,0) > F(\pi,\pi) > F(0,\pi)$. Therefore, $F_{max} = 1$ and $F_{min} = 1 - 2p_2$.

This case occurs for contours coinciding with or having very strong components on the ω_1-axis (*e.g.* an ellipse with a very low rotation angle *i.e.* $0 \leq \theta < \pi/9$ (Fig. 2.2c)).

Case (iv): $t_{01} > t_{11}$:

(iv) The condition $t_{01} > t_{11}$. along with (2.14) implies $F(0,0) > F(\pi,0) > F(0,\pi) > F(\pi,\pi)$. Therefore, $F_{max} = 1$ and $F_{min} = 1 - 2(t_{01} + t_{10})$.

This case occurs for contours having strong components on both the frequency axes (*e.g.* for an ellipse with its major-axis ($2\omega_b$) and minor-axis ($2\omega_a$) approximately of the same length (Fig. 2.2d), and circles).

---

† For the approximation of rotated elliptical contours one cannot use the transformation given by (2.1). However, they can be approximated using generalized McClellan transformation which has cosine and sine terms. Further details can be found in Chapter 5.

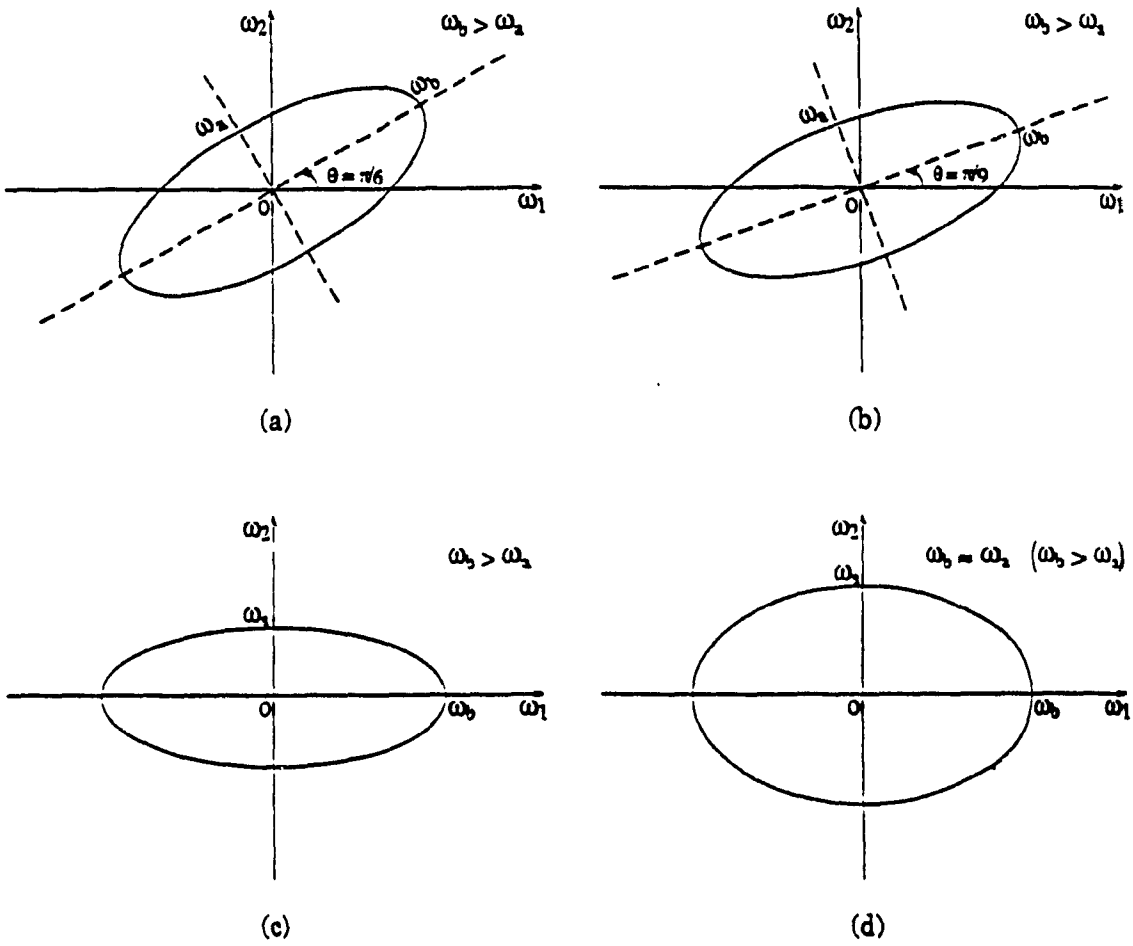

Fig. 2.2 Rotated Type-B Elliptical Cutoff Contours for Various Cases.
(a) Example for Case (i) with $\theta = \pi/6$,
(b) Example for Case (ii) with $\theta = \pi/9$,
(c) Example for Case (iii) with a large value ($>>$ 1) of the ratio ω_b / ω_a, and
(d) Example for Case (iv) with a small value ($\approx$ 1) of the ratio ω_b / ω_a.

Example 2.1: The rotation angles given above for the various cases as examples correspond to a type-B elliptical contour with $\omega_a = 0.125\pi$ and $\omega_b = 0.375\pi$. Initially, when $\theta = 0$, the minor-axis ($2\omega_a$) was on the ω_2-axis. The coefficients were calculated by taking $\omega_0 = 0.25\pi$ and using the formulas presented in Chapters 3 and 5. The scaling of the coefficients was performed by using the F_{max} and F_{min} values found from the above formulas in (2.5), and substituting the resulting values of C_1 and C_2 in (2.4).

In [52], formulas for F_{max} and F_{min} have been presented assuming that the smaller cutoff frequency is on the ω_1-axis (type-A contours). An example is shown in Fig. 2.3. The locations of the global maximum and minimum for all the contours of type-A and B are illustrated in Fig. 2.4. From this figure it is seen that the location of F_{min} for cases (i)-(iii) is different, and the location of F_{max} for cases (i)-(iv), and F_{min} for case (iv) are the same for types A and B contours. Comparing the derived results with those in [52], it is found that the actual value of F_{min} for cases (i)-(iii) is different (p_1 is replaced by p_2), and the actual value of F_{max} for cases (i)-(iv), and that of F_{min} for case (iv) are the same for both the types of contours. Also, in the conditions for cases (ii)-(iv), t_{01} is replaced by t_{10} and vice-versa.

2.3.3 Type-C Contours

When a horizontal (type-B: ω_a is on ω_2-axis) or vertical (type-A: ω_a is on ω_1-axis) elliptical contour is rotated, it no longer possesses quadrantal symmetry, but possesses centro-symmetry [50]. When $\theta = \pm\pi/4$ an interesting contour arises (Fig. 2.5a) *i.e.* the contour has equal components on both the axes. This type of contours that have equal cutoff frequencies on both the axes will be referred as type-C contours. A circular contour (Fig. 2.5b) is another example of a type-C contour.

Type-C contours must satisfy the condition

$$p_1 = p_2 > 0. \tag{2.16}$$

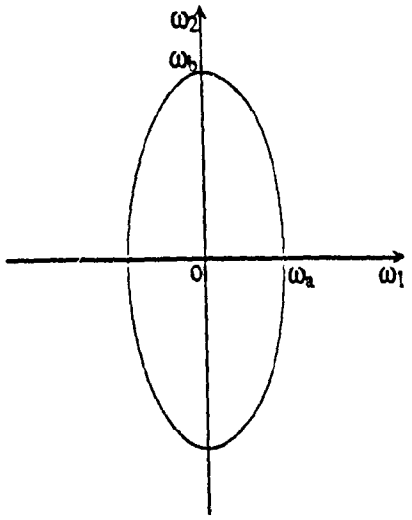

Fig. 2.3 Example of a Type-A (Vertical) Elliptical Cutoff Contour ($\omega_b > \omega_a$).

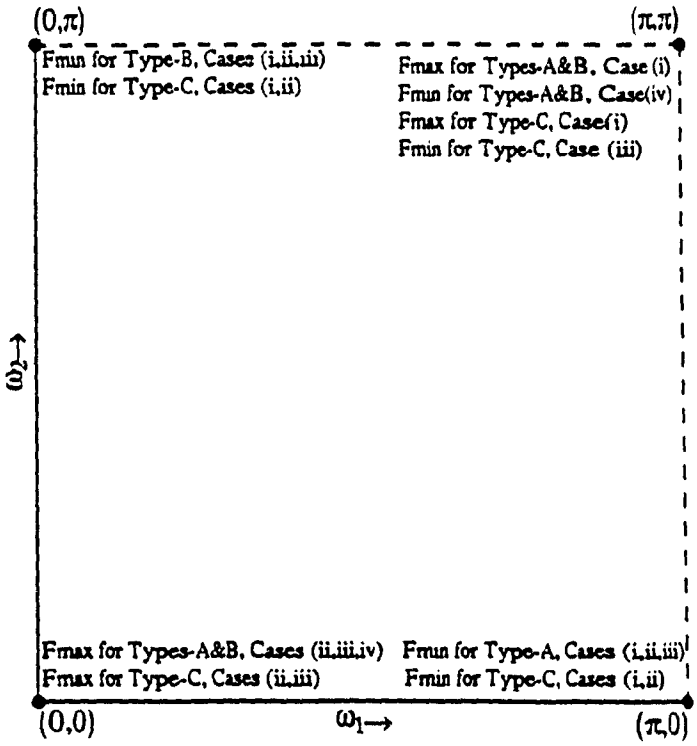

Fig. 2.4 Locations of the Global Maximum and Minimum for Various Cases of Different Types of Cutoff Contours.

(For type-A, $F(0,0) > F(0,\pi) > F(\pi,0)$;
(for type-B, $F(0,0) > F(\pi,0) > F(0,\pi)$; and
(for type-C, $F(0,0) > F(0,\pi) = F(\pi,0)$.)

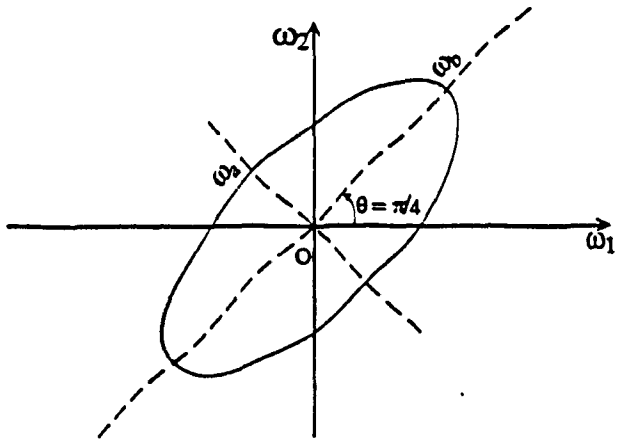

(a)

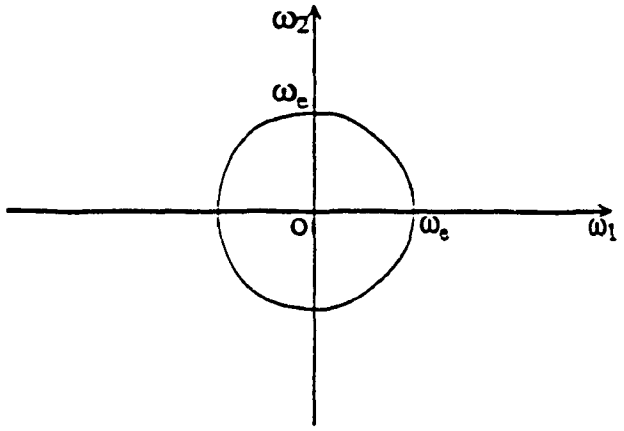

(b)

Fig. 2.5 Example of Type-C Cutoff Contours.
(a) A Type-B Elliptical Cutoff Contour with a Rotation Angle, $\theta = \pi/4$, and
(b) A Circular Cutoff Contour.

Using (2.16) in (2.13), gives

$$F(0,0) > F(0,\pi) = F(\pi,0) \tag{2.17}$$

Let $p_1 = p_2 = p$, and $t_{10} = t_{01} = t$. Following similar derivation as before, there results three different cases depending on the value of $(t_{01} + t_{10}) = 2t$.

Case (i): $2t < 0$:

The condition $2t < 0$ along with (2.16) implies $F(\pi,\pi) > F(0,0) > F(0,\pi) = F(\pi,0)$. Therefore, $F_{max} = 1 - 4t$ and $F_{min} = 1 - 2p$.

Case (ii): $t_{11} > t$:

The condition $t_{11} > t$ along with (2.16) implies $F(0,0) > F(\pi,\pi) > F(0,\pi) = F(\pi,0)$. Therefore, $F_{max} = 1$ and $F_{min} = 1 - 2p$.

Case (iii): $t > t_{11}$:

The condition $t > t_{11}$ along with (2.16) implies $F(0,0) > F(0,\pi) = F(\pi,0) > F(\pi,\pi)$. Therefore, $F_{max} = 1$ and $F_{min} = 1 - 4t$.

Example 2.2: For the elliptical contour in Example 2.1, when $\theta = 0.25\pi$, type-C case (i) formulas are used to scale the coefficients.

Example 2.3: For a circular contour of radius 0.5π, designed from a 1-D prototype filter with $\omega_0 = 0.5\pi$, the optimized coefficients are given in [52]. Using type-C case (iii) formulas the following results are obtained.

$F_{max} = 1.00000000$	$F_{min} = 1.55115200$
$C_1 = 0.78305056$	$C_2 = 0.21604044$
$\omega_0' = 0.43068570\pi$	
$T_{00} = 0.28391684$	$T_{01} = 0.50000533$
$T_{10} = 0.49999467$	$T_{11} = 0.28391683$

$T_{01} \approx T_{10}$, since $t_{01} \approx t_{10}$ in [52].

Comparing the above results for type-C contours with those for type-B discussed earlier, and type-A in [52], it is seen that the condition of case (iii) for types A and B are absent in type-C. Also, in the conditions of cases (i), (ii), and (iv) for types A and B, when the inequality between p_1 and p_2 is replaced by equality, cases (i), (ii), and (iii) for type-C are obtained. This is also seen in the F_{min} values of cases (i) and (ii) for type-C which are now located at both the points $(0,\pi)$ and $(\pi,0)$ in Fig. 2.4. The value and location of F_{max} of cases (i), (ii), and (iii) for type-C are the same as those for cases (i), (ii), and (iv) for types A and B. All these results are summarized in Appendix C.

2.4 Simple Formulas for Scaling Factors and Scaled McClellan Transformations

In this section, the scaling factors and the scaled McClellan transformations for all types of general contours are derived. If the unscaled coefficients are known, the scaled coefficients can be evaluated directly by using the conditions in Appendix C and the derived formulas.

2.4.1 Type-A Contours

For type-A contours, the scaled transformation is obtained by substituting the F_{max} and F_{min} formulas from [52] in (2.5) and by using (2.4). The following results are obtained for the four cases.

Case (i): $C_1 = 1 / (t_{11} - t_{01})$ and $C_2 = (t_{00} - t_{10}) / (t_{11} - t_{01})$.

$$F'(\omega_1,\omega_2) = U_{10} + U_{01}\cos(\omega_2) + U_{10}\cos(\omega_1) + (1 + U_{01})\cos(\omega_1)\cos(\omega_2) \quad (2.18)$$

and

$$G'(\omega_1,\omega_2) = -(U_{01} + U_{10}) + (1 + 2U_{01})\sin^2(\omega_2/2) + (1+U_{01}+U_{10})\sin^2(\omega_1/2) - 2(1 + U_{01})\sin^2(\omega_1/2)\sin^2(\omega_2/2) \quad (2.19)$$

where $U_{ij} = t_{ij} / (t_{11} - t_{01})$.

Cases (ii) and (iii): $C_1 = 1 / p_1 = 1 / (t_{10} + t_{11})$ and

$$C_2 = C_1 - 1 = (1 - p_1) / p_1 = (t_{00} + t_{01}) / (t_{10} + t_{11}).$$

$$F'(\omega_1,\omega_2) = - U_{01} + U_{01}\cos(\omega_2) + U_{10}\cos(\omega_1) + (1 - U_{10})\cos(\omega_1)\cos(\omega_2) \quad (2.20)$$

and

$$G'(\omega_1,\omega_2) = (1 + U_{01} - U_{10})\sin^2(\omega_2/2) + \sin^2(\omega_1/2) + 2(U_{10} - 1)\sin^2(\omega_1/2)\sin^2(\omega_2/2) \quad (2.21)$$

where $U_{ij} = t_{ij} / p_1 = t_{ij} / (t_{10} + t_{11})$.

Case (iv): $C_1 = 1 / (t_{01} + t_{10})$ and $C_2 = C_1 - 1 = (t_{00} + t_{11}) / (t_{01} + t_{10})$ [52]

$$F'(\omega_1,\omega_2) = - U_{11} + (1 - U_{10})\cos(\omega_2) + U_{10}\cos(\omega_1) + U_{11}\cos(\omega_1)\cos(\omega_2) \quad (2.22)$$

and

$$G'(\omega_1,\omega_2) = (1 + U_{11} - U_{10})\sin^2(\omega_2/2) + (U_{10} + U_{11})\sin^2(\omega_1/2) - 2U_{11}\sin^2(\omega_1/2)\sin^2(\omega_2/2) \quad (2.23)$$

where $U_{ij} = t_{ij} / (t_{01} + t_{10})$.

In the above results, only (2.20) is reported in [51] and [52]. For common elliptical contours (2.20) and (2.21) apply, and if the response of the 1-D prototype filter is preserved on the ω_1-axis, *i.e.* the axis of the lower cutoff frequency, then the necessary scaling is achieved.

2.4.2 Type-B Contours

Employing similar procedure as before with the F_{max} and F_{min} formulas derived in Sec. 2.3.2, the following scaling factors and scaled transformations are obtained for the four cases.

Case (i): $C_1 = 1 / (t_{11} - t_{10})$ and $C_2 = (t_{00} - t_{01}) / (t_{11} - t_{10})$.

$$F'(\omega_1,\omega_2) = U_{01} + U_{01}\cos(\omega_2) + U_{10}\cos(\omega_1) + (1 + U_{10})\cos(\omega_1)\cos(\omega_2) \quad (2.24)$$

and

$$G'(\omega_1,\omega_2) = -U_{01} + U_{10}) + (1 + U_{01} + U_{10})\sin^2(\omega_2/2) + (1 + 2U_{10})\sin^2(\omega_1/2) - 2(1 + U_{10})\sin^2(\omega_1/2)\sin^2(\omega_2/2) \quad (2.25)$$

where $U_{ij} = t_{ij} / (t_{11} - t_{00})$.

Cases (ii) and (iii): $C_1 = 1 / p_2 = 1 / (t_{01} + t_{11})$ and $C_2 = C_1 - 1 = (1 - p_2) / p_2$

$= (t_{00} + t_{10}) / (t_{01} + t_{11})$ [51].

$$F'(\omega_1,\omega_2) = -U_{10} + U_{01}\cos(\omega_2) + U_{10}\cos(\omega_1) + (1 - U_{01})\cos(\omega_1)\cos(\omega_2) \quad (2.26)$$

and

$$G'(\omega_1,\omega_2) = \sin^2(\omega_2/2) + (1 + U_{10} - U_{01})\sin^2(\omega_1/2) + 2(U_{01} - 1)\sin^2(\omega_1/2)\sin^2(\omega_2/2) \quad (2.27)$$

where $U_{ij} = t_{ij} / p_2 = t_{ij} / (t_{01} + t_{11})$.

Case (iv): The same results as for case (iv) for type-A contours *i.e.* the same C_1 and C_2, and the same expression for F' and G' as given by (2.22) and (2.23), respectively.

Cases (ii) and (iii) are applicable for contours having strong components near or on the ω_1-axis. Using the C_1 and C_2 values, (2.12b) can be rewritten as

$$\cos(\omega_2) = \{F(0,\omega_2) / p_2\} - \{(1 - p_2) / p_2\} = C_1F(0,\omega_2) - C_2. \quad (2.28)$$

Comparison of (2.28) with (2.4), yields,

$$\cos(\omega_2) = \cos(\omega') = F'(0,\omega_2). \quad (2.29)$$

The physical interpretation of (2.29) is that if the response of the 1-D prototype filter is preserved on the ω_2-axis, *i.e.* the axis of the lower cutoff frequency, then the necessary scaling is achieved.

Comparing the above results with those for type-A contours, the following differences are noticed. For case (i), the U_{ij}'s for type-B are obtained from the U_{ij}'s for

type-A by replacing t_{01} in the denominator by t_{10}. Eq. (2.24) is obtained from (2.18) by interchanging U_{10} and U_{01} in the first and last coefficients. Eq. (2.25) is obtained from (2.19) by interchanging U_{01} and U_{10} in the constant term and last term, interchanging the coefficients of two sine terms in the middle, and then by interchanging U_{01} and U_{10} in all the coefficients. For cases (ii) and (iii), U_{ij}'s for type-B are obtained from the U_{ij}'s for A by replacing t_{10} in the denominator by t_{01}. Eq. (2.26) is obtained from (2.20), and (2.27) is obtained from (2.21) by the same procedure as for case (i).

2.4.3 Type-C Contours

Employing similar procedure as for type-A contours, with the F_{max} and F_{min} formulas derived in Sec. 2.3.3, the following scaling factors and scaled transformations are obtained for the three cases where $t_{01} = t_{10} = t$.

Case (i): $C_1 = 1 / (t_{11} - t)$ and $C_2 = (t_{00} - t) / (t_{11} - t)$.

$$F'(\omega_1,\omega_2) = U + U\cos(\omega_2) + U\cos(\omega_1) + (1 + U)\cos(\omega_1)\cos(\omega_2) \tag{2.30}$$

and

$$G'(\omega_1,\omega_2) = -2U + (1 + 2U)\sin^2(\omega_2/2) + (1 + 2U)\sin^2(\omega_1/2) - 2(1 + U)\sin^2(\omega_1/2)\sin^2(\omega_2/2) \tag{2.31}$$

where $U = t / (t_{11} - t)$.

Case (ii): $C_1 = 1 / (t + t_{11})$ and $C_2 = C_1 - 1 = (t + t_{00}) / (t + t_{11})$.

$$F'(\omega_1,\omega_2) = -U + U\cos(\omega_2) + U\cos(\omega_1) + (1 - U)\cos(\omega_1)\cos(\omega_2) \tag{2.32}$$

and

$$G'(\omega_1,\omega_2) = \sin^2(\omega_2/2) + \sin^2(\omega_1/2) + 2(U - 1)\sin^2(\omega_1/2)\sin^2(\omega_2/2) \tag{2.33}$$

where $U = t / (t + t_{11})$.

Case (iii): $C_1 = 1 / (2t)$ and $C_2 = C_1 - 1 = (1 - 2t) / (2t)$.

$$F'(\omega_1,\omega_2) = -U_{11} + 0.5\cos(\omega_2) + 0.5\cos(\omega_1) + U_{11}\cos(\omega_1)\cos(\omega_2) \tag{2.34}$$

and

$$G'(\omega_1,\omega_2) = (0.5 + U_{11})\sin^2(\omega_2/2) + (0.5 + U_{11})\sin^2(\omega_1/2) - 2U_{11}\sin^2(\omega_1/2)\sin^2(\omega_2/2) \quad (2.35)$$

where $U_{11} = t_{11} / (2t)$.

Comparing the above results with those for types A and B contours, the following points are noticed. For case (i), the expression U for type-C is obtained as a special case from U_{ij}'s for type-A case (i) or from U_{ij}'s for type-B case (i) in which $t_{01} = t_{10} = t$ and hence, $U_{01} = U_{10} = U$. Using this relationship, (2.30) and (2.31) are obtained as special cases from (2.18) and (2.24), and (2.19) and (2.25), respectively. For case (ii), the expression of U for type-C is obtained as a special case from U_{ij}'s for type- A or B and cases (ii) or (iii) under the same relationship. Thus, (2.32) and (2.33) are obtained as special cases from (2.20) and (2.26), and (2.21) and (2.27), respectively. For case (iii), the expression U_{11} for type-C is obtained as a special case from U_{ij}'s for type A or B and case (iv) in which $t_{01} = t_{10} = t$ and hence, $U_{01} = U_{10} = 0.5$. Using this condition, (2.34) and (2.35) are obtained as a special case of (2.22) and (2.23), respectively.

2.5 Scaling-Free McClellan Transformations

In (2.20) and (2.21), if the coefficients U_{01} and U_{10} are used as optimization parameters, then no scaling is required for the transformation [51] [52]

$$\cos(\omega) = F'(\omega_1,\omega_2) \quad (2.36)$$

or

$$\sin^2(\omega/2) = G'(\omega_1,\omega_2) \quad (2.37)$$

where F' and G' are defined by (2.20) and (2.21), respectively. A question arises: "Even though it represents a scaled transformation, why is it scaling-free?" The reasons will be clear from the following discussion.

The McClellan transformation given by (2.1) is scaling-free if and only if

$$F_{max} = 1 \qquad \text{and} \qquad F_{min} = -1. \tag{2.38}$$

In this section, using (2.38), the necessary and sufficient conditions and the scaling-free transformation for each case are derived. It is shown that the number of independent coefficients to be optimized varies from 0 to 2 depending on the case, compared to 3 in the original transformation [17]. It is hoped that this critical study will provide clear understanding of different choices of the coefficients used in the literature [17], [28], [34], [40]. The scaling-free transformations are very useful in deriving analytical expressions for the coefficients (Given in Sec. 2.5.4). Also, in digital filtering, they reduce the number of multiplications per output sample [34].

To use the scaling-free transformations presented in this section, the conditions for the various cases given in Appendix C which are in terms of the unscaled coefficients must be checked first.

2.5.1 Type-A Contours

Case (i): In (2.6) if F' is defined by (2.18), then $F_{max} = 1 - 2(T_{01} + T_{10})$ and $F_{min} = 1 - 2p_1 = 1 - 2(T_{10} + T_{11})$ where $T_{ij} = f\,^{\dagger}(U_{ij})$. The condition (2.38) is satisfied when $T_{01} + T_{10} = 0$ and $T_{10} + T_{11} = 1$ or equivalently $U_{01} + U_{10} = 0$ and $U_{10} + 1 + U_{01} = 1$. The latter condition is the same as the former one and it is satisfied when $U_{10} = -U_{01}$. Thus, the scaling free transformation is

$$\cos(\omega) = -U_{01} + U'_{01}\cos(\omega_2) - U_{01}\cos(\omega_1) + (1 + U_{01})\cos(\omega_1)\cos(\omega_2) \tag{2.39}$$

or

$$\begin{aligned}\sin^2(\omega/2) = {} & (1 + 2U_{01})\sin^2(\omega_2/2) + \sin^2(\omega_1/2) \\ & - 2(1 + U_{01})\sin^2(\omega_1/2)\sin^2(\omega_2/2)\end{aligned} \tag{2.40}$$

It should be noted that in the above transformation, the number of coefficients to be optimized is only 1 compared to 3 in the original transformation [17].

---

† $f \triangleq$ function of

Cases (ii) and (iii): In (2.36), $F_{max} = 1$ and $F_{min} = 1 - 2p_1 = 1 - 2(T_{10} + T_{11}) = 1 - 2(U_{10} + 1 - U_{10}) = -1$. In these cases no condition is required. Hence, (2.36) or (2.37) *i.e.*

$$\cos(\omega) = - U_{01} + U_{01}\cos(\omega_2) + U_{10}\cos(\omega_1) + (1 - U_{10})\cos(\omega_1)\cos(\omega_2) \quad (2.41)$$

or

$$\sin^2(\omega/2) = (1 + U_{01} - U_{10})\sin^2(\omega_2/2) + \sin^2(\omega_1/2) + 2(U_{10} - 1)\sin^2(\omega_1/2)\sin^2(\omega_2/2) \quad (2.42)$$

itself is a scaling-free transformation with only 2 coefficients.

Case (iv): In (2.36), if F' is defined by (2.22), then $F_{max} = 1$ and $F_{min} = 1 - 2(T_{01} + T_{10}) = 1 - 2(1 - U_{10} + U_{10})$ or $1 - 2(U_{01} + 1 - U_{01}) = -1$. Therefore, again no condition is required and

$$\cos(\omega) = - U_{11} + (1 - U_{10})\cos(\omega_2) + U_{10}\cos(\omega_1) + U_{11}\cos(\omega_1)\cos(\omega_2) \quad (2.43)$$

or

$$\sin^2(\omega/2) = (1 + U_{11} - U_{10})\sin^2(\omega_2/2) + (U_{10} + U_{11})\sin^2(\omega_1/2) - 2U_{11}\sin^2(\omega_1/2)\sin^2(\omega_2/2) \quad (2.44)$$

itself is a scaling-free transformation with only 2 coefficients. In the above results, only (2.41) and (2.42) are reported in [51] and only (2.44) is reported in [52].

2.5.2 Type-B Contours

Using similar procedure as in Sec. 2.5.1, the following scaling-free transformations are obtained for the four cases.

Case (i):

$$\cos(\omega) = U_{01} + U_{01}\cos(\omega_2) - U_{01}\cos(\omega_1) + (1 - U_{01})\cos(\omega_1)\cos(\omega_2) \quad (2.45a)$$

$$= - U_{10} - U_{10}\cos(\omega_2) + U_{10}\cos(\omega_1) + (1 + U_{10})\cos(\omega_1)\cos(\omega_2) \quad (2.45b)$$

$$\sin^2(\omega/2) = \sin^2(\omega_2/2) + (1 - 2U_{10})\sin^2(\omega_1/2) + 2(U_{01} - 1)\sin^2(\omega_1/2)\sin^2(\omega_2/2) \quad (2.46)$$

Cases (ii) and (iii):

$$\cos(\omega) = -U_{10} + U_{01}\cos(\omega_2) + U_{10}\cos(\omega_1) + (1 - U_{01})\cos(\omega_1)\cos(\omega_2) \quad (2.47)$$

$$\sin^2(\omega/2) = \sin^2(\omega_2/2) + (1 + U_{10} - U_{01})\sin^2(\omega_1/2) + 2(U_{01} - 1)\sin^2(\omega_1/2)\sin^2(\omega_2/2) \quad (2.48)$$

Case (iv):

The same results as in case (iv) for type-A contours *i.e.* (2.43) and (2.44) hold.

The conditions and the number of coefficients for each case are not changed.

Comparing the above results with those for type-A contours, the following points are noticed. For case (i), (2.45) is obtained from (2.39) by replacing $\mp U_{01}$ by $\pm U_{01}$ in the first and last coefficients. Eq.s (2.46) is obtained from (2.40) by interchanging the coefficients of two sine terms, and then replacing $\mp U_{01}$ by $\pm U_{01}$. For cases (ii) and (iii), (2.47) and (2.48) are obtained from (2.41) and (2.42), respectively, by the same procedure as for case (i).

2.5.3 Type-C Contours

Using similar procedure as for type-A contours, the following scaling-free transformations are obtained for the three cases.

Case (i):

$$\cos(\omega) = \cos(\omega_1)\cos(\omega_2) \quad (2.49)$$

$$\sin^2(\omega/2) = \sin^2(\omega_2/2) + \sin^2(\omega_1/2) - 2\sin^2(\omega_1/2)\sin^2(\omega_2/2) \quad (2.50)$$

Case (ii):

$$\cos(\omega) = -U + U\cos(\omega_2) + U\cos(\omega_1) + (1 - U)\cos(\omega_1)\cos(\omega_2) \quad (2.51)$$

$$\sin^2(\omega/2) = \sin^2(\omega_2/2) + \sin^2(\omega_1/2) + 2(U - 1)\sin^2(\omega_1/2)\sin^2(\omega_2/2) \quad (2.52)$$

Case (iii):

$$\cos(\omega) = -U_{11} + 0.5\cos(\omega_2) + 0.5\cos(\omega_1) + U_{11}\cos(\omega_1)\cos(\omega_2) \quad (2.53)$$

$$\sin^2(\omega/2) = (0.5 + U_{11})\sin^2(\omega_2/2) + (0.5 + U_{11})\sin^2(\omega_1/2) - 2U_{11}\sin^2(\omega_1/2)\sin^2(\omega_2/2) \quad (2.54)$$

The transformations in case (i) are derived by using the condition $U = 0$ in (2.30) and (2.31). In cases (ii) and (iii), no condition is required. The number of coefficients to be optimized is 0 in case (i) and only 1 in cases (ii) and (iii), compared to 3 in the original transformation [17].

Comparing the above results with those for types A and B contours, the following points are noted. Eq. (2.49) is a special case of (2.39) and (2.45) in which $U_{01} = 0$. Hence, (2.50) is also a special case of (2.40) and (2.46) under the same conditions. Eq. (2.51) becomes a special case of (2.41) and (2.47) when the octagonal symmetry condition $U_{01} = U_{10}\ (= U)$ is applied. Therefore, (2.52) also becomes a special case of (2.42) and (2.48) under the same condition. Eq. (2.53) is a special case of (2.43) in which $U_{10} = 0.5$. Hence, (2.54) is also a special case of (2.44) under the same condition.

2.5.4 Reasons for Different Choices of Coefficients

Eq. (9) of [28] *i.e.*

$$\sin^2(\omega/2) = \sin^2(\omega_2/2) + \sin^2(\omega_1/2) + t'_{11}\sin^2(\omega_1/2)\sin^2(\omega_2/2) \quad (2.55)$$

is the same as (2.51) with $2(U - 1) = t'_{11}$. Therefore, (2.55) is inherently a scaling-free transformation and when t'_{11} is found by using an optimization technique, it yields more nearly circular contours than the original McClellan transformation [17], where $t'_{11} = -1$ or $U = 0.5$ in (2.51) and (2.52).

By imposing the suboptimal constraint $F(0,\pi) = F(\pi,\pi) = F_{min}$ on the transformation for type-B case (iv) contours (Sec. 2.3.2), then the conditions in cases (iii) and (iv) are the same, yielding, $t_{11} = t_{10}$. Imposing a similar constraint, $F(\pi,0) = F(\pi,\pi) = F_{min}$, on the transformation for type-A case (iv) contours, $t_{11} = t_{01}$ is obtained. When π is mapped onto (π,π) *i.e.* $\pi \rightarrow (\pi,\pi)$, it results in

$$t_{00} - t_{01} - t_{10} + t_{11} = -1 \tag{2.56}$$

These three equations when solved together with (2.3), give,

$$-t_{00} = t_{01} = t_{10} = t_{11} = 0.5 \tag{2.57}$$

which are the original McClellan transformation coefficients for approximately circular contours [17]. For the original transformation defined by (2.57), $F'_{max} = 1$ and $F_{min} = -1$ and, therefore, no scaling is necessary. Under this constraint, it can be easily verified that the two scaling-free transformations (2.51) and (2.58) or (2.52) and (2.54) are identical.

Comparing the scaled coefficients in Example 2.3, with the coefficients in (2.53), $-T_{00} = T_{11} = U_{11}$ and $T_{01} = T_{10} = 0.5$ are obtained. From this observation, it is concluded that for circular contours, (2.53) can be directly used in an optimization technique instead of (2.1). Since the former equation has only 1 coefficient, the error minimization using this equation will be faster than by using the latter which has 3 coefficients. Also, when (2.53) is employed no scaling is necessary

Hazra and Reddy [40] have given formulas to find the sine-form coefficients in (2.8) for 2-D circularly symmetric digital filters. They are:

$$p_{00} = 0, \quad p_{01} = p_{10} = g^{-1}, \quad \text{and} \quad p_{11} = 1 - (2g^{-1}) \tag{2.58}$$

where g is as defined in [40]. These coefficients are the same as the coefficients in (2.54) where $U_{11} = g^{-1} - 0.5$, and therefore, no scaling is required when (2.58) is used to evaluate them. Substituting the derived value of U_{11} in (2.53), and comparing it with (2.1), the corresponding cosine-form coefficients are obtained as

$$-t_{00} = t_{11} = g^{-1} - 0.5 \quad \text{and} \quad t_{01} = t_{10} = 0.5 \tag{2.59}$$

In [34], formulas are given to find the cosine-form coefficients in (2.1) for 2-D type-A elliptically symmetric digital filters. They are:

$$-t_{00} = \quad t_{01} = -0.5 + \{b_1(g_2 + 1) / (2b_2)\} \tag{2.60a}$$

$$t_{10} = 1 - t_{11} = \quad 0.5 + \{b_1(g_2 - 1) / (2b_2)\} \tag{2.60b}$$

for *case A i.e.* $b_1 g_2 < b_2$,

$$-t_{00} = \quad t_{11} = -0.5 + \left[\{(b_2 / b_1) + 1\} / (2g_2)\right] \tag{2.61a}$$

$$t_{10} = 1 - t_{01} = \quad 0.5 + \left[\{(b_2 / b_1) - 1\} / (2g_2)\right] \tag{2.61b}$$

for *case B i.e.* $b_1 g_2 > b_2$, where b_1, b_2, and g_2 are as defined in [34]. The coefficients in (2.60) and (2.61) satisfy the coefficient relationships in (2.41) and (2.43), respectively, and therefore, no scaling is required when (2.60) and (2.61) are used to evaluate them. Also, the expressions for U_{ij}'s in (2.41) and (2.43) can be easily obtained by comparison. Substituting them in (2.42) and (2.44), and comparing the resulting transformation with (2.8), the corresponding sine-form coefficients are obtained as

$$p_{00} = 0, \quad p_{01} = b_1 / b_2, \quad p_{10} = 1, \quad \text{and} \quad p_{11} = (b_1 / b_2)(g_2 - 1) - 1 \tag{2.62}$$

for *case A*, and

$$p_{00} = 0, \quad p_{01} = g_2^{-1}, \quad p_{10} = (b_2 / b_1) g_2^{-1} \quad \text{and}$$
$$p_{11} = 1 - \left[\{1 + (b_2 / b_1)\} g_2^{-1}\right] \tag{2.63}$$

for *case B*. Eq. (2.61) and the coefficients of (11) in [34] converge to (2.59) when $b_1 = b_2$ and $g_2 = g$. Thus, it is seen that the scaling-free transformations not only require fewer coefficients but also are very useful in deriving analytical expressions (More expressions are derived in the next few chapters.) for the coefficients. Also, the filters designed by using them have lesser number of multiplications per output sample [34].

2.6 A New Formula for Scaling

A new formula is presented in this section for scaling McClellan transformation coefficients. It is derived by making a mapping assumption reverse to that proposed by Mersereau *et al*'s [27] where they obtain the scaling formula (2.4) defined by (2.5). The properties and the effects of new formula on those derived in the previous sections are

also discussed.

2.6.1 New Scaling Formula and Its Properties

Replacing C_1 and C_2 in (2.4) by (2.5), and substituting $F = F_{max}$, $F' = 1$ is obtained and with $F = F_{min}$, $F' = -1$ is obtained. The opposite scaling is that when $F = F_{max}$, $F' = -1$, and when $F = F_{min}$, $F' = 1$. Substituting these values in (2.4), and solving for C_1 and C_2, yields,

$$C_1 = -2 / (F_{max} - F_{min}) \quad \text{and} \quad C_2 = C_1 F_{max} + 1. \tag{2.64}$$

Now, (2.4) with C_1 and C_2 as specified by (2.64) is the new scaling formula.

Comparing (2.64) with (2.5), it is observed that C_1 and C_2 in (2.64) are negative of the C_1 and C_2 in (2.5). Let ω_n' be the new 1-D frequency obtained by using (2.64) in (2.7). It can be proved that $\omega_n' = \pi - \omega'$. When ω' varies from 0 to π, ω_n' varies from π to 0 which is a reverse frequency mapping.

2.6.2 Scaled and Scaling-Free Transformations

The cosine-form coefficients scaled by using (2.64) are easily obtained as the negative of the scaled coefficients in Sec. 2.4. The corresponding sine-form coefficients can be derived easily from them. It is found that in the sine-form, except the constant coefficient, the other coefficients are negative of the scaled coefficients obtained in Sec. 2.4. Also, if the constant coefficient is originally 0, it becomes 1 in the new scaling, otherwise it is one minus the original constant coefficient. Thus, the scaled transformations are found for all the three types of contours

The scaling-free transformations are derived from the scaled transformations using a procedure similar to that in Sec. 2.5, and noting that F_{max} and F_{min} locations are interchanged in the new scaling. For case (i), the necessary and sufficient condition is $U_{10} = -(1 + U_{01})$ for types A and B contours, and $U = -0.5$ for type-C contours. For other cases, no condition is necessary and the scaled transformation itself is the scaling-

free transformation. The number of coefficients to be optimized varies from 0 to 2 depending on the case, compared to 3 in the original transformation. Since the scaled and scaling-free transformations for the three types of contours can be obtained easily using the above procedure, they are not presented here.

2.6.3 Examples

Consider the scaling of coefficients corresponding to a 2-D elliptically symmetric low-pass filter obtained from a 1-D low-pass filter. For a horizontal elliptical contour (type-B case (iii)), if the coefficients are scaled by using the scaling formula given by Mersereau *et al.'s*, the maximum and minimum value of the function before and after scaling remain at the same location *i.e.* at (0,0) and $(0,\pi)$, respectively. If the coefficients are scaled by using the new scaling formula, the maximum and minimum value of the function after scaling is at the interchanged location *i.e.* at $(0,\pi)$ and (0,0), respectively. As a result, a 2-D filter with elliptical contours is obtained. An example is given in the next chapter (Sec. 3.13).

The scaling formula of Mersereau *et al.'s* preserves the type of 1-D filter in the resulting 2-D filter. But the new scaling formula does not preserve the type of 1-D filter. An advantage of the new scaling formula is that from the coefficients for a given class of filters, coefficients for a different class of filters can be generated.

2.7 SUMMARY

In this chapter, the conventional method of scaling 2-D McClellan transformation coefficients for both cosine- and sine- form transformations have been described. The scaling problem of elliptical (type-B) and circular (type-C) cutoff contours have been analyzed, and some new simple formulas for finding the maximum and minimum values of the transformation function (F_{max} & F_{min}) have been derived. Using these extreme values, simple formulas for the scaling factors (C_1 & C_2), and scaled McClellan transformations for all types (elliptical- type-A & B, and circular- type-C) of contours for the

various cases have been derived. In this context, the similarities and differences between them are brought out.

Scaling-free McClellan transformations have been presented for all types of contours for the various cases, which satisfy the necessary and sufficient condition: $F_{max} = 1$ and $F_{min} = -1$. It has been shown that in this transformation, the number of independent coefficients to be optimized varies from 0 to 2 depending on the case, compared to 3 in the original transformation. Two-dimensional digital filters designed by employing these transformations have a smaller number of multiplications per output sample. A critical study of the scaling-free transformations reveals the reasons for different choices of the coefficients by various authors for 2-D filter design.

A new scaling formula has been found, by assuming a different kind of scaling as compared to the assumption in the derivation of the conventional scaling formula. Some of its properties and its effects on the derived formulas have been discussed. An advantage of the new scaling formula is that from the coefficients for a given class of filters, coefficients for a different class of filters can be generated.

All the analytical formulas presented in this chapter are extremely simple and the calculations can be done easily using hand calculators. They are suitable for real-time and adaptive digital filtering applications. In the next chapter, these formulas will be used to derive the formulas for finding the transformation coefficients

CHAPTER 3

APPROXIMATION DESIGN OF 2-D ELLIPTICALLY SYMMETRIC DIGITAL FILTERS USING MCCLELLAN TRANSFORMATION

3.1 INTRODUCTION

In this Chapter, some analytical methods are developed for finding the coefficients of the first-order McClellan transformation [17] for the design of 2-D elliptically symmetric digital filters from 1-D digital filters. Existing unconstrained linear [27] and nonlinear [4] optimization methods give the optimum results, but they are computationally very expensive. Therefore, these methods are not suitable for real-time adaptive design of 2-D digital filters. Recently proposed analytical methods [34] and [35] overcome this problem with only very few computations. Even though the results of these methods are approximate, still they are very close to those obtained by the optimization methods.

In this chapter, several new simple formulas other than those in [34] and [35] are derived for finding the coefficients by forcing the lower order significant terms in the power series expansion of the linear error function to zero. Formulas are presented for both the original and the scaling-free McClellan transformation coefficients for all the four cases [(i)-(iv)] of both the types (A & B) of elliptical cutoff contours [36], [37]. Many examples are given. The results obtained by using the derived formulas agree well with the results of the optimization methods, and the accuracy of the formulas is sufficient for many engineering applications. The number of multiplications required to implement the designed filters is shown to be small.

3.2 TWO-DIMENSIONAL ELLIPTICALLY SYMMETRIC DIGITAL FILTERS

A vital application of 2-D digital filters is in digital image processing. In applications like automatic quality control, computer vision, and robotics, there is need for real-time image processing due to large volume of data. The 2-D image signal to be

processed, may have unequal spatial variation in the direction of the spatial coordinates along which the sampling is performed. To process such signals, 2-D elliptically symmetric digital filters are employed.

When the 2-D signal has unequal spatial variation along the spatial coordinates, there may be compelling reasons to use different sampling rates along them. In such cases, the design of filters with circularly symmetric response changes to the design of filters with elliptically symmetric response.

3.3 Review of Existing Design Methods

3.3.1 Design of 2-D FIR and IIR Digital Filters

One of the important methods for the design of 2-D zero-phase filters (FIR/IIR) is to transform a corresponding 1-D zero-phase filter using McClellan transformation [17]. This method is very popular, since it is simple and fast, and efficient implementations exist for the designed filters [27]. Since the 2-D zero-phase IIR filter obtained by using the transformation is unstable, it is spectrally factorized into 4 quarter-plane [4], [18], [45] or 2 half-plane [46], [47] filters which are stable. A stable 2-D zero-phase IIR filter can be obtained by proper combination of two or more of these factorized filters. Also, one can achieve 2-D zero-phase response or other useful symmetries, by properly processing the input data through one of the factorized filters [4]. The methods which have been developed so far for finding the coefficients are either optimization [4], [27] or analytical [34], [35] methods.

3.3.2 Unconstrained Nonlinear Optimization Method

Mersereau *et al.* [27] have suggested unconstrained nonlinear and linear optimization methods to find the coefficients for a 2-D elliptical cutoff contour. Here, they are presented to understand our approximation technique.

The equation of a desired type-A elliptical pass-band cutoff contour is given by

$$(\omega_1 / \omega_a)^2 + (\omega_2 / \omega_b)^2 = 1 \tag{3.1}$$

where ω_1 and ω_2 are the 2-D frequency variables, and ω_a and ω_b are the 2-D pass-band cutoff frequencies on the ω_1-axis and ω_2-axis, respectively. If both the 1-D filter and the desired 2-D filter are low-pass, a valid mapping assumption is that the 1-D origin must be mapped onto the 2-D origin, *i.e.* $0 \rightarrow (0,0)$. This gives the constraint equation (2.3), using which the number of independent coefficients to be optimized are reduced from 4 to 3 in the original McClellan transformation (2.1). Another required mapping is that the 1-D pass-band cutoff frequency ω_0 must be mapped onto the desired 2-D pass-band cutoff contour described by (3.1). To find the coefficients, we solve (2.1) for ω_2, using the mapping assumptions, giving

$$\begin{aligned} \omega_2 &= \cos^{-1}\left\{ \frac{\cos(\omega_0) - t_{00} - t_{10}\cos(\omega_1)}{t_{01} + \{1 - (t_{00} + t_{01} + t_{10})\}\cos(\omega_1)} \right\} \\ &= G_n(\omega_1, \omega_0, t_{00}, t_{01}, t_{10}). \end{aligned} \tag{3.2}$$

From (3.1),

$$\begin{aligned} \omega_2 &= \omega_b \left[1 - (\omega_1 / \omega_a)^2 \right]^{1/2} \qquad \omega_1 \leq \omega_a \\ &= G_d(\omega_1, \omega_a, \omega_b). \end{aligned} \tag{3.3}$$

Using the above two equations, a nonlinear error function is defined as

$$E_1(\omega_1) = G_n - G_d. \tag{3.4}$$

The objective function is

$$J_1(t) = \sum_{n_1 \in R_p} \left[E_1(\omega_1) \right]^p \tag{3.5}$$

where p is a positive even integer, n_1 is the ω_1 frequency index, R_p is the discrete set of frequency points on the ω_1-axis in the range $0 \leq \omega_1 \leq \omega_a$, and t is the vector of transformation coefficients to be optimized *i.e.* $[t_{00}\ t_{01}\ t_{10}]^T$† For least mean square

† $T \triangleq$ matrix transpose

(LMS) approximation (l_2 error norm) $p = 2$, and for minimax or Chebyshev approximation (l_∞ error norm) $p \rightarrow \infty$. $J_1(t)$ is minimized using an unconstrained nonlinear optimization technique.

3.3.3 Unconstrained Linear Optimization Method

A suboptimum approach reformulates the above problem as a linear approximation problem. Assume that the 1-D pass-band cutoff frequency ω_0 exactly maps onto the desired 2-D pass-band cutoff contour given by (3.1). In this case, $F(\omega_1,\omega_2)$ in (2.1) will be a constant and is given by

$$\cos(\omega_0) = t_{00} + t_{01}\cos(\omega_2) + t_{10}\cos(\omega_1) + t_{11}\cos(\omega_1)\cos(\omega_2) = F(\omega_1, \omega_2). \quad (3.6a)$$

In (3.6a), ω_2 is defined by (3.3) and t_{11} can be expressed as a function of the other three coefficients from (2.3). Eq. (3.6a) can be rewritten as

$$\begin{aligned}\cos(\omega_0) &= t_{00} + t_{01}\cos\left\{\omega_b \left(1 - (\omega_1 / \omega_a)^2\right)^{1/2}\right\} + t_{10}\cos(\omega_1) \\ &\quad + \{1 - (t_{00} + t_{01} + t_{10})\}\cos(\omega_1)\cos\left\{\omega_b \left(1 - (\omega_1 / \omega_a)^2\right)^{1/2}\right\} \\ &= G_l(\omega_1, \omega_a, \omega_b, t_{00}, t_{01}, t_{10}). \end{aligned} \quad (3.6b)$$

If the mapping is not exact, the equality in (3.6a) will only be approximate and a linear error function can be defined as

$$E_2(\omega_1) = \cos(\omega_0) - G_l . \quad (3.7)$$

The objective function is

$$J_2(t) = \sum_{n_1 \in R_p} \left(E_2(\omega_1)\right)^p \quad (3.8)$$

where p, n_1, R_p, and t are as defined earlier. $J_2(t)$ is minimized using an unconstrained linear optimization technique.

Mersereau *et al.* [27] discussed the nonlinear and linear problem formulations only for type-A contours. For type-B contours, they are identical except for the following differences. The equation of a type-B elliptical pass-band cutoff contour is given by

$$(\omega_1 / \omega_b)^2 + (\omega_2 / \omega_a)^2 = 1 \tag{3.9}$$

and ω_2 becomes

$$\omega_2 = \omega_a \left(1 - (\omega_1 / \omega_b)^2\right)^{1/2} \qquad \omega_1 \leq \omega_b \,. \tag{3.10}$$

In (3.3), now, G_d is defined by (3.10), and in (3.5) and (3.8), R_p is defined in the range $0 \leq \omega_1 \leq \omega_b$. Also in (3.6a), ω_2 is defined by (3.10).

As a practical matter, the transformation will only be useful if the coefficients satisfy the constraint (2.2). The constrained optimization methods are computationally very expensive. Therefore, Mersereau *et al.* [27] preferred to find the coefficients by the unconstrained linear optimization method and to scale them by (2.4) and (2.5). Also, they found that for a first-order transformation, at least, the minimization of $E_2(\omega_1)$ effectively minimizes $E_1(\omega_1)$ Based on computational considerations, it has been proven in [4] that the unconstrained nonlinear optimization method followed by the scaling procedure is superior to other methods for finding the optimum coefficients. Even then, the amount of computations in these two methods exceeds the arithmetic and/or speed capability of low cost, stand-Alone 2-D signal processors and therefore, they are not suitable for real-time applications. Also, the nonlinear optimization method normally provides a local minima unlike the linear optimization method which always provides the global minima.

3.3.4 Analytical Methods

To overcome the above mentioned problems, some analytical methods [34], [35] have been proposed recently, which involve only very few computations. Nguyen and Swamy's method [35] gives good approximation for lower values of frequency

specifications than for higher values. It is the simplest of all the methods Reddy and Hazra's method [34] involves more calculations than the method of [35], but it gives results very close to the best one obtained by the optimization methods.

Even though the methods [34] and [35] aim to solve the same problem, their approaches are different. Method of [35] presents formulas for the coefficients (t_{ij}'s) for a given 1-D and 2-D pass-band cutoff frequencies (ω_0, and ω_a & ω_b). Method of [34], however, presents formulas for the 1-D pass-band and stop-band cutoff frequencies (ω_0 and ω_s), and the coefficients (t_{ij}'s) for a given 2-D pass-band and stop-band cutoff frequencies (ω_a & ω_b and ω_c & ω_d). Some of the mapping assumptions in both the methods are different. For example, in [35] ω_0 is assumed to map exactly onto the 2-D elliptical contour (3.1), whereas in [34] ω_0 is assumed to map onto $(\omega_a, 0)$, $(0, \omega_b)$, and $(\omega_a/\sqrt{2}, \omega_b/\sqrt{2})$ simultaneously.

3.4 Developed Analytical Methods

In the following sections, some analytical methods are developed for finding the McClellan transformation coefficients for the design of 2-D elliptically symmetric digital filters from 1-D digital filters. Several new extremely simple analytical formulas other than those in [34] and [35] for finding the coefficients are presented. Some of the derived formulas give scaling-free coefficients directly and therefore, are referred to as *scaling-free formulas*. The results obtained by using these formulas, are close to those obtained by using the optimization method. It is shown through several examples that the formulas are, in fact, good approximate solutions to the linear optimization problem itself. The derived formulas are well suited for low cost, stand-alone 2-D signal processors and make the real-time adaptive design of 2-D elliptically symmetric digital filters possible. These filters have lesser number of multiplications per output sample.

3.5 Approximation for Coefficients for Type-A Contours

The function $\cos(x)$ can be approximated by its truncated power series as

$$\cos(x) \approx 1 - \frac{x^2}{2} + \frac{x^4}{24}. \tag{3.11}$$

Using this in the original McClellan transformation as given by (2.1), and neglecting the sixth- and higher- order powers, yields,

$$1 - \frac{\omega^2}{2} + \frac{\omega^4}{24} = (t_{00} + t_{01} + t_{10} + t_{11}) - \frac{1}{2}(p_1\omega_1^2 + p_2\omega_2^2) + \frac{1}{24}(p_1\omega_1^4 + p_2\omega_2^4 + 6t_{11}\omega_1^2\omega_2^2) \tag{3.12}$$

where p_1 and p_2 are as defined in (2.11a) and (2.11b), respectively.

Assume that the 1-D pass-band cutoff frequency ω_0 is exactly mapped onto the desired 2-D elliptical pass-band cutoff contour given by (3.1). First, consider the type-A contours *i.e.* contours with ω_a on the ω_1-axis. The linear error function given by (3.7) can be rewritten using (3.12) and (2.3) as

$$\frac{1}{2}\left[-\omega_0^2\left\{1 - \frac{\omega_0^2}{12}\right\} + \omega_b^2\left\{1 - \frac{\omega_b^2}{12}\right\}p_2\right] + \frac{\omega_1^2}{2}\left[p_1 + \frac{\omega_b^2}{\omega_a^2}\left\{\frac{\omega_b^2}{6} - 1\right\}p_2 - \frac{\omega_b^2}{2}t_{11}\right] - \frac{\omega_1^4}{24}\left[p_1 + \frac{\omega_b^4}{\omega_a^4}p_2 - 6\frac{\omega_b^2}{\omega_a^2}t_{11}\right] = 0. \tag{3.13}$$

Since the error must be zero, the right side of (3.13) is taken to be zero. Equating the constant, ω_1^2, and ω_1^4 term coefficients to zero, the following equations are obtained.

$$\omega_b^2\left\{1 - \frac{\omega_b^2}{12}\right\}p_2 = \omega_0^2\left\{1 - \frac{\omega_0^2}{12}\right\} \tag{3.14}$$

$$p_1 - \frac{\omega_b^2}{2}t_{11} = \frac{\omega_b^2}{\omega_a^2}\left\{1 - \frac{\omega_b^2}{6}\right\}p_2 \tag{3.15}$$

$$p_1 - 6\frac{\omega_b^2}{\omega_a^2}t_{11} = -\frac{\omega_b^4}{\omega_a^4}p_2 \tag{3.16}$$

Solving the above three equations, gives,

$$p_1 = \frac{\omega_0^2\left\{1 - \frac{\omega_0^2}{12}\right\}}{\omega_a^2\left\{1 - \frac{\omega_a^2}{12}\right\}} \tag{3.17a}$$

$$p_2 = \frac{\omega_0^2\left\{1 - \frac{\omega_0^2}{12}\right\}}{\omega_b^2\left\{1 - \frac{\omega_b^2}{12}\right\}} \tag{3.17b}$$

and

$$t_{11} = \frac{1}{6}\,\omega_0^2\left\{1 - \frac{\omega_0^2}{12}\right\}\left[\frac{1}{\omega_a^2\left\{1 - \frac{\omega_b^2}{12}\right\}} + \frac{1}{\omega_b^2\left\{1 - \frac{\omega_a^2}{12}\right\}}\right] \tag{3.17c}$$

This derivation is different from that in [35]. The results, however, are identical

From this derivation, it can be concluded that the analytical formulas given by (3.17) are approximate solutions to the linear optimization problem itself defined by (3.8). The above derivation is more straight forward, easy to understand, and useful in deriving the scaling-free formulas than the derivation in [35] The constant term and the lower-order ω_1 terms, depending on the number of unknowns, are forced to assume a zero value. The higher-order ω_1 terms are also assumed to be zero, since their values are negligible, particularly for low frequencies. The approximate solution agrees well with the optimal solution [35] and its accuracy is sufficient for many engineering applications To prove these points, some examples are given in an up-coming section.

The formulas provide good accuracy when ω_0, ω_a, and ω_b are much smaller than $\sqrt{12} \approx 1.1\pi$ rad./sec. For a given ω_0, ω_a, and ω_b, let this condition be satisfied and let t_{ij}'s be the coefficients found by using the formulas After scaling let T_{ij}'s be the scaled coefficients and ω_0' be the new 1-D pass-band cutoff frequency. For another 1-D pass-band cutoff frequency $\omega_p < \omega_0$, and for the same ω_a and ω_b, different coefficients are

obtained by using the formulas. However, it is observed that after scaling, the same scaled coefficients and approximately the same new 1-D pass-band cutoff frequency are obtained. Therefore, it is concluded that the same T_{ij}'s would transform a given $\omega_p < \omega_0$ into an ellipse.

3.5.1 Finding the Coefficients

To find the coefficients, first p_1, p_2, and t_{11} are evaluated using (3.17a)-(3.17c) from the given frequency specifications (ω_0, ω_a, and ω_b). Substituting the value of t_{11} in (2.11a) and (2.11b), the values of t_{10} and t_{01} are found. Finally, t_{00} is evaluated from (2.3) The corresponding sine-form transformation coefficients are

$$p_{00} = 0, \quad p_{01} = p_2, \quad p_{10} = p_1, \quad \text{and} \quad p_{11} = -2t_{11}. \tag{3.18}$$

3.5.2 Special Cases

Consider two special cases $\omega_0 = \omega_a$ and $\omega_0 = \omega_b$. When $\omega_0 = \omega_a$, the equations given by (3.17), respectively become

$$p_1 = 1 \tag{3.19a}$$

$$p_2 = \frac{\omega_a^2\left\{1 - \frac{\omega_a^2}{12}\right\}}{\omega_b^2\left\{1 - \frac{\omega_b^2}{12}\right\}} \tag{3.19b}$$

and

$$t_{11} = \frac{1}{6}\left[\frac{1 - \frac{\omega_a^2}{12}}{1 - \frac{\omega_b^2}{12}} + \frac{\omega_a^2}{\omega_b^2}\right]. \tag{3.19c}$$

Using $p_1 = 1$ in (2.20), the scaled transformation for the cases (ii) and (iii), it is seen that the scaled and the unscaled coefficients are the same. Also, $C_1 = 1$ and $C_2 = 0$ or $F_{max} = 1$ and $F_{min} = -1$ and therefore, no scaling is necessary.

When $\omega_0 = \omega_b$, the equations given by (3.17), respectively become

$$p_1 = \frac{\omega_b^2\left\{1 - \frac{\omega_b^2}{12}\right\}}{\omega_a^2\left\{1 - \frac{\omega_a^2}{12}\right\}} \tag{3.20a}$$

$$p_2 = 1 \tag{3.20b}$$

and

$$t_{11} = \frac{1}{6}\left[\frac{\omega_b^2}{\omega_a^2} + \frac{1 - \frac{\omega_b^2}{12}}{1 - \frac{\omega_a^2}{12}}\right]. \tag{3.20c}$$

These simplified formulas are useful for the fast evaluation of the coefficients, when the specifications satisfy the special conditions

3.5.3 Comparison of Approximation and Optimization Methods

To demonstrate the accuracy of the above approximation for the coefficients, consider the same design example given in [27]

Example 3.1: The specifications for a type-A contour are $\omega_0 = \omega_b = 0.5\pi$ and $\omega_a = 0.25\pi$.

Mersereau *et al* [27] minimized the objective function $J_2(t)$ as given by (3.8) in the LMS sense and arrived at the following optimum results,

$$\begin{aligned} t_{00} &= -2.58366000 & t_{01} &= 0.16411000 \\ t_{10} &= 2.58426000 & t_{11} &= 0.83529000 \\ p_1 &= 3.41955000 & p_2 &= 0.99940000 \\ E_{2\,MSE} &= 0.26083329\times10^{-6} & E_{2\,\max} &= 0.15630064\times10^{-2} \\ E_{1\,MSE} &= 0.16728813\times10^{-5} & E_{1\,\max} &= 0.12166497\times10^{-1}, \end{aligned}$$

where $E_{2\,MSE}$ and $E_{2\,\max}$, respectively, are the mean square error (MSE) and the maximum absolute error of the linear error function $E_2(\omega_1)$ given by (3.7), and $E_{1\,MSE}$ and $E_{1\,\max}$ are defined, similarly, for the nonlinear error function $E_1(\omega_1)$ given by (3.4) The values of MSE and maximum absolute error are obtained in order to compare the results of several methods. Since the minimization of $J_2(t)$ as given by (3.8) is suboptimum, the

equivalent error values for $J_1(t)$ given by (3.5), which is a better objective function, are presented.

The results obtained by using the simplified formulas given by (3.20) are as follows.

$$t_{00} = -2.54348430 \qquad t_{01} = 0.19376155$$
$$t_{10} = 2.54348430 \qquad t_{11} = 0.80623845$$
$$p_1 = 3.34972275 \qquad p_2 = 1.00000000$$
$$E_{2\,MSE} = 0.63906240 \times 10^{-4} \qquad E_{2\,\max} = 0.18888922 \times 10^{-1}$$
$$E_{1\,MSE} = 0.63381249 \times 10^{-3} \qquad E_{1\,\max} = 0.22284909$$

By comparing the error values, it is concluded that the results of the approximation method agree very well with the results of the optimization method, considering the practical tolerance allowed in many engineering applications. Also, it should be noted that in this example, ω_0 and ω_b are not so small. To see the effect of small values of the specifications, in the next example, ω_0, ω_a, and ω_b are reduced by a factor of 2.

Example 3.2: The specifications for a type-A contour are $\omega_0 = \omega_b = 0.25\pi$ and $\omega_a = 0.125\pi$.

Nguyen and Swamy [35] minimized the objective function $J_2(t)$ given by (3.8) in the LMS sense and arrived at the following optimum results.

$$t_{00} = -3.01372180 \qquad t_{01} = 0.16555910$$
$$t_{10} = 3.01375500 \qquad t_{11} = 0.83440770$$
$$p_1 = 3.84816270 \qquad p_2 = 0.99996680$$
$$E_{2\,MSE} = 0.75549476 \times 10^{-10} \qquad E_{2\,\max} = 0.30724883 \times 10^{-4}$$
$$E_{1\,MSE} = 0.15498727 \times 10^{-8} \qquad E_{1\,\max} = 0.37620023 \times 10^{-3}$$

The results obtained by using the simplified formulas given by (3.20) are as follows.

$$t_{00} = -3.01695570 \qquad t_{01} = 0.17317584$$
$$t_{10} = 3.01695570 \qquad t_{11} = 0.82682416$$
$$p_1 = 3.84377986 \qquad p_2 = 1.00000000$$
$$E_{2\,MSE} = 0.16130892 \times 10^{-7} \qquad E_{2\,\max} = 0.30289895 \times 10^{-3}$$
$$E_{1\,MSE} = 0.35394782 \times 10^{-5} \qquad E_{1\,\max} = 0.25426693 \times 10^{-1}$$

By comparing the error values of the above two examples, it is observed that both the methods give better results for lower values of frequency specifications.

It should be pointed out that the basic difference between the two methods is that, while the optimization method finds the best fit to the overall shape of the ellipse, the approximation method gives a close fit to the four cutoff frequency points (minor- and major- axis cutoff frequency points on the ω_1 and ω_2 axes) of the ellipse. For this reason, the results of both the methods agree most in the values of p_1 and p_2. Finally, it should be pointed out that the approximation method is the simplest of all the existing methods.

3.6 Approximation for Scaling-Free Coefficients for Type-A Contours

Using the coefficients of the scaling-free transformations given in (2.39)-(2.41) in (3.14)-(3.16), the following four cases of scaling-free formulas are obtained

Case (i):

$$U_{01} = \frac{1}{2}\left[\frac{\omega_0^2\left\{1 - \frac{\omega_0^2}{12}\right\}}{\omega_b^2\left\{1 - \frac{\omega_b^2}{12}\right\}} - 1\right] \tag{3.21}$$

Cases (ii) and (iii):

$$U_{10} = \frac{2}{\omega_b^2}\left[\frac{\omega_0^2\left\{1 - \frac{\omega_0^2}{12}\right\}\left\{1 - \frac{\omega_b^2}{6}\right\}}{\omega_a^2\left\{1 - \frac{\omega_b^2}{12}\right\}} - 1\right] + 1 \tag{3.22a}$$

$$U_{01} = \frac{\omega_0^2\left\{1 - \frac{\omega_0^2}{12}\right\}}{\omega_b^2\left\{1 - \frac{\omega_b^2}{12}\right\}} + U_{10} - 1 \tag{3.22b}$$

Case (iv):

$$U_{11} = \frac{1}{2\left\{1 - \frac{\omega_b^2}{4}\right\}} \left[\frac{\omega_0^2\left\{1 - \frac{\omega_0^2}{12}\right\}}{1 - \frac{\omega_b^2}{12}} \left[\frac{1 - \frac{\omega_b^2}{6}}{\omega_a^2} + \frac{1}{\omega_b^2} \right] - 1 \right] \tag{3.23a}$$

$$U_{10} = 1 + U_{11} - \frac{\omega_0^2\left\{1 - \frac{\omega_0^2}{12}\right\}}{\omega_b^2\left\{1 - \frac{\omega_b^2}{12}\right\}} \tag{3.23b}$$

Comparing the scaling-free transformations as given by (2.39)-(2.44) with the original transformations given by (2.1) and (2.8), the following cases of the scaling-free cosine- and sine- form coefficients result.

Case (i):

$$t_{00} = t_{10} = -U_{01}, \quad t_{01} = U_{01}, \quad \text{and} \quad t_{11} = 1 + U_{01} \tag{3.24}$$

$$p_{00} = 0, \quad p_{01} = 1 + 2U_{01}, \quad p_{10} = 1, \quad \text{and} \quad p_{11} = -2(1 + U_{01}) \tag{3.25}$$

Cases (ii) and (iii):

$$t_{00} = -U_{01}, \quad t_{01} = U_{01}, \quad t_{10} = U_{10}, \quad \text{and} \quad t_{11} = 1 - U_{10} \tag{3.26}$$

$$p_{00} = 0, \quad p_{01} = 1 + U_{01} - U_{10}, \quad p_{10} = 1, \quad \text{and} \quad p_{11} = 2(U_{10} - 1) \tag{3.27}$$

Case (iv).

$$t_{00} = -U_{11}, \quad t_{01} = 1 - U_{10}, \quad t_{10} = U_{10}, \quad \text{and} \quad t_{11} = U_{11} \tag{3.28}$$

$$p_{00} = 0, \quad p_{01} = 1 + U_{11} - U_{10},$$
$$p_{10} = U_{10} + U_{11}, \quad \text{and} \quad p_{11} = -2U_{11}. \tag{3.29}$$

It should be emphasized that to determine the case and to select the corresponding scaling-free formulas for given specifications, the unscaled coefficients must first be evaluated by using (3.17) and Appendix C used.

3.6.1 Advantages

The advantage of the scaling-free formulas given by (3.21)-(3.23) is that they yield the scaling-free coefficients given in (3.24)-(3.29) directly. Also, the 1-D pass-band cutoff frequency ω_0 remains the same. On the other hand, the coefficients evaluated by using the set of equations given in (3.17), (3.18), or (3.20) require scaling and changing ω_0 to ω_0'.

3.6.2 Special Cases

Under the special case $\omega_0 = \omega_a$, the equations in (3.22), respectively, become

$$U_{10} = \frac{2}{\omega_b^2}\left[\frac{\left\{1 - \frac{\omega_a^2}{12}\right\}\left\{1 - \frac{\omega_b^2}{6}\right\}}{1 - \frac{\omega_b^2}{12}} - 1\right] + 1 \tag{3.30a}$$

and

$$U_{01} = \frac{\omega_a^2\left\{1 - \frac{\omega_a^2}{12}\right\}}{\omega_b^2\left\{1 - \frac{\omega_b^2}{12}\right\}} + U_{10} - 1. \tag{3.30b}$$

Similarly, under the special case $\omega_0 = \omega_b$, the corresponding equations are

$$U_{10} = 2\left[\frac{1 - \frac{\omega_b^2}{6}}{\omega_a^2} - \frac{1}{\omega_b^2}\right] + 1 \tag{3.31a}$$

and

$$U_{01} = U_{10}. \tag{3.31b}$$

These simplified scaling-free formulas further reduce the computations for the special cases of specifications

3.6.3 Examples

Example 3.3: The specifications for a type-A contour are $\omega_0 = \omega_a = 0.25\pi$ and

$\omega_b = 0.5\pi$.

Using the simplified scaling-free formulas for type-A contours given by (3.30) the following results are obtained.

$$U_{01} = 0.57844060\times10^{-1} \qquad U_{10} = 0.75931189$$
$$E_{2\,MSE} = 0.19662967\times10^{-4} \qquad E_{2\,\max} = 0.56389512\times10^{-2}$$
$$E_{1\,MSE} = 0.25562594\times10^{-3} \qquad E_{1\,\max} = 0.19003112\times10^{-1}$$

The scaling-free coefficients for the cosine- and sine- form transformations are obtained by substituting these values in (3.26) and (3.27), respectively.

The scaled coefficients for the unscaled coefficients of the optimum and approximation solutions in Example 3.1 were obtained by using (2.20). After scaling, $\omega_0' \approx 0.25\pi$. The scaling-free coefficients of Example 3.3 have the same values as those of the scaled coefficients of the approximation solution in Example 3.1.

The results in Example 3.3 are same as those in column 1 of Table I, of [35], even though (3.30a) is different from Eq. (30) of [35]. The formulas in [35] (*i.e.* Eq.s (30) and (31)) are valid only if $\omega_0 = \omega_a$; the formulas given by (3.22a) and (3.22b) of this section are, however, valid even if $\omega_0 \neq \omega_a$.

The sine-form transformation coefficients corresponding to the cosine-form transformation coefficients defined by Eq.s (30) and (31) in [35] are:

$$P_{00} = 0, \qquad P_{01} = \frac{\omega_a^2\left\{1 - \dfrac{\omega_a^2}{12}\right\}}{\omega_b^2\left\{1 - \dfrac{\omega_b^2}{12}\right\}},$$

$$P_{10} = 1, \quad \text{and} \quad P_{11} = -\frac{1}{3}\left[\frac{\omega_a^2}{\omega_b^2} + \frac{1 - \dfrac{\omega_a^2}{12}}{1 - \dfrac{\omega_b^2}{12}}\right]. \tag{3.32}$$

Example 3.4. The specifications for a type-A contour are $\omega_0 = \omega_a = 0.125\pi$ and $\omega_b = 0.25\pi$.

Using the simplified scaling-free formulas given by (3.30) for type-A contours, the following results are obtained.

$$U_{01} = 0.45053527\times10^{-1} \qquad U_{10} = 0.78489295$$
$$E_{2\,MSE} = 0.39241793\times10^{-8} \qquad E_{2\,\max} = 0.78861587\times10^{-4}$$
$$E_{1\,MSE} = 0.14436219\times10^{-6} \qquad E_{1\,\max} = 0.44398185\times10^{-3}$$

The scaling-free coefficients for the cosine- and sine- form transformations are obtained by substituting these values in (3.26) and (3.27), respectively.

The scaled coefficients of the optimum and approximation solutions in Example 3.2 were obtained by using (2.20). After scaling, $\omega_0' \approx 0.25\pi$. The scaling-free coefficients of Example 3.4 have the same values as those of the scaled coefficients of the approximation solution in Example 3.2.

3.7 Approximation for Coefficients for Type-B Contours

For type-B contours *i.e.* contours with ω_a on the ω_2 axis, the derivation for finding the coefficients is carried out in a similar way as for the derivation for type-A contours using (3.9) and (3.10). The linear error function given by (3.7) can be rewritten as

$$\begin{aligned}
&\frac{1}{2}\left[-\omega_0^2\left\{1-\frac{\omega_0^2}{12}\right\}+\omega_a^2\left\{1-\frac{\omega_a^2}{12}\right\}p_2\right]\\
&+\frac{\omega_1^2}{2}\left[p_1+\frac{\omega_a^2}{\omega_b^2}\left\{\frac{\omega_a^2}{6}-1\right\}p_2-\frac{\omega_a^2}{2}t_{11}\right]\\
&-\frac{\omega_1^4}{24}\left[p_1+\frac{\omega_a^4}{\omega_b^4}p_2-6\frac{\omega_a^2}{\omega_b^2}t_{11}\right]=0.
\end{aligned} \tag{3.33}$$

Equating the constant, ω_1^2, and ω_1^4 term coefficients to zero, the following equations which are parallel to (3.14)-(3.16) are obtained.

$$\omega_a^2\left\{1-\frac{\omega_a^2}{12}\right\}p_2 = \omega_0^2\left\{1-\frac{\omega_0^2}{12}\right\} \tag{3.34}$$

$$p_1-\frac{\omega_a^2}{2}t_{11} = \frac{\omega_a^2}{\omega_b^2}\left\{1-\frac{\omega_a^2}{6}\right\}p_2 \tag{3.35}$$

$$p_1-6\frac{\omega_a^2}{\omega_b^2}t_{11} = -\frac{\omega_a^4}{\omega_b^4}p_2 \tag{3.36}$$

The equations (3.33)-(3.36) can also be obtained easily from the corresponding Eq.s (3.13)-(3.16) for type-A contours by interchanging ω_a and ω_b. Solving (3.34)-(3.36) gives,

$$p_1 = \frac{\omega_0^2\left\{1 - \frac{\omega_0^2}{12}\right\}}{\omega_b^2\left\{1 - \frac{\omega_b^2}{12}\right\}} \tag{3.37a}$$

$$p_2 = \frac{\omega_0^2\left\{1 - \frac{\omega_0^2}{12}\right\}}{\omega_a^2\left\{1 - \frac{\omega_a^2}{12}\right\}} \tag{3.37b}$$

and

$$t_{11} = \frac{1}{6}\,\omega_0^2\left\{1 - \frac{\omega_0^2}{12}\right\}\left[\frac{1}{\omega_b^2\left\{1 - \frac{\omega_a^2}{12}\right\}} + \frac{1}{\omega_a^2\left\{1 - \frac{\omega_b^2}{12}\right\}}\right] \tag{3.37c}$$

3.7.1 Finding the Coefficients

The cosine-form transformation coefficients (t_{ij}'s) are found by using the above formulas and substituting the value of t_{11} in the defining equations for p_1 and p_2 given by (2.11). The corresponding sine-form transformation coefficients (p_{ij}'s) are obtained from (3.18).

3.7.2 Special Cases

Under the special case $\omega_0 = \omega_a$, the equations given by (3.37), respectively become

$$p_1 = \frac{\omega_a^2\left\{1 - \frac{\omega_a^2}{12}\right\}}{\omega_b^2\left\{1 - \frac{\omega_b^2}{12}\right\}} \tag{3.38a}$$

$$p_2 = 1 \tag{3.38b}$$

and

$$t_{11} = \frac{1}{6}\left[\frac{\omega_a^2}{\omega_b^2} + \frac{1 - \frac{\omega_a^2}{12}}{1 - \frac{\omega_b^2}{12}}\right]. \tag{3.38c}$$

Using $p_2 = 1$ (2.26), in the scaled transformation for cases (ii) and (iii), it is seen that the scaled and unscaled coefficients are the same. Also, $C_1 = 1$ and $C_2 = 0$ or $F_{\max} = 1$ and $F_{\min} = -1$ and therefore, no scaling is necessary.

Similarly, for the special case $\omega_0 = \omega_b$, the equation in (3.37), respectively become

$$p_1 = 1 \tag{3.39a}$$

$$p_2 = \frac{\omega_b^2\left\{1 - \frac{\omega_b^2}{12}\right\}}{\omega_a^2\left\{1 - \frac{\omega_a^2}{12}\right\}} \tag{3.39b}$$

and

$$t_{11} = \frac{1}{6}\left[\frac{1 - \frac{\omega_b^2}{12}}{1 - \frac{\omega_a^2}{12}} + \frac{\omega_b^2}{\omega_a^2}\right]. \tag{3.39c}$$

These simplified formulas are useful for a quick evaluation of the coefficients, when the specifications fall under the special cases.

3.7.3 Comparison of Formulas for Type-A and Type-B Contours

Comparing the above results [(3.37), (3.38), and (3.39)] with those for type-A contours [(3.17), (3.19), and (3.20)], the following points are noticed. The formulas for p_1 and p_2 for type-B contours can be obtained, respectively, from the right side of the formulas for p_2 and p_1 for type-A contours. The formula for t_{11} for type-B contours is same as the corresponding formula for type-A contours. As a consequence, the values of p_1 and p_2, t_{10} and t_{01}, and p_{10} and p_{01} for type-B contours can be obtained by interchanging the values of p_1 and p_2, t_{10} and t_{01}, and p_{10} and p_{01} in the type-A contours

for the same specifications. The values of t_{00} and t_{11}, and p_{00} and p_{11} are the same for both the types of contours.

3.7.4 Comparison of Approximation and Optimization Methods

Example 3.5: The specifications for a type-B contour are $\omega_0 = \omega_b = 0.5\pi$ and $\omega_a = 0.25\pi$.

The optimum results for this contour are easily obtained from the optimum results of the corresponding type-A contour in Example 3.1 by following the procedure described in Sec. 3.7.2. These results are as follows.

$$t_{00} = -2.58366000 \qquad t_{01} = 2.58426000$$
$$t_{10} = 0.16411000 \qquad t_{11} = 0.83529000$$
$$p_1 = 0.99940000 \qquad p_2 = 3.41955000$$
$$E_{2\,MSE} = 0.26083329\times10^{-6} \qquad E_{2\,\max} = 0.15630064\times10^{-2}$$
$$E_{1\,MSE} = 0.10728813\times10^{-5} \qquad E_{1\,\max} = 0.12166497\times10^{-1}$$

The results obtained by using the simplified formulas given in (3.39) are

$$t_{00} = -2.51348430 \qquad t_{01} = 2.54348430$$
$$t_{10} = 0.19376155 \qquad t_{11} = 0.80623845$$
$$p_1 = 1.00000000 \qquad p_2 = 3.34972275$$
$$E_{2\,MSE} = 0.63963249\times10^{-4} \qquad E_{2\,\max} = 0.18888922\times10^{-1}$$
$$E_{1\,MSE} = 0.63381249\times10^{-3} \qquad E_{1\,\max} = 0.22284909.$$

These results can also be obtained easily from the results of the approximation method in Example 3.1 by following the procedure described in Sec. 3.7.2.

Example 3.6: The specifications for a type-B contour are $\omega_0 = \omega_b = 0.25\pi$ and $\omega_a = 0.125\pi$.

Similar to Example 3.5, the optimum results for this contour can be obtained easily from the optimum results of the corresponding type-A contour in Example 3.2, giving

$$t_{00} = -3.01372180 \qquad t_{01} = 3.01375500$$
$$t_{10} = 0.16555010 \qquad t_{11} = 0.83440770$$
$$p_1 = 0.99996680 \qquad p_2 = 3.84816270$$
$$E_{2\,MSE} = 0.75549476\times10^{-10} \qquad E_{2\,\max} = 0.30724883\times10^{-4}$$
$$E_{1\,MSE} = 0.15498727\times10^{-8} \qquad E_{1\,\max} = 0.37620023\times10^{-3}.$$

The results obtained by using the simplified formulas given in (3.39) are

$$t_{00} = -3.01695570 \qquad t_{01} = 3.01695570$$
$$t_{10} = 0.17317584 \qquad t_{11} = 0.82682416$$
$$p_1 = 1.00000000 \qquad p_2 = 3.84377086$$
$$E_{2\,MSE} = 0.16130892\times10^{-7} \qquad E_{2\,\max} = 0.30289895\times10^{-3}$$
$$E_{1\,MSE} = 0.35394782\times10^{-5} \qquad E_{1\,\max} = 0.25426603\times10^{-1}.$$

Again, these results can also be obtained easily from the results of the approximation method

In the above two examples, the error values for the optimization and approximation methods are the same as those in Examples 3.1 and 3.2. Hence, the conclusions made in Sec. 3.5.3 are also true here. Fig. 3.1 shows the contours of the original McClellan transformation with the coefficients given by the unscaled optimized and approximated values of Example 3.5.

3.8 Approximation for Scaling-Free Coefficients for Type-B Contours

Using the coefficients of the scaling-free transformations given in (2.43), (2.44), and (2.45)-(2.48) in Sec. 2.5.2 in (3.34)-(3.36), the following four cases of scaling-free formulas are obtained.

Case (i):

$$U_{01} = \frac{1}{2\left\{1 - \dfrac{\omega_a^2}{4}\right\}}\left[\frac{\omega_a^2}{\omega_b^2}\left\{\frac{\omega_a^2}{6} - 1\right\} + 1 - \frac{\omega_a^2}{2}\right] \tag{3.40}$$

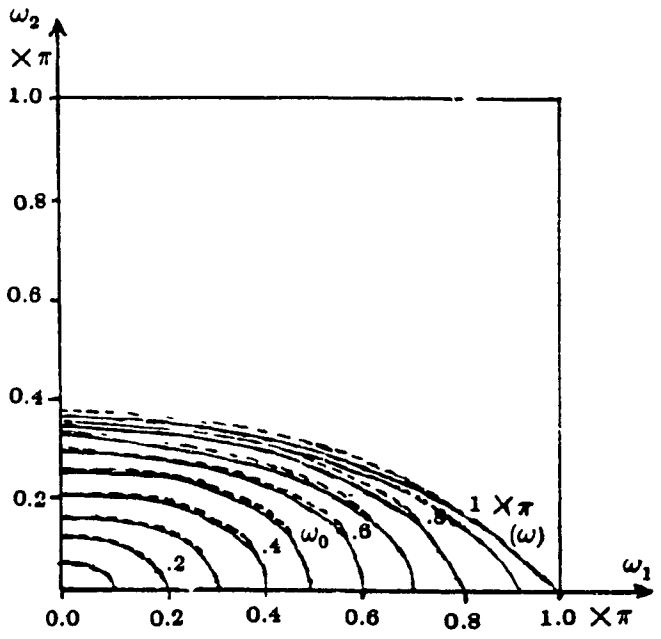

Fig. 3.1 Contours of the Original McClellan Transformation Obtained by Using the Unscaled Optimized (Solid Line) and Approximated (Dotted Line) Coefficients in Example 3.6.

(The specifications for a type-B contour are $\omega_0 = \omega_b = 0.5\pi$ and $\omega_a = 0.25\pi$. In the area outside the outer most contour $| F(\omega_1,\omega_2) | > 1$.)

Cases (ii) and (iii):

$$U_{01} = \left[\frac{1 + \omega_a^2 \left(\frac{1}{\omega_b^2} - \frac{1}{6} \right)}{\frac{\omega_b^2}{2} - 6} \right] + 1 \tag{3.41a}$$

$$U_{10} = \left\{ \frac{\omega_a^2}{2} - 1 \right\} (1 - U_{01}) + \frac{\omega_a^2}{\omega_b^2} \left\{ 1 - \frac{\omega_a^2}{6} \right\} \tag{3.41b}$$

Case (iv):

$$U_{11} = \frac{1}{2\left\{ 1 - \frac{\omega_a^2}{4} \right\}} - \left[\frac{\omega_0^2 \left\{ 1 - \frac{\omega_0^2}{12} \right\}}{1 - \frac{\omega_a^2}{12}} \left[\frac{1 - \frac{\omega_a^2}{6}}{\omega_b^2} + \frac{1}{\omega_a^2} \right] - 1 \right] \tag{3.42a}$$

$$U_{10} = 1 + U_{11} - \frac{\omega_0^2 \left\{ 1 - \frac{\omega_0^2}{12} \right\}}{\omega_a^2 \left\{ 1 - \frac{\omega_a^2}{12} \right\}} \tag{3.42b}$$

The condition to be satisfied, to use the formulas for Cases (i)-(iii) is

$$\omega_0 = \omega_a \tag{3.43}$$

Comparing the Case (iv) formulas with the corresponding formulas of Case (iv) for type-A, (3.42a) and (3.42b) are obtained, respectively, from (3.23a) and (3.23b) by interchanging ω_a and ω_b. The advantages of the scaling-free formulas have been discussed in Sec. 3.6.1.

Comparing the scaling-free transformations as given by (2.43)-(2.48) with the original transformations given by (2.1) and (2.8), the following four cases of scaling-free coefficients result.

Case (i):

$$t_{00} = t_{01} = U_{01}, \quad t_{10} = -U_{01}, \quad \text{and} \quad t_{11} = 1 - U_{01} \tag{3.44}$$

$$p_{00} = 0, \quad p_{01} = 1, \quad p_{10} = 1 - 2U_{01}, \quad \text{and} \quad p_{11} = 2(U_{01} - 1) \tag{3.45}$$

Cases (ii) and (iii):

$$t_{00} = -U_{10}, \quad t_{01} = U_{01}, \quad t_{10} = U_{10}, \quad \text{and} \quad t_{11} = 1 - U_{01} \tag{3.46}$$

$$p_{00} = 0, \quad p_{01} = 1, \quad p_{10} = 1 + U_{10} - U_{01}, \quad \text{and} \quad p_{11} = 2(U_{01} - 1) \tag{3.47}$$

Case (iv).

The same results as Case (iv) for type-A contours (Eq.s (3.28) and (3.29)).

It should be emphasized that to determine the case and to select the corresponding scaling free formulas for given specifications, the unscaled coefficients must first be evaluated by using (3 37) and Appendix C used

3.8.1 Examples

Example 3 7. The specifications for a type-B contour are $\omega_0 = \omega_a = 0.25\pi$ and $\omega_b = 0.5\pi$

Using the scaling-free formulas given by (3.41) for type-B contours, the following results are obtained.

$$U_{01} = 0.75031180 \qquad U_{10} = 0.57844060 \times 10^{-1}$$
$$E_{2\,MSE} = 0.19662967 \times 10^{-4} \qquad E_{2\,\max} = 0.56380512 \times 10^{-2}$$
$$E_{1\,MSE} = 0.2556250 1 \times 10^{-3} \qquad E_{1\,\max} = 0.19003112 \times 10^{-1}$$

The scaling-free coefficients for the cosine- and sine- form transformations are obtained by substituting these values in (3.46) and (3.47), respectively.

The scaled coefficients of the optimum or approximation solution in Example 3.5 were obtained by using (2.26). After scaling, $\omega_0' \approx 0.25\pi$. The scaling-free coefficients of Example 3.7 have the same values as those of the scaled coefficients of the approximation solution in Example 3.5. Fig. 3.2 shows the contours of the original McClellan transformation with the coefficients given by the scaled optimized and approximated values.

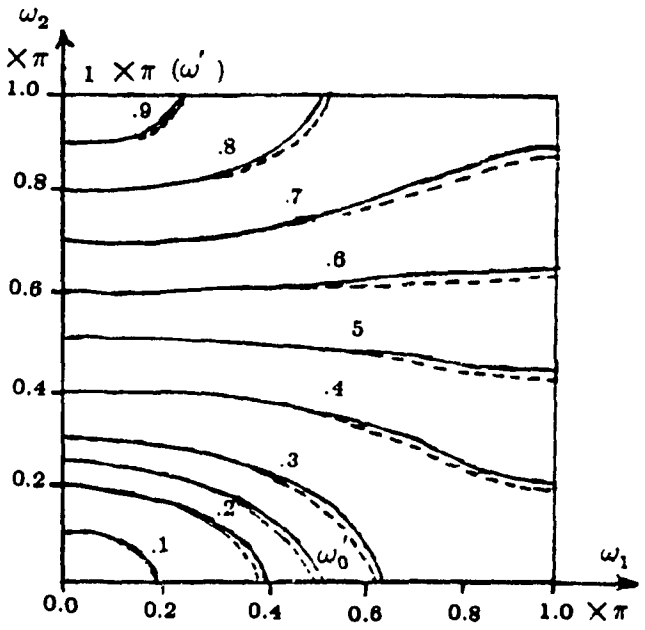

Fig. 3.2 Contours of the Original McClellan Transformation Obtained by Using the Scaled Optimimum (Solid Line) and Approximated (Dotted Line) Coefficients.

(The specifications for a type-B contour are $\omega_0 = \omega_b = 0.5\pi$ and $\omega_a = 0.25\pi$. After scaling, $\omega_0' \approx 0.25\pi$. For the approximated case, the scaled coefficients are same as the scaling-free coefficients in Example 3.7.)

Example 3.8: The specifications for a type-B contour are $\omega_0 = \omega_a = 0.125\pi$ and $\omega_b = 0.25\pi$.

Using the scaling-free formulas given by (3.41), for type-B contours the following results are obtained.

$$U_{01} = 0.78480295 \qquad U_{10} = 0.45053527 \times 10^{-1}$$
$$E_{2\,MSE} = 0.39241793 \times 10^{-8} \qquad E_{2\,\max} = 0.78861587 \times 10^{-4}$$
$$E_{1\,MSE} = 0.14436219 \times 10^{-6} \qquad E_{1\,\max} = 0.44398185 \times 10^{-3}$$

The scaling-free coefficients for the cosine- and sine- form transformations are obtained by substituting these values in (3.46) and (3.47), respectively.

The scaled coefficients of the optimum or approximation solution in Example 3.6 were obtained by using (2.26). After scaling, $\omega_0' \approx 0.125\pi$. Again, for the approximation solution, it can be shown from Examples 3.6 and 3.8 that the values of the scaled and scaling-free coefficients are the same.

3.9 An Analytical Method for Finding Coefficients for Type-B Contours

Reddy and Hazra [34] have proposed an analytical method for finding the McClellan transformation coefficients for type-A elliptical cutoff contours. Some of the advantages and differences of this method, when compared with the method of [35] have been presented in Sec. 3.3.4. Since the method of [34] gives results which are very close to those of the optimization methods, and has other advantages, it is worthwhile to extend this method for type-B elliptical cutoff contours as well. In this section, the derivation of the conditions and formulas for this extension are presented.

The desired frequency specifications for a 2-D type-B elliptically symmetric digital filter are shown in Fig. 3.3, where ω_a and ω_b are 2-D minor and major axes pass-band cutoff frequencies, and ω_c and ω_d are the 2-D minor and major axes stop-band cutoff frequencies. Let ω_0 and ω_s be the 1-D pass-band and stop-band cutoff frequencies of the prototype digital filter as shown in Fig. 3.4. Assume that both the filters are low-pass

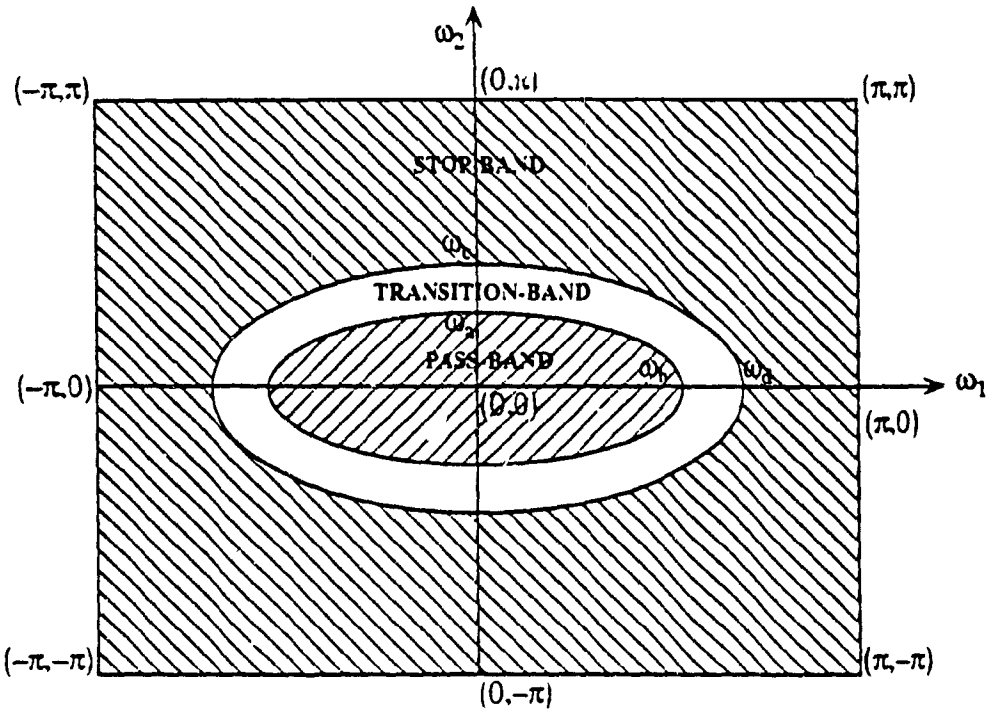

Fig. 3.3 Desired Frequency Specifications for a 2-D Type-B Elliptically Symmetric Digital Filter.

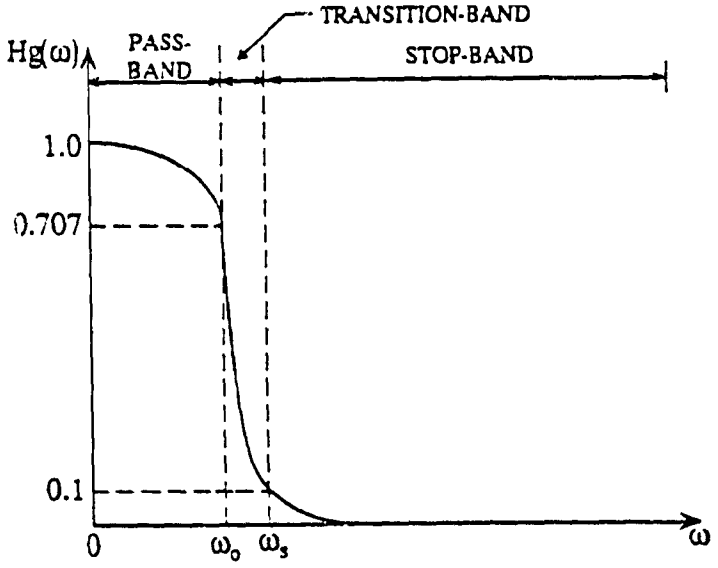

Fig. 3.4 Frequency Specifications for a 1-D Prototype Digital Filter.

filters. The coefficients p_{ij}'s of the original McClellan transformation in sine-form as given in (2.8) are found by making the following mapping assumptions: (i) $0 \rightarrow (0,0)$, (ii) $\omega_0 \rightarrow (0,\omega_a)$, (iii) $\omega_0 \rightarrow (\omega_b,0)$, and (iv) $\omega_0 \rightarrow (\omega_b/\sqrt{2}, \omega_a/\sqrt{2})$. The p_{ij} coefficients are given by

$$p_{00} = 0, \quad p_{01} = a / b_2, \quad p_{10} = a / b_1, \quad \text{and}$$
$$p_{11} = a\{b_2 - (b_2 / b_1)c_1 - c_2\} / (b_2 c_1 c_2) \tag{3.48}$$

where a, b_1, b_2, c_1, and c_2 are defined as

$$a = \sin^2(\omega_0/2) \tag{3.49a}$$
$$b_1 = \sin^2(\omega_b/2) \tag{3.49b}$$
$$b_2 = \sin^2(\omega_a/2) \tag{3.49c}$$
$$c_1 = \sin^2\left(\omega_b/(2\sqrt{2})\right) \tag{3.49d}$$

and

$$c_2 = \sin^2\left(\omega_a/(2\sqrt{2})\right) \tag{3.49e}$$

The value of ω_0 must be $0 \leq \omega_0 \leq \pi$. Accordingly, the value of a given by (3.49a) is chosen such that

$$0 \leq G(\omega_1,\omega_2) \leq 1 \tag{3.50}$$

for $|\omega_1| \leq \pi$ and $|\omega_2| \leq \pi$. When $\omega_1 = \alpha$, where α is a constant, *i.e.* on a line parallel to the ω_2-axis in the (ω_1,ω_2)-plane, (2.8) becomes

$$G(\alpha,\omega_2) = \{p_{00} + p_{10}\sin^2(\alpha/2)\} + \{p_{01} + p_{11}\sin^2(\alpha/2)\}\sin^2(\omega_2/2)$$
$$= G_\alpha(\omega_2) \quad \text{(say)} \tag{3.51}$$

From (3.51), it is observed that $G_\alpha(\omega_2)$ is a monotonically increasing or decreasing function of ω_2 for $0 \leq \omega_2 \leq \pi$. Similarly, $G_\alpha(\omega_1)$ is a monotonically increasing or decreasing function of ω_1 on a line parallel to the ω_1-axis. Therefore, the extreme values of $G(\omega_1,\omega_2)$ can occur only at the corner frequency points $(0,0)$, $(0,\pi)$, $(\pi,0)$, and (π, π) in the first quadrant of the (ω_1,ω_2)-plane. The values of the transformation function at these points, with the choice of the coefficients in (3.48), are

$$G(0,0) = 0, \quad G(0,\pi) = a \ / \ b_2, \quad G(\pi,0) = a \ / \ b_1, \quad \text{and}$$
$$G(\pi,\pi) = ag_2 \ / \ b_2 \tag{3.52}$$

where

$$g_2 \triangleq 1 + (b_2 \ / \ b_1) + \{ \left(b_2 - (b_2 \ / \ b_1)c_1 - c_2 \right) \ / \ (c_1 c_2) \} \tag{3.53}$$

and $g_2 > 1$ for $\omega_a \geq 10^{-6}$ rad./sec. There are two cases, that arise in the derivation of formulas depending on where the maximum value of $G(\omega_1,\omega_2)$ occurs.

Case A: The Maximum Value at $(0,\pi)$

For $G(0,\pi) \leq 1$, it follows from (3.52) that $a/b_2 \leq 1$. Taking $a = b_2$ gives $G(0,\pi) = 1$, maps the point $\omega = \pi$ onto $(0,\pi)$, and makes the frequency response of the 2-D filter along the ω_2-axis, i.e. the axis of lowest cutoff frequency identical to the frequency response of the 1-D filter. When $a = b_2$, $G(\pi,\pi) \leq 1$ becomes $g_2 < 1$. Thus, the condition for this case is $g_2 < 1$. The following formulas are obtained for the coefficients by substituting $a = b_2$ in (3.48) and using (3.53).

$$p_{00} = 0, \quad p_{01} = 1, \quad p_{10} = b_2 \ / \ b_1, \quad \text{and} \quad p_{11} = g_2 - \{1 + (b_2 \ / \ b_1)\}. \tag{3.54}$$

Case B: The Maximum Value at (π,π)

For $G(\pi,\pi) \leq 1$, it follows from (3.52) that $ag_2 \ / \ b_2 \leq 1$ Taking $a = b_2 \ / \ g_2$ gives $G(\pi,\pi) = 1$ and maps the point $\omega = \pi$ onto (π,π) The condition for this case is $g_2 > 1$. Substituting $a = b_2 \ / \ g_2$ in (3.48) and using (3.53), the same formulas as for type-A, case B contours and given by (2.63) are obtained.

Given the 2-D frequency specifications (ω_a & ω_b and ω_c & ω_d), the 1-D frequency specifications (ω_0 & ω_s) are found by proceeding as follows. The 1-D pass-band cutoff frequency, ω_0 for case A is found from

$$a = b_2 \tag{3.55}$$

i.e. $\omega_0 = \omega_b$, and for case B, is found from

$$a = b_2 / g_2. \tag{3.56}$$

To find the 1-D stop-band cutoff frequency ω_s, let

$$d = \min^{\dagger}\{ae_1 / b_1 , ae_2 / b_2\} \tag{3.57}$$

where d, e_1, and e_2 are given by

$$d = \sin^2(\omega_s /2) \tag{3.58a}$$

$$e_1 = \sin^2(\omega_d /2) \tag{3.58b}$$

and

$$e_2 = \sin^2(\omega_c /2). \tag{3.58c}$$

For case A, ω_s is obtained by substituting (3.55) in (3.57) which becomes

$$d = \min\{b_2 e_1 / b_1 , e_2\}, \tag{3.59}$$

and for case B, ω_s is obtained by substituting (3.56) in (3.57), in which case

$$d = \min\{(b_2 e_1) / (g_2 b_1) , e_2 / g_2\}. \tag{3.60}$$

The coefficients in (3.54) satisfy the coefficient relationships in (2.48), and therefore, no scaling is required when (3.54) is used to calculate them. Also, the expressions for U_{ij}'s in (2.48) can be easily obtained by comparing this equation with (3.54). Substituting the coefficients U_{ij}'s in (2.47), and comparing it with (2.1), the coefficients for the corresponding cosine-form transformation for case A are obtained as

$$-t_{00} = \quad t_{10} = -0.5 + \{(b_1 g_2 + b_2) / (2b_1)\} \tag{3.61a}$$

$$t_{01} = 1 - t_{11} = \quad 0.5 + \{(b_1 g_2 - b_2) / (2b_1)\}. \tag{3.61b}$$

The coefficients of the cosine-form transformation for case B are same as those in (2.61) which are for case B of type-A contours. It should be noted that the expressions of b_1 & b_2, c_1 & c_2, e_1 & e_2, and g_2 for type-B contours are different from those for type-A contours.

---

† $\min\{x , y\} \triangleq$ minimum of x and y

3.9.1 Discussion on the Transition-Band

In [34], the authors have not provided any discussion on the transformation of the transition-width from 1-D to 2-D. Therefore, the transition-band of both type-A and type-B filters are now discussed.

For case A of type-A contours, $a / b_1 \leq 1$. For case A of type-B contours, $a / b_2 \leq 1$. For case B of both types A and B contours, $ag_2 / b_2 \leq 1$. From these relationships, and from (3.57) it is seen that for given values of b_1 & b_2 and c_1 & c_2, there are wide range of values that a and d can assume, i.e. for given values of ω_a & ω_b and ω_c & ω_d, there are a number of choices for ω_0 and ω_s. The converse statement, that is, for given values of ω_0 and ω_s, there are a wide range of values ω_a & ω_b and ω_c & ω_d, is also true. It is noted that when $a = b_1$, $a = b_2$, and $a = b_2 / g_2$, $\omega = \pi$ maps onto $(\pi,0)$, $(0,\pi)$, and (π,π), respectively, and $\omega = 0$ maps onto (0,0) for both the cases.

For a 2-D type-A filter, define the transition-ratio for the ω_1-axis and ω_2-axis as

$$r_{a1} = \omega_c / \omega_a \qquad \text{and} \qquad r_{a2} = \omega_d / \omega_b , \tag{3.62}$$

and the transition-width for the respective axes as

$$w_{a1} = \omega_c - \omega_a \qquad \text{and} \qquad w_{a2} = \omega_d - \omega_b . \tag{3.63}$$

For a 2-D type-B filter, these quantities are similarly defined as

$$r_{b1} = \omega_d / \omega_b \qquad \text{and} \qquad r_{b2} = \omega_c / \omega_a , \quad \text{and} \tag{3.64}$$

$$w_{b1} = \omega_d - \omega_b \qquad \text{and} \qquad w_{b2} = \omega_c - \omega_a . \tag{3.65}$$

For a 1-D filter, the transition-ratio and the transition-width are defined as

$$r_\omega = \omega_s / \omega_0 \qquad \text{and} \qquad w_\omega = \omega_s - \omega_0 . \tag{3.66}$$

These two quantities can be considered either on the ω_1-axis or ω_2-axis, since the design criteria applied with respect to either of the two axes will lead to the same filter. It is desirable to minimize the transition- ratio and width of the 2-D filter, and to maximize the same for the 1-D filter. In other words, it is desirable to minimize the ratio of the

transition- ratio or width of the 2-D filter to that of the 1-D filter.

The stop-band cutoff frequency on either the ω_1-axis or the ω_2-axis of the 2-D filter is derived, for each of the cases A and B, by substituting the corresponding mappings in (2.8). For case A of type-A and type-B 2-D filter, ω_c can be expressed as a function of ω_a, ω_0, and ω_s $(= r_\omega \omega_0)$ as

$$\omega_c = 2 \sin^{-1}\left\{\sin(r_\omega \omega_0/2)\sin(\omega_a/2) \,/\, \sin(\omega_0/2)\right\}. \tag{3.67}$$

For case B of type-A 2-D filter, $\omega_c\,(\omega_d)$ can be expressed as a function of $\omega_d\,(\omega_c)$ and ω_s $(= r_\omega \omega_0)$ as

$$\omega_c = 2 \sin^{-1}\left\{\left[\frac{\sin^2(r_\omega \omega_0/2) - p_{01}\sin^2(\omega_d/2)}{p_{10} + p_{11}\sin^2(\omega_d/2)}\right]^{1/2}\right\} \tag{3.68a}$$

$$\omega_d = 2 \sin^{-1}\left\{\left[\frac{\sin^2(r_\omega \omega_0/2) - p_{10}\sin^2(\omega_c/2)}{p_{01} + p_{11}\sin^2(\omega_c/2)}\right]^{1/2}\right\}. \tag{3.68b}$$

For case B of type-B 2-D filter, ω_d (ω_c) can be expressed as a function of ω_c (ω_d) and ω_s $(= r_\omega \omega_0)$ as

$$\omega_d = 2 \sin^{-1}\left\{\left[\frac{\sin^2(r_\omega \omega_0/2) - p_{01}\sin^2(\omega_c/2)}{p_{10} + p_{11}\sin^2(\omega_c/2)}\right]^{1/2}\right\} \tag{3.69a}$$

$$\omega_c = 2 \sin^{-1}\left\{\left[\frac{\sin^2(r_\omega \omega_0/2) - p_{10}\sin^2(\omega_d/2)}{p_{01} + p_{11}\sin^2(\omega_d/2)}\right]^{1/2}\right\}. \tag{3.69b}$$

For case A of type-A (type-B) 2-D filter, the ratios of r_{a1} to r_ω (r_{b1} to r_ω) and w_{a1} to w_ω ($w_{b\ell}$ to w_ω) can be viewed as functions of variables b_1 / a (b_2 / a) and d for various values of r_ω for a given ω_a & ω_b and ω_c & ω_d. Eq. (3.67) is used for $a / b_1 \leq 1$ $(a / b_2 \leq 1)$, and (3.68) [(3.69)] is used for $ag_2 / b_2 \leq 1$. The values of r_{a1} / r_ω $(r_{b\ell} / r_\omega)$ and w_{a1} / w_ω $(w_{b\ell} / w_\omega)$ will be greater than one for all values of b_1 a $(b_2 \; a)$, d, and r_ω. They will be minimum when $a = b_1$ $(a = b_2)$, and d is given by (3.57). For case B of both types A and B contours, they will be minimum when

$a = b_2 / g_2$ and d is given by (3.57). In the case of 2-D elliptically symmetric filters, the mentioned functions are 2-variable functions. But, in the case of 2-D circularly symmetric filters, they are functions of 1-variable, since $\omega_a = \omega_b$ and $\omega_c = \omega_d$, and the d-axis is not necessary. The proof for the assertion about the behavior of the 2-D function directly follows from Fig. 2 in [40].

3.9.2 Implementation

For case A of type-A 2-D elliptically symmetric digital filter, the original McClellan transformation (2.1) with the coefficients of (2.60) can be written as

$$\cos(\omega) = - U_1 + U_1\cos(\omega_2) + (0.5 + U_2)\cos(\omega_1) + (0.5 - U_2)\cos(\omega_1)\cos(\omega_2) \tag{3.70}$$

where

$$U_1 = - 0.5 + \{b_1(g_2 + 1) / (2b_2)\} \quad \text{and} \quad U_2 = b_1(g_2 - 1) / (2b_2).$$

For case A of type-B 2-D filter, the transformation (2.1) with the coefficients given by (3.61) can be written as

$$\cos(\omega) = - U_3 + (0.5 + U_4)\cos(\omega_2) + U_3\cos(\omega_1) + (0.5 - U_4)\cos(\omega_1)\cos(\omega_2) \tag{3.71}$$

where

$$U_3 = - 0.5 + \{(b_1 g_2 + b_2) / (2b_1)\} \quad \text{and} \quad U_4 = (b_1 g_2 - b_2) / (2b_1).$$

For case B of both types A and B filters, the transformation (2.1) with the coefficients given by (2.61) can be written as

$$\cos(\omega) = - U_5 + (0.5 - U_6)\cos(\omega_2) + (0.5 + U_6)\cos(\omega_1) + U_5\cos(\omega_1)\cos(\omega_2) \tag{3.72}$$

where

$$U_5 = -0.5 + \left[\{(b_2 / b_1) + 1\} / (2g_2)\right]$$

and

$$U_6 = \{(b_2 / b_1) - 1\} / (2g_2).$$

The 2-D filters obtained by the transformations (3.70)-(3.72) can be implemented by using the scheme described in [16]. The number of multiplications required per output sample is only two. Multiplications by a power of 2 are not counted, since they are done by bit shifting. The total number of multiplications per output sample for a filter of order M×M is $\{2(M-1)/2\} + \{(M+1)/2\} = (3M-1)/2$.

3.9.3 Comparison of Analytical and Optimization Methods

The following two examples illustrate the comparison of analytical and optimization methods of finding the transformation coefficients.

Example 3.9: The specifications for a 2-D type-B elliptically symmetric digital filter are $\omega_a = 0.25\pi$ & $\omega_b = 0.5\pi$, and $\omega_c = 0.5\pi$ & $\omega_d = 0.75\pi$.

Using the formulas for case B of type-B filters, given by (2.61), (3.56), and (3.60), the following results are obtained.

$$\omega_0 = 0.25000000\pi \qquad \omega_s = 0.33333333\pi$$
$$t_{00} = -0.50664618\times10^{-1} \qquad t_{01} = 0.75777140$$
$$t_{10} = 0.50664618\times10^{-1} \qquad t_{11} = 0.24222860$$
$$E_{2\,MSE} = 0.57204307\times10^{-7} \qquad E_{2\,\max} = 0.36810137\times10^{-3}$$
$$E_{1\,MSE} = 0.14437507\times10^{-5} \qquad E_{1\,\max} = 0.25908047\times10^{-2}$$

The scaled optimum coefficients were obtained by scaling the coefficients in Example 3.5 using (2.26). After scaling, $\omega_0' = 0.24070418\pi$. The other results are as follows.

$$T_{00} = -0.47991700\times10^{-1} \qquad T_{01} = 0.75573102$$
$$T_{10} = 0.47991700\times10^{-1} \qquad T_{11} = 0.24426898$$
$$E_{2\,MSE} = 0.22306101\times10^{-7} \qquad E_{2\,\max} = 0.45709033\times10^{-3}$$
$$E_{1\,MSE} = 0.16728171\times10^{-5} \qquad E_{1\,\max} = 0.12166175\times10^{-1}$$

By comparing the error values, it is seen that the results of the analytical method are very close to those of the optimization method. In the next example, specifications ω_a & ω_b are reduced by one half of their value and the transition-width is kept the same (0.25π).

Example 3.10: The specifications for a 2-D type-B elliptically symmetric digital filter are $\omega_a = 0.125\pi$ & $\omega_b = 0.25\pi$, and $\omega_c = 0.375\pi$ & $\omega_d = 0.5\pi$.

Using the formulas for case B of type-B filters, given by (2.61), (3.56), and (3.60), the following results are obtained.

$$\omega_0 = 0.12500000\pi \qquad \omega_s = 0.18261013\pi$$
$$t_{00} = -0.43710115\times10^{-1} \qquad t_{01} = 0.78381859$$
$$t_{10} = 0.43710115\times10^{-1} \qquad t_{11} = 0.21618141$$
$$E_{2\,MSE} = 0.13481030\times10^{-10} \qquad E_{2\,\max} = 0.55685973\times10^{-5}$$
$$E_{1\,MSE} = 0.10244047\times10^{-8} \qquad E_{1\,\max} = 0.70639645\times10^{-4}$$

The scaled optimum results were obtained by scaling the coefficients in Example 3.6 using (2.26). After scaling, $\omega_0' = 0.12499336\pi$. The other results are as follows.

$$T_{00} = -0.43022895\times10^{-1} \qquad T_{01} = 0.78316725$$
$$T_{10} = 0.43022895\times10^{-1} \qquad T_{11} = 0.21683275$$
$$E_{2\,MSE} = 0.51017793\times10^{-11} \qquad E_{2\,\max} = 0.79826424\times10^{-5}$$
$$E_{1\,MSE} = 0.15492537\times10^{-8} \qquad E_{1\,\max} = 0.37611299\times10^{-3}$$

By comparing the above results with those in the previous example, it is observed that the analytical method provides results quite close to those obtained by the optimization method even for large values of frequency specification. Therefore, the use of the analytical method is justified in view of its computational simplicity.

3.10 Approximation of Analytical Method for Type-A Contours

The formulas given by (2.60)-(2.63) used to find the McClellan transformation coefficients for a 2-D type-A elliptically symmetric digital filters involve parameters defined in the form $\sin^2(x/2)$ and $\sin^2\left(x/(2\sqrt{2})\right)$. Thus, to implement these formulas in

hardware, either a ROM lookup table or a numeric data processor is required. For the lookup table method, more memory space is needed. The numeric data processor may not have enough mathematical capability. Mathematical identities should be used., if instead of a sine function other trigonometric function is given. However, both the approaches will increase the over all chip count and hardware cost, though they are fast. The built in function subroutine in a general-purpose computer is relatively slow, and it is not suitable for real-time adaptive digital filtering. To overcome these problems, simple approximate formulas which can be implemented even in a general-purpose signal processor are presented.

The functions $\sin^2(x/2)$ and $\sin^2\left(x/(2\sqrt{2})\right)$ can be approximated by their truncated power series as

$$\sin^2(x/2) \approx (x^2/4)\{1-(x^2/12)\} \tag{3.73a}$$

and

$$\sin^2\left(x/(2\sqrt{2})\right) \approx (x^2/8)\{1-(x^2/24)\}. \tag{3.73b}$$

Using these expressions, the equations for type-A contours are approximated as

$$a = (\omega_0^2/4)\{1-(\omega_0^2/12)\} \tag{3.74a}$$
$$b_1 = (\omega_a^2/4)\{1-(\omega_a^2/12)\} \tag{3.74b}$$
$$b_2 = (\omega_b^2/4)\{1-(\omega_b^2/12)\} \tag{3.74c}$$
$$c_1 = (\omega_a^2/8)\{1-(\omega_a^2/24)\} \tag{3.74d}$$
$$c_2 = (\omega_b^2/8)\{1-(\omega_b^2/24)\} \tag{3.74e}$$
$$d = (\omega_s^2/4)\{1-(\omega_s^2/12)\} \tag{3.74f}$$
$$e_1 = (\omega_c^2/4)\{1-(\omega_c^2/12)\} \tag{3.74g}$$
$$e_2 = (\omega_d^2/4)\{1-(\omega_d^2/12)\}. \tag{3.74h}$$

Substituting (3.74) in (3.53), (3.57), (2.60), and (2.62), the resulting equations are simplified by neglecting sixth- and higher- order powers. Using the binomial series and simplifying, the following results are obtained for case A.

$$f_{a1} + f_{a2} < 0 \tag{3.75}$$

where

$$f_{a1} = \frac{\omega_a^2}{\omega_b^2}\left\{1 + \frac{1}{12}(\omega_b^2 - \omega_a^2) + \frac{1}{144}(\omega_b^4 - \omega_a^2\omega_b^2)\right\}$$

and

$$f_{a2} = -\frac{1}{3}\left[1 + \omega_a^2\left\{\frac{1}{12} + \frac{1}{\omega_b^2}\right\} + \frac{1}{24}\left\{\omega_b^2 + \frac{\omega_a^4}{\omega_b^2}\right\} + \frac{\omega_a^2}{288}(\omega_a^2 + \omega_b^2) + \frac{\omega_b^4}{576}\right].$$

If the condition given by (3.75) is satisfied, then,

$$\omega_0 = \omega_a \tag{3.76}$$

and

$$d = \min\{d_{a1}, d_{a2}\} \tag{3.77a}$$

where

$$d_{a1} = e_1 \tag{3.77b}$$

and

$$d_{a2} = f_{a1}\omega_d^2 / 4, \tag{3.77c}$$

and

$$\omega_s = \omega_c \quad \text{if} \quad d = d_{a1} \tag{3.78a}$$

$$\omega_s = (\omega_a \omega_d) / \omega_b \quad \text{if} \quad d = d_{a2}. \tag{3.78b}$$

The cosine-form transformation coefficients are

$$-t_{00} = \quad t_{01} = f_{a1} + (f_{a2} / 2) \tag{3.79a}$$

and

$$t_{10} = 1 - t_{11} = 1 + (f_{a2} / 2). \tag{3.79b}$$

The corresponding sine-form transformation coefficients are

$$p_{00} = 0, \quad p_{01} = f_{a1}, \quad p_{10} = 1, \quad \text{and} \quad p_{11} = f_{a2}. \tag{3.80}$$

The above formulas are directly in terms of the given 2-D frequency specifications and are very simple. They give good accuracy for lower values of cutoff frequencies than for higher values. Some examples are given in Sec. 3.12.4.

3.11 Approximation of Analytical Metiiod for Type-B Contours

Using (3.73), the expressions given by (3.49) and (3.58) can be approximated as

$$a = (\omega_0^2 / 4)\{1 - (\omega_0^2 / 12)\} \tag{3.81a}$$

$$b_1 = (\omega_b^2 / 4)\{1 - (\omega_b^2 / 12)\} \tag{3.81b}$$

$$b_2 = (\omega_a^2 / 4)\{1 - (\omega_a^2 / 12)\} \tag{3.81c}$$

$$c_1 = (\omega_b^2 / 8)\{1 - (\omega_b^2 / 24)\} \tag{3.81d}$$

$$c_2 = (\omega_a^2 / 8)\{1 - (\omega_a^2 / 24)\} \tag{3.81e}$$

$$d = (\omega_s^2 / 4)\{1 - (\omega_s^2 / 12)\} \tag{3.81f}$$

$$e_1 = (\omega_d^2 / 4)\{1 - (\omega_d^2 / 12)\} \tag{3.81g}$$

$$e_2 = (\omega_c^2 / 4)\{1 - (\omega_c^2 / 12)\}. \tag{3.81h}$$

Carrying out a derivation similar to type-A contours, by substituting (3.81) in (3.53), (3.54), (3.57), and (3.61), the following results are obtained for case A.

$$f_{b1} + f_{b\ell} < 0 \tag{3.82}$$

where

$$f_{b1} = \frac{\omega_a^2}{\omega_b^2}\left\{1 + \frac{1}{12}(\omega_b^2 - \omega_a^2) + \frac{1}{144}(\omega_b^4 - \omega_a^2\omega_b^2)\right\}$$

and

$$f_{b\ell} = -\frac{1}{3}\left[1 + \omega_a^2\left\{\frac{1}{12} + \frac{1}{\omega_b^2}\right\} + \frac{1}{24}\left\{\omega_b^2 + \frac{\omega_a^4}{\omega_b^2}\right\} + \frac{\omega_a^2}{288}(\omega_a^2 + \omega_b^2) + \frac{\omega_b^4}{576}\right].$$

If the condition given by (3.82) is satisfied, then,

$$\omega_0 = \omega_a \tag{3.83}$$

and

$$d = \min\{d_{b1}, d_{b2}\} \tag{3.84a}$$

where

$$d_{b1} = e_2 \tag{3.84b}$$

and

$$d_{b2} = f_{b1}\omega_d^2 / 4, \tag{3.84c}$$

and

$$\omega_s = \omega_c \quad \text{if} \quad d = d_{b1} \tag{3.85a}$$

$$\omega_s = (\omega_a \omega_d) / \omega_b \quad \text{if} \quad d = d_{b2}. \tag{3.85b}$$

The cosine-form transformation coefficients are

$$-t_{00} = \quad t_{10} = f_{b1} + (f_{b2} / 2) \tag{3.86a}$$

and

$$t_{01} = 1 - t_{11} = 1 + (f_{b2} / 2). \tag{3.86b}$$

The corresponding sine-form transformation coefficients are

$$p_{00} = 0, \quad p_{01} = 1, \quad p_{10} = f_{b1}, \quad \text{and} \quad p_{11} = f_{b2}. \tag{3.87}$$

Comparing the above results [(3.82)-(3.87)] with those for type-A contours [(3.75)-(3.80)], the following points are noticed. The formulas for f_{b1} and f_{b2} for type-B can be obtained, respectively, from the right side of the formulas for f_{a1} and f_{a2} for type-A. Using (3.74) in (3.77b) and (3.77c), and (3.81) in (3.84b) and (3.84c), it is found that $d_{a1} = d_{b1}$ and $d_{a2} = d_{b2}$. Because of these reasons, the formulas for ω_0, ω_s, t_{00}, t_{11}, p_{00}, and p_{11} are the same for both the types of contours. For a given specification, the values of t_{01}, t_{10}, p_{01}, and p_{10} in type-B contours, respectively become the values of t_{10}, t_{01}, p_{10}, and p_{01} for type-A contours. specifications.

3.11.1 Comparison of Approximate and Exact Analytical Methods

The following examples illustrate the difference between the approximate and exact analytical methods.

Example 3.11: Assume a type-B filter with the same specifications as of Example 3.9, *i.e.* $\omega_a = 0.25\pi$ & $\omega_b = 0.5\pi$, and $\omega_c = 0.5\pi$ & $\omega_d = 0.75\pi$.

Using the formulas in (3.82)-(3.86), the following results are obtained.

$$\omega_0 = 0.25000000\pi \qquad \omega_s = 0.37500000\pi$$
$$t_{00} = -0.58511375\times10^{-1} \qquad t_{01} = 0.76203106$$
$$t_{10} = 0.58511375\times10^{-1} \qquad t_{11} = 0.23796894$$
$$E_{2\,MSE} = 0.89290240\times10^{-5} \qquad E_{2\,\max} = 0.36851832\times10^{-2}$$
$$E_{1\,MSE} = 0.11896471\times10^{-3} \qquad E_{1\,\max} = 0.12894790\times10^{-1}$$

Comparing the above error values with those in Example 3.9, it is observed that the results of the approximate analytical method agree well with those of the exact analytical method. Also, it should be noted that in this example, ω_b and ω_c & ω_d are not so small. To see that effect of smaller values of these critical frequencies, in the next example, ω_a and ω_b are reduced by a factor of 2 and keeping the transition-width the same.

Example 3.12: The specifications for a type-B filter are same as in Example 3.10, *i.e.* $\omega_a = 0.125\pi$ & $\omega_b = 0.25\pi$, and $\omega_c = 0.375\pi$ & $\omega_d = 0.5\pi$.

Using the formulas given in (3.82)-(3.86), the following results are obtained.

$$\omega_0 = 0.12500000\pi \qquad \omega_s = 0.18750000\pi$$
$$t_{00} = -0.44928233\times10^{-1} \qquad t_{01} = 0.78479450$$
$$t_{10} = 0.44928233\times10^{-1} \qquad t_{11} = 0.21520550$$
$$E_{2\,MSE} = 0.32063920\times10^{-8} \qquad E_{2\,\max} = 0.71129552\times10^{-4}$$
$$E_{1\,MSE} = 0.11773916\times10^{-6} \qquad E_{1\,\max} = 0.40275310\times10^{-3}$$

Comparing the above error values with those in Example 3.10, once again it is observed that they agree well with those of the exact analytical method. By comparing the error values of the above two examples, it is seen notice that the approximate analytical method gives better results for lower values of frequency specifications.

3.12 Filter Design Examples

The McClellan transformation is used to design 2-D zero-phase FIR and IIR digital filters. FIR filter design examples are there in many papers [16], [17], [27], [28], [34], [40]. Therefore, in this section, some IIR filter design examples are presented to demonstrate the applications of the derived formulas.

A 1-D zero-phase filter obtained by multiplying the transfer function of a second-order digital Butterworth filter and its conjugate is used as a prototype filter ($\omega_0 = 0.24281303\pi$). The 2-D specifications for a type-B elliptically symmetric filter are $\omega_a = 0.25\pi$ and $\omega_b = 0.5\pi$. The transformation coefficients are obtained by using (3.37). The scaled coefficients are obtained by using (2.26). The unscaled (scaled) coefficients are same as the coefficients for type-A contours in which t_{01} and t_{10} (T_{01} and T_{10}) are interchanged. Applying the scaled transformation on the 1-D zero-phase filter, the required 2-D zero-phase filter is obtained. The magnitude response of this filter is shown in Fig. 3.5. When the new scaling formula given by (2.64) is used, the scaled coefficients are negative of the previously scaled coefficients. In this case, a 2-D zero-phase filter with elliptical contours shown in Fig. 3.6 is obtained.

3.13 Comparison of Analytical and Optimization Methods

To compare several analytical methods and the optimization method, it becomes necessary to solve the same problem and to compute the same type of error values in all the methods employed. Therefore, the mean square error and the maximum absolute error of the error functions $E_1(\omega_1)$ and $E_2(\omega_1)$ are used as figures of merit.

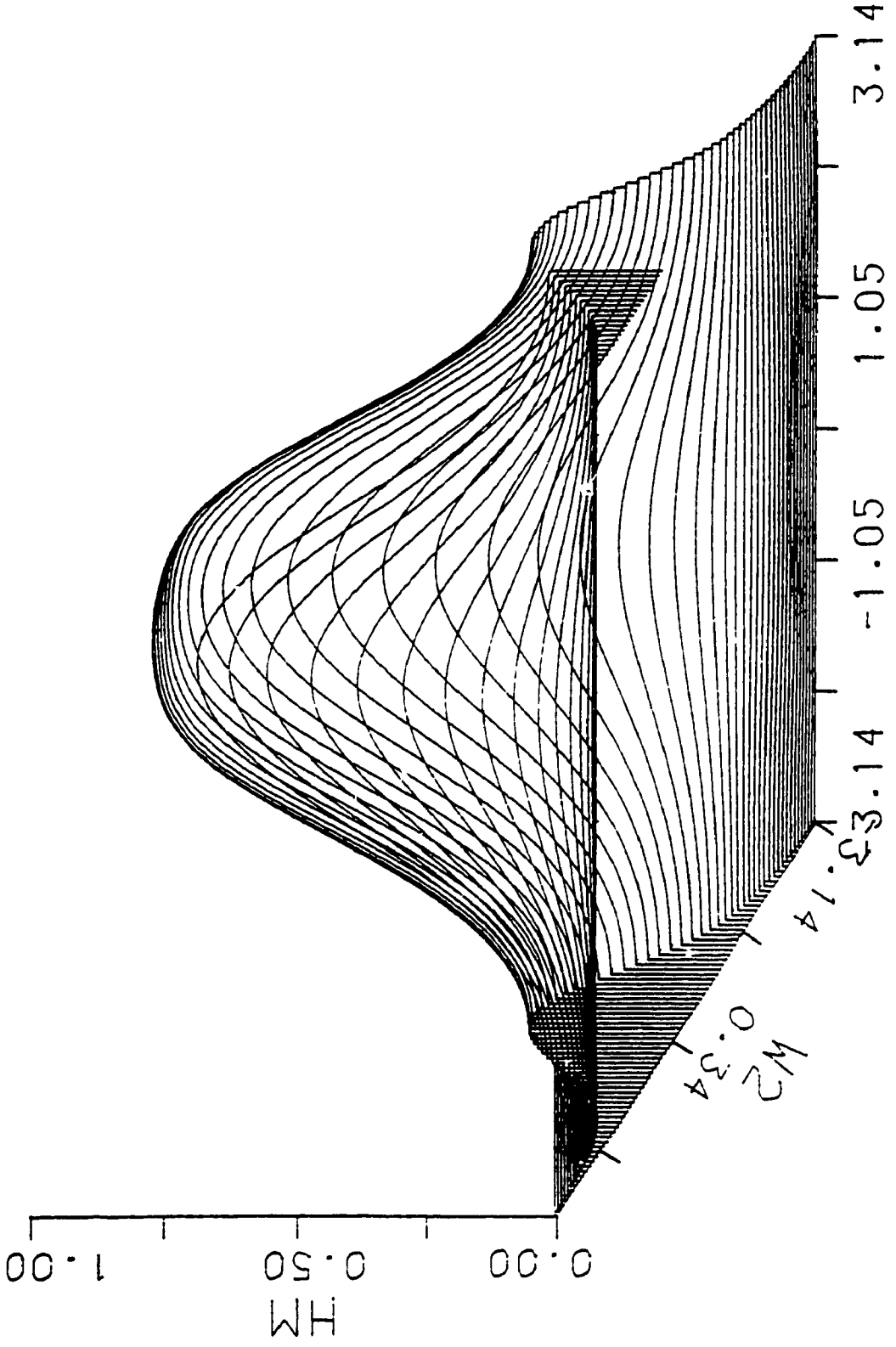

Fig. 3.5 Magnitude Response of a 2-D Zero-Phase Type-B Elliptical Fan Filter Designed From the Specifications $\omega_0 \approx 0.24\pi$, $\omega_s = 0.25\pi$, and $\omega_p = 0.5\pi$.

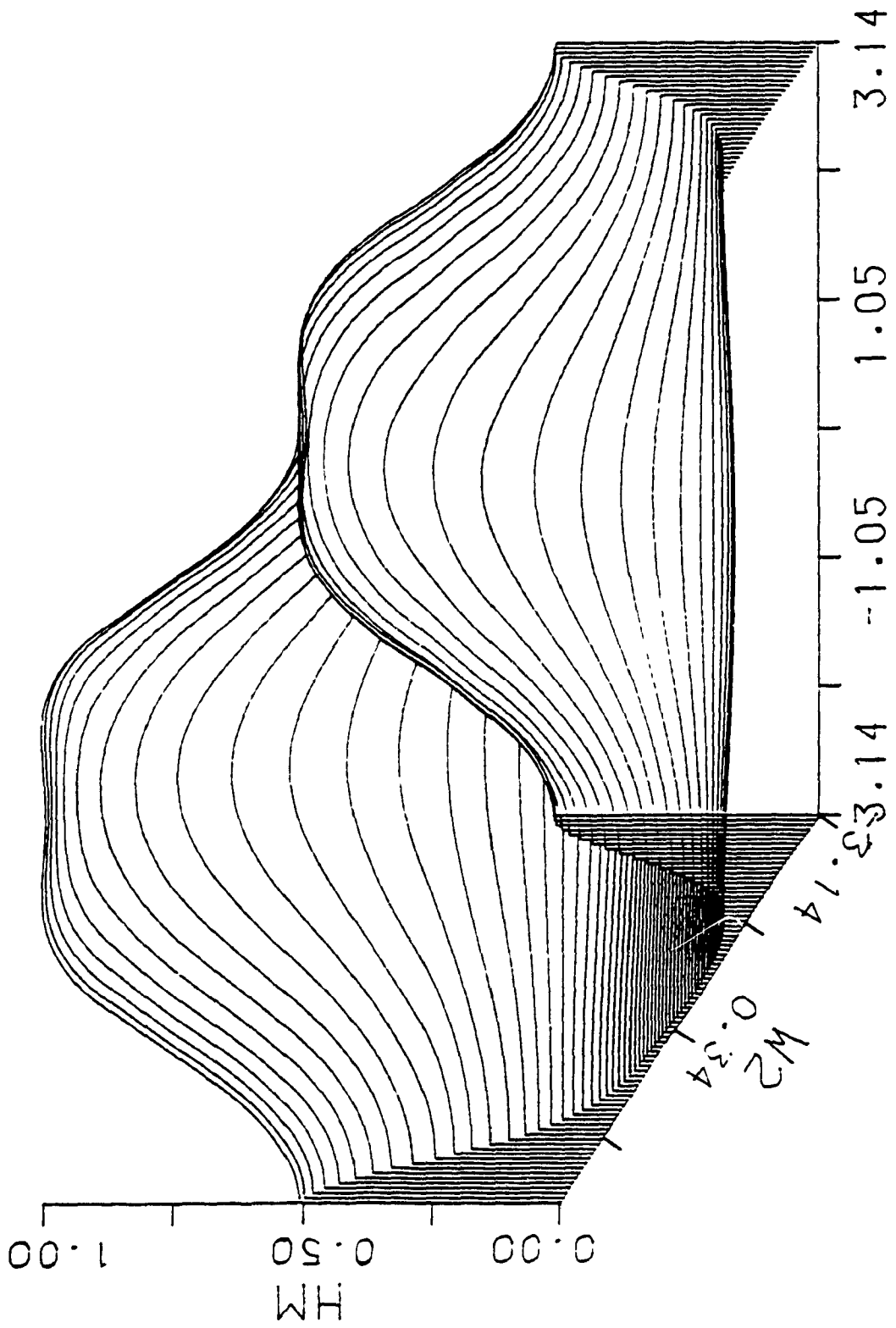

Fig. 3.6 Magnitude Response of a 2-D Zero-Phase Type-B Elliptical Fan Filter Designed by Using the New Scaling Formula From the Specifications $\omega_0 \approx 0.24\pi$, $\omega_a = 0.25\pi$, and $\omega_b = 0.5\pi$.

3.13.1 Mean Square Error

Define the mean square error (MSE) as

$$E_{i\ MSE} = \{ \sum_{j=1}^{N_f} \left(E_i(\omega_1) \right)^2 \} / N_f \qquad i = 1, 2. \tag{3.88}$$

where N_f is the total number of equally-spaced frequency points in the range 0 to ω_a for type-A contours, and 0 to ω_b for type-B contours. The root mean square (RMS) error is defined as

$$E_{i\ RMS} = \sqrt{E_{i\ MSE}}. \tag{3.89}$$

Our definition of MSE is different from that used in [35] and it is the same as that used in [34]. The MSE definition used in [35] is obtained by multiplying the right side of (3.88) by ω_a.

3.13.2 Further Solutions

Computer simulations were carried out using (3.88) with $N_f = 201$, to verify the error values reported in [34] and [35]. Since some numerical mistakes were found, the correct error values are presented along with the error values of other methods and further solutions.

On page 600, in column 1 of [35], the $E_{2\ MSE}$ values for the optimal and approximated cases were given. The recalculated values for the respective cases are $0.29668210 \times 10^{-10}$ and $0.63345864 \times 10^{-8}$. Also, the items given in Table I of [35] were recalculated. This table is reproduced with appropriate corrections as Table 3.1.

Two additional solutions are given in Table 3.2 so that some of the significant differences between the proposed method and that of [35] become clear. The results of this table are obtained by scaling the coefficients in Example 3.1 by using (2.20). Comparing the values in the first and last columns of Table 3.2 with those of Table 3.1, it is observed that the scaled approximation (optimum) solution is better than the scaling-

Parameter	Scaling-free Approx. Solution (3.30) $\omega_0 = \omega_a$	Scaled Optimum Solution (3.8)&(2.20) $\omega_0' \approx \omega_a$	Scaling-free Optimum Solution (2.41)&(3.8) $\omega_0 = \omega_a$
U_{01}	$0.57844060 \times 10^{-1}$	$0.47528400 \times 10^{-1}$	$0.51795200 \times 10^{-1}$
U_{10}	0.75931189	0.75532360	0.75613420
$E_{2\,MSE}$	$0.15443258 \times 10^{-4}$	$0.22779727 \times 10^{-6}$	$0.30229494 \times 10^{-7}$

Table 3.1 Recalculated Values of MSE for the Three Solutions in Table I of Reference [35]. (Specifications. $\omega_0 = 0.5\pi$, $\omega_a = 0.25\pi$ and $\omega_b = 0.5\pi$.)

Parameter	Scaled Approx. Solution† (3.20)&(2.20)	Scaled Optimum Solution* (3.8)&(2.20)
U_{01}	$0.57844060 \times 10^{-1}$	$0.47091690 \times 10^{-1}$
U_{10}	0.75931189	0.75573102
$E_{2\,MSE}$	$0.44794445 \times 10^{-5}$	$0.17519171 \times 10^{-7}$

† $\omega_0' = 0.25252840\pi$ * $\omega_0' = 0.24979418\pi$

Table 3.2 Values of U_{01}, U_{10}, and $E_{2\,MSE}$ for Scaled Approximate and Scaled Optimum Solutions. (Specifications: $\omega_0 = 0.5\pi$, $\omega_a = 0.25\pi$, and $\omega_b = 0.5\pi$.)

free approximation (optimum) solution. The reason is that the number of independent coefficients are 3 in the former solution, compared to only 2 in the latter solution. Because of the increased degree of freedom, the former case gives lesser error; but, in the latter case, the solution is achieved more quickly due to a smaller number of coefficients. The unscaled coefficient values corresponding to the scaled values given in the middle column of Table 3.1 are not known. Using the C_1 and C_2 values given in [27] for scaling the unscaled optimum coefficients in Example 3.1, the U_{01} and U_{10} values are obtained which are very close to those in the last column of Table 3.2. The relationships $T_{00} = -T_{01}$ and $T_{11} = 1 - T_{10}$ are approximately satisfied. In this case, $E_{2\,MSE} = 0.17510682 \times 10^{-7}$ and this is slightly higher than that in the last column of Table 3.2. From this, it is concluded that the analytical method of finding F_{max} and F_{min} and hence, C_1 and C_2 is better than the numerical method employing the scaling scheme of [27].

3.13.3 Analytical Versus Optimization Method

In Table I of [34], the authors have compared the results of analytical and optimization methods through the error values $E_{1\,RMS}$ and $E_{1\,max}$. Since there are numerical errors in the optimization results for the elliptical contour, the correct values of these quantities are reevaluated and presented in Table 3.3. It is apparent from this table that the results of both the methods are nearly identical.

Similarly, the results for the circular contour of [34] are corrected and presented in Table 3.4. Once again it is seen that there is close proximity between the results of these two methods.

3.13.4 A Comparison of the Proposed and Other Analytical and Optimization Methods

The results of several methods for a type-A elliptical cutoff contour with

Parameter	Optimization Method† (3.8)&(2.20)	Analytical Method* (2.60)
$-t_{00} = t_{01}$	$0.47991700 \times 10^{-1}$	$0.50664618 \times 10^{-1}$
$t_{10} = 1 - t_{11}$	0.75573102	0.75777140
$E_{1\,RMS}$	$0.12933743 \times 10^{-2}$	$0.12015618 \times 10^{-2}$
$E_{1\,max}$	$0.12166175 \times 10^{-1}$	$0.25908047 \times 10^{-2}$

† $\omega_0 = 0.5\pi$ (Specification), $\omega_0' = 0.24979418\pi$.
* $\omega_0 = 0.25\pi$

Table 3.3 Comparison of Results by Optimization and Analytical Methods for a Type-A Elliptical Cutoff Contour with $\omega_a = 0.25\pi$ and $\omega_b = 0.5\pi$.

Parameter	Optimization Method† (3.8)&(2.34)	Analytical Method* (2.59)
$-t_{00} = t_{11}$	0.33708360	0.33733770
$t_{10} = 1 - t_{01}$	0.49993930	0.50000000
$E_{1\,RMS}$	$0.82764915 \times 10^{-2}$	$0.30363783 \times 10^{-2}$
$E_{1\,max}$	0.11282790	$0.83589189 \times 10^{-2}$

† $\omega_0 = 0.75\pi$ (Specification), $\omega_0' = 0.64148950\pi$.
* $\omega_0 = 0.64128370\pi$

Table 3.4 Comparison of Results by Optimization and Analytical Methods for a Circular (Type-C) Cutoff Contour with $\omega_c = 0.75\pi$.

$\omega_a = 0.25\pi$ and $\omega_b = 0.5\pi$ are summarized in Table 3.5. From this, it is observed that the error $E_{2\,MSE}$ ($E_{1\,MSE}$) for the scaled approximation solution and the approximate analytical solution are nearly the same and it is of the order of 10^{-5} (10^{-3}). Similarly, the error $E_{2\,MSE}$ ($E_{1\,MSE}$) for the analytical solution and the scaled optimum solution are nearly the same and it is of the order of 10^{-7} (10^{-5}). The scaled approximation solution gives a smaller value† of $E_{2\,MSE}$ than the scaling-free approximation solution for the reasons mentioned in Sec. 3.13.1. The same conclusion holds for the optimum solution. In all the solutions, the value of $E_{1\,MSE}$ is larger than that of $E_{2\,MSE}$.

Comparing $E_{2\,MSE}$ and $E_{1\,MSE}$ in the first two and the last two columns of the table, it is observed that a decrease in the value of $E_{2\,MSE}$ may not result in a decrease in the value of $E_{1\,MSE}$. Therefore, the conclusion of Mersereau *et al.* [27] as given in Sec. 3.3.3. is modified as follows. For a first-order McClellan transformation, at least, the minimization of $E_2(\omega_1)$ generally minimizes $E_1(\omega_1)$, but this may not be true at or near the optimum point of $E_2(\omega_1)$

From the results in Tables 3.5 and 3.2, it can be concluded that the scaled or scaling-free approximation solution agrees well with the scaled or scaling-free optimum solution, even if the values of ω_0, ω_a, and ω_b are not small. Similarly, the approximate analytical solution agrees well with the exact analytical solution.

To illustrate the improvements in the results as the cutoff frequencies are made smaller, let $\omega_a = 0.125\pi$ and $\omega_b = 0.25\pi$. The results obtained by using several methods are summarized in Table 3.6. From this table, it is observed that the error $E_{2\,MSE}$ ($E_{1\,MSE}$) of all the approximate solutions is of the order of 10^{-8} ($\approx 10^{-6}$), while that of the analytical and scaled optimum solutions is of the order of 10^{-10} (10^{-8}) and 10^{-11} (10^{-10}), respectively. For all the solutions, the error $E_{1\,MSE}$ is larger than the error $E_{2\,MSE}$.

† Ideally, the scaled and scaling-free approximation solutions should be the same. The slight difference arises due to the approximations used.

Parameter	Scaled Approx. Solution* (3.20)&(2.20)	Scaling-free Approx. Solution (3 30)	Approx. Analytical Solution† (3.75)-(3.79b)	Analytical Solution† (2.60)	Scaled Optimum Solution* (3.8)&(2.20)
t_{00}	-0.57844060×10^{-1}	-0.57811060×10^{-1}	-0.58511375×10^{-1}	-0.50664618×10^{-1}	-0.47991700×10^{-1}
t_{01}	0.57844060×10^{-1}	0.57844060×10^{-1}	0.58511375×10^{-1}	0.50664618×10^{-1}	0.47991690×10^{-1}
t_{10}	0.75931189	0.75931189	0.76203106	0.75777140	0.75573102
t_{11}	0.24068811	0.24068811	0.23796894	0.24222860	0.24426898
ω_0'	0.25252840π	0.25000000π	0.25000000π	0.25000000π	0.24979418π
ω_0	0.50000000π†	0.25000000π	0.25000000π	0.25000000π	0.50000000π†
ω_s	–	–	0.37500000π	0.33333333π	–
$E_{2\,MSE}$	0.57034059×10^{-5}	0.19662967×10^{-4}	0.89290240×10^{-5}	0.57204307×10^{-7}	0.22306101×10^{-7}
$E_{2\,max}$	0.56380407×10^{-2}	0.56380512×10^{-2}	0.36851832×10^{-2}	0.36810137×10^{-3}	0.45709033×10^{-3}
$E_{1\,MSE}$	0.63381048×10^{-3}	0.25562594×10^{-3}	0.11896471×10^{-3}	0.14437507×10^{-5}	0.16728171×10^{-5}
$E_{1\,max}$	0.22284889	0.19003112×10^{-1}	0.12804790×10^{-1}	0.25908047×10^{-2}	0.12166175×10^{-1}

* The coefficients are actually T_{ij}'s. † One of the specification. ‡ Other specifications are $\omega_c = 0.5\pi$ and $\omega_d = 0.75\pi$.

Table 3.5 Comparison of Results by Several Analytical Methods and Optimization Method for Type-A Elliptical Cutoff Contour with $\omega_a = 0.25\pi$, and $\omega_b = 0.5\pi$.

Parameter	Scaled Approx. Solution* (3.20)&(2.20)	Scaling-free Approx. Solution (3.30)	Approx. Analytical Solution† (3.75)-(3.79b)	Analytical Solution‡ (2.60)	Scaled Optimum Solution* (3.8)&(2.20)
t_{00}	-0.45053527×10^{-1}	-0.45053527×10^{-1}	-0.44928233×10^{-1}	-0.43710115×10^{-1}	-0.43022895×10^{-1}
t_{01}	0.45053527×10^{-1}	0.45053527×10^{-1}	0.44928233×10^{-1}	0.43710115×10^{-1}	0.43022895×10^{-1}
t_{10}	0.78189295	0.78489295	0.78479150	0.78381859	0.78316725
t_{11}	0.21510705	0.21510705	0.21520550	0.21618141	0.21683275
ω_0'	0.12506553π	0.12500000π	0.12500000π	0.12500000π	0.12499336π
ω_0	0.25000000π†	0.12500000π	0.12500000π	0.12500000π	0.25000000π†
ω_1	–	–	0.18750000π	0.18281013π	–
$E_{2\ MSE}$	0.10917970×10^{-8}	0.39241793×10^{-8}	0.32063920×10^{-8}	0.13481930×10^{-10}	0.51017703×10^{-11}
$E_{2\ max}$	0.78802067×10^{-4}	0.78861587×10^{-4}	0.71129552×10^{-4}	0.55685973×10^{-5}	0.79826424×10^{-5}
$E_{1\ MSE}$	0.35394645×10^{-5}	0.14436219×10^{-6}	0.11773916×10^{-6}	0.10244047×10^{-8}	0.15402537×10^{-8}
$E_{1\ max}$	0.25426645×10^{-1}	0.44308185×10^{-3}	0.40275310×10^{-3}	0.70639645×10^{-4}	0.37611299×10^{-3}

* The coefficients are actually T_{ij}'s. † One of the specification. ‡ Other specifications are $\omega_c = 0.375\pi$ and $\omega_d = 0.5\pi$.

Table 3.6 Comparison of Results by Several Analytical Methods and Optimization Method for Type-A Elliptical Cutoff Contour with $\omega_c = 0.125\pi$, and $\omega_b = 0.25\pi$.

Comparing the results in Tables 3.5 and 3.6, it is observed that for all the methods, lower the frequency specifications, the smaller is the MSE. The scaled or scaling-free optimization method gives the best MSE results and it is followed in performance by the analytical method. The methods proposed in this chapter are approximations to these methods and they are simpler and the error performance is good. The advantages of approximation methods have already been discussed. The results for type-B contours with the same specifications are easily obtained by interchanging the t_{01} and the t_{10} values in Tables 3.5 and 3.6. The MSE and the maximum error values do not change.

3.14 SUMMARY

To overcome the problem of optimization techniques such as larger amount of computations and unreliability due to local minima, several analytical methods have been developed for finding the coefficients of the first-order McClellan transformation for the design of 2-D elliptically symmetric digital filters from 1-D digital filters. Two types of elliptically symmetric filters have been considered: those with vertical elliptical contours (type-A) and those with horizontal elliptical contours (type-B). Several new simple analytical formulas have been derived for calculating the coefficients by forcing the lower order significant terms in the power series expansion of the linear error function to zero. Specifically, the following methods have been developed. (i) Approximation Method for Type-A Contours, (ii) Scaling-free Approximation Method for Type-A Contours, (iii) Approximation Method for Type-B Contours, (iv) Scaling-free Approximation Method for Type-B Contours. (v) Analytical Method for Type-B Contours, (vi) Approximate Analytical Method for Type-A Contours, and (vii) Approximate Analytical Method for Type-B Contours.

In these methods, based on the locations of the extreme values of the McClellan transformation, there could be up to four different cases of coefficient evaluation. Even though the results of Method (i) are identical to those in [35], the derivation is different,

more straight forward, easy to understand, and useful in deriving the scaling-free formulas. The scaling-free formulas given in [35] are for the cases (ii) & (iii), and they are valid only when $\omega_0 = \omega_a$. But, the formulas derived in this chapter for type-A contour, in Method (ii), are for all the cases [(i)-(iv)], and the formulas for the cases (ii) & (iii) are valid even when $\omega_0 \neq \omega_a$. The advantages of the scaling-free formulas are that they give the scaling-free coefficients directly and the 1-D pass-band cutoff frequency ω_0 remains the same. On the other hand, the coefficients calculated by using the formulas of the approximation method require scaling and the 1-D pass-band cutoff frequency ω_0 changes after scaling. A simplified version of the formulas for the Methods (i) and (ii) has also been presented. They are useful for fast calculation of the coefficients, when the specifications satisfy some special conditions. Similarly, in Methods (iii) and (iv), new formulas have been derived for type-B contours. For a given 1-D and 2-D pass-band cutoff frequencies (ω_0 and ω_a & ω_b), the Methods (i)-(iv), provide the coefficients t_{ij}'s.

The analytical method for type-A contours in [34] has been extended to type-B contours in Method (v). The conditions and formulas have been presented. The results of this method are very close to those of the optimization methods. For a given 2-D frequency specifications ω_a & ω_b and ω_c & ω_d, the method gives the 1-D frequency specifications ω_0 and ω_s and the coefficients t_{ij}'s. They are chosen in such a way that the ratios of the transition- ratio and width of the 2-D filter to those of the 1-D filter are minimum. The total number of multiplications per output sample required to implement the designed filters are shown to be small. This is true for the Methods (ii), (iv), (vi), and (vii) as well. The Methods (vi) and (vii) are approximate analytical methods and they do not require a ROM lookup table or a numeric data processor for their hardware implementation. The formulas are directly in terms of the 2-D frequency specifications and can easily be implemented even on a general purpose signal processor.

For all the methods, formulas have been presented for the coefficients of both the cosine- and sine- form representations of the McClellan transformation. Also, many

examples have been provided to demonstrate the usefulness of the formuias. The error values of all the methods have been compared. For all the methods, lower the frequency specifications, the smaller is the mean square error. The results of the approximation methods agree well with those of the optimization and other analytical methods. Some filter design examples have been provided to illustrate the application of the formulas and the transformations. All the formulas presented in this chapter are extremely simple and they are suitable for real-time adaptive filter design and filtering applications. In the next two chapters, the approximation theory and some of the formulas of this chapter are used to find the coefficients for circularly symmetric filters and elliptically symmetric filters with arbitrary orientations.

CHAPTER 4

APPROXIMATION DESIGN OF 2-D CIRCULARLY SYMMETRIC DIGITAL FILTERS USING MCCLELLAN TRANSFORMATION

4.1 INTRODUCTION

In this chapter, some analytical methods are developed for finding the coefficients of the first-order McClellan transformation [17] for the design of 2-D circularly symmetric digital filters from 1-D digital filters. Existing unconstrained linear [27], [29]-[31] and nonlinear [4], [28] optimization methods give the optimum transformation coefficients; but, they are computationally very expensive. Therefore, these methods are not suitable for real-time adaptive design of 2-D digital filters. Fettweis's method [38] uses appropriate power series expansions and higher order transformations to fulfill the circular symmetry requirements for filters with arbitrary precision. Kurogochi and Makino's method [39] is similar in principle; but, it uses a modified McClellan transformation. In both the methods, the order of the designed filters is high, and they are not suitable for designing filters for use in real-time applications. Methods described in [17], [38], and [39] do not succeed in giving circular contours over a band of frequencies in the 2-D plane.

To overcome these problems, in this chapter, some analytical methods are presented which involve only very few computations [41]. Even though the results of these methods are approximate, they are still very close to those obtained by the optimization methods. Several new simple formulas are derived for finding the coefficients by forcing the lower order significant terms in the power series expansion of the linear error function to zero. Formulas are presented for both the original and the scaling-free McClellan transformation coefficients for all the three cases [(i)-(iii)] of circular cutoff (type-C) contours. Many examples are given. Some of the commonly used mappings and their advantages are discussed. The coefficients obtained by using the proposed

analytical methods approximate a circular contour with higher degree of accuracy than the McClellan's coefficients given by (2.57). Formulas are also derived for finding N-D McClellan transformation coefficients for the design of N-D approximately hyperspherically symmetric filters. The results of these methods agree well with the results of a recently proposed analytical method of [40] and the optimization methods. The accuracy of the formulas is sufficient for many engineering applications. The number of multiplications required to implement the designed filters is shown to be small.

4.2 Two-Dimensional Circularly Symmetric Digital Filters

Two-dimensional circularly symmetric digital filters have a lot of applications in the area of digital image processing such as smoothing, sharpening, and restoration of images. When the 2-D signal has equal spatial variation along all radial directions, the sampling rates along the spatial coordinates are same. To process such signals, 2-D circularly symmetric digital filters are employed.

The requirement of circular symmetry for 2-D filters is indeed necessary and sufficient for ensuring that a circularly symmetric input signal always leads to a circularly symmetric output signal. More generally, one can say that in such a filtering, rotating an arbitrary input signal does not produce any other effect except rotating the corresponding output signal.

4.3 Review of Existing Design Methods

4.3.1 Optimization Methods

The unconstrained, nonlinear and linear optimization methods have been discussed in Sec.s 3.3.2 and 3.3.3, respectively. The modifications for a circular contour are given below.

The equation of a desired circular pass-band cutoff contour (type-C contour) is

$$\omega_1^2 + \omega_2^2 = \omega_c^2 \tag{4.1}$$

where ω_1 and ω_2 are the 2-D frequency variables, and ω_e is the 2-D pass-band cutoff radius. From (4.1),

$$\begin{aligned}\omega_2 &= (\omega_e^2 - \omega_1^2)^{1/2} \qquad \omega_1 \leq \omega_e \\ &= G_d(\omega_1, \omega_e).\end{aligned} \tag{4.2}$$

The discrete set of frequency points on the ω_1-axis denoted as R_p in (3.5) and (3.8), is now defined in the range $0 \leq \omega_1 \leq \omega_e$. Eq. (3.6b) becomes

$$\begin{aligned}\cos(\omega_0) &= t_{00} + t_{01}\cos\{(\omega_e^2 - \omega_1^2)^{1/2}\} + t_{10}\cos(\omega_1) \\ &\quad + \{1 - (t_{00} + t_{01} + t_{10})\}\cos(\omega_1)\cos\{(\omega_e^2 - \omega_1^2)^{1/2}\} \\ &= G_l(\omega_1, \omega_e, t_{00}, t_{01}, t_{10}).\end{aligned} \tag{4.3}$$

The constrained optimization methods are computationally more expensive than the unconstrained optimization methods [4]. Both the methods exceed the arithmetic and/or speed capability of low cost, stand-alone 2-D signal processors and they are not suitable for real-time applications. The nonlinear optimization method normally provides a local minima rather than the global minima.

The McClellan's coefficients [17] given by (2.57) yield nearly circular contours for low values of ω (1-D frequency variable) and increasingly square contours for larger values of ω. Thus, the original McClellan transformation with these coefficients is quite useful for the design of low-pass or high-pass filters with a low cutoff radius. However, if either a large cutoff radius or a broad-band, band-pass or band-stop filter is required, it is not quite suitable, since it is not capable of providing circular contours in the transition region.

A solution to this problem, suggested by Mersereau *et al.* [27], is to find the coefficients using an optimization method, and if the desired accuracy cannot be obtained by employing a first-order transformation, one can use a higher order transformation. The use of higher order transformation will naturally result in a higher order filter. Ahmadi and King [31] have extended the methods of [17] and [27], to N-D low-pass filters with hyper-spherical cutoff boundary. Yan and Venetsanopoulos [29] have

designed 3-D low-pass and high-pass spherically symmetric FIR filters using this method. Venetsanopoulos and Zervakis [30] have applied symmetry conditions on the transformation, and used the linear optimization method to design 3-D fan- and spherically symmetric- FIR filters. They have observed that the imposition of symmetries is a good compromise between the realization cost and the quality of the filter.

It has been shown in [1] that the unconstrained nonlinear optimization method followed by scaling is computationally efficient and has some advantages over the unconstrained linear optimization method followed by scaling, which has been adopted in [27], [29], and [30]. Rajan and Swamy [28] have optimized the overall response of a circularly symmetric filter by using a nonlinear optimization technique and different transformations for different first- and second-order factors of the prototype 1-D filter in which only one parameter is varied. Even though nearly circular contours are obtained over a band of frequencies, the type of 2-D responses one can get is restricted in this method.

4.3.2 Analytical Methods

A different approach of determining the coefficients which will yield nearly circular contours at any specified cutoff radius in the 2-D plane, has been suggested by Fettweis [38]. This method uses higher order transformations for better circular symmetry, and does not succeed in providing circular contours over a band of frequencies in the 2-D plane. Also, the entire region in the (ω_1,ω_2)-plane outside the contour $\omega = \pi$, does not map onto a real frequency point on the ω-axis.

Kurogochi and Makino's method [39] is based on a modified McClellan transformation and presents the optimal coefficients for a specified cutoff radius in the form of a graph. The order of the filters designed by this method is high and they do not possess circular contours over a band of frequencies.

Hazra and Reddy [40] have proposed an analytical method for choosing the coefficients of a first-order McClellan transformation for the design of 2-D circularly

symmetric FIR filters. This method gives results very close to those obtained by the optimization methods which yield the optimum results. The better approximation of the circular contour is achieved by mapping an additional point on the 2-D cutoff contour *i.e.* $(\omega_e/\sqrt{2}, \omega_e/\sqrt{2})$ onto the 1-D cutoff frequency ω_0, and this is done by making ω_0 as one of the design parameters. Consequently, the response of the 2-D filter on the ω_1-axis and ω_2-axis will not be identical to the response of the 1-D filter. This method presents formulas for the 1-D pass-band and stop-band cutoff frequencies (ω_0 and ω_s), and the coefficients (t_{ij}'s) for a given 2-D pass-band and stop-band cutoff radii (ω_e and ω_f). Also, the method maximizes the 1-D transition-width, $\omega_s - \omega_0$ for a given 2-D transition-width, $\omega_f - \omega_e$.

4.4 Development of Analytical Methods for Circularly Symmetric Filters

In the following sections, some analytical methods are developed for finding the first-order McClellan transformation coefficients for the design of 2-D circularly symmetric digital filters from 1-D digital filters. Several new extremely simple analytical formulas, some of them are scaling-free, are presented for finding the coefficients. The results obtained by using these formulas, are close to those obtained by using the optimization method. It is shown through several examples that the formulas are, in fact, good approximate solutions to the linear optimization problem itself. Some of the commonly used mappings and their advantages are discussed. The coefficients obtained by the scaled approximation method are constants, and they approximate a circular contour with a higher degree of accuracy than the McClellan's coefficients given by (2.57). Formulas for finding N-D McClellan transformation coefficients are also presented. These filters have fewer number of multiplications per output sample compared to filters designed using the original McClellan transformation.

4.5 APPROXIMATION FOR COEFFICIENTS FOR TYPE-C CONTOURS

Assume that the 1-D pass-band cutoff frequency ω_0 is exactly mapped onto the desired 2-D circular pass-band cutoff contour (type-C contour) given by (4.1). For this contour, the linear error function given by (3.7) is now derived from (4.3). It can be rewritten using (3.12) and (2.3) as

$$\begin{aligned} &\frac{1}{2}\left[-\omega_0^2\left\{1-\frac{\omega_0^2}{12}\right\} + \omega_e^2\left\{1-\frac{\omega_e^2}{12}\right\}p_2\right] \\ &+\frac{\omega_1^2}{2}\left[p_1+\left\{\frac{\omega_e^2}{6}-1\right\}p_2-\frac{\omega_e^2}{2}t_{11}\right] \\ &-\frac{\omega_1^4}{24}\left[p_1+p_2-6t_{11}\right]=0. \end{aligned} \tag{4.4}$$

Since the error must be zero, the right side of (4.4) is taken to be zero. Equating the constant, ω_1^2, and ω_1^4 term coefficients to zero, the following equations are obtained.

$$\omega_e^2\left\{1-\frac{\omega_e^2}{12}\right\}p_2 = \omega_0^2\left\{1-\frac{\omega_0^2}{12}\right\} \tag{4.5}$$

$$p_1-\frac{\omega_e^2}{2}t_{11} = \left\{1-\frac{\omega_e^2}{6}\right\}p_2 \tag{4.6}$$

$$p_1-6t_{11} = -p_2 \tag{4.7}$$

Solving these equations simultaneously, yields,

$$p_1 = p_2 = K \tag{4.8a}$$

and

$$t_{11} = K/3 \tag{4.8b}$$

where

$$K = \frac{\omega_0^2\left\{1-\frac{\omega_0^2}{12}\right\}}{\omega_e^2\left\{1-\frac{\omega_e^2}{12}\right\}} \tag{4.8c}$$

From this derivation, it can be concluded that the analytical formulas given by (4.8) are approximate solutions to the linear optimization problem itself defined by (3.8). The above derivation is straight forward, easy to understand, and useful in deriving the

scaling-free formulas. The constant term and certain number of lower-order ω_1 terms, depending on the number of unknowns, are forced to assume a zero value. The higher-order ω_1 terms are also assumed to be zero, since their values are negligible, particularly for low frequencies. The approximate solution thus obtained agrees well with the optimal solution [52] and its accuracy is sufficient for many engineering applications. To prove these points, an example is given in an up-coming Sec. 4.5.4.

The formulas provide good accuracy when ω_0 and ω_e are much smaller than $\sqrt{12} \approx 1.1\pi$ rad./sec. For a given ω_0 and ω_e, let this condition be satisfied and let t_{ij}'s be the coefficients found by using the formulas. After scaling let T_{ij}'s be the scaled coefficients and ω_0' be the new 1-D pass-band cutoff frequency. For another 1-D pass-band cutoff frequency $\omega_p < \omega_0$, and for the same ω_e, different coefficients are obtained by using the formulas. However, it is observed that after scaling, the same scaled coefficients and approximately the same new 1-D pass-band cutoff frequency are obtained. Therefore, it is concluded that the same T_{ij}'s would transform a given $\omega_p < \omega_0$ into a circle.

4.5.1 Unscaled Coefficients

The formulas for the other coefficients *viz* t_{00}, t_{01}, and t_{11} are derived using the following procedure. Substituting the expressions of p_1 and p_2 given by (2.11a) and (2.11b), respectively, in (4.8a), and using the expression for t_{11} from (4.8b), the formulas for t_{10} and t_{01} are found. Using these formulas in (2.3), the formula for t_{00} is deduced The cosine form transformation coefficients are

$$t_{00} = 1 - (5K / 3), \quad t_{01} = t_{10} = 2K / 3, \quad \text{and} \quad t_{11} = K / 3 \tag{4.9}$$

and the corresponding sine-form transformation coefficients are

$$p_{00} = 0, \quad p_{01} = p_{10} = K, \quad \text{and} \quad p_{11} = 2K / 3 \tag{4.10}$$

where K is defined by (4.8c). It should be noted that the coefficients as obtained above

are directly in terms of the given frequency specifications, ω_0 and ω_e. The computations involved for finding these coefficients are less than those for the elliptical contours, and those for the circular contours in [40].

4.5.2 Scaled Coefficients

For all practical values of ω_0 and ω_e, $K > 0$, and therefore, $t_{01} = t_{10} > t_{11}$. The scaled cosine- and sine- form transformation coefficients are obtained by using (2.34) and (2.35), respectively, giving

$$T_{00} = T_{11} = 0.25, \quad T_{01} = T_{10} = 0.5 \tag{4.11}$$

and

$$P_{00} = 0, \quad P_{01} = P_{10} = 0.75, \quad P_{11} = -0.5. \tag{4.12}$$

It should be noted that these scaled coefficients are constants. They are independent of K, and therefore, they are independent of ω_0 and ω_e. After scaling, ω_0 changes to ω_0' as given by

$$\omega_0' = \cos^{-1}\left\{\frac{3}{4K}\{\cos(\omega_0) - 1\} + 1\right\}. \tag{4.13}$$

Since T_{ij}'s and P_{ij}'s are constants, only ω_0' has to be calculated for each specification.

4.5.3 Special Case

When the 1-D cutoff frequency, ω_0, is equal to the radius, ω_e, of the 2-D cutoff contour, $K = 1$, and the unscaled coefficients in (4.9) and (4.10) become

$$t_{00} = t_{01} = t_{10} = (2 / 3), \quad \text{and} \quad t_{11} = 1 / 3, \tag{4.14}$$

and

$$p_{00} = 0, \quad p_{01} = p_{10} = 1, \quad \text{and} \quad p_{11} = -(2 / 3), \tag{4.15}$$

respectively. The scaled coefficients in (4.11) and (4.12) are not affected. The formula for ω_0' reduces to

$$\omega_0' = \cos^{-1}\left\{\frac{1}{4}\{3\cos(\omega_0) + 1\}\right\}. \tag{4.16}$$

This simplified formula further reduces the computations for the specified special case.

The circular contour is a subclass of the elliptical contour, since when the minor- and major- axes cutoff frequencies are equal, *i.e.*

$$\omega_a = \omega_l = \omega_e \quad (\text{say}) \tag{4.17}$$

the elliptical contour becomes a circular contour, and thus, some of the above formulas can also be derived from the formulas for the elliptical contour in the previous chapter. For example, by substituting (4.17) in (3.13) or (3.33), (4.8) is obtained.

4.5.4 Comparison of Approximation and Optimization Methods

To demonstrate the accuracy of the above approximation of the coefficients, the same specifications as in Example 2.3 are used.

Example 4.1: The specifications for a type-C contour are $\omega_0 = 0.5\pi$ and $\omega_e = 0.5\pi$.

Nguyen and Swamy [52] minimized the objective function $J_2(t)$ as given by (3.8) in the least mean square sense and arrived at the following optimum results.

$$\begin{aligned} t_{00} &= -0.63773350 & t_{01} &= 0.63779480 \\ t_{10} &= 0.63778120 & t_{11} &= 0.36215750 \\ p_1 &= 0.99993870 & p_2 &= 0.99995230 \\ E_{2\,MSE} &= 0.99188318\times10^{-9} & E_{2\,\max} &= 0.61300000\times10^{-4} \\ E_{1\,MSE} &= 0.95960385\times10^{-6} & E_{1\,\max} &= 0.13864441\times10^{-1} \end{aligned}$$

The results obtained by using the simplified formula given by (4.14) are as follows.

$$\begin{aligned} t_{00} &= -0.66666667 & t_{01} &= 0.66666667 \\ t_{10} &= 0.66666667 & t_{11} &= 0.33333333 \\ p_1 &= 1.00000000 & p_2 &= 1.00000000 \\ E_{2\,MSE} &= 0.32630577\times10^{-4} & E_{2\,\max} &= 0.89285533\times10^{-2} \\ E_{1\,MSE} &= 0.69532636\times10^{-4} & E_{1\,\max} &= 0.13361769\times10^{-1} \end{aligned}$$

By comparing these error values, it is concluded that the results of the approximation method agree well with those of the optimization method. Fig. 4.1 shows the contours of the original McClellan transformation using the above unscaled optimized and approximated coefficients. It should be noted that in this example, ω_0 and ω_e are not so small. To see the effect of smaller values of the specifications, ω_0 and ω_e in the next example are reduced by a factor of 2.

4.5.5. Comparison of Approximation and Analytical Methods

Example 4.2: The specifications for a type-C contour are $\omega_0 = 0.25\pi$ and $\omega_e = 0.25\pi$.

Since the analytical method [40] gives results very close to those of the optimization method, in this example, the results of the approximation method are compared with those of the analytical method. The additional specification required for the analytical method is $\omega_f = 0.4\pi$. The results of this method are as follows.

$$\omega_0 = 0.21622507\pi \qquad \omega_s = 0.34197443\pi$$
$$t_{00} = -0.25789298 \qquad t_{01} = 0.50000000$$
$$t_{10} = 0.50000000 \qquad t_{11} = 0.25789298$$
$$E_{2\,MSE} = 0.28004852\times10^{-13} \qquad E_{2\,\max} = 0.27308599\times10^{-6}$$
$$E_{1\,MSE} = 0.80121456\times10^{-10} \qquad E_{1\,\max} = 0.12666750\times10^{-3}$$

It should be noted that the above coefficients are scaling-free coefficients. Therefore, these coefficients cannot be compared with the unscaled coefficients of approximation and optimization methods. However, the magnitude of the error will provide the basis of comparing this method with the approximation method. The results obtained by using the simplified formula given by (4.14) are as follows.

$$t_{00} = -0.66666667 \qquad t_{01} = 0.66666667$$
$$t_{10} = 0.66666667 \qquad t_{11} = 0.33333333$$
$$p_1 = 1.00000000 \qquad p_2 = 1.00000000$$
$$E_{2\,MSE} = 0.99728806\times10^{-8} \qquad E_{2\,\max} = 0.15681301\times10^{-1}$$
$$E_{1\,MSE} = 0.44774566\times10^{-7} \qquad E_{1\,\max} = 0.34122203\times10^{-3}$$

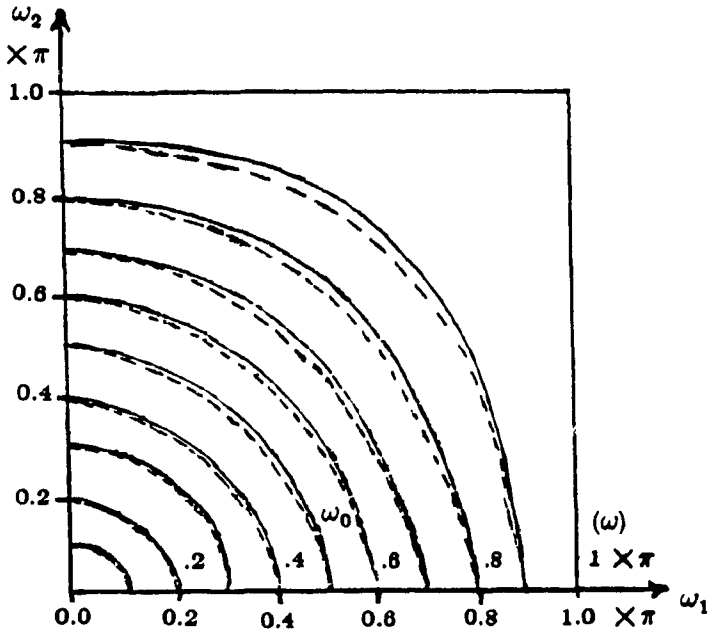

Fig. 4.1 Contours of the Original McClellan Transformation Obtained by Using the Unscaled Optimimum (Solid Line) and Approximated (Dotted Line) Coefficients in Example 4.1.

(The specifications for a type-C contour are $\omega_0 = 0.5\pi$ and $\omega_c = 0.5\pi$.)

By comparing the error values obtained in Examples 4.1 and 4.2, it is observed that both the methods gives better results for lower values of frequency specifications.

It should be pointed out that the basic difference between the optimization and approximation methods is that, while the optimization method finds the best fit to the overall shape of the circle, the approximation method gives a close fit to the four cutoff frequency points on the ω_1 and ω_2 axes of the circle. For this reason, the results of both the methods agree most in the values of p_1 and p_2. Finally, it should be pointed out that the approximation method is the simplest of all the existing methods.

4.6 Approximation for Scaling-Free Coefficients for Type-C Contours

Using the coefficients of the scaling-free transformations given by (2.51)-(2.54) in (4.5)-(4.7), the following three cases of scaling-free formulas are obtained.

Case (i):

The scaling-free coefficients are given directly by (2.49) and (2.50)

Case (ii):

The condition to be satisfied for this case is $\omega_0 = \omega_e$, and then, the scaling-free coefficient is given by

$$U = 2 / 3 \tag{4.18}$$

Case (iii):

$$U_{11} = \frac{\omega_0^2\left\{1 - \dfrac{\omega_0^2}{12}\right\}}{\omega_e^2\left\{1 - \dfrac{\omega_e^2}{12}\right\}} - \frac{1}{2} \tag{4.19}$$

Eq. (4.18) can also be obtained by using the condition of (4.17) in the scaling-free formulas given by (3.30) or (3.31) or (3.41) for elliptical contours.

Comparing the scaling-free transformations as given by (2.49)-(2 54) with the original transformations given by (2.1) and (2.8), the following cases of the scaling-free cosine- and sine- form transformation coefficients result.

Case (i):

$$t_{00} = t_{01} = t_{10} = 0, \quad \text{and} \quad t_{11} = 1 \tag{4.20}$$

$$p_{00} = 0, \quad p_{01} = p_{10} = 1 \quad \text{and} \quad p_{11} = -2 \tag{4.21}$$

Case (ii):

$$t_{00} = -U, \quad t_{01} = t_{10} = U, \quad \text{and} \quad t_{11} = 1 - U \tag{4 22}$$

$$p_{00} = 0, \quad p_{01} = p_{10} = 1, \quad \text{and} \quad p_{11} = 2(U - 1) \tag{4 23}$$

Case (iii):

$$t_{00} = -U_{11}, \quad t_{01} = t_{10} = 0.5, \quad \text{and} \quad t_{11} = U_{11} \tag{4.24}$$

$$p_{00} = 0, \quad p_{01} = p_{10} = 0.5 + U_{11} \quad \text{and} \quad p_{11} = -2U_{11}. \tag{4.25}$$

It should be emphasized that to determine the case and to select the corresponding scaling-free formulas for given specifications, the unscaled coefficients must first be evaluated by using (4.9) and Appendix C used.

4.6.1 Advantages

The advantage of the scaling-free formulas given by (4.18) and (4.19) is that they yield directly the scaling-free coefficients given in (4.20)-(4.25). Also, the 1-D pass-band cutoff frequency ω_0 remains the same. On the other hand, the coefficients evaluated by using (4.9) or (4.10), or the simplified formulas given by (4.14) or (4.15) require scaling which changes ω_0 to ω_0'.

4.6.2 Special Case

Under the special case $\omega_0 = \omega_e$, (4.19) becomes $U_{11} = 0.5$ and the coefficients in (4.24) become equal to those in (2.57), which are the original McClellan transformation coefficients for approximately circular contours. Therefore, the coefficients in (4.24) belong to a general class in the sense that ω_0 and ω_e need not be equal. The McClellan's coefficients given by (2.57) are, in fact, simplified scaling-free coefficients, which further reduce the computations for the special case of specification: $\omega_0 = \omega_e$.

4.6.3 Examples

Example 4.3: The specifications for a type-C contour are the same as in Example 4.1, *i.e.*, $\omega_0 = 0.5\pi$ and $\omega_e = 0.5\pi$.

In this example, since $\omega_0 = \omega_e$, the McClellan's coefficients given by (2.57) are obtained. The value of the U_{11} coefficient and other results obtained are as follow.

$$U_{11} = 0.50000000$$

$$E_{2\,MSE} = 0.73093292\times10^{-3} \qquad E_{2\,\max} = 0.42589350\times10^{-1}$$

$$E_{1\,MSE} = 0.19601775\times10^{-2} \qquad E_{1\,\max} = 0.72940096\times10^{-1}$$

Example 4.4: The specifications for a type-C contour are $\omega_0 = 0.43068820\pi$ and $\omega_e = 0.5\pi$.

In this example $\omega_0 \neq \omega_e$. Using the scaling-free formula given by (4.19) for type-C contours, the following results are obtained.

$$U_{11} = 0.29396723$$

$$E_{2\,MSE} = 0.81305446\times10^{-4} \qquad E_{2\,\max} = 0.99999882\times10^{-2}$$

$$E_{1\,MSE} = 0.55420406\times10^{-3} \qquad E_{1\,\max} = 0.15688316$$

Example 4.5: The specifications for a type-C contour are $\omega_0 = 0.25\pi$ and $\omega_e = 0.25\pi$, which are the same as in Example 4.2.

Since $\omega_0 = \omega_e$, the McClellan's coefficients given by (2.57) are obtained. In this case, the following are the results.

$$U_{11} = 0.50000000$$

$$E_{2\,MSE} = 0.52615227\times10^{-5} \qquad E_{2\,max} = 0.36075431\times10^{-2}$$

$$E_{1\,MSE} = 0.55309631\times10^{-4} \qquad E_{1\,max} = 0.78441580\times10^{-1}$$

Example 4.6: The specifications for a type-C contour are $\omega_0 = 0.21622507\pi$ and $\omega_e = 0.25\pi$.

Since $\omega_0 \neq \omega_e$, (4.19) is used, and the following results are obtained.

$$U_{11} = 0.25826564$$

$$E_{2\,MSE} = 0.11311613\times10^{-7} \qquad E_{2\,max} = 0.10914410\times10^{-3}$$

$$E_{1\,MSE} = 0.13123175\times10^{-6} \qquad E_{1\,max} = 0.20620254\times10^{-2}$$

In all the above examples, the scaling-free coefficients for the cosine- and sine- form transformations are obtained by substituting the value of U_{11} in (4.24) and (4.25), respectively.

The scaled coefficients of the optimum and/or approximation solutions in Examples 4.1 and 4.2 can be obtained by using (2.34). After scaling, $\omega_0' \approx 0.42\pi$. The scaled coefficients for the approximation solution are, in fact, constants and they are given by (4.11). Fig. 4.2 shows the contours of the original McClellan transformation using the scaled optimized and approximated coefficients.

4.7 Approximation of Analytical Method for Type-C Contours

Hazra and Reddy [40] have proposed an analytical method for finding the McClellan transformation coefficients for circular cutoff (type-C) contours. The advantages and differences of this method, when compared to the other analytical methods [38] and [39], have been discussed in Sec. 4.3.2. The formulas given by (2.58) and (2.59) used to find the McClellan transformation coefficients for 2-D circularly symmetric (type-C) digital filters are now approximated to very simple forms providing certain implementation advantages as discussed in Sec. 3.10.

Using (3.73), the equations for type-C contours in [40] are approximated as

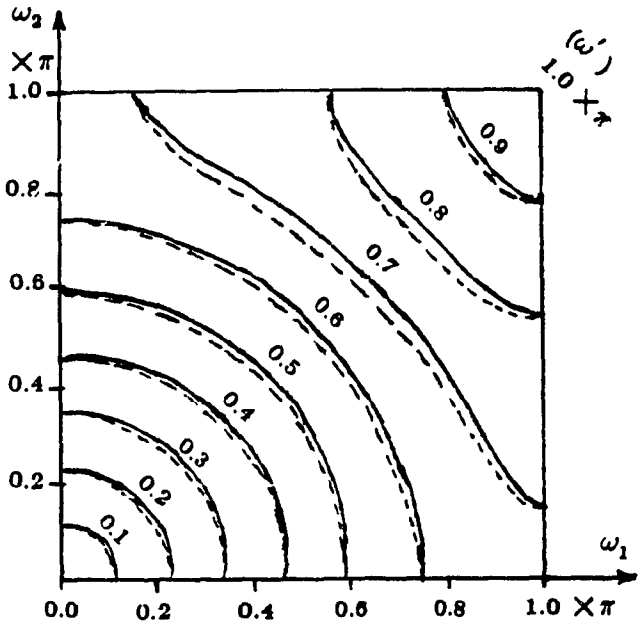

Fig. 4.2 Contours of the Original McClellan Transformation Obtained by Using the Scaled Optimimum (Solid Line) and Approximated (Dotted Line) Coefficients in Table 4.1.

(The specifications for a type-C contour are $\omega_0 = 0.5\pi$ and $\omega_c = 0.5\pi$. After scaling, $\omega_0' \approx 0.42\pi$.)

$$a = (\omega_0^2 / 4)\{1 - (\omega_0^2 / 12)\} \tag{4.26a}$$
$$b = (\omega_c^2 / 4)\{1 - (\omega_c^2 / 12)\} \tag{4.26b}$$
$$c = (\omega_c^2 / 8)\{1 + (\omega_c^2 / 24)\} \tag{4.26c}$$
$$d = (\omega_s^2 / 4)\{1 - (\omega_s^2 / 12)\} \tag{4.26d}$$
$$e = (\omega_f^2 / 4)\{1 - (\omega_f^2 / 12)\}. \tag{4.26e}$$

The quantities g and d have been defined in [40] as

$$g = 2 + \{(b - 2c) / c^2\} \tag{4.27}$$
$$d = e / g. \tag{4.28}$$

Eq.s (4.26) and (4.27) are substituted in (2.58) and (2.59) and the resulting equations are simplified by neglecting sixth- and higher- order terms. Finally, using binomial series and simplifying further, the following results are obtained.

$$\omega_0 = (\sqrt{3} / 2)\omega_c \tag{4.29}$$
$$\omega_s = (\sqrt{3} / 2)\omega_f . \tag{4.30}$$

The cosine-form transformation coefficients are

$$-t_{00} = t_{11} = (1 / 4)\{1 + (\omega_c^2 / 8)\}, \quad \text{and} \quad t_{01} = t_{10} = 0.5 \tag{4.31}$$

The corresponding sine-form transformation coefficients are

$$p_{00} = 0, \quad p_{01} = p_{10} = (3 / 4)\{1 + (\omega_c^2 / 24)\}, \quad \text{and}$$
$$p_{11} = (-1 / 2)\{1 + (\omega_c^2 / 8)\}. \tag{4.32}$$

The above formulas are directly in terms of the given 2-D frequency specifications, and very simple to use, and they provide good accuracy for lower values of cutoff frequencies.

4.7.1 Comparison of Approximate and Exact Analytical Methods

In order to illustrate the points mentioned above, some examples are given below.

Example 4.7: The specifications for a 2-D circularly symmetric (type-C) digital filter are $\omega_c = 0.5\pi$ and $\omega_f = 0.65\pi$.

Using the approximate formulas given by (4.29)-(4.31), the following results are obtained.

$$\omega_0 = 0.43301270\pi \qquad \omega_s = 0.56291651\pi$$
$$t_{00} = -0.32710628 \qquad t_{01} = 0.50000000$$
$$t_{10} = 0.50000000 \qquad t_{11} = 0.32710628$$
$$E_{2\,MSE} = 0.10030168\times10^{-2} \qquad E_{2\,\max} = 0.36003153\times10^{-1}$$
$$E_{1\,MSE} = 0.56523184\times10^{-2} \qquad E_{1\,\max} = 0.34903858$$

Using the exact formulas given by (2.59), (4.27), and (4.28), the following results are obtained.

$$\omega_0 = 0.43068820\pi \qquad \omega_s = 0.54467197\pi$$
$$t_{00} = -0.28396723 \qquad t_{01} = 0.50000000$$
$$t_{10} = 0.50000000 \qquad t_{11} = 0.28396723$$
$$E_{2\,MSE} = 0.18774845\times10^{-8} \qquad E_{2\,\max} = 0.70236681\times10^{-4}$$
$$E_{1\,MSE} = 0.94687513\times10^{-8} \qquad E_{1\,\max} = 0.26214851\times10^{-3}$$

Comparing the above two results, it is observed that the results of the approximate analytical method agree well with those of the exact analytical method. Also, it should be noted that in this example, ω_e and ω_f are not so small. To see the effect of smaller values of these critical frequencies, in the next example, the values of ω_e and ω_f are reduced by a factor of 2 and the value of the transition-width is kept the same .

Example 4.8: The specifications for a 2-D circularly symmetric (type-C) digital filter are $\omega_e = 0.25\pi$ and $\omega_f = 0.4\pi$.

Using the approximate formulas given by (4.29)-(4.31), the following results are obtained.

$$\omega_0 = 0.21650635\pi \qquad \omega_s = 0.34641016\pi$$
$$t_{00} = -0.26927657 \qquad t_{01} = 0.50000000$$
$$t_{10} = 0.50000000 \qquad t_{11} = 0.26927657$$
$$E_{2\,MSE} = 0.72333961\times10^{-5} \qquad E_{2\,\max} = 0.27787106\times10^{-2}$$
$$E_{1\,MSE} = 0.10689203\times10^{-3} \qquad E_{1\,\max} = 0.78441580\times10^{-1}$$

Results using the exact formulas have been given in Example 4.2. Comparing the two sets of results, once again it is observed that the results of the approximate analytical method agree well with those of the exact analytical method. By comparing the error values of the above Examples 4.7 and 4.8, it is seen that the approximate analytical method gives better results for lower values of frequency specifications, and it is simpler than the exact analytical method.

4.8 Mapping Conditions

Mapping conditions are useful to reduce the number of independent coefficients, to derive formulas which guarantee certain mappings, and to predict the error performance of the transformation along a particular direction in the (ω_1,ω_2)-plane. Here, some of the mappings and the resulting conditions are discussed, and some examples for the elliptical and circular contours are given.

4.8.1 Mapping Conditions for Cosine-Form Transformation

Consider the 1-D to 2-D mapping $\omega \rightarrow (\omega_1,\omega_2)$ given by (2.1). Some of the commonly used mappings in 2-D filter design and the resulting conditions are given below.

	Mapping	Condition	
1)	$0 \rightarrow (0,0)$	Given by (2.3).	
2)	$\pi \rightarrow (\pi,\pi)$	Given by (2.56).	
3)	$\omega \rightarrow (\omega_1,0)$	$t_{00} + t_{01} = 0$	(4.33a)
		$t_{10} + t_{11} = 1$	(4.33b)
4)	$\omega \rightarrow (0,\omega_2)$	$t_{00} + t_{10} = 0$	(4.34a)
		$t_{01} + t_{11} = 1$	(4.34b)
5)	$\omega \rightarrow (\omega_1,\omega_1)$	$t_{00} = 0$	(4.35a)
or	$\omega \rightarrow (\omega_2,\omega_2)$	$t_{11} = 0$	(4.35b)

$$i.e. \quad \omega_2 = \omega_1 \qquad\qquad t_{01} + t_{10} = 1 \tag{4.35c}$$

Mappings 1) and 2) when applied together, the equivalent conditions are obtained from (2.3) and (2.56), and they are:

$$t_{00} + t_{11} = 0 \qquad \text{and} \qquad t_{01} + t_{10} = 1. \tag{4.36}$$

Similarly, when the mappings 3) and 4) are applied together the equivalent condition is

$$-t_{00} = t_{01} = t_{10} = 1 - t_{11}. \tag{4.37}$$

Thus, the equivalent conditions can be derived for several other combinations of mapping assumptions. If the transformation coefficients satisfy the conditions derived, then the assumed mappings are guaranteed. It has been shown previously that (2.3) reduces the number of independent coefficients from 4 to 3. Similarly, (4.36) reduces the number of independent coefficients from 4 to 2 and (4.37) from 4 to 1.

Example 4.9: Consider the coefficients of a type-A elliptical contour for the cases (ii) and (iii), which satisfy (2.41). The coefficient relationships are

$$-t_{00} = t_{01} \qquad \text{and} \qquad t_{10} = 1 - t_{11}. \tag{4.38}$$

The coefficients satisfy the conditions given by (2.3) and (4.33), and hence, the mappings 1) and 3) are assured. The 1-D origin is mapped onto the 2-D origin, and the 1-D frequency response is preserved only on the ω_1-axis, but not on the ω_2-axis.

To satisfy the mappings 2) and 4), the required condition is obtained from (2.56) and (4.34), and it is given by: $-t_{00} = t_{10} = t_{11} = 1 - t_{01}$.

Example 4.10: Consider the coefficients of a type-B elliptical contour for the cases (ii) and (iii), which satisfy (2.47). The coefficient relationships are

$$-t_{00} = t_{10} \qquad \text{and} \qquad t_{01} = 1 - t_{11}. \tag{4.39}$$

The coefficients satisfy the conditions (2.3) and (4.34), and hence, the mappings 1) and 4) are assured. The 1-D origin is mapped onto the 2-D origin, and the 1-D frequency response is preserved on the ω_2-axis, but not on the ω_1-axis.

To satisfy the mappings 2) and 3), the required condition is obtained from (2.56) and (4.33), and it is given by: $-t_{00} = t_{01} = t_{11} = 1 - t_{10}$.

Example 4.11: Consider the coefficients of a circular (type-C) contour for the case (iii), which satisfy (2.53). The coefficient relationships are

$$-t_{00} = t_{11} \qquad \text{and} \qquad t_{01} = t_{10} = 0.5. \tag{4.40}$$

The coefficients satisfy the conditions given by (2.3) and (2.56), and hence, the mappings 1) and 2) are assured. Also, the condition given by (4.35c) is satisfied, and hence, the mapping 5) is approximately satisfied. The value of $-t_{00} = t_{11}$ serves as a measure of the mapping error along the diagonal $\omega_2 = \omega_1$.

Example 4.12: The McClellan's coefficients for approximately circular contours given by (2.57) are obtained by solving (4.36) and (4.37). Therefore, the mappings 1)-4) are assured. The condition given by (4.35c) is satisfied, and hence, the mapping 5) is approximately satisfied. The value of $-t_{00} = t_{11}$ in (2.57) is greater than that in (4.11). Therefore, for the contours along the diagonal $\omega_2 = \omega_1$, the McClellan's coefficients given by (2.57) will result in more mapping error than that for the coefficients given by (4.11). However, the former coefficients map the 1-D frequency exactly on the ω_1 and ω_2 axes, while the latter coefficients do the same approximately.

4.8.2 Error Function for the Diagonal Line

An error function $E(\omega)$ for the diagonal $\omega_2 = \omega_1$ can be written as

$$E(\omega) = \cos(\omega) - \{t_{00} + (t_{01} + t_{10})\cos(\omega) + t_{11}\cos^2(\omega)\}. \tag{4.41}$$

Fig. 4.3 illustrates $E(\omega)$ for the coefficients given by (2.57) and (4.11) The curves are symmetrical with respect to the vertical line at $\omega = 0.5\pi$. From the figure it is observed that the maximum error for the McClellan's coefficients given by (2.57) is twice the maximum error for the proposed coefficients given by (4.11). Thus, the assertion made in Example 4.12 is verified to be correct. Fig. 4.4 illustrates the contours of the original

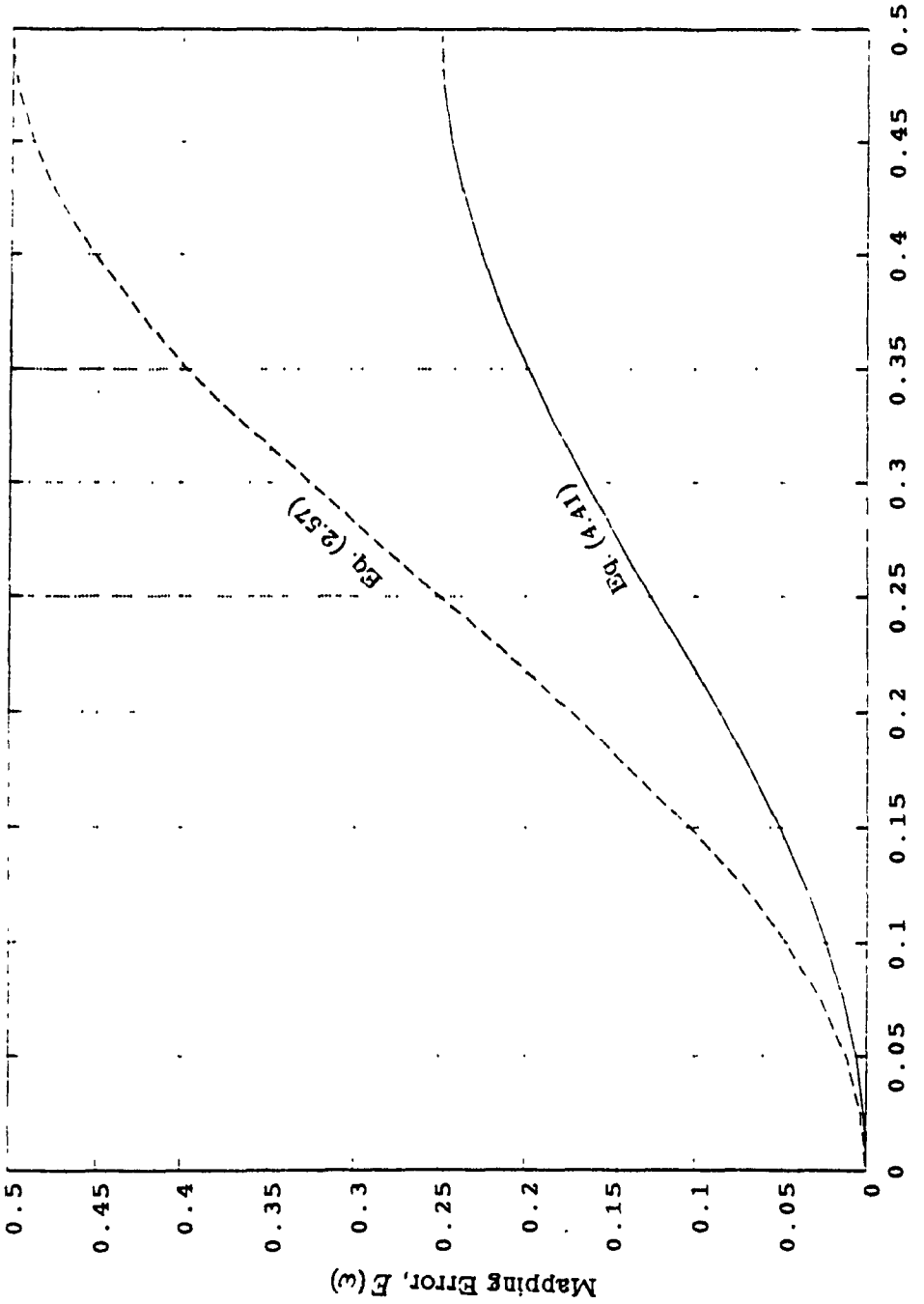

Fig. 4.3 Mapping Error, $E(\omega)$, (Eq. (1.11)) Along the Diagonal $\omega_2 = \omega_1$ for the McClellan's Coefficients (Eq. (2.57)) and the Proposed Coefficients (Eq. (4.11)).

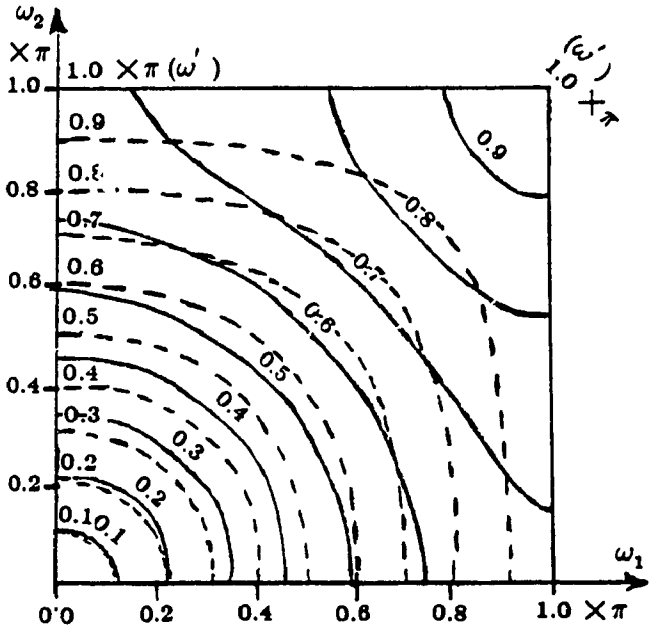

Fig. 4.4 Contours of the Original McClellan Transformation Obtained by Using the McClellan's Coefficients (Eq. (2.57); Dotted Line) and the Proposed Coefficients (Eq. (4.11); Solid Line).

McClellan transformation using the coefficients given by (2.57) and (4.11), respectively.

4.8.3 Mapping Conditions for Arbitrary Angles

The equation of a line passing through the origin in the (ω_1,ω_2)-plane is $\omega_2 = \tan(\theta)\omega_1$ where θ is the angle of inclination of the line measured from the ω_1-axis in the anticlockwise direction. Substituting this expression in (2.1), yields

$$\cos(\omega) = t_{00} + t_{01}\cos\{\tan(\theta)\omega_1\} + t_{10}\cos(\omega_1) + t_{11}\cos(\omega_1)\cos\{\tan(\theta)\omega_1\}. \quad (4.42)$$

From (4.42), the conditions for an exact mapping with an arbitrary angle can be derived. For example, when $\theta = \pi / 4$ and the mapping is exact, (4.42) gives the same conditions as given by (4.35).

4.8.4 Mapping Conditions for Sine-Form Transformation

The equivalent mapping conditions for the sine-form transformation are given below.

	Mapping	Condition	
1)	$0 \rightarrow (0,0)$	$p_{00} = 0$	(4.43)
2)	$\pi \rightarrow (\pi,\pi)$	$p_{00} + p_{01} + p_{10} + p_{11} = 1$	(4.44)
3)	$\omega \rightarrow (\omega_1,0)$	$p_{00} = 0$	(4.45a)
		$p_{10} = 1$	(4.45b)
4)	$\omega \rightarrow (0,\omega_2)$	$p_{00} = 0$	(4.46a)
		$p_{01} = 1$	(4.46b)
5)	$\omega \rightarrow (\omega_1,\omega_1)$	$p_{00} = 0$	(4.47a)
	or $\omega \rightarrow (\omega_2,\omega_2)$	$p_{11} = 0$	(4.47b)
	i.e. $\omega_2 = \omega_1$	$p_{01} + p_{10} = 1$	(4.47c)

For the mappings 1) and 2) the condition is

$$p_{01} + p_{10} + p_{11} = 1. \tag{4.48}$$

For the mappings 3) and 4) the conditions are

$$p_{00} = 0 \qquad \text{and} \qquad p_{01} = p_{10} = 1. \tag{4.49}$$

Similarly, the equivalent conditions can be derived for several other combinations of mapping assumptions.

4.9 Implementation of 2-D Circularly Symmetric Digital Filters

For a 2-D circularly symmetric digital filter (type-C), the original McClellan transformation (2.1) defined by (2.59) can be written as

$$\cos(\omega) = -U_7 + 0.5\cos(\omega_2) + 0.5\cos(\omega_1) + U_7\cos(\omega_1)\cos(\omega_2) \tag{4.50}$$

where

$$U_7 = -0.5 + g^{-1}$$

The 2-D filters obtained by the transformation above can be implemented by using the scheme described in [16]. While counting the number of multiplications, the multiplications by a power of 2 are not counted since, they are done by bit shifting. The total number of multiplications per output sample for a filter of order M×M is M.

The McClellan transformation defined by using the coefficients in (4.24) and (4.31) can also be written in the form of (4.50). Therefore, the 2-D filters obtained by using them will also have M multiplications per output sample.

4.10 N-Dimensional McClellan Transformation

4.10.1 N-D Original McClellan Transformation

The N-D original McClellan transformation of order $I_1 \times I_2 \times \cdots \times I_N$ is given by

$$\begin{aligned}\cos(\omega) &= \sum_{i_1=0}^{I_1} \sum_{i_2=0}^{I_2} \cdots \sum_{i_N=0}^{I_N} t_{i_1 i_2 \cdots i_N} \cos(i_1\omega_1)\cos(i_2\omega_2) \cdots \cos(i_N\omega_N) \\ &= F_O(\omega_1, \omega_2, \cdots, \omega_N)\end{aligned} \tag{4.51}$$

where $t_{i_1 i_2 \cdots i_N}$'s are the N-D original McClellan transformation coefficients. For $0 \leq \omega \leq \pi$, the left side of (4.51) *i.e.* $\cos(\omega)$ varies between -1 and 1. Therefore, the right side of (4.51) must satisfy the constraint

$$| F_O(\omega_1,\omega_2,\cdots,\omega_N) | \leq 1, \quad 0 \leq \omega_i \leq \pi, \quad i = 1,2,...,N. \tag{4.52}$$

4.10.2 N-D Generalized McClellan Transformation

The transformation given by (4.51) contains only cosine terms and, therefore, can produce only quadrantally symmetric frequency response. For filters with general frequency response, one should use the generalized transformation which has sine terms also [50]. The *N-D generalized McClellan transformation* of order $I_1 \times I_2 \times \cdots \times I_N$ is given by

$$\begin{aligned}\cos(\omega) = & \sum_{i_1=0}^{I_1} \sum_{i_2=0}^{I_2} \cdots \sum_{i_N=0}^{I_N} t_{i_1 i_2 \cdots i_N} \cos(i_1\omega_1)\cos(i_2\omega_2)\cdots\cos(i_N\omega_N) \\ & + \sum_{i_1=1}^{I_1} \sum_{i_2=1}^{I_2} \cdots \sum_{i_N=1}^{I_N} s_{i_1 i_2 \cdots i_N} \sin(i_1\omega_1)\sin(i_2\omega_2)\cdots\sin(i_N\omega_N) \\ = & F_G(\omega_1,\omega_2,\cdots,\omega_N)\end{aligned} \tag{4.53}$$

where $t_{i_1 i_2 \cdots i_N}$'s and $s_{i_1 i_2 \cdots i_N}$'s are the N-D generalized McClellan transformation coefficients. For $0 \leq \omega \leq \pi$, the left side of (4.53) *i.e.* $\cos(\omega)$ varies between -1 and 1. Therefore, the right side of (4.53) must satisfy the constraint

$$| F_G(\omega_1,\omega_2,\cdots,\omega_N) | \leq 1, \quad 0 \leq \omega_i \leq \pi, \quad i = 1,2,...,N. \tag{4.54}$$

4.10.3 Formulas for N-D McClellan Transformation Coefficients

The 2-D original McClellan transformation used in the design of 2-D approximately circularly symmetric digital filters is given by (2.1) in which the values of the coefficients are as in (2.57) [17], *i.e.*

$$\cos(\omega) = -0.5 + 0.5\cos(\omega_1) + 0.5\cos(\omega_2) + 0.5\cos(\omega_1)\cos(\omega_2). \tag{4.55}$$

Using the trigonometric identity

$$\cos(x) = 2\cos^2(x/2) - 1 \tag{4.56}$$

in (4.55), rearranging, and then taking the square root of both sides, yields,

$$\cos(\omega/2) = \prod_{i=1}^{2} \cos(\omega_i/2). \tag{4.57}$$

The advantages of (4.57) are that it has a simpler form than (4.55), and it can easily be generalized to N-D ($N \geq 2$). The essential properties of (4.55) can also be derived from (4.57).

The N-D first-order original McClellan transformation used in the design of N-D approximately hyper-spherically symmetric digital filters is obtained by replacing the upper limit 2 of the product in (4.57) by N, giving

$$\cos(\omega/2) = \prod_{i=1}^{N} \cos(\omega_i/2). \tag{4.58}$$

In [49], this equation is written erroneously with a summation sign. Squaring both sides of this equation, using the trigonometric identity

$$\cos^2(x/2) = \{1 + \cos(x)\} / 2, \tag{4.59}$$

and rearranging, yields,

$$\cos(\omega) = -1 + 2^{1-N} \prod_{i=1}^{N} \{1 + \cos(\omega_i)\}. \tag{4.60}$$

Eq. (4.60) is a generalization of (4.55) to N-D, and it maintains the essential properties of (4.55). For example, the N-D basic frequency range $|\omega_i| \leq \pi$ ($i = 1$ to N) is mapped onto the 1-D basic frequency range $|\omega| \leq \pi$. Also, in this range, the mapping is convex *i.e.* when $|\omega_i|$ ($i = 1$ to N) increase monotonically from 0 to π, $|\omega|$ also increases monotonically from 0 to π. In (4.60), $\omega = 0$ when $\omega_i = 0$ for $i = 1$ to N, and $|\omega| = \pi$ when any $|\omega_i|$'s is equal to π.

Replacing all the cosine terms in (4.60) by their power-series expansion (using (3.11)) and neglecting all terms of order 4 and higher, (4.60) reduces to

$$\omega = (\omega_1^2 + \omega_2^2 + \cdots + \omega_N^2)^{1/2}. \tag{4.61}$$

This equation shows that the required hyper-spherical symmetry is obtained at least in the neighborhood of the N-D origin in the $(\omega_1,\omega_2, \cdots \omega_N)$-plane.

Consider the N-D first-order original McClellan transformation *i.e.* (4.51) in which $I_1 = I_2 = \cdots = I_N = 1$. The formulas for finding its coefficients for the design of N-D approximately spherically symmetric digital filters are obtained by comparing this transformation with (4.60). In the case of three dimensions, the following values for the coefficients are obtained.

$$t_{000} = -0.75\ ; \quad t_{001} = t_{010} = \cdots = t_{111} = 0.25 \tag{4.62}$$

In the case of four dimensions, the following values for the coefficients are obtained.

$$t_{0000} = -0.875\ ; \quad t_{0001} = t_{0010} = \cdots = t_{1111} = 0.125 \tag{4.63}$$

The results can be generalized to the N-dimensional case, giving the following formulas.

$$t_{00\cdots0} = -1 + 2^{1-N} \tag{4.64a}$$

$$t_{i_1 i_2 \cdots i_N} = 2^{1-N} \quad (i_1,i_2, \cdots ,i_N) \in (0, 1), (i_1,i_2, \cdots ,i_N) \neq (0.0, \cdots ,0) \tag{4.64b}$$

4.10.4 Sine-Form N-D Original McClellan Transformation

The *sine-form N-D original McClellan transformation* of order $I_1 \times I_2 \times \cdots \times I_N$ is obtained by replacing the cosine terms in (4.51) by their equivalent sine terms. It is given by

$$\sin^2(\omega/2) = \sum_{i_1=0}^{I_1} \sum_{i_2=0}^{I_2} \cdots \sum_{i_N=0}^{I_N} p_{i_1 i_2 \cdots i_N} \sin^{2i_1}(\omega_1/2) \sin^{2i_2}(\omega_2/2) \cdots \sin^{2i_N}(\omega_N/2)$$

$$= G_O(\omega_1,\omega_2, \cdots ,\omega_N) \tag{4.65}$$

where $p_{i_1 i_2 \cdots i_N}$'s are the transformation coefficients. The advantages of this form were outlined in Sec. 2.2.2.

4.10.5 Sine-Form N-D Generalized McClellan Transformation

The *sine-form N-D generalized McClellan transformation* of order $I_1 \times I_2 \times \cdots \times I_N$ is obtained by replacing the cosine terms in (4.53) by their equivalent sine terms and it is given by

$$\sin^2(\omega/2) = \sum_{i_1=0}^{I_1} \sum_{i_2=0}^{I_2} \cdots \sum_{i_N=0}^{I_N} p_{i_1 i_2 \cdots i_N} \sin^{2i_1}(\omega_1/2) \sin^{2i_2}(\omega_2/2) \cdots \sin^{2i_N}(\omega_N/2)$$
$$+ \sum_{i_1=1}^{I_1} \sum_{i_2=1}^{I_2} \cdots \sum_{i_N=1}^{I_N} q_{i_1 i_2 \cdots i_N} \sin(i_1\omega_1) \sin(i_2\omega_2) \cdots \sin(i_N\omega_N)$$
$$= G_G(\omega_1, \omega_2, \cdots, \omega_N) \tag{4.66}$$

where $p_{i_1 i_2 \cdots i_N}$'s and $q_{i_1 i_2 \cdots i_N}$'s are the transformation coefficients. This transformation is suitable for the design of N-D filters with arbitrary frequency responses.

4.10.6 Formulas for Sine-Form N-D McClellan Transformation Coefficients

The sine-form N-D first-order original McClellan transformation used in the design of N-D approximately hyper-spherically symmetric digital filters is derived by squaring both sides of (4.58), using the trigonometric identity

$$\cos^2(x/2) = 1 - \sin^2(x/2), \tag{4.67}$$

and rearranging. It is given by

$$\sin^2(\omega/2) = 1 - \prod_{i=1}^{N} \{1 - \sin^2(\omega_i/2)\}. \tag{4.68}$$

Consider the sine-form N-D first-order original McClellan transformation given by (4.65) with $I_1 = I_2 = \cdots = I_N = 1$. The formulas for finding the coefficients are obtained by comparing this transformation with (4.68). The values of the sine-form transformation coefficients corresponding to the 2-D cosine-form transformation coefficients in (2.57) are given by

$$p_{00} = 0, \quad p_{01} = p_{10} = 1, \quad \text{and} \quad p_{11} = -1. \tag{4.69}$$

In the case of three dimensions, the following values for the coefficients are obtained

$$p_{000} = 0\,; \quad p_{001} = p_{010} = p_{100} = p_{111} = 1\,; \quad p_{011} = p_{101} = p_{110} = -1 \tag{4.70}$$

In the case of four dimensions, the following values for the coefficients are obtained.

$$p_{0000} = 0\,; \quad p_{0001} = p_{0010} = p_{0100} = p_{0111} = p_{1000} = p_{1011} = p_{1101} =$$
$$p_{1110} = 1\,; \quad p_{0011} = p_{0101} = p_{0110} = p_{1001} = p_{1010} = p_{1100} = p_{1111} = -1 \qquad (4.71)$$

The results can be generalized to the N-dimensional case, giving the following formulas given below.

$$p_{00\cdots0} = 0 \qquad (4.72a)$$

$$p_{i_1 i_2 \cdots i_N} = 1 \; (i_1, i_2, \cdots, i_N) \in (0, 1), \; (i_1 + i_2 + \cdots + i_N) = 1, 3, 5, \ldots \qquad (4.72b)$$

$$p_{i_1 i_2 \cdots i_N} = -1 \; (i_1, i_2, \cdots, i_N) \in (0, 1), \; (i_1 + i_2 + \cdots + i_N) = 2, 4, 6, \ldots \qquad (4.72c)$$

4.10.7 Optimality of N-D Digital Filters

McClellan [17] has shown that if the 1-D prototype filter is optimal in the Chebyshev sense, the 2-D filters obtained by the transformation given by (4.55) are also optimal in the Chebyshev sense. Here, it is proved that the N-D transformation given by (4.58) or the first-order version of (4.51) in which the values of the coefficients are given by (4.64) possesses the same property.

For convenience, (4.58) is used for the proof. Consider the mapping $\omega \rightarrow (\omega_1, \omega_2, \ldots, \omega_k, \ldots, \omega_N)$ in (4.58). When $\omega_j = 0$, $(j = 1,2,\ldots N;\ j \neq k)$ the N-D frequency response on the ω_k-axis is exactly same as the 1-D frequency response on the ω-axis. So, the deviation of the 1-D filter is a lower bound for the deviation of the N-D filter. Also, since the N-D transformation preserves the equiripple nature of the error, the deviation of the N-D response is equal to this lower bound, and if the 1-D prototype filter is optimal in the Chebyshev sense, the N-D filter is also optimal in the Chebyshev sense.

4.11 Comparison of Analytical and Optimization Methods

To compare several methods the same problem is solved and the same type of error values are computed by all the methods. The results obtained for a circular cutoff (type-C) contour with $\omega_c = 0.5\pi$ are summarized in Table 4.1. Comparing these results,

Parameter	Scaled Approx. Solution* (4.11)&(4.16)	McClellan's Coefficients (2.57)	Approx. Analytical Solution† (4.29)&(4.31)	Analytical Solution† (2.59)	Scaled Optimum Solution* + (3.8)&(2.34)	Scaling-free Approx. Solution (4.19)	Scaling-free Approx. Solution (4.19)
t_{00}	− 0.25000000	− 0.50000000	− 0.32710628	− 0.28396723	− 0.28391684	− 0.29396723	− 0.25807535
t_{01}	0.50000000	0.50000000	0.50000000	0.50000000	0.50000533	0.50000000	0.50000000
t_{10}	0.50000000	0.50000000	0.50000000	0.50000000	0.49999467	0.50000000	0.50000000
t_{11}	0.25000000	0.50000000	0.32710628	0.28396723	0.28391683	0.29396723	0.25807535
ω_0'	0.41956938π	0.50000000π	0.43301270π	0.43068820π	0.43068570π	0.43068820π	0.41956938π
ω_0	0.50000000π†	0.50000000π†	0.43301270π	0.43068820π	0.50000000π†	0.43068820π†	0.41956938π†
ω_s	–	–	0.56291651π	0.54467197π	–	–	–
$E_{2\,MSE}$	0.18354699×10^{-4}	0.73093292×10^{-3}	0.10030168×10^{-2}	0.18774845×10^{-6}	0.60960688×10^{-9}	0.81305446×10^{-4}	0.12020137×10^{-3}
$E_{2\,max}$	0.66964150×10^{-2}	0.42589350×10^{-1}	0.36003153×10^{-1}	0.70236681×10^{-4}	0.48063338×10^{-4}	0.99999882×10^{-2}	0.13179756×10^{-1}
$E_{1\,MSE}$	0.69532535×10^{-4}	0.19601775×10^{-2}	0.56523184×10^{-2}	0.94687513×10^{-6}	0.95973594×10^{-6}	0.55420406×10^{-3}	0.68441314×10^{-3}
$E_{1\,max}$	0.13361746×10^{-1}	0.72940098×10^{-1}	0.34903858	0.26214851×10^{-3}	0.13865395×10^{-1}	0.15688316	0.15688316

* The coefficients are actually T_{ij}'s. † One of the specification. ‡ Other specification is $\omega_f = 0.65\pi$ + Example 2.3 answers are given.

Table 4.1 Comparison of Results by Several Analytical Methods and Optimization Method for Type-C Circular Cutoff Contour with $\omega_c = 0.5\pi$.

it is observed that the error $E_{2\,MSE}$ ($E_{1\,MSE}$) for the approximate analytical solution is the highest of all and it is of the order of 10^{-2} (10^{-1}). The main reason for this is the inaccuracy in the value of $-t_{00} = t_{11}$ because of the approximation. The scaled optimum solution gives the lowest value of the error, $E_{2\,MSE}$ ($E_{1\,MSE}$), and it is of the order of 10^{-9} (10^{-4}). The error $E_{2\,MSE}$ ($E_{1\,MSE}$) for the analytical solution is very close to this value *i.e.* it is of the order of 10^{-8} (10^{-4}).

The McClellan's coefficients give the error $E_{2\,MSE}$ ($E_{1\,MSE}$) of the order of 10^{-3} (10^{-2}). The error $E_{2\,MSE}$ ($E_{1\,MSE}$) for the scaled approximate solution is less than this value *i.e.* it is of the order of 10^{-4} (10^{-4}). This is because, the errors along and near the diagonal $\omega_2 = \omega_1$ are smaller than those obtained with the McClellan's coefficients given by (2.57). Hence, for circular contours, the coefficients of the scaled approximate solution are better than the McClellan's coefficients. A difference to be noted is that in the former case $\omega_0' < \omega_0$, but in the latter case $\omega_0' = \omega_0$. In all the solutions, the error $E_{1\,MSE}$ is larger than the error $E_{2\,MSE}$.

In order to compare the scaling-free approximate solution with the analytical and scaled approximate solutions (columns 4 and 1), the respective ω_0' values are used. The results are presented in the last two columns. It is observed that the scaling-free approximate solution gives a smaller value of the error $E_{2\,MSE}$ ($E_{1\,MSE}$) than the approximate analytical solution (column 3).

The expression for U_{11} as given by Hazra and Reddy [40] can be written after some manipulation as

$$U_{11} = \frac{1 - \cos(\omega_0)}{1 - \cos(\omega_e)} - \frac{1}{2}. \tag{4.73}$$

By having a series expansion of $\cos(\omega_0)$ and $\cos(\omega_e)$ in (4.73) and truncating sixth- and higher- order terms, (4.73) reduces to (4.19). Therefore, the scaling-free approximate solution obtained by (4.19) is a good approximation to the exact analytical solution [40].

The error $E_{2\,MSE}$ ($E_{1\,MSE}$) for the scaling-free approximate solution (last column) is roughly 10 times higher than that of the scaled approximate solution (first column). The reason for this is that the former solution is obtained by forcing only the constant term in the error function to zero, whereas the latter solution is obtained by forcing the constant, ω_1^2, and ω_1^4 terms in the error function to zero. Thus, the errors are kept to a small value in the scaled approximate solution compared with the scaling-free approximate solution.

To check the error performance of various methods at higher frequencies, the value of ω_e is increased from 0.5π to 0.75π. The results obtained are presented in Table 4.2. As expected, the errors for all the methods are relatively larger. Even though the value of ω_e is larger for the above two examples, the scaled and scaling-free approximation solutions agree well with the optimization and analytical solutions.

For all the methods, the accuracy of contour approximation improves for smaller values of frequency specifications. To prove this point, the results of various methods are presented in Table 4.3 for $\omega_e = 0.25\pi$. The error $E_{2\,MSE}$ for different values of ω_e for three selected methods are given in Table 4.4. Comparing these values, it is observed that lower the cutoff frequency, the smaller is the MSE of the scaled approximate method compared to that by using the McClellan's coefficients (Eq. (2.57)), and closer to that of the analytical method. The coefficients obtained by the scaled approximation method are constants just like the McClellan's coefficients (Eq (2.57)). Only ω_0' has to be calculated by using (4.16) or (4.13). This method and other approximation methods are simple and hence, they have relatively simpler calculations compared to the analytical and optimization methods.

4.12 Filter Design Examples

For reasons as explained in Sec. 3.12, in this section, some IIR filter design examples are chosen to demonstrate the applications of the derived formulas.

Parameter	Scaled Approx. Solution* (4.11)&(4.16)	McClellan's Coefficients (2.57)	Approx. Analytical Solution† (4.20)-(4.31)	Analytical Solution† (2.50)	Scaled Optimum Solution* (3.8)&(2.34)	Scaling-free Approx. Solution (4.10)	Scaling-free Approx. Solution (4.19)
t_{00}	− 0.25000000	− 0.50000000	− 0.42348914	− 0.33733770	− 0.33708360	− 0.40035607	− 0.32266018
t_{01}	0.50000000	0.50000000	0.50000000	0.50000000	0.50006070	0.50000000	0.50000000
t_{10}	0.50000000	0.50000000	0.50000000	0.50000000	0.49993930	0.50000000	0.50000000
t_{11}	0.25000000	0.50000000	0.42348914	0.33733770	0.33708360	0.40035607	0.32266018
ω_0'	0.59044392π	0.75000000π	0.64951905π	0.64128370π	0.64148950π	0.64128370π	0.59044392π
ω_0	0.75000000π‡	0.75000000π‡	0.64951905π	0.64128370π	0.75000000π‡	0.64128370π‡	0.59044392π‡
ω_s	–	–	0.77042286π	0.71846181π	–	–	–
$E_{2\,MSE}$	0.16278420×10^{-2}	0.53395863×10^{-2}	0.89689521×10^{-2}	0.11888991×10^{-5}	0.38520153×10^{-6}	0.74192667×10^{-2}	0.17038151×10^{-1}
$E_{2\,max}$	0.62545617×10^{-1}	0.11648752	0.12385086	0.17673487×10^{-2}	0.11211957×10^{-2}	0.10757909	0.13454999
$E_{1\,MSE}$	0.82558693×10^{-2}	0.35235414×10^{-1}	0.64537523×10^{-1}	0.92195930×10^{-5}	0.88500311×10^{-4}	0.55894777×10^{-1}	0.10957566
$E_{1\,max}$	0.14144065	0.32249458	0.86604171	0.83589189×10^{-2}	0.11282790	0.83561899	0.92343588

* The coefficients are actually $T_{i,j}$'s. † One of the specification. ‡ Other specification is $\omega_f = 0.9\pi$.

Table 4.2 Comparison of Results by Several Analytical Methods and Optimization Method for Type-C Circular Cutoff Contour with $\omega_c = 0.75\pi$.

Parameter	Scaled Approx. Solution* (4.11)&(4.16)	McClellan's Coefficients (2.57)	Approx. Analytical Solution† (4.20)&(4.31)	Analytical Solution† (2.59)	Scaling-free Approx. Solution (4.19)	Scaling-free Approx. Solution (4.19)
t_{00}	− 0.25000000	− 0.50000000	− 0.26927657	− 0.25789298	− 0.25826564	− 0.25037878
t_{01}	0.50000000	0.50000000	0.50000000	0.50000000	0.50000000	0.50000000
t_{10}	0.50000000	0.50000000	0.50000000	0.50000000	0.50000000	0.50000000
t_{11}	0.25000000	0.50000000	0.26927657	0.25789298	0.25826564	0.25037878
ω_0'	0.21505107π	0.25000000π	0.21650635π	0.21622507π	0.21622507π	0.21505107π
ω_0	0.25000000π‡	0.25000000π‡	0.21650630π	0.21622507π	0.21622507π‡	0.21505107π‡
ω_s	–	–	0.34641016π	0.34197443π	–	–
$E_{2\ MSE}$	0.56097454×10^{-8}	0.52615227×10^{-5}	0.72333961×10^{-5}	0.28004852×10^{-13}	0.11311613×10^{-7}	0.30606561×10^{-7}
$E_{2\ max}$	0.11760975×10^{-3}	0.28075431×10^{-2}	0.27787106×10^{-2}	0.27308599×10^{-6}	0.10914410×10^{-3}	0.22290156×10^{-3}
$E_{1\ MSE}$	0.41774566×10^{-7}	0.55309631×10^{-4}	0.10689203×10^{-3}	0.80121456×10^{-10}	0.13123175×10^{-6}	0.30056438×10^{-6}
$E_{1\ max}$	0.34122203×10^{-3}	0.78441580×10^{-1}	0.78441580×10^{-1}	0.12666750×10^{-3}	0.20620254×10^{-2}	0.22038739

* The coefficients are actually T_{ij}'s. † One of the specification. ‡ Other specification is $\omega_f = 0.4\pi$.

Table 4.3 Comparison of Results by Several Analytical Methods and Optimization Method for Type-C Circular Cutoff Contour with $\omega_c = 0.25\pi$.

ω_e	Mean Square Error of $E_2(\omega_1)$		
	McClellan's Coefficients* † (2.57)	Scaled Approx. Solution* ‡ (4.11)&(4.16)	Analytical Solution† ‡ (2.59)
0.05π	0.16141094×10^{-10}	0.24676357×10^{-16}	0.48760338×10^{-17}
0.25π	0.52615227×10^{-5}	0.56097454×10^{-8}	0.28004852×10^{-13}
0.50π	0.73093292×10^{-3}	0.18354699×10^{-4}	0.18774845×10^{-8}
0.75π	0.53395863×10^{-2}	0.16278420×10^{-2}	0.11888991×10^{-5}
1.00π	0.17982284×10^{-2}	0.29755967×10^{-1}	0.11803166×10^{-3}

* $\omega_0 = \omega_e$ † $\omega_0' = \omega_0$ ‡ $\omega_0' < \omega_e$

Table 4.4 Comparison of Mean Square Error of $E_2(\omega_1)$ for Various 2-D Cutoff Radii (ω_e's) for Three Methods.

A 1-D zero-phase filter obtained by multiplying the transfer function of a second-order digital Butterworth filter and its conjugate is used as a prototype filter ($\omega_0 = 0.24281303\pi$). The 2-D specification for a circularly symmetric filter (type-C) is $\omega_e = \omega_0$. Using the McClellan's coefficients (Eq. (2.57)) derived from (4.19), a 2-D zero-phase approximately circularly symmetric filter is obtained. The magnitude response of this filter is shown in Fig. 4.5.

Consider the design of another circularly symmetric filter (type-C) with the specification $\omega_e = \omega_0 = 0.28284134\pi$. The unscaled and scaled coefficients are given by (4.14) and (4.11), respectively. The ω_0' value obtained from (4.16) is same as the cutoff frequency of the prototype filter. Using the scaled coefficients, a 2-D zero-phase circularly symmetric filter is obtained. The magnitude response of this filter is shown in Fig. 4.6. The contours of the response in Fig. 4.6 are more circular than the contours of the response in Fig. 4.5. The improvements are larger for contours at smaller frequencies as seen from Table 4.4. The transition-width of the filter response shown in Fig. 4.6 is slightly more than that in Fig. 4.5.

Nguyen and Swamy [48] have proposed a technique for designing a class of 2-D separable denominator zero-phase IIR filters using McClellan transformation. Fig. 4.7 shows the magnitude response of an 8th-order IIR filter with a bandwidth corresponding to $c = 1$ (Used in (26) of [48]), designed by them using the scaled optimum coefficients given in Table 4.1. The coefficients found by the analytical formulas presented in this chapter can readily be used in their design. Fig. 4.8 shows the magnitude response of an IIR filter with the same filter order and with the same value of c, but designed by using the scaled approximation coefficients given in Table 4.1. This filter has slightly smaller transition-width and better stop-band response near the frequency points $(\pm\pi,0)$ and $(0,\pm\pi)$ compared to the one corresponding to Fig. 4.7.

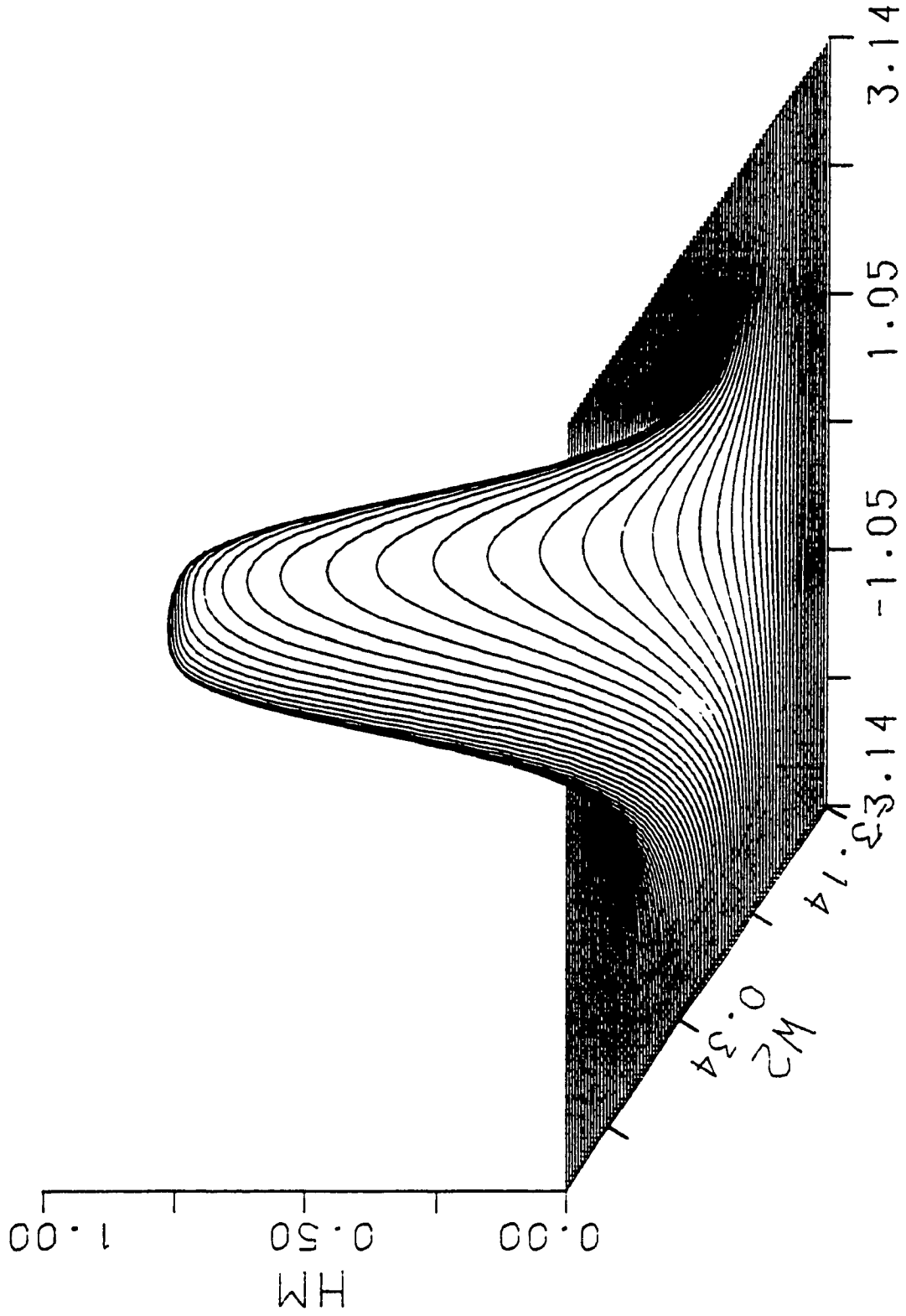

Fig. 4.5 Magnitude Response of a 2-D Zero-Phase Approximately Circularly Symmetric Filter (Type-C) Designed by Using the McClellan's Coefficients (Eq. (2.57)) From the Specification $\omega_c = \omega_0 \approx 0.24\pi$.

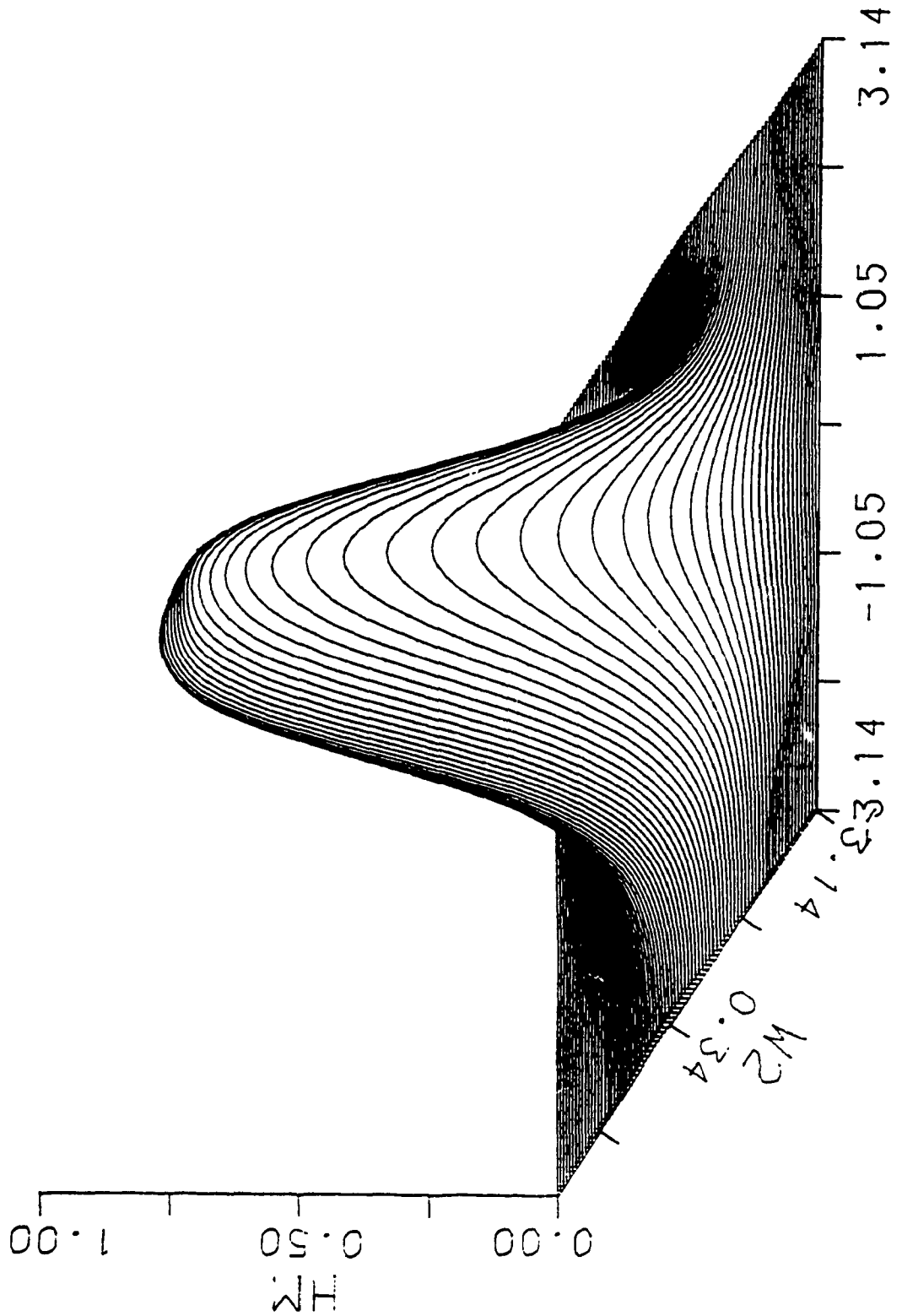

Fig. 4.6 Magnitude Response of a 2-D Zero-Phase Approximately Circularly Symmetric Filter (Type-C) Designed by Using the Scaled Coefficients (Eq. (4.11)) From the Specification $\omega_c = \omega_0 \approx 0.28\pi$.

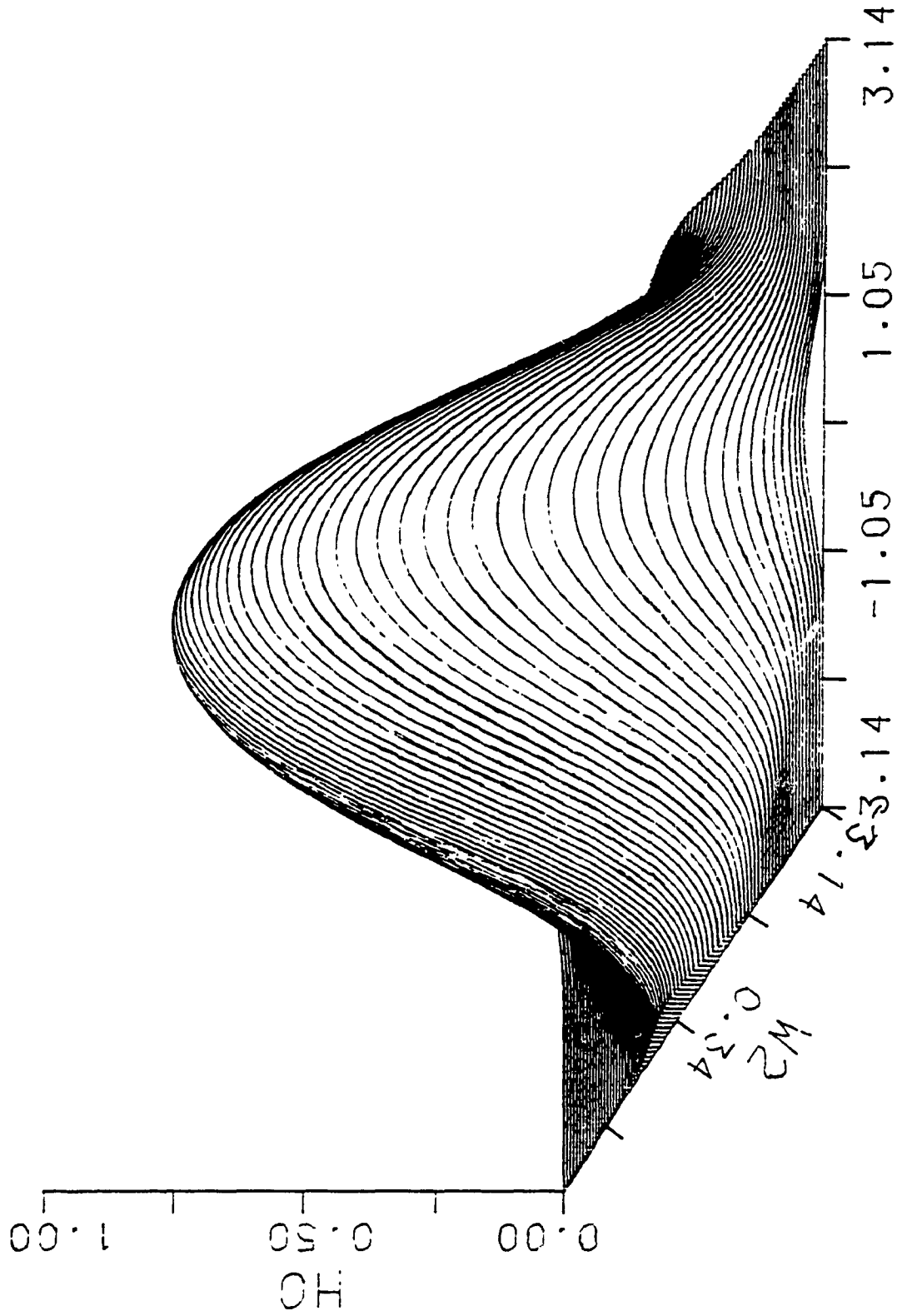

Fig. 4.7 Magnitude Response of an 8th-Order Separable Denominator 2-D IIR Filter Designed by Using the Scaled Optimum Coefficients (Given in Table 4.1) and a Band-Width Corresponding to $c = 1$ (Eq. (26) of [4.12]).

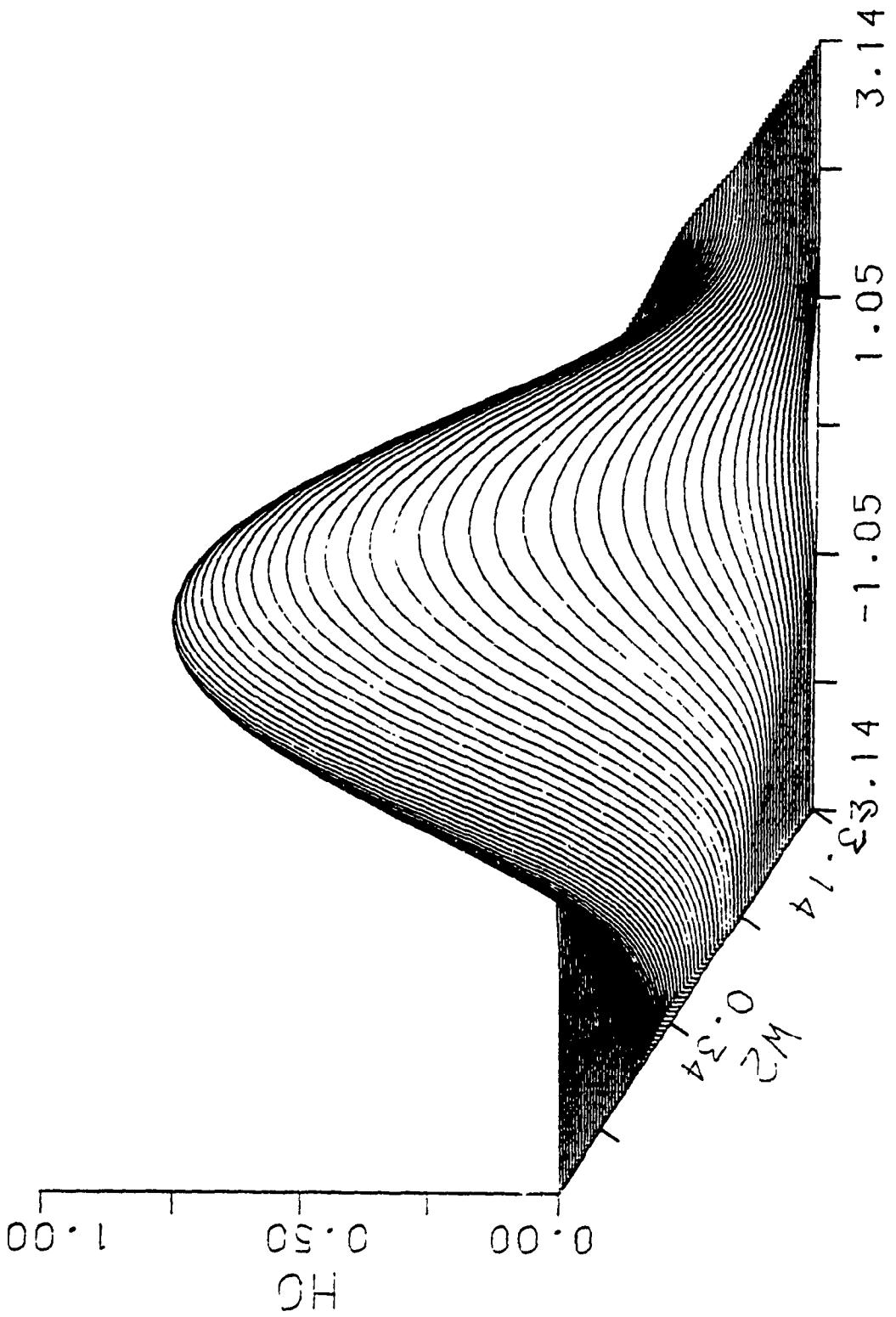

Fig. 4.8 Magnitude Response of an 8th-Order Separable Denominator 2-D IIR Filter Designed by Using the Scaled Approximation Coefficients (Given in Table 4.1) and a Band-Width Corresponding to $c = 1$ (Eq. (26) of [4.12]).

4.13 SUMMARY

In this chapter, some analytical methods have been developed for finding the coefficients of the first-order McClellan transformation for the design of 2-D circularly symmetric digital filters from 1-D digital filters. Several new extremely simple analytical formulas have been derived for calculating the transformation coefficients by forcing the coefficients of lower order significant terms in the power series expansion of the linear error function to zero. Specifically, the following methods have been developed. (i) Approximation Method, (ii) Scaling-free Approximation Method, and (iii) Approximate Analytical Method.

In Methods (i) and (ii), ordinary and simplified formulas have been presented. It has been proven that the scaled coefficients of Method (i) are constants and are independent of frequency specifications. fast calculation of the coefficients, when the specifications The McClellan's coefficients given by (2.57) have been shown to be the simplified scaling-free coefficients of (4.24) for the special case of specification $\omega_0 = \omega_e$. The proposed coefficients given by (4.24) belong to a general class in the sense that ω_0 and ω_e need not be equal. In Method (iii), approximate formulas have been derived for the exact formulas of the analytical method, and they offer some implementation advantages. Also, Method (iii), retains the advantages of the original analytical method.

For all the methods, formulas have been presented for the coefficients of both the cosine- and sine- form McClellan transformations. Also, many numerical and filter design examples have been provided to demonstrate the usefulness of the formulas. The error values of several methods have been compared in Tables 4.1 and 4.2. For all the methods, lower the frequency specifications, the smaller is the MSE. To prove this point, additional results have been given in Tables 4.3 and 4.4. The results of the approximation methods are found to agree well with those of the other analytical and optimization methods. In the next chapter, some new methods are developed to find the generalized transformation coefficients for elliptically symmetric filters with arbitrary orientations.

CHAPTER 5

APPROXIMATION DESIGN OF 2-D ELLIPTICALLY SYMMETRIC DIGITAL FILTERS WITH ARBITRARY ORIENTATIONS USING GENERALIZED MCCLELLAN TRANSFORMATION

5.1 INTRODUCTION

Two-dimensional digital filters find wide range of applications in digital image processing. The 2-D image signal, to be processed, may have a spatial variation along a certain direction and it may not coincide with the spatial coordinates along which the sampling is performed. To process such signals, 2-D elliptically symmetric digital filters of arbitrary orientation are employed.

In this chapter, some analytical methods are developed for finding the coefficients of the generalized McClellan transformation with two sine terms (approach I) and one sine term (approach II) for the design of 2-D elliptically symmetric digital filters with arbitrary orientations from 1-D digital filters.

5.1.1 Review of Existing Optimization Methods

Existing unconstrained linear [27] and nonlinear [4] optimization methods use the original transformation [17]. They can be extended to use the generalized transformation as well. Though these methods give optimum results, they are computationally expensive. The constrained linear and nonlinear optimization methods are computationally even more expensive [4]. Both the methods exceed the arithmetic and/or speed capability of low cost, stand-alone 2-D signal processors and they are not suitable for real-time applications. Also, the nonlinear optimization method normally provides a local minima rather than the global minima.

5.1.2 Review of Existing Analytical Methods

Nguyen and Swamy [35], and Reddy and Hazra [42] have proposed analytical methods and they involve quite a few computations. The method in [35] uses two second-order sine terms and gives good approximation for lower values of frequency specifications. It is much simpler than the method of [42]. A disadvantage of the method is that its scaled coefficients produce two extra pass-bands around (π, π) and $(-\pi, \pi)$, in addition to the normal pass-band around (0, 0) in the upper half of the (ω_1,ω_2)-plane. On the other hand, the method of [42] uses a first-order sine term and gives reasonably good approximation for higher values of frequency specifications as well. But, it is more complex than the method in [35], and it does not give good results for lower values of the ratio of minor-axis $(2\omega_a)$ to major-axis $(2\omega_b)$.

5.1.3 Proposed Analytical Methods

The analytical methods developed in this chapter [43], do not have the disadvantages of the methods of [1], [27], [35], and [42] and have the advantages of the method in [35]. Several new simple formulas other than those in [35] and [42] are derived for finding the coefficients by forcing the lower order significant terms in the power series expansion of the linear error function to zero. Using both the approaches I and II, formulas are presented for both the original and the scaling-free generalized McClellan transformation coefficients for all the four cases [(i)-(iv)] of elliptical cutoff contours with arbitrary orientations. Many examples are given. The results obtained by using the derived formulas agree well with the results of the optimization methods, and the accuracy of the formulas is sufficient for many engineering applications. The number of multiplications required to implement the designed filters is small. As in the cases of elliptical and circular contours, since they involve only very few computations, the derived formulas are very useful for real-time 2-D adaptive filter design and filtering.

5.2 Approach I - Approximation with Two Sine Terms

5.2.1 Approximation for Coefficients for Type-A Contours

Consider a vertical *i.e.* type-A elliptical cutoff contour rotated about the 2-D origin by an angle θ in the anticlockwise direction, as depicted in Fig. 5.1. The equation of the rotated elliptical contour is

$$\frac{\omega_1^2}{\omega_A^2} + \frac{\omega_2^2}{\omega_B^2} + \frac{\omega_1\omega_2}{\omega_C} = 1 \tag{5.1a}$$

where

$$\omega_A^2 = \omega_a^2\left[1 - \left\{1 - \frac{\omega_a^2}{\omega_b^2}\right\}\sin^2(\theta)\right]^{-1} \tag{5.1b}$$

$$\omega_B^2 = \omega_b^2\left[1 - \left\{1 - \frac{\omega_b^2}{\omega_a^2}\right\}\sin^2(\theta)\right]^{-1} \tag{5.1c}$$

and

$$\omega_C = \omega_a\,\omega_b\left[\left\{\frac{\omega_a}{\omega_b} - \frac{\omega_b}{\omega_a}\right\}\sin(2\theta)\right]^{-1}. \tag{5.1d}$$

The original McClellan transformation given by (2.1) has only cosine terms, therefore, it is suitable for designing only 2-D quadrantally symmetric filters [50] When an elliptical cutoff contour is rotated, it no longer possesses quadrantal symmetry. However, it possesses centro-symmetry [72]. Therefore, in order to have a better approximation for this type of contours, the generalized McClellan transformation which has sine terms also [32], [50] must be used. Therefore, in approach I, a generalized transformation with two sine terms as given below is used.

$$\begin{aligned}\cos(\omega) &= t_{00} + t_{01}\cos(\omega_2) + t_{10}\cos(\omega_1) + t_{11}\cos(\omega_1)\cos(\omega_2) \\ &\quad + s_{12}\sin(\omega_1)\sin(2\omega_2) + s_{21}\sin(2\omega_1)\sin(\omega_2) \\ &= F_{g_2}(\omega_1,\omega_2)\end{aligned} \tag{5.2a}$$

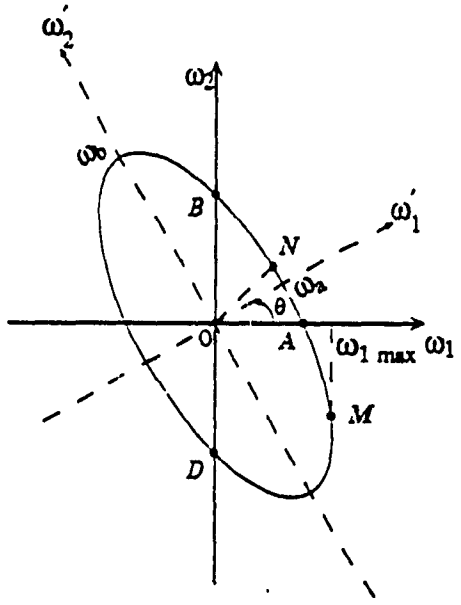

Fig. 5.1 Geometry of a Rotated Type-A Elliptical Cutoff Contour.

Eq. (5.2a) is only one of the many possible choices of a 2-D version of (4.53) in which for the sine terms, (i_1, i_2) assumes the ordered pairs (1, 2) and (2, 1). The terms corresponding to $(i_1, i_2) = (1, 1)$ or (2, 2) is not included in (5.2a), since they will introduce two extra coefficients to be determined. It should be noted that the first- and second- order terms are used to provide the quadrantally symmetric and centrosymmetric components, respectively. Eq. (5.2a) can be rewritten as

$$\cos(\omega) = t_{00} + t_{01}\cos(\omega_2) + t_{10}\cos(\omega_1) + t_{11}\cos(\omega_1)\cos(\omega_2) + 2\sin(\omega_1)\sin(\omega_2)\{s_{12}\cos(\omega_2) + s_{21}\cos(\omega_1)\}. \tag{5.2b}$$

The function $\sin(x)$ can be approximated by its truncated power series expansion as

$$\sin(x) \approx x - \frac{x^3}{6} + \frac{x^5}{120}. \tag{5.3}$$

Using (3.11) and (5.3) in (5.2b), and neglecting the terms with sixth- and higher- order powers, yields,

$$1 - \frac{\omega^2}{2} + \frac{\omega^4}{24} = (t_{00} + t_{01} + t_{10} + t_{11}) - \frac{1}{2}(p_1\omega_1^2 + p_2\omega_2^2) + \frac{1}{24}(p_1\omega_1^4 + p_2\omega_2^4 + 6t_{11}\omega_1^2\omega_2^2) - \frac{1}{2}\{-\frac{6}{5}(q_1 + q_2)\omega_1\omega_2 + q_1\omega_1^3\omega_2 + q_2\omega_1\omega_2^3\} \tag{5.4a}$$

where

$$q_1 = \frac{2}{3}s_{12} + \frac{8}{3}s_{21}, \tag{5.4b}$$

$$q_2 = \frac{8}{3}s_{12} + \frac{2}{3}s_{21}, \tag{5.4c}$$

and p_1 and p_2 are as defined in (2.11a) and (2.11b), respectively.

Assume that the 1-D pass-band cutoff frequency ω_0 is exactly mapped onto the desired rotated 2-D elliptical pass-band cutoff contour given by (5.1a). Substituting in (5.4a), $\omega = \omega_0$, and ω_2^2 value from (5.1a), and using (2.3), the linear error function (3.7) (now derived for the generalized transformation (5.2b)) is rewritten as

$$\frac{1}{2}\left[-\omega_0^2\left\{1-\frac{\omega_0^2}{12}\right\}+\omega_B^2\left\{1-\frac{\omega_B^2}{12}\right\}p_2\right]$$

$$+\frac{\omega_1^2}{2}\left[p_1+\frac{\omega_B^2}{\omega_A^2}\left\{\frac{\omega_B^2}{6}-1\right\}p_2-\frac{Q_a}{12}\right]$$

$$+\frac{\omega_1\omega_2}{2}\left[\frac{\omega_B^2}{\omega_C}\left\{\frac{\omega_B^2}{6}-1\right\}p_2-\frac{6}{5}q_1+\left\{\omega_B^2-\frac{6}{5}\right\}q_2\right]$$

$$+\frac{\omega_1^3\omega_2}{2}\left[q_1+\frac{Q_a}{12\omega_C}-\frac{\omega_B^2}{\omega_A^2}\left\{q_2+\frac{\omega_B^2}{6\omega_C}p_2\right\}\right]$$

$$-\frac{\omega_1^4}{24}\left[p_1+\frac{\omega_B^4}{\omega_A^4}p_2-\frac{Q_a}{\omega_A^2}\right]=0 \tag{5.5a}$$

where

$$Q_a=\omega_B^2\left[\frac{\omega_B^2}{\omega_C}\left\{\frac{\omega_B^2}{\omega_C}p_2+12q_2\right\}+6t_{11}\right]. \tag{5.5b}$$

Since the error must be zero, the right side of (5.5a) has been taken to be zero. Equating the constant, and the ω_1^2-, $\omega_1\omega_2$-, $\omega_1^3\omega_2$- and ω_1^4-, term coefficients to zero, the following equations are obtained.

$$\omega_B^2\left\{1-\frac{\omega_B^2}{12}\right\}p_2=\omega_0^2\left\{1-\frac{\omega_0^2}{12}\right\} \tag{5.6}$$

$$p_1-\frac{\omega_B^2}{2}t_{11}-\frac{\omega_B^4}{\omega_C}q_2=\frac{\omega_B^2}{\omega_A^2}\left\{1+\frac{\omega_A^2\omega_B^4}{12\omega_C^2}-\frac{\omega_B^2}{6}\right\}p_2 \tag{5.7}$$

$$-\frac{6}{5}q_1+\left\{\omega_B^2-\frac{6}{5}\right\}q_2=\frac{\omega_B^2}{\omega_C}\left\{1-\frac{\omega_B^2}{6}\right\}p_2 \tag{5.8}$$

$$\frac{\omega_B^2}{2\omega_C} t_{11} + q_1 + \omega_B^2 \left\{ \frac{\omega_B^2}{\omega_C^2} - \frac{1}{\omega_A^2} \right\} q_2 = \frac{\omega_B^4}{6\omega_C} \left\{ \frac{1}{\omega_A^2} - \frac{\omega_B^2}{2\omega_C^2} \right\} p_2 \tag{5.9}$$

$$- p_1 + \frac{6\omega_B^2}{\omega_A^2} t_{11} + \frac{12\omega_B^4}{\omega_A^2 \omega_C} q_2 = \frac{\omega_B^4}{\omega_A^2} \left\{ \frac{1}{\omega_A^2} - \frac{\omega_B^2}{\omega_C^2} \right\} p_2 \tag{5.10}$$

Solving the above five equations, yields the following formulas.

$$p_1 = \frac{\omega_0^2 \left\{ 1 - \frac{\omega_0^2}{12} \right\}}{\omega_A^2 \left\{ 1 - \frac{\omega_A^2}{12} \right\}} \tag{5.11a}$$

$$p_2 = \frac{\omega_0^2 \left\{ 1 - \frac{\omega_0^2}{12} \right\}}{\omega_B^2 \left\{ 1 - \frac{\omega_B^2}{12} \right\}} \tag{5.11b}$$

$$q_2 = \frac{\omega_A^2 \left[\omega_A^2 p_1 + \frac{5}{6} \omega_B^4 p_2 - 10\omega_0^2 \left\{ 1 - \frac{\omega_0^2}{12} \right\} \right] - \omega_B^4 p_2}{12\omega_C \left\{ \omega_A^2 + \omega_B^2 - \frac{5}{6} \omega_A^2 \omega_B^2 \right\}} \tag{5.11c}$$

$$q_1 = \frac{5}{6\omega_C} \left[\frac{\omega_B^4}{12} \cdot p_2 - \omega_0^2 \left\{ 1 - \frac{\omega_0^2}{12} \right\} + \left\{ \frac{5\omega_B^2}{6} - 1 \right\} q_2 \right] \tag{5.11d}$$

$$t_{11} = \frac{1}{6} \left[\frac{\omega_A^2}{\omega_B^2} p_1 + \omega_B^2 \left\{ \frac{1}{\omega_A^2} - \frac{\omega_B^2}{\omega_C^2} \right\} p_2 - 12 \frac{\omega_B^2}{\omega_C} q_2 \right] \tag{5.11e}$$

This derivation is different from that in [35]. The results, however, are identical.

From this derivation, it can be concluded that the analytical formulas given by (5.11) are approximate solutions to the linear optimization problem as defined by (3.8) itself for the generalized transformation. Also, it is more straight forward and easy to understand the formulas derived in [35]. Further it is more useful in deriving the scaling-free formulas. The constant term and certain number of lower-order ω_1 and ω_2

terms are forced to assume a zero value depending on the number of unknowns. The higher-order ω_1 and ω_2 terms are assumed to be zero, since their values are negligible particularly for low frequencies. The approximation solution thus obtained agrees well with the optimal solution [35] and its accuracy is sufficient for many engineering applications. To illustrate these points, some examples are given in Sec. 5.2.1.3.

Since on a rotated ellipse, the ratios ω_1^2/ω_A^2 and ω_2^2/ω_B^2 are not necessarily less than one, the formulas derived in this section and in later sections are valid only if ω_0, ω_a, and ω_b are less than $1 \approx 0.3183\pi$ rad/sec. Also, these formulas are not as accurate as for the case of the type-A or type-B elliptical contours.

5.2.1.1 Finding the Coefficients

To find the coefficients, first ω_A^2, ω_B^2, and ω_C are evaluated from the given frequency specifications (ω_0, ω_a, ω_b, and θ) using (5.1b)-(5.1d). Then p_1 and p_2 are evaluated from (5.11a) and (5.11b), respectively, followed by the evaluation of q_2 from (5.11c). Quantities q_1 and t_{11} are evaluated using (5.11d) and (5.11e). Other t_{ij}'s are found in the same way as for the type-A contours using (2.11), and (2.3). Finally, s_{ij}'s are found from the following formulas which are derived from (5.4b) and (5.4c).

$$s_{12} = -\frac{1}{10}q_1 + \frac{2}{5}q_2 \tag{5.12a}$$

$$s_{21} = \frac{2}{5}q_1 - \frac{1}{10}q_2 \tag{5.12b}$$

The sine-form generalized transformation corresponding to (5.2a) is obtained from the 2-D version of (4.66) in which for the additional sine terms, (i_1, i_2) assumes the ordered pairs (1, 2) and (2, 1). The transform, in this case, is then given by

$$\begin{aligned}\sin^2(\omega/2) &= p_{00} + p_{01}\sin^2(\omega_2/2) + p_{10}\sin^2(\omega_1/2) + p_{11}\sin^2(\omega_1/2)\sin^2(\omega_2/2) \\ &\quad + q_{12}\sin(\omega_1)\sin(2\omega_2) + q_{21}\sin(2\omega_1)\sin(\omega_2) \\ &= G_{q_2}(\omega_1,\omega_2).\end{aligned} \tag{5.13}$$

The formulas for the coefficients in (5.13) are

$$p_{00} = 0, \quad p_{01} = p_2, \quad p_{10} = p_1, \quad p_{11} = -2t_{11},$$
$$q_{12} = -s_{12}/2, \quad \text{and} \quad q_{21} = -s_{21}/2. \tag{5.14}$$

5.2.1.2 Special Cases

For $\theta = 0$, one can obtain $\omega_A = \omega_a$, $\omega_B = \omega_b$, $\omega_C = \infty$, $q_1 = q_2 = 0$, and $s_{12} = s_{21} = 0$. The formulas (5.11a), (5.11b), and (5.11e) reduce to (3.17a), (3.17b), and (3.17c), respectively, which are the formulas for the type-A contours. Similarly, for $\theta = 0.5\pi$, one can obtain $\omega_A = \omega_b$, $\omega_B = \omega_a$, $\omega_C = \infty$, $q_1 = q_2 = 0$, and $s_{12} = s_{21} = 0$. The formulas (5.11a), (5.11b), and (5.11e) reduce to (3.37a), (3.37b), and (3.37c), respectively, which are the formulas for the type-B contours Finally, for $\theta = 0.25\pi$, the following simplified formulas are obtained

$$\omega_A^2 = \omega_B^2 = \frac{2\omega_a^2\omega_b^2}{\omega_a^2 + \omega_b^2} \tag{5.15a}$$

$$\omega_C = \frac{\omega_a^2\omega_b^2}{\omega_a^2 - \omega_b^2} \tag{5.15b}$$

$$p_1 = p_2 = \frac{\omega_0^2\left\{1 - \dfrac{\omega_0^2}{12}\right\}}{\omega_A^2\left\{1 - \dfrac{\omega_A^2}{12}\right\}} \tag{5.16a}$$

$$q_1 = q_2 = \frac{\omega_0^2\left\{1 - \dfrac{\omega_0^2}{12}\right\} - \dfrac{\omega_A^4}{12}p_1}{\omega_C\left\{\omega_A^2 - \dfrac{12}{5}\right\}} \tag{5.16b}$$

$$t_{11} = \frac{1}{3}\left\{1 - \frac{\omega_A^4}{2\omega_C^2}\right\}p_1 - 2\frac{\omega_A^2}{\omega_C}q_1 \tag{5.16c}$$

Since $p_1 = p_2$ and $q_1 = q_2$, $t_{10} = t_{01} = p_1 - t_{11}$, $t_{00} = 1 - (2t_{01} + t_{11})$, and $s_{12} = s_{21} = (3/10)q_1$ are obtained. These simplified formulas reduce the amount of computations for the specifications with $\theta = 0.25\pi$ and with different values of ω_0, ω_a, and ω_b.

5.2.1.3 Comparison of Approximation and Optimization Methods

The following two examples illustrate the comparison of approximation and optimization methods for finding the generalized transformation coefficients.

Example 5.1: The specifications for a rotated type-A contour are $\omega_0 = \omega_b = 0.5\pi$, $\omega_a = 0.25\pi$, and $\theta = \pi/6$. The results obtained by using the formulas given by (5.11) are

$$t_{00} = -0.22875051 \qquad t_{01} = -1.52736540$$
$$t_{10} = -0.34650530 \qquad t_{11} = 3.10262120$$
$$s_{12} = 0.23046834 \qquad s_{21} = 0.56657502$$
$$p_1 = 2.75611590 \qquad p_2 = 1.57525580$$
$$q_1 = 1.66451230 \qquad q_2 = 0.99229892$$
$$E_{2\,MSE} = 0.39245036 \times 10^{-1} \qquad E_{2\,\max} = 0.30832894$$
$$E_{1\,MSE} = 0.23648141 \times 10^{-1} \qquad E_{1\,\max} = 0.61049285.$$

Using (2.18), the following scaled coefficients are obtained.

$$T_{00} = -0.74839375 \times 10^{-1} \qquad T_{01} = -0.32988549$$
$$T_{10} = -0.74839375 \times 10^{-1} \qquad T_{11} = 0.67011451$$
$$S_{12} = 0.49777324 \times 10^{-1} \qquad S_{21} = 0.12237077$$
$$\omega_0' = 0.50800647\pi$$
$$E_{2\,MSE} = 0.18307336 \times 10^{-2} \qquad E_{2\,\max} = 0.66593911 \times 10^{-1}$$
$$E_{1\,MSE} = 0.23648144 \times 10^{-1} \qquad E_{1\,\max} = 0.61049290$$

It should be noted that in this example, ω_0 and ω_b are not less than 1 rad/sec. Even then, the MSE values are reasonably good. For lower frequency specifications, the MSE will be still less. To reinforce this point, in the next example, the frequency specifications are reduced by a factor of 2 and the rotation angle is kept the same.

Example 5.2: The specifications for a rotated type-A contour are $\omega_0 = \omega_b = 0.25\pi$, $\omega_a = 0.125\pi$, and $\theta = \pi/6$.

Nguyen and Swamy [35] minimized the objective function $J_2(t)$ given by (3.8) in the LMS sense and arrived at the following optimum results.

$$t_{00} = -1.30679770 \qquad t_{01} = -0.82845540$$
$$t_{10} = 0.59535250 \qquad t_{11} = 2.53990060$$
$$s_{12} = 0.20531900 \qquad s_{21} = 0.46497150$$
$$p_1 = 3.13525310 \qquad p_2 = 1.71144520$$
$$q_1 = 1.37680333 \qquad q_2 = 0.85749833$$
$$E_{2\,MSE} = 0.10360509 \times 10^{-8} \qquad E_{2\,max} = 0.45230907 \times 10^{-4}$$
$$E_{1\,MSE} = 0.40639974 \times 10^{-8} \qquad E_{1\,max} = 0.30603276 \times 10^{-3}$$

The results obtained by using the formulas given by (5.11) are

$$t_{00} = -1.14016150 \qquad t_{01} = -0.99232028$$
$$t_{10} = 0.42988141 \qquad t_{11} = 2.70260040$$
$$s_{12} = 0.20032028 \qquad s_{21} = 0.47196517$$
$$p_1 = 3.13248181 \qquad p_2 = 1.71028012$$
$$q_1 = 1.39212064 \qquad q_2 = 0.84883086$$
$$E_{2\,MSE} = 0.94607476 \times 10^{-5} \qquad E_{2\,max} = 0.48000056 \times 10^{-2}$$
$$E_{1\,MSE} = 0.75012721 \times 10^{-4} \qquad E_{1\,max} = 0.61230245 \times 10^{-1}.$$

The scaled coefficients are obtained by using (2.18) and they are given in Table 5.1 (p. 165). By comparing the error values of the above two examples, it is observed that the approximation method gives better results for lower values of frequency specifications than for higher values.

It should be pointed out that the basic difference between the two methods is that, while the optimization method finds the best fit to the overall shape of the rotated ellipse, the approximation method finds a close fit to the frequency points A, B, and N on the rotated ellipse (Fig. 5.1).

5.2.1.4 Effects of Rotation Angle on the Coefficient Values

An elliptical contour is symmetrical about its major and minor axes. Therefore, an anticlockwise rotation by an angle θ ($0 \leq \theta \leq \pi$) itself is equivalent to a rotation by an angle $(\pi + \theta)$.

For an angle θ ($0 \leq \theta \leq \pi/2$) replacing θ by $(\pi - \theta)$, $\sin(\theta)$ becomes $\sin(\pi - \theta) = \sin(\theta)$, and $\sin(2\theta)$ becomes $\sin\{2(\pi - \theta)\} = -\sin(2\theta)$. Substituting these

results in (5.1b)-(5.1d), it is observed that the values of ω_A^2 and ω_B^2 are the same for both the angles, θ and $(\pi - \theta)$, and the value of ω_C for the latter angle is negative of that for the former. Consequently, the values of q_1 and q_2 and hence, the values of s_{12} and s_{21} for the angle $(\pi - \theta)$ are negative of those for the angle θ.

For an angle θ $(0 \leq \theta \leq \pi/4)$, replacing θ by $\{(\pi/2) - \theta)\}$, $\sin(\theta)$ becomes $\sin\{(\pi/2) - \theta\} = \cos(\theta)$, and $\sin(2\theta)$ becomes $\sin\{2\left((\pi/2) - \theta\right)\} = \sin(2\theta)$. Substituting these results in (5.1b)-(5.1d), it is observed that the values of ω_A^2 and ω_B^2 for the angle $\{(\pi/2) - \theta)\}$ is equal to the values of ω_B^2 and ω_A^2 for the angle θ, respectively, and the value of ω_C is the same for both the angles. Accordingly, the values of p_1, p_2, q_1, q_2, t_{10}, t_{01}, s_{12}, and s_{21} for the angle $\{(\pi/2 - \theta)\}$ are the values of p_2, p_1, q_2, q_1, t_{01}, t_{10}, s_{21}, and s_{12}, respectively, of the angle θ.

The same kind of symmetry is also noticed in the scaled values of the coefficients. The values of F_{max} and F_{min} and hence, the values of C_1 and C_2, and the value of ω_0' remain unchanged With these properties, the results for any angle of rotation $(0 \leq \theta \leq 2\pi)$ can be obtained from the results of a corresponding angle θ where $0 \leq \theta \leq \pi/4$

Example 5.3: The specifications for a rotated type-A contour are $\omega_0 = \omega_b = 0.25\pi$, $\omega_a = 0.125\pi$, and $\theta = (5/6)\pi$.

These specifications are the same as those in the Example 5.2 except for the rotation angle θ which is $\pi/6$. Using the above properties, it is seen that when $\theta = (5/6)\pi$ (or $\theta = -\pi/6$), the coefficients are same as in the Example 5.2 except for the values of s_{12} and s_{21} that are negative of their previous values.

Example 5.4: The specifications for a rotated type-A contour are $\omega_0 = \omega_b = 0.25\pi$, $\omega_a = 0.125\pi$, and $\theta = \pi/6$

Since the coefficients for $\theta = \pi/3$ are known from Example 5.2, using the above properties, the coefficients for $\theta = \pi/3$ are easily obtained by interchanging the values of

t_{01} and t_{10}, and s_{12} and s_{21}.

The scaled coefficients for both these examples can be obtained by making similar changes in the appropriate values given in Table 5.1 (p. 165).

5.2.2 Formulas for Scaling the Coefficients of Sine Terms

Before considering the scaling-free coefficients, the formulas for scaling the coefficients of sine terms in the generalized transformation given by (5.2a) are presented The addition of sine terms to (2.1) would not affect the derivations of Chapter 2. Therefore, the maximum and minimum values of the function (F_{max} and F_{min}) and their locations do not change. They depend only upon the values of t_{ij}'s. Let S_{ij}'s be the scaled coefficients of s_{ij}'s. For all the three types (A-C) of contours

$$S_{ij} = C_1 s_{ij} \tag{5.17}$$

where C_1 is the scaling factor defined by (2.5). The scaled coefficient S_{ij}'s can also be obtained from the expressions for U_{ij}'s ($T_{ij} = f(U_{ij})$ as given in Sec. 2.4) by replacing t_{ij}'s or t in their numerator by s_{ij}'s.

Using (5.17) in (5.2a), the scaled original transformation of Sec. 2.4 is now to the *scaled generalized McClellan transformation* By adding the sine terms, $S_{ij}\sin(i\omega_1)\sin(j\omega_2)$ $[(i, j) = (1, 2), (2, 1)]$, to the scaling-free original transformation of Sec. 2.5, the *scaling-free generalized McClellan transformation* is obtained. The number of independent coefficients in this transformation varies from 0 to 4 compared to 5 in the generalized transformation.

5.2.3 Approximation for Scaling-Free Coefficients for Type-A Contours

Defining P_1 and P_2 in a way similar to p_1 and p_2 by replacing t_{ij}'s in (2.11) by T_{ij}'s, gives,

$$P_1 = T_{10} + T_{11} \tag{5.18a}$$

$$P_2 = T_{01} + T_{11}. \tag{5.18b}$$

Similarly Q_1 and Q_2, as given below, are they can be obtained by replacing s_{ij}'s in (5.4b) and (5.4c) by S_{ij}'s.

$$Q_1 = \frac{2}{3}S_{12} + \frac{8}{3}S_{21} \tag{5.19a}$$

$$Q_2 = \frac{8}{3}S_{12} + \frac{2}{3}S_{21} \tag{5.19b}$$

Using the coefficients (U_{ij}'s and S_{ij}'s) of type-A scaling-free generalized transformations in (5.6)-(5.10), the scaling-free formulas are obtained.

For all the four cases encountered the common formula for P_2 is

$$P_2 = \frac{\omega_0^2\left\{1 - \frac{\omega_0^2}{12}\right\}}{\omega_B^2\left\{1 - \frac{\omega_B^2}{12}\right\}}. \tag{5.20}$$

The values of S_{12} and S_{21} are obtained from Q_1 and Q_2. The formulas for their evaluation are similar to (5.12) in which q_1 and q_2 are replaced by Q_1 and Q_2, respectively, giving

$$S_{12} = -\frac{1}{10}Q_1 + \frac{2}{5}Q_2 \tag{5.21a}$$

$$S_{21} = \frac{2}{5}Q_1 - \frac{1}{10}Q_2 \tag{5.21b}$$

Additional formulas for different cases are as follows.

Case (i)

$$Q_2 = \frac{\omega_C}{\omega_B^2}\left[\frac{1}{\omega_B^2}\left\{1 - \frac{\omega_B^2}{4}\right\} - \left\{\frac{1}{\omega_A^2} + \frac{\omega_B^2}{6}\left\{\frac{\omega_B^2}{2\omega_C^2} - \frac{1}{\omega_A^2}\right\} + \frac{1}{4}\right\}P_2\right] \tag{5.22a}$$

$$Q_1 = \frac{5}{6}\left[\left\{\omega_B^2 - \frac{6}{5}\right\}Q_2 + \frac{\omega_B^2}{\omega_C}\left\{\frac{\omega_B^2}{6} - 1\right\}P_2\right] \tag{5.22b}$$

$$U_{01} = (P_2 - 1)/2 \tag{5.22c}$$

Cases (ii) and (iii):

$$Q_2 = \frac{\omega_B^2\left[\frac{1}{\omega_A^2} + \frac{5}{6}\left\{1 - \frac{\omega_B^2}{6}\right\}\right]P_2 - 1}{\omega_C\left[\omega_B^2\left\{\frac{5}{6} - \frac{1}{\omega_A^2}\right\} - 1\right]} \tag{5.23a}$$

$$Q_1 = \frac{5\omega_B^2}{6\omega_C}\left\{\frac{\omega_B^2}{6} - 1\right\}P_2 + \left\{\frac{5\omega_B^2}{6} - 1\right\}Q_2 \tag{5.23b}$$

$$U_{01} = \frac{2\omega_B^2}{\omega_C}Q_2 + \left[1 + \frac{2}{\omega_A^2} + \frac{\omega_B^2}{3}\left\{\frac{\omega_B^2}{2\omega_C^2} - \frac{1}{\omega_A^2}\right\}\right]P_2 - \frac{2}{\omega_B^2} \tag{5.23c}$$

$$U_{10} = 1 + U_{01} - P_2 \tag{5.23d}$$

Case (iv):

$$Q_2 = \frac{\omega_B^2\left[\omega_B^2\left[\left\{\frac{1}{\omega_A^2} - \frac{\omega_B^2}{2\omega_C^2}\right\}\left\{\frac{\omega_B^2}{6} + \frac{2}{3}\left\{1 - \frac{\omega_B^2}{4}\right\}\right\} - \left\{\frac{1}{\omega_A^2} + \frac{5}{6}\left\{1 - \frac{\omega_B^2}{4} + \frac{1}{4}\right\}\right]P_2 + \left[\left\{1 - \frac{\omega_B^2}{4}\right\}\left\{1 + \frac{7}{3}P_2\right\} + \frac{\omega_B^2}{4}\right]\right]}{4\omega_C\left\{1 - \frac{\omega_B^2}{4}\right\}\left[\omega_B^2\left\{-\frac{1}{\omega_A^2} + \frac{\omega_B^2}{\omega_C} + \frac{5}{6}\right\} - 1\right] + \omega_B^6} \tag{5.24a}$$

$$Q_1 = \frac{5\omega_B^2}{6\omega_C}\left\{\frac{\omega_B^2}{6} - 1\right\}P_2 + \left\{\frac{5\omega_B^2}{6} - 1\right\}Q_2 \tag{5.24b}$$

$$P_1 = \frac{\omega_B^2\left[\left\{\frac{1}{\omega_A^2} + \frac{\omega_B^2}{6}\left\{\frac{\omega_B^2}{2\omega_C^2} - \frac{1}{\omega_A^2}\right\} + \frac{1}{4}\right\}P_2 + \frac{\omega_B^2}{\omega_C}Q_2 - \frac{1}{4}\right]}{\left\{1 - \frac{\omega_B^2}{4}\right\}} \tag{5.24c}$$

$$U_{11} = (P_1 + P_2 - 1)/2 \tag{5.24d}$$

$$U_{10} = P_1 - U_{11} \tag{5.24e}$$

The scaling-free coefficients are obtained by using the U_{ij}'s in (3.24)-(3.26) and from the

following formulas.

$$s_{12} = S_{12} \tag{5.25a}$$

$$s_{21} = S_{21} \tag{5.25b}$$

$$q_{12} = -S_{12} / 2 \tag{5.26a}$$

$$q_{21} = -S_{21} / 2 \tag{5.26b}$$

It should be emphasized that to determine the case and to select the corresponding scaling-free formulas for given specifications, the unscaled coefficients must first be evaluated by using (5.11) and Appendix C used.

For $\theta = 0$, one can obtain $\omega_A = \omega_a$, $\omega_B = \omega_b$, $\omega_C = \infty$, $Q_1 = Q_2 = 0$, and $S_{12} = S_{21} = 0$. The above formulas for each case converge to the scaling-free formulas [(3.21)-(3.23b)] of the corresponding case for type-A contours.

5.2.3.1 Advantages

The advantage of the scaling-free formulas given by (5.20)-(5.24e) is that they give the scaling-free coefficients directly. Also, the 1-D cutoff frequency ω_0 remains the same. On the other hand, the coefficients evaluated by using (5.11a)-(5.16c) require scaling, changing ω_0 to ω_0'

5.2.3.2 Examples

The following two examples serve to illustrate the simplicity and effectiveness of the scaling-free formulas.

Example 5.5: The specifications for a rotated type-A contour are $\omega_0 = \omega_a = 0.25\pi$, $\omega_b = 0.5\pi$, and $\theta = \pi/12$.

Using the scaling-free formulas given by (5.20), (5.21), and (5.23) for the rotated type-A contours, the following results are obtained.

$$U_{01} = -0.13823764 \qquad U_{10} = 0.51812057$$

$$S_{12} = 0.15126460 \times 10^{-1} \qquad S_{21} = 0.11580589$$

$$E_{2\,MSE} = 0.13215546 \times 10^{-3} \qquad E_{2\,\max} = 0.15000616 \times 10^{-1}$$

$$E_{1\,MSE} = 0.16386627 \times 10^{-1} \qquad E_{1\,\max} = 0.77677981$$

Example 5.6: The specifications for a rotated type-A contour are $\omega_0 = \omega_a = 0.125\pi$, $\omega_b = 0.25\pi$, and $\theta = \pi/12$.

Using scaling-free formulas given by (5.20), (5.21), and (5.23) for the rotated type-A contours, the following results are obtained.

$$U_{01} = -0.17996313 \qquad U_{10} = 0.51040163$$
$$S_{12} = 0.49268836 \times 10^{-3} \qquad S_{21} = 0.96329199 \times 10^{-1}$$
$$E_{2\,MSE} = 0.58901451 \times 10^{-5} \qquad E_{2\,\max} = 0.50720035 \times 10^{-2}$$
$$E_{1\,MSE} = 0.30726512 \times 10^{-2} \qquad E_{1\,\max} = 0.30100081$$

In the above two examples, the scaling-free coefficients for the cosine- and sine-form transformations are obtained by substituting these values in (3.26) and (5.25), and (5.26) and (3.27), respectively.

5.2.4 Approximation for Coefficients for Type-B Contours

Consider a horizontal *i.e.* type-B elliptical cutoff contour rotated about the 2-D origin by an angle θ in the anticlockwise direction. The equation of this contour is

$$\frac{\omega_1^2}{\omega_B^2} + \frac{\omega_2^2}{\omega_A^2} - \frac{\omega_1\omega_2}{\omega_C} = 1 \tag{5.27}$$

where ω_A^2, ω_B^2, and ω_C are as defined by (5.1b)-(5.1d). Here, a similar derivation as for the rotated type-A contours is followed. Substituting $\omega = \omega_0$ and ω_2^2 value from (5.27), in (5.4), and using (2.3), the linear error function (3.7) (now derived for the generalized transformation (5.2b)) is rewritten as

$$\frac{1}{2}\left[-\omega_0^2\left\{1 - \frac{\omega_0^2}{12}\right\} + \omega_A^2\left\{1 - \frac{\omega_A^2}{12}\right\}p_2\right]$$

$$+ \frac{\omega_1^2}{2}\left[p_1 + \frac{\omega_A^2}{\omega_B^2}\left\{\frac{\omega_A^2}{6} - 1\right\}p_2 - \frac{Q_b}{12}\right]$$

$$+\frac{\omega_1\omega_2}{2}\left[-\frac{\omega_A^2}{\omega_C}\left\{\frac{\omega_A^2}{6}-1\right\}p_2-\frac{6}{5}q_1+\left\{\omega_A^2-\frac{6}{5}\right\}q_2\right]$$

$$+\frac{\omega_1^3\omega_2}{2}\left[q_1-\frac{Q_b}{12\omega_C}-\frac{\omega_A^2}{\omega_B^2}\left\{q_2-\frac{\omega_A^2}{6\omega_C}p_2\right\}\right]$$

$$-\frac{\omega_1^4}{24}\left[p_1+\frac{\omega_A^4}{\omega_B^4}p_2-\frac{Q_b}{\omega_B^2}\right]=0 \tag{5.28a}$$

where

$$Q_b=\omega_A^2\left[-\frac{\omega_A^2}{\omega_C}\left\{-\frac{\omega_A^2}{\omega_C}p_2+12q_2\right\}+6t_{11}\right]. \tag{5.28b}$$

Equating the constant, and the ω_1^2-, $\omega_1\omega_2$-, $\omega_1^3\omega_2$-, and ω_1^4- term coefficients of (5.28a) to zero, the following equations are obtained.

$$\omega_A^2\left\{1-\frac{\omega_A^2}{12}\right\}p_2=\omega_0^2\left\{1-\frac{\omega_0^2}{12}\right\} \tag{5.29}$$

$$p_1-\frac{\omega_A^2}{2}t_{11}+\frac{\omega_A^4}{\omega_C}q_2=\frac{\omega_A^2}{\omega_B^2}\left\{1+\frac{\omega_B^2\omega_A^4}{12\omega_C^2}-\frac{\omega_A^2}{6}\right\} \tag{5.30}$$

$$-\frac{6}{5}q_1+\left\{\omega_A^2-\frac{6}{5}\right\}q_2=-\frac{\omega_A^2}{\omega_C}\left\{1-\frac{\omega_A^2}{6}\right\}p_2 \tag{5.31}$$

$$-\frac{\omega_A^2}{2\omega_C}t_{11}+q_1+\omega_A^2\left\{\frac{\omega_A^2}{\omega_C^2}-\frac{1}{\omega_B^2}\right\}q_2=-\frac{\omega_A^4}{6\omega_C}\left\{\frac{1}{\omega_B^2}-\frac{\omega_A^2}{2\omega_C^2}\right\}p_2 \tag{5.32}$$

$$-p_1+\frac{6\omega_A^2}{\omega_B^2}t_{11}-\frac{12\omega_A^4}{\omega_B^2\omega_C}q_2=\frac{\omega_A^4}{\omega_B^2}\left\{\frac{1}{\omega_B^2}-\frac{\omega_A^2}{\omega_C^2}\right\}p_2 \tag{5.33}$$

The equations (5.28a)-(5.33) can also be obtained easily from the corresponding equations (5 5a)-(5.10) for the type-A contours, by replacing ω_A, ω_B, ω_C, and Q_a by ω_B, ω_A,

$-\omega_c$, and Q_b, respectively. Solving equations (5.29)-(5.33), the following formulas are obtained.

$$p_1 = \frac{\omega_0^2\left\{1 - \frac{\omega_0^2}{12}\right\}}{\omega_B^2\left\{1 - \frac{\omega_B^2}{12}\right\}} \tag{5.34a}$$

$$p_2 = \frac{\omega_0^2\left\{1 - \frac{\omega_0^2}{12}\right\}}{\omega_A^2\left\{1 - \frac{\omega_A^2}{12}\right\}} \tag{5.34b}$$

$$q_2 = \frac{\omega_B^2\left[\omega_B^2 p_1 + \frac{5}{6}\omega_A^4 p_2 - 10\omega_0^2\left\{1 - \frac{\omega_0^2}{12}\right\}\right] - \omega_A^4 p_2}{-12\omega_c\left\{\omega_B^2 + \omega_A^2 - \frac{5}{6}\omega_B^2\omega_A^2\right\}} \tag{5.34c}$$

$$q_1 = -\frac{5}{6\omega_c}\left[\frac{\omega_A^4}{12}p_2 - \omega_0^2\left\{1 - \frac{\omega_0^2}{12}\right\} + \left\{\frac{5\omega_A^2}{6} - 1\right\}q_2\right] \tag{5.34d}$$

$$t_{11} = \frac{1}{6}\left[\frac{\omega_B^2}{\omega_A^2}p_1 + \omega_A^2\left\{\frac{1}{\omega_B^2} - \frac{\omega_A^2}{\omega_c^2}\right\}p_2 + 12\frac{\omega_A^2}{\omega_c}q_2\right] \tag{5.34e}$$

5.2.4.1 Finding the Coefficients

To find the coefficients, first ω_A^2, ω_B^2, and ω_c are evaluated from the given frequency specifications (ω_0, ω_a, ω_b, and θ) using (5.1b)-(5.1d). Then p_1 and p_2 are evaluated from (5.34a) and (5.34b), respectively followed by the evaluation of q_2 from (5.34c). The quantities q_1 and t_{11} are evaluated using (5.34d) and (5.34e) Other t_{ij}'s are found in the same way as for the type-A contours using (2.11a), (2.11b), and (2.3). Finally, s_{ij}'s are found from (5.12). The corresponding sine-form coefficients p_{ij}'s and q_{ij}'s are obtained by using (5.14).

5.2.4.2 Special Cases

For $\theta = 0$, one can obtain $\omega_A = \omega_a$, $\omega_B = \omega_b$, $\omega_C = \infty$, $q_1 = q_2 = 0$, and $s_{12} = s_{21} = 0$. The formulas (5.34a), (5.34b), and (5.34e) reduce to (3.37a), (3.37b), and (3.37c), respectively, which are the formulas for the type-B contours. Similarly, for $\theta = 0.5\pi$, $\omega_A = \omega_b$, $\omega_B = \omega_a$, $\omega_C = \infty$, $q_1 = q_2 = 0$, and $s_{12} = s_{21} = 0$. The formulas (5.34a), (5.34b), and (5.34e) reduce to (3.17a), (3.17b), and (3.17c), respectively, which are the formulas for the type-A contours. Finally, for $\theta = 0.25\pi$, the same simplified formulas as given by (5.15a)-(5.16a) are obtained. Additionally, the simplified formulas for $q_1 = q_2$ and t_{11} are given by

$$q_1 = q_2 = \frac{\omega_0^2\left\{1 - \frac{\omega_0^2}{12}\right\} - \frac{\omega_A^4}{12}p_1}{-\omega_C\left\{\omega_A^2 - \frac{12}{5}\right\}} \tag{5.35a}$$

$$t_{11} = \frac{1}{3}\left\{1 - \frac{\omega_A^4}{2\omega_C^2}\right\}p_1 + 2\frac{\omega_A^2}{\omega_C}q_1. \tag{5.35b}$$

Since $p_1 = p_2$ and $q_1 = q_2$, $t_{10} = t_{01} = p_1 - t_{11}$, $t_{00} = 1 - (2t_{01} + t11)$, and $s_{12} = s_{21} = (3 / 10)q_1$ are obtained. These simplified formulas reduce the amount of computations for the specifications with $\theta = 0.25\pi$ and different with values of ω_0, ω_a, and ω_b.

5.2.4.3 Comparison of Approximation and Optimization Methods

The following two examples illustrate the comparison of approximation and optimization methods for finding the generalized transformation coefficients.

Example 5.7: The specifications for a rotated type-B contour are $\omega_0 = \omega_b = 0.5\pi$, $\omega_a = 0.25\pi$, and $\theta = \pi/6$.

The results obtained by using the formulas given by (5.34) are

$$t_{00} = -0.22875051 \qquad t_{01} = -0.34650530$$
$$t_{10} = -1.52736540 \qquad t_{11} = 3.10262120$$
$$s_{12} = -0.56657502 \qquad s_{21} = -0.23046834$$
$$p_1 = 1.57525580 \qquad p_2 = 2.75611590.$$
$$q_1 = -0.99229892 \qquad q_2 = -1.66451230$$
$$E_{2\,MSE} = 0.39245036 \times 10^{-1} \qquad E_{2\,\max} = 0.30832894$$
$$E_{1\,MSE} = 0.23648141 \times 10^{-1} \qquad E_{1\,\max} = 0.61049285$$

Example 5.8: The specifications for a rotated type-B contour are $\omega_0 = \omega_b = 0.25\pi$, $\omega_a = 0.125\pi$, and $\theta = \pi/6$.

Similar to Example 5.7, the optimum results for this contour can be obtained easily from the optimum results of the corresponding rotated type-A contour in the Example 5.2, giving

$$t_{00} = -1.30679770 \qquad t_{01} = 0.59535250$$
$$t_{10} = -0.82845540 \qquad t_{11} = 2.53990060$$
$$s_{12} = -0.46497150 \qquad s_{21} = -0.20531960$$
$$p_1 = 1.71144520 \qquad p_2 = 3.13525310$$
$$q_1 = -0.85749833 \qquad q_2 = -1.37680333$$
$$E_{2\,MSE} = 0.10360509 \times 10^{-8} \qquad E_{2\,\max} = 0.45230907 \times 10^{-4}$$
$$E_{1\,MSE} = 0.40639974 \times 10^{-8} \qquad E_{1\,\max} = 0.30603276 \times 10^{-3}.$$

The results obtained by using the formulas given by (5.34) are

$$t_{00} = 1.14016150 \qquad t_{01} = 0.42088141$$
$$t_{10} = -0.99232028 \qquad t_{11} = 2.70260040$$
$$s_{12} = -0.47196517 \qquad s_{21} = -0.20032028$$
$$p_1 = 1.71028012 \qquad p_2 = 3.13248181$$
$$q_1 = -0.84883086 \qquad q_2 = -1.39212064$$
$$E_{2\,MSE} = 0.94607476 \times 10^{-5} \qquad E_{2\,\max} = 0.48000056 \times 10^{-2}$$
$$E_{1\,MSE} = 0.75012721 \times 10^{-4} \qquad E_{1\,\max} = 0.61230245 \times 10^{-1}.$$

In the above two examples, the error values for the optimization and approximation methods are the same as those in the Examples 5.1 and 5.2. Hence, the conclusions made in Sec. 5.3.3 are also true here.

5.2.5 Comparison of Formulas for Rotated Type-A and Type-B Contours

Comparing the results of the rotated type-B contours [(5.34), (5.15a)-(5.16a), and (5.35)] with those for the rotated type-A contours [(5.11) and (5.15a)-(5.16c)], the following points are observed. The formulas for p_1 and p_2 for the rotated type-B contours are simply the formulas for p_2 and p_1, respectively for the rotated type-A contours. The formulas for q_2, q_1, and t_{11} for the rotated type-B contours can be obtained from the corresponding formula for the rotated type-A contours by replacing ω_A, ω_B, and ω_C by ω_B, ω_A, and $-\omega_C$, respectively. As a consequence, the expressions for p_1, p_2, t_{10}, t_{01}, p_{10}, and p_{01} for the rotated type-B contours become, respectively, the expressions for p_2, p_1, t_{01}, t_{10}, p_{01}, and p_{10} for rotated type-A contours. Similar differences are also noted in the formulas of q_1, q_2, s_{12}, s_{21}, q_{12}, and q_{21} corresponding to types A and B contours. The values of t_{00} and t_{11}, and p_{00} and p_{11} remain the same for both the types of contours. When $\theta = 0.25\pi$, the formula for $q_1 = q_2$ for the rotated type-B contours is negative of that for the rotated type-A contours. Hence, s_{12} and s_{21}, and q_{12} and q_{21} values can be obtained as the negative of the corresponding values of the rotated type-A contours. Since the value of q_1 in the formula for the rotated type-B contours is negative of that for the rotated type-A contours, the value of t_{11} does not change. Therefore, the values of t_{ij}'s and p_{ij}'s remain the same for both types of rotated contours.

The comparisons between the formulas for types A and B contours as discussed in this section are also apparent from the numerical results of Examples 5.7 and 5.8.

5.2.6 Approximation for Scaling-Free Coefficients for Type-B Contours

Using the coefficients (U_{ij}'s and S_{ij}'s) of the type-B scaling-free generalized transformations in (5.29)-(5.33), the scaling-free formulas are obtained.

For all the four cases of scaling-free formulas, the common formula for P_2 is

$$P_2 = \frac{\omega_0^2\left\{1 - \frac{\omega_0^2}{12}\right\}}{\omega_A^2\left\{1 - \frac{\omega_A^2}{12}\right\}}. \tag{5.36}$$

With the condition that

$$\omega_0 = \omega_A \tag{5.37}$$

other formulas for Cases (i)-(iii) are as follows.

Case (i):

$$P_1 = \frac{\omega_C\left[\frac{\omega_A^2}{6}\left\{\frac{\omega_A^2}{2\omega_C^2} - \frac{1}{\omega_B^2}\right\} + \frac{1}{\omega_B^2} + \frac{1}{4}\right]\left\{\frac{1}{\omega_A^2} + \frac{1}{\omega_B^2} - \frac{\omega_A^2}{\omega_C} - \frac{5}{6}\right\} + \frac{\omega_A^2}{2\omega_C}\left[\frac{\omega_A^2}{3}\left\{\frac{\omega_A^2}{2\omega_C^2} - \frac{1}{\omega_B^2}\right\} + \frac{5}{3}\left\{\frac{\omega_A^2}{6} - 1\right\} + \frac{1}{2}\right]}{\omega_C\left\{\frac{1}{\omega_A^2} - \frac{1}{4}\right\}\left\{\frac{1}{\omega_A^2} + \frac{1}{\omega_B^2} - \frac{5}{6}\right\} + \frac{\omega_A^2}{4}\left\{1 - \frac{1}{\omega_C}\right\}} \tag{5.38a}$$

$$Q_2 = \frac{\omega_C}{\omega_A^2}\left[\frac{1}{\omega_B^2}\left\{1 - \frac{\omega_A^2}{6}\right\} + \frac{1}{4}\left\{1 + \frac{\omega_A^2}{3\omega_C^2}\right\} + \left\{\frac{1}{4} - \frac{1}{\omega_A^2}\right\}P_1\right] \tag{5.38b}$$

$$Q_1 = \frac{5\omega_A^2}{6\omega_C}\left\{1 - \frac{\omega_A^2}{6}\right\} + \left\{\frac{5\omega_A^2}{6} - 1\right\}Q_2 \tag{5.38c}$$

$$U_{01} = (1 - P_1) / 2 \tag{5.38d}$$

Cases (ii) and (iii):

$$Q_2 = \frac{\omega_A^2}{\omega_C^2}\left[\frac{\omega_A^2}{6}\left\{\frac{5}{6} - \frac{1}{\omega_B^2}\right\} - \left[1 - \omega_A^2\left\{\frac{1}{\omega_B^2} - \frac{1}{6}\right\}\right]\left\{\omega_C^2 - 12\right\}^{-1} - \frac{5}{6}\right]\left[\omega_A^2\left\{\frac{5}{6} - \frac{1}{\omega_B^2}\right\} - 1\right]^{-1} \tag{5.39a}$$

$$U_{01} = \left[1 + \omega_A^2\left\{\frac{1}{\omega_B^2} - \frac{1}{6}\right\}\right]\left\{\frac{\omega_B^2}{2} - 6\right\}^{-1} + \frac{\omega_A^2}{\omega_C}\left\{\frac{\omega_A^2}{6\omega_C} - 2Q_2\right\} + 1 \qquad (5.39b)$$

$$Q_1 = \frac{5\omega_A^2}{6\omega_C}\left\{1 - \frac{\omega_A^2}{6}\right\} + Q_2\left\{\frac{5\omega_A^2}{6} - 1\right\} \qquad (5.39c)$$

$$P_1 = \omega_A^2\left[\frac{1}{\omega_B^2}\left\{1 - \frac{\omega_A^2}{6}\right\} + \frac{1}{2}(1 - U_{01}) + \frac{\omega_A^2}{\omega_C}\left\{\frac{\omega_A^2}{12\omega_C} - Q_2\right\}\right] \qquad (5.39d)$$

$$U_{10} = P_1 + U_{01} - 1 \qquad (5.39e)$$

Finally, the formulas for Case (iv), in addition to the one given by (5.31) are as follows.

Case (iv):

$$Q_2 = \frac{\omega_A^2\left[\omega_A^2\left[\left\{\frac{1}{\omega_B^2} - \frac{\omega_A^2}{2\omega_C^2}\right\}\left\{\frac{\omega_A^2}{6} + \frac{2}{3}\left\{1 - \frac{\omega_A^2}{4}\right\}\right\} - \left\{\frac{1}{\omega_B^2} + \frac{5}{9}\left\{1 - \frac{\omega_A^2}{4} + \frac{1}{4}\right\}\right]P_2 + \left[\left\{1 - \frac{\omega_A^2}{4}\right\}\left\{1 + \frac{7}{3}P_2\right\} + \frac{\omega_A^2}{4}\right]\right]}{-4\omega_C\left\{1 - \frac{\omega_A^2}{4}\right\}\left[\omega_A^2\left\{-\frac{1}{\omega_B^2} - \frac{\omega_A^2}{\omega_C} + \frac{5}{6}\right\} - 1\right] + \omega_A^6} \qquad (5.40a)$$

$$Q_1 = -\frac{5\omega_A^2}{\omega_C}\left\{\frac{\omega_A^2}{6} - 1\right\}P_2 + \left\{\frac{5\omega_A^2}{6} - 1\right\}Q_2 \qquad (5.40b)$$

$$P_1 = \frac{\omega_A^2\left[\left\{\frac{1}{\omega_B^2} + \frac{\omega_A^2}{6}\left\{\frac{\omega_A^2}{2\omega_C^2} - \frac{1}{\omega_B^2}\right\} + \frac{1}{4}\right\}P_2 - \frac{\omega_A^2}{\omega_C}Q_2 - \frac{1}{4}\right]}{\left\{1 - \frac{\omega_A^2}{4}\right\}} \qquad (5.40c)$$

$$U_{11} = (P_1 + P_2 - 1) / 2 \qquad (5.40d)$$

$$U_{10} = P_1 - U_{11} \qquad (5.40e)$$

The scaling-free coefficients are obtained by substituting the values of U_{ij}'s in

(3.28), (3.29), and (3.44)-(3.47) and by substituting the value of S_{ij}'s in (5.25) and (5.26).

It should be emphasized that to determine the case and to select the corresponding scaling-free formulas for given specifications, the unscaled coefficients must first be evaluated by using (5.34) and Appendix C used.

For $\theta = 0$, the above formulas for each case converge to the scaling-free formulas of the corresponding case for type-B contours and they are given by (3.40)-(3.42).

Comparing the above case (iv) formulas with the case (iv) formulas for the rotated type-A contours, it is found that (5.40a)-(5.40c) can be obtained, respectively, from (5.24a)-(5.24c) by replacing ω_A, ω_B, and ω_C by ω_B, ω_A, and $-\omega_C$, respectively. The advantages of these scaling-free formulas have been discussed in the Sec 5.2.3.1.

5.2.6.1 Examples

The following two examples serve to illustrate the simplicity and effectiveness of the scaling-free formulas.

Example 5.9: The specifications for a rotated type-B contour are $\omega_a = 0.25\pi$, $\omega_b = 0.5\pi$, and $\theta = \pi/12$.

From (5.1b) and (5.37), $\omega_0 = \omega_A = 0.25652706\pi$. Using the scaling-free formulas for the rotated type-B contours given by (5.21), (5.36), (5.37), and (5.39) the following results are obtained.

$$U_{01} = 0.48997078 \qquad U_{10} = -0.14217765$$
$$S_{12} = -0.12386888 \qquad S_{21} = -0.19048321\times10^{1}$$
$$E_{2\,MSE} = 0.25584515\times10^{-3} \qquad E_{2\,\max} = 0.21734841\times10^{1}$$
$$E_{1\,MSE} = 0.19827200\times10^{-2} \qquad E_{1\,\max} = 0.16440175$$

Example 5.10: The specifications for a rotated type-B contour are $\omega_a = 0.125\pi$, $\omega_b = 0.25\pi$, and $\theta = \pi/12$.

From (5.1b) and (5.37), $\omega_0 = \omega_A = 0.12826353\pi$. Using the scaling-free formulas for the rotated type-B contours given by (5.21), (5.36), (5.37), and (5.39) the following

results are obtained.

$$U_{01} = 0.59845542 \qquad U_{10} = -0.75372201 \times 10^{-1}$$
$$S_{12} = -0.90187637 \times 10^{-1} \qquad S_{21} = -0.16047103 \times 10^{-1}$$
$$E_{2\,MSE} = 0.41865687 \times 10^{-7} \qquad E_{2\,\max} = 0.27605462 \times 10^{-3}$$
$$E_{1\,MSE} = 0.13504137 \times 10^{-5} \qquad E_{1\,\max} = 0.72030070 \times 10^{-2}$$

In the above two examples, the scaling-free coefficients for the cosine- and sine-form transformations are obtained by substituting the values of U_{ij}'s in (5.25) and (3.26), and (5.26) and (3.27), respectively.

5.2.7 Comparison of Analytical and Optimization Methods

For the purpose of comparing analytical and optimization methods using two sine terms, a type-A elliptical cutoff contour with $\omega_0 = \omega_b = 0.25\pi$, $\omega_a = 0.125\pi$, and $\theta = \pi/6$ is chosen. In this example, all the frequency specifications are less than 1 rad./sec. The results of scaled and scaling-free approximation methods, and optimization method are summarized in Table 5.1.

The scaled optimum solution gives the lowest value of the error $E_{2\,MSE}$ ($E_{1\,MSE}$) and it is of the order of 10^{-10} (10^{-6}). The scaled approximation solution gives the next lowest value of the error $E_{2\,MSE}$ ($E_{1\,MSE}$), and it is of the order of 10^{-6} (10^{-4}). To compare the scaling-free approximation solution with the scaled approximation solution, a ω_0 value which is equal to the ω_0' value obtained from the latter solution is used. The errors $E_{1\,MSE}$ and $E_{2\,MSE}$ for the scaling free approximation solution is not close to that of the scaled approximation solution. The reason for this is that the former solution is obtained by forcing only the first 3 terms in the error function to zero, whereas the latter solution is obtained by forcing all the 5 terms (the constant term, and ω_1^2, $\omega_1\omega_2$, $\omega_1^3\omega_2$, and ω_1^4 terms) to zero. In all the solutions, the error $E_{1\,MSE}$ is larger than the error $E_{2\,MSE}$.

The scaled and scaling-free approximation solutions for two other values of θ, $\pi/12$ and π 1, are presented in Table 5.2. Comparing the results in Tables 3.6, 5.1, and 5.2, it

Parameter	Scaled Approx. Solution* (5.11) & (2.18) $\omega_0 = 0.25\pi$†	Scaled Optimum Solution* (5.2b) & (2.18) $\omega_0 = 0.25\pi$†	Scaling-free Approx. Solution (5.20)-(5.22c) $\omega_0 = \omega_0'$ †
t_{00}	0.11634388	0.17674869	- 0.61929677
t_{01}	- 0.26856335	- 0.24595245	0 61929677
t_{10}	0.11634388	0.17674869	- 0.61929677
t_{11}	0.73143665	0.75404755	1.61929677
s_{12}	0.54215041×10^{-1}	0.60955255×10^{-1}	2.74621150
s_{21}	0.12773351	0.13804108	- 1.4011 4020
ω_0'	0.28863415π	0.21703203π	0 28863415π
$E_{2\,MSE}$	0.69295848×10^{-6}	0.91294727×10^{-10}	0 8843 4295$\times10^{-1}$
$E_{2\,max}$	0.12900742×10^{-2}	0.13436741×10^{-4}	0.59912096
$E_{1\,MSE}$	0.75011609×10^{-4}	0.22082309×10^{-6}	0 22478457$\times10^{-1}$
$E_{1\,max}$	0.61229920×10^{-1}	0.46811285×10^{-2}	0 4673 4709

* The coefficients are actually T_{ij}'s, S_{12}, and S_{21}. † One of the specification.

Table 5.1 Comparison of Results by Analytical Methods and Optimization Method for a Rotated Type-A Elliptical Cutoff Contour with $\omega_a = 0.125\pi$, $\omega_b = 0.25\pi$, and $\theta = \pi/6$.

Parameter	Scaled Approximate Solution* $\omega_0 = 0.25\pi$†		Scaling-free Approximate Solution $\omega_0 = \omega_0'$†	
	$\theta = \pi/12$ (5.11) & (2.20)	$\theta = \pi/4$ (5.15), (5.16), & (2.18)	$\theta = \pi/12$ (5.20) & (5.23)	$\theta = \pi/4$ (5.20)-(5.22c)
t_{00}	$0.71042777 \times 10^{-1}$	-0.21455892	$0.68785237 \times 10^{-1}$	$-0.32746657 \times 10^{1}$
t_{01}	$-0.71042777 \times 10^{-1}$	-0.21455892	$-0.68785237 \times 10^{-1}$	0.32746657×10^{1}
t_{10}	0.60316738	-0.21455892	0.60509009	$-0.32746657 \times 10^{1}$
t_{11}	0.39683262	0.78544108	0.39490991	0.42746657×10^{1}
s_{12}	$0.16047103 \times 10^{-1}$	$0.91519843 \times 10^{-1}$	$0.16360192 \times 10^{-1}$	0.10594241×10^{2}
s_{21}	$0.90187637 \times 10^{-1}$	$0.91519843 \times 10^{-1}$	$0.90060313 \times 10^{-1}$	$-0.69663759 \times 10^{1}$
ω_0'	$0.1283303\,4\pi$	0.47683630π	$0.1283303\,1\pi$	0.47683630π
$E_{2\,MSE}$	$0.70697815 \times 10^{-7}$	$0.10284670 \times 10^{-5}$	$0.56600202 \times 10^{-7}$	0.10422037×10^{1}
$E_{2\,max}$	$0.37580917 \times 10^{-3}$	$0.16757531 \times 10^{-2}$	$0.31803690 \times 10^{-3}$	0.20569026×10^{1}
$E_{1\,MSE}$	$0.20092676 \times 10^{-4}$	$0.10518038 \times 10^{-3}$	$0.21451003 \times 10^{-4}$	0.35601155
$E_{1\,max}$	$0.36186539 \times 10^{-1}$	$0.67087039 \times 10^{-1}$	$0.38393376 \times 10^{-1}$	0.12085246×10^{1}

* The coefficients are actually T_{ij}'s, S_{12}, and S_{21}. † One of the specification.

Table 5.2 Comparison of Scaled and Scaling-free Approximate Solutions for Different Values of θ for Type-A Elliptical Cutoff Contour with $\omega_a = 0.125\pi$ and $\omega_b = 0.25\pi$.

is observed that for both the solutions, the MSE increases with the increasing value of the angle of rotation ($0 \leq \theta \leq \pi/4$). Also it is observed that the MSEs for the scaling-free approximation solution is much closer to those of the scaled approximation solution for $\theta = \pi/12$ than for $\theta = \pi/6$ and $\theta = \pi/4$. The reason for this is that in the scaling-free approximation solution for $\theta = \pi/12$, the number of terms in the error function forced to zero is increased to 4.

5.3 Approach II - Approximation with One Sine Term

5.3.1 Approximation for Coefficients for Type-A Contours

In order to design a better fit for the non-quadrantal contour (Fig 5.1) and to have a 2-D filter of minimum order, the following first-order generalized McClellan transformation is used.

$$\begin{aligned}\cos(\omega) &= t_{00} + t_{01}\cos(\omega_2) + t_{10}\cos(\omega_1) + t_{11}\cos(\omega_1)\cos(\omega_2) + s_{11}\sin(\omega_1)\sin(\omega_2) \\ &= F_{g1}(\omega_1,\omega_2) \end{aligned} \tag{5.41}$$

It should be noted that in (5.41), only first-order cosine terms and a sine term are used to provide the quadrantally symmetric and centro-symmetric components, respectively Fig. 5.2 shows the 2-D impulse response of the transformation given by (5.41).

Using (3.11) and (5.3) in (5.41), and neglecting the terms with sixth- and higher-order powers, yields,

$$\begin{aligned}1 - \frac{\omega^2}{2} + \frac{\omega^4}{24} &= (t_{00} + t_{01} + t_{10} + t_{11}) - \frac{1}{2}(p_1\omega_1^2 + p_2\omega_2^2) \\ &\quad + \frac{1}{24}(p_1\omega_1^4 + p_2\omega_2^4 + 6t_{11}\omega_1^2\omega_2^2) \\ &\quad + s_{11}\left\{\omega_1\omega_2 - \frac{\omega_1^3\omega_2}{6} - \frac{\omega_1\omega_2^3}{6}\right\}\end{aligned} \tag{5.42}$$

where p_1 and p_2 are as defined in (2.11a) and (2.11b), respectively. Assume that the 1-D pass-band cutoff frequency ω_0 is exactly mapped onto the rotated 2-D elliptical pass-band cutoff contour given by (5.1a). Substituting in (5.42), $\omega = \omega_0$, and ω_2^2 value

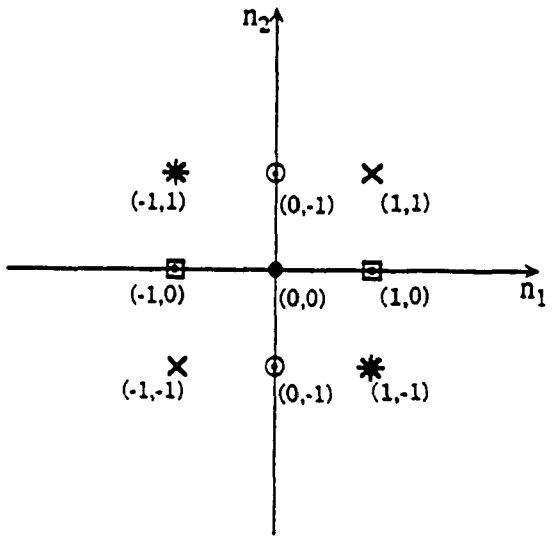

Fig. 5.2 Two-Dimensional Impulse Response $f(n_1,n_2)$ of the First-Order Generalized McClellan Transformation given by (5.41).
$f(0,0) = t_{00}$, $f(0,1) = f(0,-1) = t_{01}/2$, $f(1,0) = f(-1,0) = t_{10}/2$,
$f(1,1) = f(-1,-1) = (t_{11} - s_{11})/4$, $f(1,-1) = f(-1,1) = (t_{11} + s_{11})/4$.

(Two-dimensional impulse response $f(n_1,n_2)$ of the first-order original McClellan transformation given by (2.1) is obtained from the above equations by substituting $s_{11} = 0$. In this case, the values at the corner points (×,*) are equal.)

from (5.1a), and using (2.3), the linear error function given by (3.7) (now derived for the generalized transformation (5.41)) is rewritten as

$$\frac{1}{2}\left[-\omega_0^2\left\{1-\frac{\omega_0^2}{12}\right\}+\omega_B^2\left\{1-\frac{\omega_B^2}{12}\right\}p_2\right]$$
$$+\frac{\omega_1^2}{2}\left[p_1+\frac{\omega_B^2}{\omega_A^2}\left\{\frac{\omega_B^2}{6}-1\right\}p_2-\frac{R_a}{12}\right]$$
$$+\frac{\omega_1\omega_2}{2}\left[\left\{\frac{\omega_B^2}{\omega_C}p_2+2s_{11}\right\}\left\{\frac{\omega_B^2}{6}-1\right\}\right]$$
$$+\frac{\omega_1^3\omega_2}{6}\left[s_{11}+\frac{R_a}{4\omega_C}-\frac{\omega_B^2}{\omega_A^2}\left\{\frac{\omega_B^2}{2\omega_C}p_2+s_{11}\right\}\right]$$
$$-\frac{\omega_1^4}{24}\left[p_1+\frac{\omega_B^4}{\omega_A^4}p_2-\frac{R_a}{\omega_A^2}\right]=0 \qquad (5.43a)$$

where

$$R_a=\omega_B^2\left[\frac{\omega_B^2}{\omega_C}\left\{\frac{\omega_B^2}{\omega_C}p_2+4s_{11}\right\}+6t_{11}\right]. \qquad (5.43b)$$

Since the error must be zero, the right side of (5.43a) has been taken to be zero. Equating the constant, and the ω_1^2-, $\omega_1\omega_2$-, and $\omega_1^3\omega_2$- term coefficients to zero, the following equations are obtained.

$$\omega_B^2\left\{1-\frac{\omega_B^2}{12}\right\}p_2=\omega_0^2\left\{1-\frac{\omega_0^2}{12}\right\} \qquad (5.44)$$

$$p_1-\frac{\omega_B^2}{2}t_{11}-\frac{\omega_B^4}{3\omega_C}s_{11}=\omega_B^2\left\{\frac{1}{\omega_A^2}-\frac{\omega_B^2}{6\omega_A^2}+\frac{\omega_B^4}{2\omega_C^2}\right\}p_2 \qquad (5.45)$$

$$\left\{\frac{\omega_B^2}{3}-2\right\}s_{11}=\frac{\omega_B^2}{\omega_C}\left\{1-\frac{\omega_B^2}{6}\right\}p_2 \qquad (5.46)$$

$$\frac{\omega_B^2}{2\omega_C}t_{11}+\frac{1}{3}\left\{1-\frac{\omega_B^2}{\omega_A^2}+\frac{\omega_B^4}{\omega_C^2}\right\}s_{11}=\frac{\omega_B^4}{6\omega_C}\left\{\frac{1}{\omega_A^2}-\frac{\omega_B^2}{2\omega_C^2}\right\}p_2 \qquad (5.47)$$

Solving the above four equations, yields the following formulas.

$$p_2 = \frac{\omega_0^2\left\{1 - \frac{\omega_0^2}{12}\right\}}{\omega_B^2\left\{1 - \frac{\omega_B^2}{12}\right\}} \tag{5.48a}$$

$$p_1 = \frac{\omega_B^2}{6}\left\{1 + \frac{6 - \omega_B^2}{\omega_A^2}\right\}p_2 \tag{5.48b}$$

$$t_{11} = -\frac{1}{3}\left\{1 + \frac{\omega_B^4}{2\omega_C^2}\right\}p_2 \tag{5.48c}$$

$$s_{11} = -\frac{\omega_B^2}{2\omega_C}p_2 \tag{5.48d}$$

From this derivation, it can be concluded that the analytical formulas given by (5.48) are approximate solutions to the linear optimization problem (Eq. (3.8)) itself for the generalized transformation. Also, the derivation is straight forward and the derived formulas are easy to use. Further, in the next section, it would form the basis for deriving the scaling-free formulas. The constant term and certain number of lower-order ω_1 and ω_2 terms, depending on the number of unknowns, are forced to assume a zero value. The higher-order ω_1 and ω_2 terms are assumed to be zero, since their values are negligible particularly for low frequencies. The approximation formulas thus obtained give good results and their accuracy is sufficient for many engineering applications. To illustrate these points, some examples are given in Sec. 5.3.1.3.

5.3.1.1 Finding the Coefficients

To find the coefficients for the given frequency specifications ω_0, ω_a, ω_b, and θ, first ω_A^2, ω_B^2, and ω_C are evaluated using (5.1b)-(5.1d) and p_2 is evaluated using (5.48a). Substituting these values in (5.48b)-(5.48d), the quantities p_1, t_{11}, and s_{11} are evaluated. Finally, other t_{ij} values are found in the same way as for type-A contours using (2.11) and (2.3).

The sine-form generalized transformation corresponding to (5.41) is obtained from the 2-D version of (4.66) in which for the additional sine terms $(i_1, i_2) = (1, 1)$. The transform, in this case, is then given by

$$\begin{aligned}\sin^2(\omega/2) &= p_{00} + p_{01}\sin^2(\omega_2/2) + p_{10}\sin^2(\omega_1/2) + p_{11}\sin^2(\omega_1/2)\sin^2(\omega_2/2) \\ &\quad + q_{11}\sin(\omega_1)\sin(\omega_2) \\ &= G_{g1}(\omega_1,\omega_2). \end{aligned} \tag{5.49}$$

The formulas for the coefficients in (5.49) are

$$p_{00} = 0, \quad p_{01} = p_2, \quad p_{10} = p_1, \quad p_{11} = -2t_{11}, \quad \text{and} \quad q_{11} = -s_{11}/2. \tag{5.50}$$

5.3.1.2 Special Cases

For $\theta = 0$, one can obtain $\omega_A = \omega_a$, $\omega_B = \omega_b$, and $\omega_C = \infty$. In the set of formulas given by (5.48), s_{11} becomes zero, and the remaining formulas do not converge to the respective formulas for type-A contours. The reason is that in the derivation of (5.48) the coefficient of ω_1^4 term is not forced to zero. Similarly, for $\theta = 0.5\pi$, one can obtain $\omega_A = \omega_b$, $\omega_B = \omega_a$, $\omega_C = \infty$, and for the same reason the formulas given by (5.48b) and (5.48c) do not converge to the corresponding formulas for type-B contours. Finally, for $\theta = 0.25\pi$, the following simplified formulas are obtained.

$$\omega_A^2 = \omega_B^2 = \frac{2\omega_a^2\omega_b^2}{\omega_a^2 + \omega_b^2} \tag{5.51a}$$

$$\omega_C = \frac{\omega_a^2\omega_b^2}{\omega_a^2 - \omega_b^2} \tag{5.51b}$$

$$p_1 = p_2 = \frac{\omega_0^2\left\{1 - \dfrac{\omega_0^2}{12}\right\}}{\omega_A^2\left\{1 - \dfrac{\omega_A^2}{12}\right\}} \tag{5.52a}$$

$$t_{11} = \frac{1}{3}\left\{1 + \frac{\omega_B^4}{2\omega_C^2}\right\}p_2 \tag{5.52b}$$

$$s_{11} = -\frac{\omega_B^2}{2\omega_C}p_2 \tag{5.52c}$$

Further, for $\omega_a = \omega_b = \omega_e$ (say), one can obtain $\omega_A = \omega_B = \omega_e$ and $\omega_C = \infty$, and the formulas given by (5.52a) and (5.52b) converge to the formulas given by (4.8a) and (4.8b), respectively for the circular (type-C) contours. Since $p_1 = p_2$ in (5.52a), $t_{10} = t_{01}$. These simplified formulas reduce the amount of computations for the specifications with $\theta = 0.25\pi$.

5.3.1.3 Comparison of Approximation and Optimization Methods

The following two examples illustrate the comparison of approximation and optimization methods for finding the first-order generalized transformation coefficients.

Example 5.11: The specifications for a rotated type A contour are $\omega_0 = \omega_b = 0.5\pi$, $\omega_a = 0.25\pi$, and $\theta = \pi/6$.

The results obtained by using the formulas given by (5.48) are

$$t_{00} = -2.07969140 \qquad t_{01} = 0.47150514$$
$$t_{10} = 1.50443560 \qquad t_{11} = 1.10375070$$
$$s_{11} = 1.16932420$$
$$E_{2\,MSE} = 0.47291728\times10^{-2} \qquad E_{2\,\max} = 0.12511143$$
$$E_{1\,MSE} = 0.10775088\times10^{-1} \qquad E_{1\,\max} = 0.42234119.$$

Using (2.20) and (5.17), the following scaled coefficients are obtained.

$$T_{00} = -0.18077894 \qquad T_{01} = 0.18077894$$
$$T_{10} = 0.57681294 \qquad T_{11} = 0.42318706$$
$$S_{11} = 0.44832848 \qquad \omega_0' = 0.28851292\pi$$
$$E_{2\,MSE} = 0.69519661\times10^{-3} \qquad E_{2\,\max} = 0.47968740\times10^{-1}$$
$$E_{1\,MSE} = 0.10775088\times10^{-1} \qquad E_{1\,\max} = 0.42234115$$

It should be noted despite the values of ω_0 and ω_b being not less than 1 rad./sec., the MSE values are reasonably good. For lower frequency specifications, the MSE will be further reduced. To reinforce this point, in the next example, the frequency specifications are reduced by a factor of 2 and the rotation angle is kept the same.

Example 5.12: The specifications for a rotated type-A elliptical contour are

$\omega_0 = \omega_b = 0.25\pi$, $\omega_a = 0.125\pi$, and $\theta = \pi/6$.

The results obtained by using the formulas given by (5.48) are

$$t_{00} = -2.60203370 \qquad t_{01} = 0.51192058$$
$$t_{10} = 1.89175360 \qquad t_{11} = 1.19835950$$
$$s_{11} = 1.26955380$$
$$E_{2\,MSE} = 0.16556856\times10^{-4} \qquad E_{2\,\max} = 0.82958487\times10^{-2}$$
$$E_{1\,MSE} = 0.26051774\times10^{-3} \qquad E_{1\,\max} = 0.99643828\times10^{-1}.$$

Using (2.20) and (5.17), the scaled coefficients are obtained and they are given in column 1 of Table 5.4 (p. 181).

By comparing the error values of the above two examples, it is observed that the approximation method gives better results for lower values of frequency specifications.

5.3.2 Approximation for Scaling-Free Coefficients for Type-A Contours

The first-order scaling-free generalized McClellan transformation is obtained from the scaling-free original transformation of Sec. 2.5, by adding the sine term, $S_{11}\sin(\omega_1)\sin(\omega_2)$. The number of independent coefficients in this transformation varies from 0 to 3 compared to 4 in the original generalized transformation. Also, both for approaches I and II, the scaling-free coefficients can be expressed in sum-of-powers-of-two (SOPOT). The 2-D filters obtained by the scaling-free transformations can be implemented by using the schemes described in [16]. The number of multiplications required per output sample will be small, since the multiplications by powers of two are done by bit shifting. Multiplierless filter structures are possible for the 2-D filters obtained through the scaled transformations by quantizing the coefficients to their nearest SOPOT value. These implementations are very attractive for low cost, real-time signal processing applications.

Employing the quantities P_1 and P_2 as defined in (5.18a) and (5.18b), respectively and using the coefficients (U_{ij}'s and S_{11}) of type-A scaling-free generalized transformations in (5.44)-(5.47), the following scaling-free formulas are derived.

For all the four cases encountered, the common formula for P_2 is

$$P_2 = \frac{\omega_0^2\left\{1 - \frac{\omega_0^2}{12}\right\}}{\omega_B^2\left\{1 - \frac{\omega_B^2}{12}\right\}} \tag{5.53}$$

Additional formulas that are not common between different cases are as follows.

Case (i):

$$S_{11} = \omega_C\left[\frac{3}{\omega_B^2}\left\{\frac{1}{\omega_B^2} - P_2\left\{\frac{1}{\omega_A^2} + \frac{1}{4}\right\} - \frac{1}{4}\right\} + \frac{P_2}{2}\left\{\frac{1}{\omega_A^2} - \frac{\omega_B^2}{2\omega_C^2}\right\}\right] \tag{5.54a}$$

$$U_{01} = (P_2 - 1) / 2 \tag{5.54b}$$

Cases (ii) and (iii):

$$S_{11} = -\frac{\omega_B^2}{2\omega_C}P_2 \tag{5.55a}$$

$$U_{01} = P_2\left[\frac{2}{\omega_A^2} - \frac{\omega_B^2}{3}\left\{\frac{1}{\omega_A^2} + \frac{\omega_B^2}{2\omega_C^2}\right\} + 1\right] - \frac{2}{\omega_B^2} \tag{5.55b}$$

$$U_{10} = 1 + U_{01} - P_2 \tag{5.55c}$$

Case (iv):

$$S_{11} = -\frac{\omega_B^2}{2\omega_C}P_2 \tag{5.56a}$$

$$P_1 = \omega_B^2\left[P_2\left\{\frac{1}{\omega_A^2} - \frac{\omega_B^2}{6}\left\{\frac{1}{\omega_A^2} + \frac{\omega_B^2}{2\omega_C^2}\right\} + \frac{1}{4}\right\} - \frac{1}{4}\right]\left[1 - \frac{\omega_B^2}{4}\right]^{-1} \tag{5.56b}$$

$$U_{11} = (P_1 + P_2 - 1) / 2 \tag{5.56c}$$

$$U_{10} = P_1 - U_{11} \tag{5.56d}$$

The scaling-free coefficients are obtained by using U_{ij}'s in (3.24)-(3.29) and from the following relations.

$$s_{11} = S_{11} \tag{5.57}$$

$$q_{11} = -S_{11}/2 \tag{5.58}$$

The advantages of the scaling-free formulas have been discussed in the Sec. 5.2.3.1.

It should be emphasized that to determine the case and to select the corresponding scaling-free formulas for given specifications, the unscaled coefficients must first be evaluated by using (5.48) and Appendix C used.

For $\theta = 0$, one can obtain $\omega_A = \omega_a$, $\omega_B = \omega_b$, $\omega_C = \infty$, and $S_{11} = 0$. The above formulas for each case converge to the scaling-free formulas [(3.21)-(3.23b)] of the corresponding case for type-A contours.

5.3.3 Approximation for Coefficients for Type-B Contours

Consider a horizontal *i.e.* type-B elliptical cutoff contour rotated about the 2-D origin by an angle θ in the anticlockwise direction. The equation of this contour is given by (5.27). Here, a similar derivation as for the rotated type-A contours is carried out. Substituting $\omega = \omega_0$ and ω_2^2 value from (5.27) in (5.42), and using (2.3), the linear error function given by (3.7) (now derived for the first-order generalized transformation (5.41)) is rewritten as

$$\begin{aligned}
&\frac{1}{2}\left[-\omega_0^2\left\{1-\frac{\omega_0^2}{12}\right\}+\omega_A^2\left\{1-\frac{\omega_A^2}{12}\right\}p_2\right] \\
&+\frac{\omega_1^2}{2}\left[p_1+\frac{\omega_A^2}{\omega_B^2}\left\{\frac{\omega_A^2}{6}-1\right\}p_2-\frac{R_b}{12}\right] \\
&+\frac{\omega_1\omega_2}{2}\left[\left\{-\frac{\omega_A^2}{\omega_C}p_2+2s_{11}\right\}\left\{\frac{\omega_A^2}{6}-1\right\}\right] \\
&+\frac{\omega_1^3\omega_2}{6}\left[s_{11}-\frac{R_b}{4\omega_C}-\frac{\omega_A^2}{\omega_B^2}\left\{-\frac{\omega_A^2}{2\omega_C}p_2+s_{11}\right\}\right]
\end{aligned}$$

$$-\frac{\omega_1^4}{24}\left[p_1+\frac{\omega_A^4}{\omega_B^4}p_2-\frac{R_b}{\omega_B^2}\right]=0. \tag{5.59a}$$

where

$$R_b=\omega_A^2\left[-\frac{\omega_A^2}{\omega_C}\left\{-\frac{\omega_A^2}{\omega_C}p_2+4s_{11}\right\}+6t_{11}\right]. \tag{5.59b}$$

Equating the constant, and the ω_1^2-, $\omega_1\omega_2$-, and $\omega_1^3\omega_2$- term coefficients of (5.59a) to zero, the following equations are obtained.

$$\omega_A^2\left\{1-\frac{\omega_A^2}{12}\right\}p_2=\omega_0^2\left\{1-\frac{\omega_0^2}{12}\right\} \tag{5.60}$$

$$p_1-\frac{\omega_A^2}{2}t_{11}+\frac{\omega_A^4}{3\omega_C}s_{11}=\omega_A^2\left\{\frac{1}{\omega_B^2}-\frac{\omega_A^2}{6\omega_B^2}+\frac{\omega_A^4}{12\omega_C^2}\right\}p_2 \tag{5.61}$$

$$\left\{\frac{\omega_A^2}{3}-2\right\}s_{11}=-\frac{\omega_A^2}{\omega_C}\left\{1-\frac{\omega_A^2}{6}\right\}p_2 \tag{5.62}$$

$$-\frac{\omega_A^2}{2\omega_C}t_{11}+\frac{1}{3}\left\{1-\frac{\omega_A^2}{\omega_B^2}+\frac{\omega_A^4}{\omega_C^2}\right\}s_{11}=-\frac{\omega_A^4}{6\omega_C}\left\{\frac{1}{\omega_B^2}-\frac{\omega_A^2}{2\omega_C^2}\right\}p_2 \tag{5.63}$$

Solving (5.60)-(5.63), the following formulas are obtained.

$$p_2=\frac{\omega_0^2\left\{1-\frac{\omega_0^2}{12}\right\}}{\omega_A^2\left\{1-\frac{\omega_A^2}{12}\right\}} \tag{5.64a}$$

$$p_1=\frac{\omega_A^2}{6}\left\{1+\frac{6-\omega_A^2}{\omega_B^2}\right\}p_2 \tag{5.64b}$$

$$t_{11}=\frac{1}{3}\left\{1+\frac{\omega_A^4}{2\omega_C^2}\right\}p_2 \tag{5.64c}$$

$$s_{11} = \frac{\omega_A^2}{2\omega_C} p_2 \tag{5.64d}$$

5.3.3.1 Finding the Coefficients

To find the coefficients for the given frequency specifications ω_0, ω_a, ω_b, and θ, first ω_A^2, ω_B^2, and ω_C are evaluated using (5.1b)-(5.1d), and p_2 is evaluated using (5.64a). Substituting these values in (5.64b)-(5.64d), the quantities p_1, t_{11}, and s_{11} are evaluated. Other t_{ij} values are found as for type-A contours using (2.11b), (2.11b), and (2.3). The corresponding sine-form coefficients p_{ij}'s and q_{11} are obtained from (5.50).

5.3.3.2 Special Cases

For $\theta = 0$, one can obtain $\omega_A = \omega_a$, $\omega_B = \omega_b$, and $\omega_C = \infty$. Similarly, for $\theta = 0.5\pi$, one can obtain $\omega_A = \omega_b$, $\omega_B = \omega_a$, and $\omega_C = \infty$. For both the cases, s_{11} becomes zero. For $\theta = 0$, or $\theta = 0.5\pi$, the formula for p_2 given by (5.64a) converges to (3.37b) corresponding to type-B contours or to (3.17b) corresponding to type-A contours. The remaining two formulas given by (5.64b) and (5.64c) do not converge to the corresponding formulas for type-B or type-A contours, since in this derivation ω_1^4 term is not forced to zero. For $\theta = 0.25\pi$, the formulas given by (5.51a)-(5.52a), the same as for the rotated type-A contours, and those given by (5.64c) and (5.64d) are obtained. Further, for $\omega_a = \omega_b = \omega_e$ (say), one can obtain $\omega_A = \omega_B = \omega_e$, $\omega_C = \infty$, and the formulas given by (5.52a) and (5.64c) converge to (4.8a) and (4.8b), respectively, corresponding to the circular (type-C) contours.

5.3.4 Approximation for Scaling-Free Coefficients for Type-B Contours

Using the coefficients U_{ij}'s and S_{11} of type-B scaling-free generalized transformations given by (5.60)-(5.63), the following scaling-free formulas are derived.

For all the four cases encountered, the common formula for P_2 is

$$P_2 = \frac{\omega_0^2 \left\{ 1 - \frac{\omega_0^2}{12} \right\}}{\omega_A^2 \left\{ 1 - \frac{\omega_A^2}{12} \right\}} \tag{5.65}$$

With the condition that

$$\omega_0 = \omega_A \tag{5.66}$$

other formulas for Cases (i)-(iii) are as follows.

Case (i):

$$S_{11} = \omega_A^2 \,/\, (2\omega_C) \tag{5.67a}$$

$$P_1 = \omega_A^2 \left[\frac{\omega_A^4}{6\omega_C} \left\{ \frac{1}{2} - \frac{1}{\omega_C} \right\} + \frac{1}{\omega_B^2} \left\{ 1 - \frac{\omega_A^2}{6} \right\} + \frac{1}{4} \right] \left[1 - \frac{\omega_A^2}{4} \right]^{-1} \tag{5.67b}$$

$$U_{01} = (1 - P_1) \,/\, 2 \tag{5.67c}$$

Cases (ii) and (iii):

$$U_{01} = \frac{2}{3} \left\{ 1 - \frac{\omega_A^4}{4\omega_C} \right\} \tag{5.68a}$$

$$P_1 = \omega_A^2 \left[\frac{1}{\omega_B^2} + \frac{1}{6} \left\{ 1 - \frac{\omega_A^2}{\omega_B^2} \right\} \right] \tag{5.68b}$$

$$U_{10} = P_1 + U_{01} - 1 \tag{5.68c}$$

Finally, the formulas for Case (iv), in addition to the one given by (5.65), are as follows.

Case (iv):

$$S_{11} = \frac{\omega_A^2}{2\omega_C} P_2 \tag{5.69a}$$

$$P_1 = \omega_A^2 \left[P_2 \left\{ \frac{1}{\omega_B^2} - \frac{\omega_A^2}{6} \left\{ \frac{\omega_A^2}{2\omega_C^2} + \frac{1}{\omega_B^2} \right\} + \frac{1}{4} \right\} - \frac{1}{4} \right] \left[1 - \frac{\omega_A^2}{4} \right]^{-1} \tag{5.69b}$$

$$U_{11} = (P_1 + P_2 - 1) / 2 \tag{5.69c}$$

$$U_{10} = P_1 - U_{11} \tag{5.69d}$$

The scaling-free coefficients are obtained by substituting the values of U_{ij}'s in (3.28), (3.29), and (3.44)-(3.47), and by substituting the value of S_{11} in (5.77) and (5.58).

It should be emphasized that to determine the case and to select the corresponding scaling-free formulas for given specifications, the unscaled coefficients must first be evaluated by using (5.64) and Appendix C used.

For $\theta = 0$, the formulas for Cases (i) and (iv) converge to the corresponding scaling-free formulas for type-B contours and they are given by (3.40) and (3.42), respectively. However, the formulas for the Cases (ii) and (iii) do not have such a convergence, since in this derivation the coefficient of ω_1^4 term is not forced to zero. The convergence takes place only for the special case when the value of U_{01} for the type-B contour is 2/3.

5.3.5 Comparison of Analytical and Optimization Methods

To compare analytical and optimization methods in approach II, it is necessary to solve the same problem and to compute the same type of error values for all the methods. As in the previous chapters, the mean square error and the maximum absolute error of the linear and nonlinear error functions $E_2(\omega_1)$ and $E_1(\omega_1)$ as defined by (3.7) and (3.4) and modified for the first-order generalized transformation (5.41), are used as figures of merit.

Calculations are carried out on CYBER 835D using (3.88) with $N_f = 201$, to verify the error values reported in [42]. Some numerical errors are found in Table I of [42]. The re-calculated error values for the results of [42] are given in Table 5.3. The authors of [42] have used a MSE definition with a weighting factor of 1/2. Therefore, the $E_{2\,MSE}$ error values in Table 5.3 are divided by 2 in order to compare them with those in [42].

Example	Method	$E_{2\,MSE}$	$E_{2\,\max}$	$E_{1\,MSE}$	$E_{1\,\max}$
1) $\omega_a = 0.35\pi$ $\omega_b = 0.85\pi$ $\theta = \pi/8$	Analytical	0.10940076×10^{-2}	0.41721732×10^{-1}	0.17425964×10^{-1}	0.63931928
	Optimization	0.13669941×10^{-2}	0.43882783×10^{-1}	0.15088715×10^{-1}	0.44935431
2) $\omega_a = 0.125\pi$ $\omega_b = 0.25\pi$ $\theta = \pi/6$	Analytical	0.10034494×10^{-6}	0.32057939×10^{-3}	0.11799751×10^{-4}	0.31863704×10^{-1}
	Optimization	0.87546093×10^{7}	0.30466212×10^{-3}	0.13896269×10^{-4}	0.34061167×10^{-1}
3) $\omega_a = 0.25\pi$ $\omega_b = 0.95\pi$ $\theta = \pi/4$	Analytical	0.26547095×10^{-4}	0.58092622×10^{-2}	0.12989938×10^{-3}	0.65630631×10^{-1}
	Optimization	0.20588867×10^{-4}	0.49032940×10^{-2}	0.16683083×10^{-3}	0.90896568×10^{-1}

Table 5.3 Recalculated $E_{2\,MSE}$ Values and Other Calculated Error Values for the Three Examples in Table I of Reference [5.3].

The errors $E_{\max}$ and E_{RMS} defined in [42] are different from the errors $E_{1\,\max}$ and $E_{1\,RMS}$ defined in the thesis. Therefore, the other error values, *viz*, $E_{2\,\max}$, $E_{1\,MSE}$, and $E_{1\,\max}$ are also presented in Table 5.3 for comparison purposes.

The results of several methods for a rotated type-A elliptical cutoff contour having the specifications $\omega_0 = \omega_b = 0.25\pi$, $\omega_a = 0.125\pi$, and $\theta = \pi/6$ are summarized in Table 5.4. The scaled optimum solution gives the lowest value of the error $E_{2\,MSE}$ and is of the order of 10^{-7}. The scaled analytical solution [42] gives the next lowest value of $E_{2\,MSE}$ and is of the order of 10^{-6}. The values of the error $E_{1\,MSE}$ for both the solutions are of the order of 10^{-4}. The scaled and scaling-free approximation solutions give the value of the error $E_{2\,MSE}$ ($E_{1\,MSE}$), close to those given by scaled analytical and scaled optimum solutions, and they are of the order of 10^{-5} (10^{-3}). To compare the scaling-free approximation solution with the scaled approximation solution, a ω_0 value which is equal to the ω_0' value obtained from the latter solution is used. For both the solutions, the $E_{2\,MSE}$ ($E_{1\,MSE}$) errors are approximately the same. In all the solutions the error $E_{1\,MSE}$ is higher than the error $E_{2\,MSE}$.

The scaled and scaling-free approximation solutions for two other values of θ, $\pi/12$ and $\pi/4$, are presented in Table 5.5. Comparing the results in Tables 5.4 and 5.5, it is observed that for both these solutions, the MSE decreases with the increasing value of the angle of rotation ($0 < \theta \leq \pi/4$). This is in contrast to the methods in approach I, where the MSE value increases.

Fig. 5.3 and 5.4 show the contours of the first-order generalized McClellan transformation with the coefficients given by the scaled optimum and scaling-free approximation solutions, respectively. Fig. 5.5 shows the contours of the transformation with the coefficients given by the scaling-free approximation solution.

Parameter	Scaled Approx. Solution* (5.48) & (2.20) $\omega_0 = 0.25\pi$†	Scaled Analytical Solution* [5.4] $\omega_0 = 0.25\pi$†	Scaled Optimum Solution* (5.41) & (2.20) $\omega_0 = 0.25\pi$†	Scaling-free Approx. Solution (5.53) & (5.55) $\omega_0 = \omega_0'$†
t_{00}	− 0.16566402	− 0.10120310	− 0.14574660	− 0.17148958
t_{01}	0.16566402	0.10120310	0.14574660	0.17148958
t_{10}	0.61219558	0.55844520	0.60295680	0.61746900
t_{11}	0.38780442	0.44155480	0.39704320	0.38253100
s_{11}	0.41084377	0.39968230	0.40195920	0.41125363
ω_0'	0.13970893π	0.13843520π	0.13850030π	0.13970893π
$E_{2\,MSE}$	0.17339359×10^{-5}	0.10034191×10^{-6}	0.87546093×10^{-7}	0.16212458×10^{-5}
$E_{2\,max}$	0.26846171×10^{-2}	0.32057939×10^{-3}	0.30166212×10^{-3}	0.26605428×10^{-2}
$E_{1\,MSE}$	0.26051869×10^{-3}	0.11700751×10^{-4}	0.13806260×10^{-4}	0.25461967×10^{-3}
$E_{1\,max}$	0.99643893×10^{-1}	0.31863704×10^{-1}	0.34061167×10^{-1}	0.99600123×10^{-1}

* The coefficients are actually T_{ij}'s and S_{11}. † One of the specification.

Table 5.4 Comparison of Results by Several Analytical Methods and Optimization Method for Rotated Type-A Elliptical Cutoff Contour with $\omega_a = 0.125\pi$, $\omega_b = 0.25\pi$, and $\theta = \pi/6$.

Parameter	Scaled Approximate Solution* $\omega_0 = 0.25\pi$†		Scaling-free Approximate Solution $\omega_0 = \omega_0'$ †	
	$\theta = \pi/12$ (5.48) & (2.20)	$\theta = \pi/4$ (5.51), (5.52), (5.48c,d), & (2.20)	$\theta = \pi/12$ (5.53) & (5.55)	$\theta = \pi/4$ (5.53) & (5.55)
t_{00}	− 0.13655077	− 0.42666667	− 0.14067431	− 0.43450800
t_{01}	0.13655077	0.42666667	0.14067431	0.43450809
t_{10}	0.80077015	0.42666667	0.80455045	0.43366031
t_{11}	0.19922955	0.57333333	0.19544955	0.56633069
s_{11}	0.20060162	0.60000000	0.20000016	0.60055780
ω_0'	0.13031066π	0.15818801π	0.13031066π	0.15818804π
$E_{2\,MSE}$	0.25224430×10^{-5}	0.26017336×10^{-7}	0.24241316×10^{-5}	0.52116429×10^{-8}
$E_{2\,max}$	0.32798648×10^{-2}	0.13260160×10^{-3}	0.32780260×10^{-2}	0.13273189×10^{-3}
$E_{1\,MSE}$	0.60322057×10^{-3}	0.27795555×10^{-5}	0.59526261×10^{-3}	0.18102724×10^{-5}
$E_{1\,max}$	0.14124343	0.15587450×10^{-1}	0.14133315	0.13344013×10^{-1}

* The coefficients are actually T_{ij}'s and S_{11}. † One of the specification.

Table 5.5 Comparison of Scaled and Scaling-free Approximate Solutions for Different Values of θ for Type–A Elliptical Cutoff Contour with $\omega_a = 0.125\pi$ and $\omega_b = 0.25\pi$.

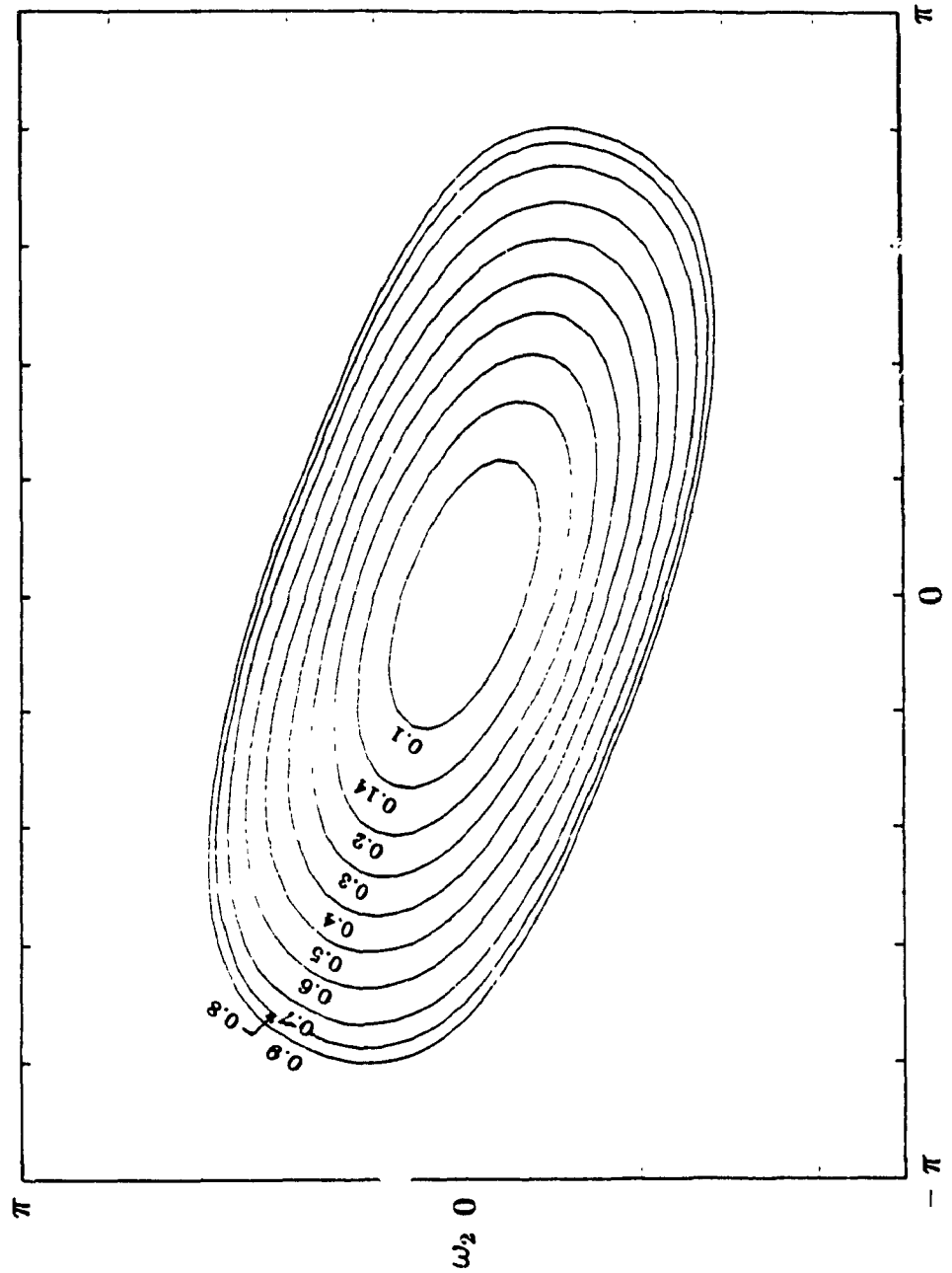

Fig. 5.3 Contours of the Generalized McClellan Transformation Using the Scaled Optimum Coefficients in Table 5.4
(The specifications for a rotated type-A contour are $\omega_a = 0.125\pi$, $\omega_0 = \omega_b = 0.25\pi$, and $\theta = \pi/6$)

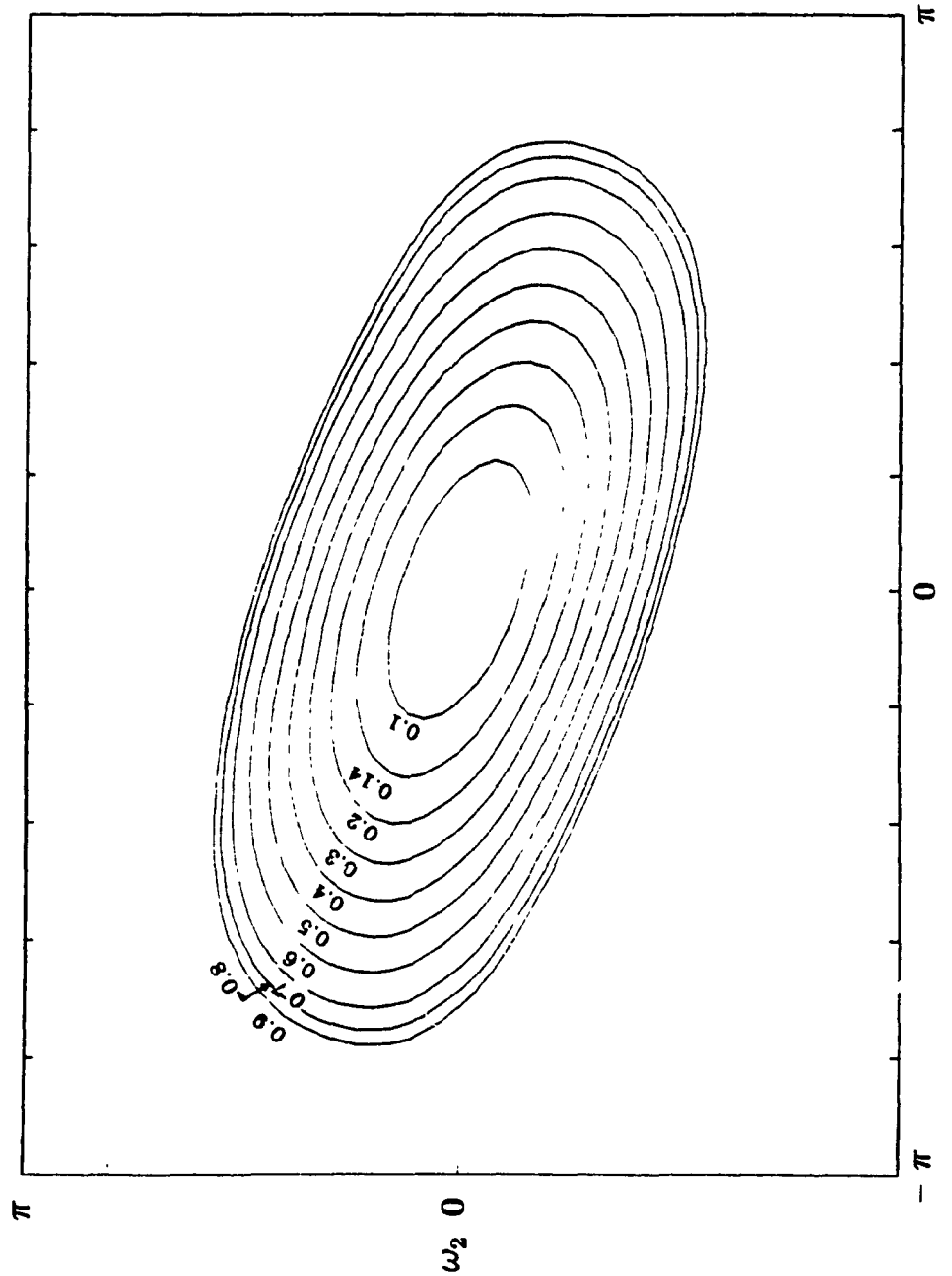

Fig. 5.4 Contours of the Generalized McClellan Transformation Using the Scaling-Free Approximation Coefficients in Table 5.4.
(The specifications for a rotated type-A contour are $\omega_a = 0.125\pi$, $\omega_0 = \omega_b = 0.25\pi$ and $\theta = \pi/6$.)

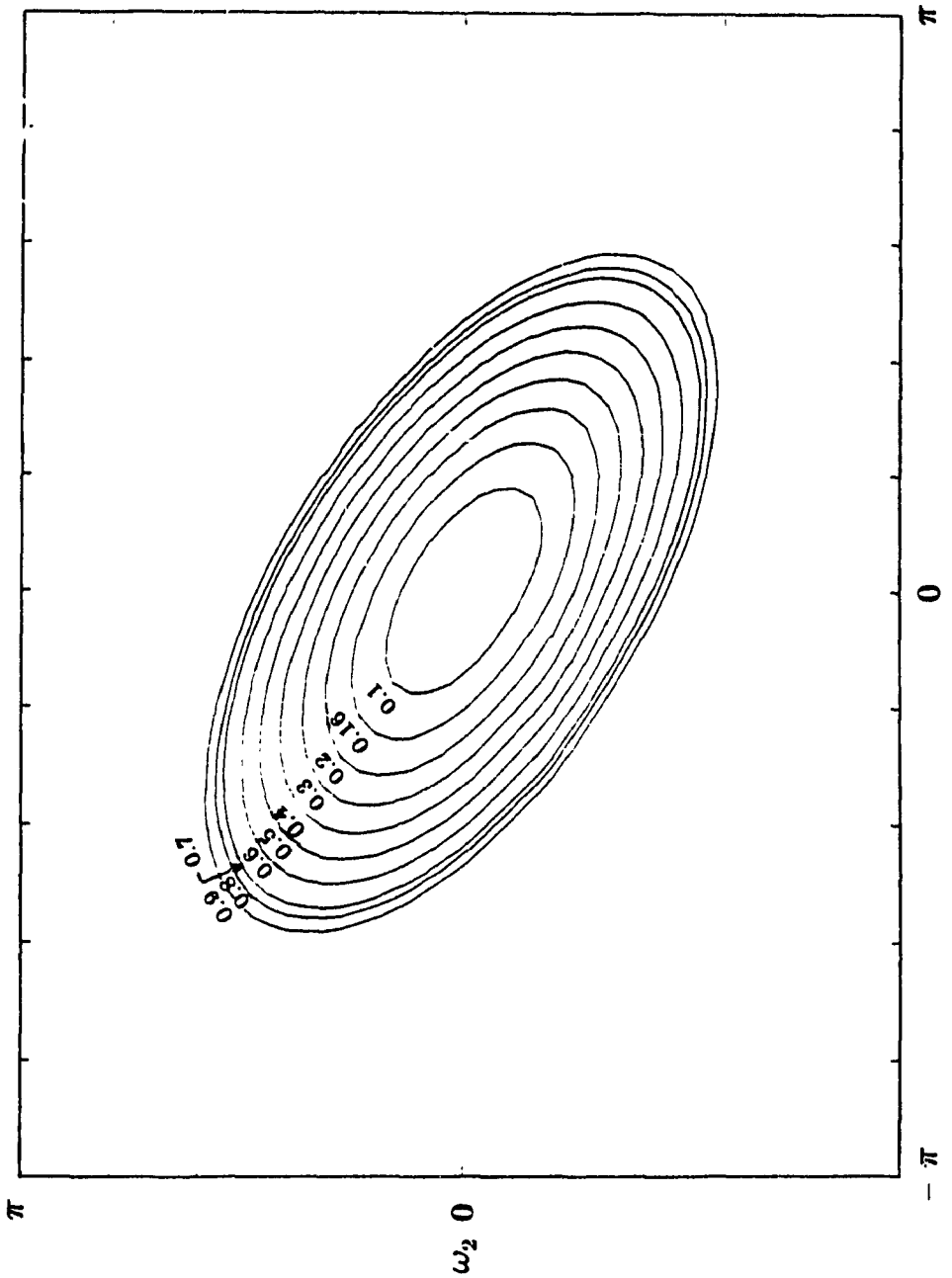

Fig. 5.5 Contours of the Generalized McClellan Transformation Using the Scaling-Free Approximation Coefficients in the Last Column of Table 5.4. (The specifications for a rotated type-A contour are $\omega_a = 0.125\pi$, $\omega_b = \omega_b = 0.25\pi$, and $\theta = \pi/4$.)

5.4 COMPARISON OF APPROACHES I AND II, AND THE METHODS OF [35] AND [42]

The $E_{2\,MSE}$ errors of the scaled optimum and the scaled approximation solutions of approach I in Table 5.1 are of the order of 10^{-10} and 10^{-6}, respectively. These are slightly lower than those of approach II in Table 5.4, since approach I uses a generalized transformation with two sine terms. The use of one more independent coefficient in approach I increases the degree of freedom in the optimization process. Even though the methods of approach I provide slightly lower error values compared to those provided by the methods of approach II, there are few points that are not in favour of approach I are worth mentioning. The methods which follow approach I, increase the order of the designed 2-D filters, since they use a generalized transformation with two second-order sine terms. Also, they produce unnecessary extra pass-bands in the 2-D plane. In order to explain this point, consider Example 5.2. The unscaled coefficients of the approximation solution give $F(0,0) = 1$, $F(\pi,\pi) = 2.1249 = F_{max}$, and $F(\pi,0) = -5.2650 = F_{min}$. Therefore, scaling of the transformation is necessary to make $F_{max} = 1$ and $F_{min} = -1$. The scaled coefficients are given in column 1 of Table 5.4. The scaled transformation maps the corner frequency (π,π) onto $\omega = 0$, and the pass-band of the 2-D filter onto the frequency segment $0.2552\pi \leq \omega \leq 0.2886\pi$. In addition, this segment maps onto two strips around the corner frequencies (π,π) and $(-\pi,\pi)$. Thus, even if the prototype 1-D filter used has a band-pass response in the mentioned frequency segment, the transformed 2-D filter will have 3 pass-bands in the upper half of the (ω_1,ω_2)-plane. The first pass-band is the desired pass-band with rotated elliptical contour around (0,0), and the second and third pass-bands are strips around (π,π) and $(-\pi,\pi)$.

The methods of approach II and the method of [42] do not have this problem of extra pass-bands. These methods use a generalized transformation with only one first-order sine term, and as a result, the designed 2-D filters are minimum order.

The method of [42] gives reasonably good approximation for higher values of frequency specifications. However, this method is more complex. Another disadvantage of the method of [42] is that it does not give good results for lower values of the ratio of the minor- to major- axes. Also, for a very small value of the ratio, F_{max} may not occur at (0,0). Thus, when scaling is employed to map the location of F_{max} onto $\omega = 0$, the 2-D origin (0,0) moves out of the pass-band segment of the ω-axis. For example, for a given value of ω_a less than 0.125π, there is a maximum value of ω_b beyond which this difficulty arises [42]. The methods of approach II do not have this problem even for low values of the ratio.

5.5 SUMMARY

In this chapter, some analytical methods have been developed for finding the coefficients of the generalized McClellan transformation with one (approach II) and two (approach I) sine terms for the design of 2-D elliptically symmetric digital filters with arbitrary orientations. Several new extremely simple analytical formulas have been derived for calculating the transformation coefficients by forcing the lower order significant terms in the power series expansion of the linear error function to zero.

Specifically, for both the approaches I and II, the following design techniques have been developed for elliptical cutoff contours with arbitrary orientations: (i) Approximation Method for Type-A Contours, (ii) Scaling-Free Approximation Method for Type-A Contours, (iii) Approximation Method for Type-B Contours, and (iv) Scaling-Free Approximation Method for Type-B Contours. Methods (i) and (ii), have been concerned with deriving ordinary and simplified formulas for type-A contours following approach I. The simplified formulas are useful for fast calculation of the coefficients when the specifications satisfy some special conditions. Similarly, in Methods (iii) and (iv), several new formulas, the ordinary, simplified, and scaling-free, have been derived for type-B contours. Effects of the angle of rotation on coefficient values have been discussed. Formulas for scaling the coefficients of the sine terms have been provided. Similar results

for types A and B contours have been established in the four methods mentioned above following approach II.

The advantages and disadvantages of all the methods in both the approaches have been discussed. For all the methods, formulas have been presented both for cosine- and sine- form generalized transformation coefficients. Many examples have been provided to demonstrate the usefulness of the formulas derived. The error values of several methods have been compared. In all the methods, lower the frequency specifications, the smaller is the MSE. For the given frequency specifications, the MSE increases with the increasing value of the angle of rotation in approach I. This trend, however, is reversed in approach II. All the formulas presented in this chapter are very simple and suitable for real-time adaptive filter design and filtering applications.

CHAPTER 6

CONCLUSIONS AND SCOPE FOR FUTURE WORK

6.1 CONCLUSIONS

This thesis has been concerned with devising fast and efficient analytical techniques for the design of 2-D elliptically and circularly symmetric FIR and IIR digital filters using McClellan transformation.

The scaling problem of vertical (type-A) and horizontal (type-B) elliptical cutoff contours and circular cutoff contours has been critically analyzed. Several new extremely simple formulas for finding the extreme values of the transformation function and the scaling factors have been presented for these contours. The advantage of the formulas derived is that they can be used directly to find scaled transformations from the unscaled coefficients. The scaled and scaling-free McClellan transformations have been derived for various cases of each type of contour. It has been shown that in the scaling-free transformations, depending on the case, the number of independent coefficients vary from 0 to 2, compared to 3 in the original McClellan transformation. They are very useful in deriving analytical expressions for the coefficients, and the 2-D filters designed have a smaller number of multiplications per output sample. In addition, these scaling-free transformations have the advantage of not changing the cutoff frequency of the 1-D prototype filter. A new formula for scaling the transformation coefficients has been developed and some of its properties given. The analytical method of scaling the coefficients has been found to be faster and more accurate than the numerical method.

Several analytical techniques have been developed for finding the coefficients of the first-order McClellan transformation for the design of 2-D zero-phase digital filters. The transformations have been determined for 2-D filters with circular and horizontal, vertical, and rotated elliptical contours. A number of new extremely simple formulas have

been presented for finding the coefficients of both the original and scaling-free transformations. An approximation approach has been followed in deriving the formulas by forcing the coefficients of the lower-order significant terms in the power series expansion of a linear error function to zero. For the rotated elliptical contours, approximations have been carried out using the generalized McClellan transformation with both one and two sine terms and their relative advantages have been discussed.

All the results have been developed both for the cosine- and sine- form transformations. It has been shown that the transformations developed in this thesis are in certain cases more general than some of the existing ones. The transformations provide more flexibility to the designer and make the comparison between different techniques easier. The scaled coefficients of circular contours have been shown to be constants and independent of the frequency specifications. These coefficients provide a better approximation of circular contours than that achieved by the McClellan's coefficients. The conditions used in determining coefficients for some of the commonly used 1-D to 2-D mappings have been obtained. N-dimensional versions of the original and generalized McClellan transformations have been given. Formulas for finding the coefficients of original N-D transformation for the design of approximately hyper-spherically symmetric filters have been presented. The effects of the angle of rotation of elliptical contours on the coefficient values have been discussed. By comparing the results of a number of design examples, it has been found that the results of the approximation techniques agree well with the those of the optimization and other analytical techniques, and the accuracy of results is sufficient for many engineering applications.

The formulas derived in this thesis are useful for real-time 2-D adaptive filter design on a low cost, stand-alone, general purpose, signal processor. The number of multiplications required to implement the designed 2-D filters has been shown to be small. The transformation coefficients obtained by using the formulas derived may serve as an excellent initial guess for the parameters of a nonlinear optimization technique and help

to accelerate the convergence process.

6.2 Scope for Future Work

The research work presented in this thesis provides a basis for further investigation of analytical design techniques of multidimensional digital filters and their applications. Some suggestions for future work are as follows.

1) It is worth investigating the designs for filters with other types of frequency response contours such as rectangular, square, and diamond shape.

2) The advantages of the new scaling-formula introduced in the thesis in generating new kinds of filters may be fully explored.

3) An investigation to establish the suitability of the designed 2-D filters in implementing various image processing functions may be carried out.

4) The approach of single contour approximation can be extended to multicontours allowing the possibility to minimize the 2-D transition-width and maximize the 1-D transition-width simultaneously.

5) The analytical method of scaling, and the scaled and scaling-free transformations can be extended to nontype preserving transformations [23] allowing the design of other types of 2-D filters from a given 1-D prototype.

6) The optimum coefficients expressible as sum-of-powers of two can be found by a discrete optimization technique using the coefficients obtained by the approximation techniques as an initial guess. These coefficients would be suitable for multiplierless filter structures which are very attractive for real-time applications.

7) The results of this thesis can be extended to higher dimensions ($N \geq 3$)

REFERENCES

[1] A. Antoniou, *Digital Filters: Analysis and Design*, New York: McGraw-Hill Book Company, 1979.

[2] F.J. Taylor, *Digital Filter Design Handbook*, New York: Marcel Dekker Inc., 1983.

[3] N. Nagamuthu, "Applications of Personal Computers in Digital Filter Design", *Proc. Fifth Canadian Conf. Eng. Education*, London, Ontario, pp. 256-274, May 12-13, 1986.

[4] N. Nagamuthu, "Transformation Design of 2-D Recursive Digital Filters Using Spectral Factorization", *M.A.Sc. Thesis*, Dept. of Elect. Eng., Univ. of Windsor, Windsor, Ont., 1982.

[5] D.E. Dudgeon and R.M. Mersereau, *Multidimensional Digital Signal Processing*, Englewood Cliffs, NJ: Prentice Hall, 1984.

[6] E.I. Jury, "Stability of Multidimensional Systems and Related Problems", Chapter 3 in *Multidimensional Systems: Techniques and Applications*, S.G. Tzafestas, Ed., New York: Marcel Dekker Inc., 1986.

[7] S.Y. Kung, Ed., "*VLSI and Modern Signal Processing*", Englewood Cliffs, NJ: Prentice-Hall, 1985.

[8] S.Y. Kung, "*VLSI Array Processors*", Englewood Cliffs, NJ: Prentice-Hall, 1988.

[9] N. Nagamuthu, "Computer Assisted Education in Digital Signal Processing", *Proc. IEEE Int. Computer Conf. and Exhibition (COMPINT'85)*, Montreal, pp. 669-671, Sep. 10-12, 1985.

[10] A.N. Venetsanopoulos, and V. Cappellini, "Real-Time Image Processing", Chapter 8 in *Multidimensional Systems: Techniques and Applications*, S.G. Tzafestas, Ed., New York: Marcel Dekker Inc., pp. 345-399, 1986.

[11] A.N. Venetsanopoulos, "Digital Image Processing and Analysis", (Les Houches, Session XLV, 12 Aout-6 Sep., 1985), Course 10 in *Signal Processing*, Vol. II, J.L. Lacoume, T.S. Durrani, and R. Stora, Eds., New York: North Holland, pp. 575-668, 1987.

[12] A.T. Chottera, "Recursive Digital Filters: Design and Applications to Image Processing", *Ph.D. Dissertation*, Dept. of Elect. Eng., Univ. of Windsor, Windsor, Ont., 1979.

[13] R.C. Gonzalez and P. Wintz, "*Digital Image Processing*", Reading, MA: Addison Wesley Publishing Company, 1977.

[14] N. Nagamuthu and M.N.S. Swamy, "Design, Implementation, and Applications of Two- and Three- Dimensional Elliptically and Circularly Symmetric Digital Filters", *Proposal Report*, Dept. of Elect. and Comp. Eng., Concordia Univ., Montreal, Que., pp. 1-11, July 1988.

[15] A.N Venetsanopoulos, "Computer Aided Design of Two-Dimensional Digital Filters", Chapter 12 in *Multidimensional Systems: Techniques and Applications*, S.G. Tzafestas, Ed., New York: Marcel Dekker Inc., pp. 527-584, 1986.

[16] R.M. Mersereau, "Two-Dimensional Nonrecursive Filter Design", Chapter 2 in *Two-Dimensional Digital Signal Processing I*, T.S. Huang, Ed. Berlin: Springer-Verlag, 1981.

[17] J.H. McClellan, "The Design of Two-Dimensional Digital Filters by Transformation", *Proc. 7th Ann. Princeton Conf. Inform. Sci. and Syst.*, pp. 247-251, March 1973.

[18] N. Nagamuthu and M.N.S. Swamy, "Spectral Transformation Design of 2-D Recursive Digital Filters - A Review and New Results", *Proc. 26th Midwest Symp. Circuits Syst.*, Puebla, Mexico, pp. 270-274, Aug. 15-16, 1983.

[19] S. Chakrabarti and S.K. Mitra, "Design of Two-Dimensional Digital Filters via Spectral Transformations", *Proc. IEEE*, Vol. 65, No. 6, pp. 905-914, June 1977.

[20] P.K. Rajan, H.C. Reddy, M.N.S. Swamy, and V. Ramachandran, "Generation of Two-Dimensional Digital Functions without Nonessential Singularities of the Second Kind", *IEEE Trans. Acoust., Speech, Signal Process.*, Vol. ASSP-28, No. 2, pp. 216-223, April 1980.

[21] J.L. Shanks, S. Treitel, and J.H. Justice, "Stability and Synthesis of Two-Dimensional Recursive Filters", *IEEE Trans. Audio Electroacoust.*, Vol. AU-20, No. 2, pp. 115-128, June 1972.

[22] J.M. Costa and A.N. Venetsanopoulos, "Design of Circularly Symmetric Two-Dimensional Recursive Filters", *IEEE Trans. Acoust., Speech, Signal Process.*, Vol. ASSP-22, No. 6, pp. 432-443, Dec. 1974.

[23] S. Chakrabarti, B.B. Bhattacharyya, and M.N.S. Swamy, "Approximation of Two-Variable Filter Specifications in Analog Domain", *IEEE Trans. Circuits Syst.*, Vol. CAS-24, No. 7, pp. 378-388, July 1977.

[24] H. Chang and J.K. Aggarwal, "Design of Two-Dimensional Recursive Filters by Interpolation", *IEEE Trans. Circuits Syst.*, Vol. CAS-24, No. 6, pp. 281-291, June 1977.

[25] R. Iijima, N. Haratani, and S.I. Takahashi, "Design Method for 2-D Circularly Symmetric Recursive Filters", *IEEE Trans. Acoust., Speech, Signal Process.*, Vol. ASSP-31, No. 5, pp. 1298-1299, Oct. 1983.

[26] A.H. Kayran and R.A. King, "Design of Recursive and Nonrecursive Fan Filters with Complex Transformations", *IEEE Trans. Circuits Syst.*, Vol. CAS-30, No. 12, pp. 849-857, Dec. 1983.

[27] R.M. Mersereau, W.F.G. Mecklenbrauker, and T.F. Quatieri, "McClellan Transformations for Two-Dimensional Digital Filtering: I-Design", *IEEE Trans. Circuits Syst.*, Vol. CAS-23, No. 7, pp. 405-414, July 1976.

[28] P.K. Rajan and M.N.S. Swamy, "Design of Circularly Symmetric Two-Dimensional FIR Digital Filters Employing Transformations with Variable Parameters", *IEEE Trans. Acoust., Speech, Signal Process.*, Vol. ASSP-31, No. 3, pp. 637-642, June 1983.

[29] C.K. Yan and A.N. Venetsanopoulos, "Three-Dimensional FIR Filter Design by Transformation of One-Dimensional Digital Filters", *Proc. IEEE Int. Elect. Electronics Conf. and Exposition (ELECTRONICOM'85)*, Toronto, Ont., pp. 202-205, Oct. 7-9, 1985.

[30] A.N. Venetsanopoulos and M.E. Zervakis, "Design of Three-Dimensional Digital Filters Using Transformation Techniques", *Proc. Int. Symp. Circuits Syst.*, San Jose, CA, pp. 498-501, May 5-7, 1986.

[31] M. Ahmadi and R.A. King, "Transformation Technique for N-Dimensional FIR Filters", *Proc. 20th Midwest Symp. Circuits Syst.*, Texas Tech. Univ., Lubbock, TX, pp. 450-453, Aug. 15-17, 1977.

[32] R.M. Mersereau, "The Design of Arbitrary 2-D Zero-phase FIR Filters Using Transformations", *IEEE Trans. Circuits Syst.*, Vol. CAS-27, No. 2, pp. 142-144, Feb. 1980.

[33] N. Nagamuthu and M.N.S. Swamy, "Scaled and Scaling-free McClellan Transformations for the Design of 2-D Low-Pass Digital Filters", *Proc. Canadian Conf. Elect. Comp. Eng.*, (CCECE'88), Vancouver, BC, pp 633-636, Nov. 3-4, 1988.

[34] M.S. Reddy and S.N. Hazra, "Design of Elliptically Symmetric Two-Dimensional FIR Filters Using the McClellan Transformation", *IEEE Trans Circuits Syst.*, Vol. CAS-34, No. 2, pp. 196-198, Feb. 1987.

[35] D.T. Nguyen and M.N.S. Swamy, "Approximation Design of 2-D Digital Filters with Elliptical Magnitude Response of Arbitrary Orientation", *IEEE Trans. Circuits Syst.*, Vol. CAS-33, No. 6, pp. 597-603, June 1986.

[36] N. Nagamuthu and M.N.S. Swamy, "Analytical Methods for the Design of 2-D Elliptically Symmetric Digital Filters Using McClellan Transformation", *Proc. IEEE Pacific Rim Conf. Commu., Comp., and Signal Process.*, Victoria, BC, pp. 198-201, June 1 & 2, 1989.

[37] N. Nagamuthu and M.N.S. Swamy, "Design Methods for 2-D Elliptically Symmetric Zero-Phase FIR and IIR Digital Filters Using McClellan Transformation", *Proc. Canadian Conf. Elect. Comp. Eng.*, (CCECE'89), Montreal, Quebec, pp. 475-478, Sep. 17-20, 1989.

[38] A. Fettweis, "Symmetry Requirements for Multidimensional Digital Filters", *Int. J. Circuit Theory Appl.*, Vol. 5, No. 4, pp. 343-353, Oct. 1977.

[39] K. Kurogochi and S. Makino, "A Design Method for Circularly Symmetric Two-Dimensional Low-Pass Digital Filters by Modified McClellan Transformation", *Trans. Inst. Electron. Comm. Eng. Japan*, Vol. J 66-A, pp. 1025-1026, Oct. 1983 (In Japanese).

[40] S.N. Hazra and M.S. Reddy, "Design of Circularly Symmetric Low-Pass Two-Dimensional FIR Digital Filters Using Transformation", *IEEE Trans. Circuits Syst.*, Vol. CAS-33, No. 10, pp. 1022-1026, Oct. 1986.

[41] N. Nagamuthu and M.N.S. Swamy, "Analytical Methods for the Design of 2-D Circularly Symmetric Digital Filters Using McClellan Transformation", *Proc. IEEE Int. Symp. Circuits Syst.*, Portland, Oregon, pp. 1095-1098, May 9-11, 1989.

[42] M.S. Reddy and S.N. Hazra, "Design of Elliptically Symmetric Two-Dimensional FIR Filters with Arbitrary Orientation", *IEEE Trans. Circuits Syst.*, (Submitted for publication.)

[43] N. Nagamuthu and M.N.S. Swamy "Analytical Methods for the Design of 2-D Elliptically Symmetric Digital Filters of Arbitrary Orientation Using Generalized McClellan Transformation", *Proc. Int. Conf. Advances in Commu. and Cont Syst.*, (ComCon'88), Baton Rouge, LA, pp. 293-304, Oct. 19-21, 1988. (Also published in the *Lecture Notes in Control and Information Sciences Series*, Springer-Verlag.)

[44] F. Bernabo, P.L. Emiliani, and V. Cappellini, "Design of 2-Dimensional Recursive Digital Filters", *Electron. Lett.*, Vol. 12, No. 11, pp. 288-289, May 27, 1976.

[45] N. Nagamuthu, M.A. Sid-Ahmad, and M. Ahmadi, "Design of 2-D Recursive Digital Filters with Constant Group-Delay Characteristics", *J. Franklin Inst.*, Vol. 320, Nos. 3/4, pp. 191-200, Sep./Oct. 1985.

[46] N. Nagamuthu and M.N.S. Swamy, "On the Transformation Design of Half-Plane 2-D Recursive Digital Filters Using Spectral Factorization", *Proc. IEEE Int Elect Electronics Conf. and Exposition (ELECTRONICOM'33)*, Toronto, Ont., pp. 520-524, Sep. 26-28, 1983.

[47] N. Nagamuthu and M.N.S. Swamy, "Transformation Design of N-D Recursive Digital Filters Using Spectral Factorization", *Proc. Int. Conf. Computers, Syst, and Signal Process.*, Bangalore, India, pp. 1632-1635, Dec. 10-12, 1981.

[48] D.T. Nguyen and M.N.S. Swamy, "A Class of 2-D Separable Denominator Filters Designed via the McClellan Transform", *IEEE Trans. Circuits Syst*, Vol. CAS-33, No. 9, pp. 874-881, Sep. 1986.

[49] P.K. Rajan and M.N.S. Swamy, "Two-Dimensional FIR Digital Filters with Maximally Flat Magnitude", *Proc. IEEE*, Vol. 66, No. 9, pp. 1086-1088, Sep. 1978

[50] P.K. Rajan and M.N.S. Swamy, "Quadrantal Symmetry Associated with Two-Dimensional Digital Transfer Functions", *IEEE Trans. Circuits Syst.*, Vol CAS-25, No. 6, pp. 340-343, June 1978.

[51] D.T. Nguyen and M.N.S. Swamy, "Scaling-Free McClellan Transform for 2-D Digital Filters", *Electron. Lett.*, Vol. 21, No. 5, pp. 176-178, Feb. 28, 1985.

[52] D.T. Nguyen and M.N.S. Swamy, "Formulas for Parameters Scaling in the McClellan Transform", *IEEE Trans. Circuits Syst.*, Vol. CAS-33, No. 1, pp. 108-109, Jan. 1986.

[53] M.Y. Dabbagh and W.E. Alexander, "Multiprocessor Implementation of 2-D Denominator-Separable Digital Filters for Real-Time Processing", *IEEE Trans. Acoust., Speech, Signal Process.*, Vol. 37, No. 6, pp. 872-881, June 1989.

[54] E. Dubois and M.L. Blostein, "A Circuit Analogy Method for the Design of Recursive Two-Dimensional Digital Filters", *Proc. IEEE Int. Symp. Circuits Syst.*, Newton, Mass., pp. 451-454, April 21-23, 1975.

[55] M. Ahmadi, A.G. Constantinides, and R.A. King, "Design Technique for a Class of Stable Two-Dimensional Recursive Digital Filters", *Proc. IEEE Int. Conf. Acoust., Speech, and Signal Process.*, Philadelphia, PA, pp. 145-147, April 1976.

[56] R.A King and A.H. Kayran, "A New Transformation Technique for the Design of 2-Dimensional Stable Recursive Digital Filters", *Proc. IEEE Int. Symp. Circuits Syst.*, Chicago, IL, pp. 196-199, April 27-29, 1981.

[57] A.M. Ali and A.G. Constantinides, "On 2-Variable Reactance Functions for 2-Dimensional Recursive Filter Design", *Electron. Lett.* Vol. 14, No. 1, pp. 12-13, Jan. 5, 1978.

[58] M.F. Fahmy and M.I. Sobhy, "A New Method for the Design of 2-D Filters with Guaranteed Stability", *IEEE Trans. Circuits Syst.*, Vol. CAS-29, No. 4, pp. 246-251, April 1982.

[59] G.V. Mendonca, A. Antoniou, and A.N. Venetsanopoulos, "Design of Two-Dimensional Pseudorotated Digital Filters Satisfying Prescribed Specifications", *IEEE Trans. Circuits Syst.*, Vol. CAS-34, No. 1, pp. 1-9, Jan. 1987.

[60] D.M. Goodman, "A Design Technique for Circularly Symmetric Low-Pass Filters", *IEEE Trans. Acoust., Speech, Signal Process.*, Vol. ASSP-26, No. 4, pp. 290-304, Aug. 1978.

[61] N.A. Pendergrass, S.K. Mitra, and E.I. Jury, "Spectral Transformations for Two-Dimensional Digital Filters", *IEEE Trans. Circuits Syst.*, Vol. CAS-23, No. 1, pp. 26-35, Jan. 1976.

[62] A.P. Gerheim, "A Synthesis Procedure for 90^{o} Fan Filters", *IEEE Trans. Circuits Syst.*, Vol. CAS-30, No. 12, pp. 858-864, Dec. 1983.

[63] K. Hirano and J.K. Aggarwal, "Design of Two-Dimensional Recursive Digital Filters", *IEEE Trans. Circuits Syst.*, Vol. CAS-25, No. 12, pp. 1066-1076, Dec. 1978.

[64] L. Harn and B.A. Shenoi, "Design of Stable Two-Dimensional IIR Filters Using Digital Spectral Transformations", *IEEE Trans. Circuits Syst.*, Vol. CAS-33, No. 5, pp. 483-490, May 1986.

[65] A.M. Ali, "Design of Inherently Stable Two-Dimensional Recursive Filters Imitating the Behavior of One-Dimensional Analog Filters", *Proc. IEEE Int. Conf. Acoust., Speech, and Signal Process.*, Tulsa, OK, pp. 765-768, April 10-12, 1978.

[66] K.S. Thyagarajan, "Design of 2-D IIR Digital Filters with Circular Symmetry by Transformation of the Variable", *Proc. IEEE Int. Conf. Acoust., Speech, and Signal Process.*, Atlanta, pp. 685-687, 1981.

[67] V. Ramachandran and M. Ahmadi, "Some Recent Advances in the Generation of VSHP and Applications in the Design of 2-D Recursive Digital Filters", *Proc. IEEE Int. Symp. Circuits Syst.*, Kyoto, Japan, pp. 1363-1366, 1985.

[68] M.S. Reddy and S.N. Hazra, "Design of Two-Dimensional Circularly Symmetric Low-Pass IIR Filters Using Transformation", *IEEE Trans. Circuits Syst.*, Vol. CAS-35, No. 9, pp. 1186-1188, Sep. 1988.

[69] M.N.S. Swamy and K.S. Thyagarajan, 'Frequency Transformations for Digital Filters", *Proc. IEEE*, pp. 165-166, Jan. 1977.

[70] S. Erfani, M. Ahmadi, and V. Ramachandran, "Alternative Approach to Digital Spectral Transformations", *IEEE Trans. Circuits Syst.*, Vol. CAS-35, No. 11, pp. 1461-1463, Nov. 1988.

[71] S. Erfani, M. Ahmadi, and V. Ramachandran, "The General Biquadratic Transformations of Polynomials", *IEEE Trans. Circuits Syst.*, Vol. CAS-35, No. 12, pp. 1547-1549, Dec. 1988.

[72] M.N.S Swamy and P.K. Rajan, "Symmetry in Two-Dimensional Digital Filters and Its Application", Chapter 9 in *Multidimensional Systems: Techniques and Applications*, S.G. Tzafestas, Ed., New York: Marcel Dekker Inc., pp. 527-584, 1986.

[73] J.K. Pitas and A.N. Venetsanopoulos, "The Use of Symmetries in the Design of Multidimensional Digital Filters", *IEEE Trans. Circuits Syst.*, Vol. CAS-33, No. 9, pp. 863-873, Sep. 1986.

[74] S.A.H. Aly and M.M. Fahmy, "Symmetry in Two-Dimensional Rectangularly Sampled Digital Filters", *IEEE Trans. Acoust., Speech, Signal Process.*, Vol. ASSP-29, No. 4, pp. 794-805, Aug. 1981.

[75] J.H. Lodge and M.M. Fahmy, "K-Cyclic Symmetries in Multi-Dimensional Sampled Signals", *IEEE Trans Acoust., Speech, Signal Process.*, Vol. ASSP-31, No. 4, pp. 847-860, Aug. 1983.

[76] P.K. Rajan and M.N.S. Swamy, "Symmetry Relations in Multidimensional Fourier Transform Pairs" *Circuits Syst. Signal Process.*, Vol. 3, No. 4, pp. 477-491, Dec. 1984.

[77] S.A.H. Aly and M.M. Fahmy, "Symmetry Exploitation in the Design and Implementation of 2-D Rectangularly Sampled Digital Filters", *IEEE Trans. Acoust., Speech, Signal Process.*, Vol. ASSP-29, No. 5, pp. 973-982, Oct. 1981.

[78] P.K. Rajan and M.N.S. Swamy, "Two-Dimensional FIR Digital Filters with Maximally Flat Magnitude", *Proc. IEEE*, Vol. 66, No. 9, pp. 1086-1088, Sep. 1978.

[79] P.K. Rajan and H.C. Reddy, "Application of Symmetrical Decomposition to 2-D FIR Filter Design", *Proc. IEEE Int. Conf. Acoust., Speech, and Signal Process.*, Tampa, FL, pp. 1321-1324, March 26-29, 1985.

[80] M.O. Ahmad, and J.D. Wang, "An Analytical Least Square Solution to the Design Problem of Two-Dimensional FIR Filters with Quadrantally Symmetric or Antisymmetric Frequency Response", *IEEE Trans. Circuits Syst.*, Vol. CAS-36, No. 7, pp. 968-979, July 1989.

[81] P.K. Rajan, H.C. Reddy, and M.N.S. Swamy, "Further Results on 4-Fold Rotational Symmetry in 2-D Functions", *Proc. IEEE Int. Conf. Acoust., Speech, and Signal Process.*, Paris, pp. 144-147, May 3-5, 1982.

APPENDIX A

CONVERSION FORMULAS FOR COSINE- AND SINE FORM McCLELLAN TRANSFORMATIONS

The first-order original McClellan transformation in cosine-form [17] is

$$\cos(\omega) = t_{00} + t_{01}\cos(\omega_2) + t_{10}\cos(\omega_1) + t_{11}\cos(\omega_1)\cos(\omega_2), \tag{A.1}$$

and in sine-form is

$$\sin^2(\omega/2) = p_{00} + p_{01}\sin^2(\omega_2/2) + p_{10}\sin^2(\omega_1/2) + p_{11}\sin^2(\omega_1/2)\sin^2(\omega_2/2). \tag{A.2}$$

The relationship between the coefficients t_{ij}'s and p_{ij}'s are derived below.

A.1 COSINE-FORM TO SINE-FORM CONVERSION FORMULAS

Using the trigonometric identity

$$\cos(x) = 1 - 2\sin^2(x/2) \tag{A.3}$$

in (A.1), rearranging, and comparing the resulting equation with (A.2), the following formulas are obtained.

$$p_{00} = -(t_{00} + t_{01} + t_{10} + t_{11} - 1)/2 \tag{A.4a}$$
$$p_{01} = t_{01} + t_{11} \tag{A.4b}$$
$$p_{10} = t_{10} + t_{11} \tag{A.4c}$$
$$p_{11} = -2t_{11} \tag{A.4d}$$

A.2 SINE-FORM TO COSINE-FORM CONVERSION FORMULAS

Sine-form to cosine-form conversion formulas can be derived by using the trigonometric identity

$$\sin^2(x/2) = \left(1 - \cos(x)\right)/2 \tag{A.5}$$

in (A.2), or by solving (A.4) for t_{ij}'s in terms of p_{ij}'s. The obtained formulas are as follows.

$$t_{00} = 1 - \left(2p_{00} + p_{01} + p_{10} + (p_{11}/2)\right) \tag{A.6a}$$

$$t_{01} = p_{01} + (p_{11}/2) \tag{A.6b}$$

$$t_{10} = p_{10} + (p_{11}/2) \tag{A.6c}$$

$$t_{11} = -(p_{11}/2) \tag{A.6d}$$

A.3 Relationship Between Scaled Coefficients

The relationship between the scaled coefficients T_{ij}'s (in Eq. (2.6)) and P_{ij}'s (in Eq. (2.9)) are obtained by replacing t_{ij}'s by T_{ij}'s and p_{ij}'s by P_{ij}'s in (A.4) and (A.6).

APPENDIX B

MAXIMA AND MINIMA OF TRANSFORMATION FUNCTION

The first-order original McClellan transformation function [17] is

$$F(\omega_1,\omega_2) = t_{00} + t_{01}\cos(\omega_2) + t_{10}\cos(\omega_1) + t_{11}\cos(\omega_1)\cos(\omega_2), \tag{B.1}$$

Hence,

$$\frac{\partial F}{\partial \omega_1} = F_{\omega_1} = -\sin(\omega_1)\left(t_{10} + t_{11}\cos(\omega_2)\right) \tag{B.2}$$

$$\frac{\partial F}{\partial \omega_2} = F_{\omega_2} = -\sin(\omega_2)\left(t_{01} + t_{11}\cos(\omega_1)\right) \tag{B.3}$$

The location of the extreme values of this function are obtained by equating the above partial derivatives to zero. Hence the possible locations of the maxima or minima are $(0,0)$, $(0,\pi)$, $(\pi,0)$, (π,π), and (θ_1,θ_2), where $\theta_1 = \cos^{-1}(-t_{01}/t_{11})$ and $\theta_2 = \cos^{-1}(-t_{10}/t_{11})$.

To determine which of these points correspond to absolute maxima or minima, the following second partial derivatives are employed.

$$\frac{\partial^2 F}{\partial \omega_1^2} = F_{\omega_1\omega_1} = -\cos(\omega_1)\left(t_{10} + t_{11}\cos(\omega_2)\right) \tag{B.4}$$

$$\frac{\partial^2 F}{\partial \omega_2^2} = F_{\omega_2\omega_2} = -\cos(\omega_2)\left(t_{01} + t_{11}\cos(\omega_1)\right) \tag{B.5}$$

$$\frac{\partial^2 F}{\partial \omega_1 \omega_2} = F_{\omega_1\omega_2} = t_{11}\sin(\omega_1)\sin(\omega_2) \tag{B.6}$$

It is known that (ω_1^*,ω_2^*) is a saddle point if, at that point

$$D \triangleq F^2_{\omega_1\omega_2}(\omega_1^*,\omega_2^*) - F_{\omega_1\omega_1}(\omega_1^*,\omega_2^*)\,F_{\omega_2\omega_2}(\omega_1^*,\omega_2^*) < 0 \tag{B.7}$$

At the point (θ_1,θ_2), $F_{\omega_1\omega_1} = F_{\omega_2\omega_2} = 0$ and hence, $D = F^2_{\omega_1\omega_2}$ is always positive. Thus, (θ_1,θ_2) is a saddle point.

Therefore, the only points at whic. $F(\omega_1,\omega_2)$ can take maximum or minimum values are the corner frequency points, $(0,0)$, $(0,\pi)$, $(\pi,0)$, and (π,π).

APPENDIX C

CONDITIONS AND VALUES OF F_{max} AND F_{min} FOR TYPES A, B, AND C CONTOURS

Contour	Case	Condition	F_{max}	F_{min}
Type-A $t_{10} + t_{11} > t_{01} + t_{11} > 0$	(i)	$t_{10} + t_{01} < 0$	$1 - 2(t_{10} + t_{01})$	$1 - 2(t_{10} + t_{11})$
	(ii)	$t_{11} > t_{10}$	1	$1 - 2(t_{10} + t_{11})$
	(iii)	$t_{10} > t_{11} > t_{01}$	1	$1 - 2(t_{10} + t_{11})$
	(iv)	$t_{10} > t_{11}$	1	$1 - 2(t_{10} + t_{01})$
Type-B $t_{01} + t_{11} > t_{10} + t_{11} > 0$	(i)	$t_{01} + t_{10} < 0$	$1 - 2(t_{01} + t_{10})$	$1 - 2(t_{01} + t_{11})$
	(ii)	$t_{11} > t_{01}$	1	$1 - 2(t_{01} + t_{11})$
	(iii)	$t_{01} > t_{11} > t_{10}$	1	$1 - 2(t_{01} + t_{11})$
	(iv)	$t_{01} > t_{11}$	1	$1 - 2(t_{01} + t_{10})$
Type-C $t_{10} = t_{01} = t > 0$	(i)	$2t < 0$	$1 - 4t$	$1 - 2(t + t_{11})$
	(ii)	$t_{11} > t$	1	$1 - 2(t + t_{11})$
	(iii)	$t > t_{11}$	1	$1 - 4t$